CHEMICAL AND THERMODYNAMIC PROPERTIES AT HIGH TEMPERATURES

A Symposium

XVIIIth International Congress of
Pure and Applied Chemistry
Montreal, Canada
August 6 - 12, 1961

Commission on Chemical Thermodynamics
Commission on High Temperatures and Refractories
INTERNATIONAL UNION OF PURE AND APPLIED CHEMISTRY

The Commissions on Thermodynamics and on High Temperatures and Refractories of the International Union of Pure and Applied Chemistry acknowledge the assistance of the National Bureau of Standards and the National Aeronautics and Space Administration, Washington 25, D. C., in the preparation and printing of this book of abstracts.

PREFACE

This book contains the program and all available abstracts of the 90 invited and contributed papers to be presented at the IUPAC Symposium on Chemical and Thermodynamic Properties at High Temperatures. The Symposium will be held in conjunction with the XVIIIth IUPAC Congress, Montreal, August 6 – 12, 1961. It has been organized by the Subcommissions on Condensed States and on Gaseous States of the Commission on High Temperatures and Refractories and by the Subcommission on Experimental Thermodynamics of the Commission on Chemical Thermodynamics, acting in conjunction with the Organizing Committee of the IUPAC Congress. All inquiries concerning participation in the Symposium should be directed to: Secretary, XVIIIth International Congress of Pure and Applied Chemistry, National Research Council, Ottawa, Canada.

Owing to the limited time and facilities available for the preparation and printing of the book, it has not been possible to refer the proofs of the abstracts to the authors for checking. Furthermore, it has not been possible to subject the manuscripts to a very thorough editorial examination. Some obvious errors in the manuscripts have been corrected; other errors undoubtedly have been introduced. Figures have been redrawn only when such a step was essential for reproduction purposes. Sincere apologies are offered to authors and readers for any errors which remain; however, in the circumstances neither the IUPAC Commissions who organized the Symposium, nor the U. S. Government Agencies who assisted in the preparation of this book can accept responsibility for the errors.

Raymond F. Walker

May 10, 1961
National Bureau of Standards
Washington 25, D. C.

CONTENTS

IUPAC – ITS FUNCTION AND MODUS OPERANDI

Many inquiries are received as to the function and operations of IUPAC. The following is a selection of excerpts from IUPAC Information Bulletin No. 10. (December, 1959), which effectively summarizes the aims and activities of the organization.

"The International Union of Pure and Applied Chemistry, IUPAC, is a voluntary body whose chief purposes are to establish and promote cooperation between the Chemical Societies of the member countries and to coordinate their scientific and technical activities. The governing body of the Union, its Council, is composed of delegates appointed by national agencies concerned with fundamental and applied chemistry in the participating countries. These agencies, which represent in each country the chemical interests of that country are the adhering bodies to IUPAC. At present there are some 36 national adhering bodies. The Union, as we know it today, originated in London in November 1918, through the joint action of Sir William Pope, the then President of the Society of Chemical Industry, and Paul Kestner, at that time President of the Societé de Chimie Industrielle, and was formally constituted at a meeting in Rome in June 1920.

The Union is essentially concerned with those aspects of chemistry, both academic and industrial, about which international agreement or uniform practice is desirable. Examples are nomenclature, atomic weights, symbols and terminology, physicochemical constants, and certain methods of analysis and assay. At the biennial conferences of the Union reports on such subjects are presented by the numerous Commissions dealing with them, discussed, and, after approval, are published.

Thus the Union, through its Commissions, offers an international forum where outstanding specialists in many fields of interest can meet to exchange opinions and experiences with the object of reaching agreements that will promote the progress of chemistry throughout the world. The adoption of these agreements or recommendations is not mandatory for the adhering countries – it is wholly voluntary. Nevertheless, the expertness of judgment that goes into them and the care taken to consider all points of view ensure their general acceptance.

The Union also sponsors international congresses and symposia organized by its Sections or Commissions in their respective fields of interest. With the aim of better dissemination of scientific knowledge a new international journal "Pure and Applied Chemistry" has been created by the Union.

All the officers of IUPAC accomplish their duties on the honorary basis and without cost to the Union. Administrative expenses are therefore neglected. The Union's funds are derived from two sources: national contributions and grants-in-aid from UNESCO, with which the Union is affiliated through the International Council of Scientific Unions.

THE SPONSORING COMMISSIONS

Commission on Chemical Thermodynamics

F. D. Rossini	(USA), President
K. Schäfer	(Germany), Secretary
J. Coops	(Netherlands)
D. M. Newitt	(UK)
K. S. Pitzer	(USA)
H. A. Skinner	(UK)
B. Vodar	(France)
G. Waddington	(USA)

Subcommission on Experimental Thermodynamics

D. M. Newitt	(UK), President
G. Waddington	(USA), Secretary
L. Deffet	(Belgium)
S. D. Hamann	(Australia)
A. Michels	(Netherlands)
J. A. Morrison	(Canada)
K. S. Pitzer	(USA)
B. Vodar	(France)

Commission on High Temperatures and Refractories

G. Chaudron	(France), President

Subcommission on Gases

B. L. Lewis	(USA), President
L. Brewer	(USA), Secretary
P. Laffitte	(France)
W. Lochte-Holtgreven	(Germany)
M. W. Thring	(UK)

Subcommission on Condensed States

G. Chaudron	(France), President
B. L. Lewis	(USA), Vice President
M. Foex	(France), Secretary
A. Franklin	(USA)
G. Hägg	(Sweden)
F. Trombe	(France)
Atma Ram	(India)
R. L. Barrett	(UK)
G. Brauer	(Germany
N. F. H. Bright	(Canada)
J. J. Diamond	(USA)
E. R. McCartney	(Australia)
H. Mii	(Japan)
H. Nowotny	(Austria)
R. Thakur	(India)
R. F. Walker	(USA)

The above is a list of titular and associate members of the Commissions as of 1959, and may be subject to change at the XXIst IUPAC Conference, Montreal, August 2 – 5, 1961. The following individuals have also contributed to the activities of the High Temperature Commission in the interim period: J. P. Shaw (U. K.); G. D. Rieck (Netherlands); E. Starkman (USA).

The following individuals were primarily responsible for the detailed planning and organization of the Symposium in conjunction with the Organizing Committee of the Congress:

The Presidents of the Commissions and Subcommissions.

L. Brewer	(USA)
N. F. Bright	(Canada)
M. Foex	(France)
A. D. Franklin	(USA)
E. Starkman	(USA)
G. Waddington	(USA)
R. F. Walker	(USA)

PROGRAM

MONDAY, AUGUST 7

Morning Session: GASEOUS STATES: KINETICS OF THERMAL AND RADIATED REACTIONS IN HIGH TEMPERATURE GASES AND PLASMAS.

Location: Moyse Hall, McGill University.

Chairman: Prof. N. Manson, Poitiers, France.

Co-Chairman: Dr. Ian Fells, University of Sheffield, England.

9:00 Introduction to Symposium by Professor G. Chaudron, President of the Commission on High Temperatures and Refractories of the International Union of Pure and Applied Chemistry.

9:10 A3-1 Sessional Lecture
FLAMES AUGMENTED BY ELECTRIC POWER

B. Karlovitz, Combustion and Explosives Research Inc., Pittsburgh, U.S.A.

10:10 A3-2 SOME NEW MEASURING TECHNIQUES IN HIGH-TEMPERATURES GASES

P. L. Blackshear and L.M. Fingerson, University of Minnesota, U.S.A.

10:30 Recess

10:40 A3-3 SHOCK WAVES IN CHEMICAL KINETICS: THE DISSOCIATION OF MOLECULAR CHLORINE

M. van Thiel and D. Britton, University of Minnesota, U.S.A.

11:00 A3-4 FAST REACTIONS IN ADIABATICALLY COMPRESSED GASES

W. Jost, A. Martinengo and H. Gg. Wagner, University of Göttingen, Germany.

11:20 A3–5 IONENDISSOZIATION VON HF UND NH_3 IN KOMPRIMIERTEM WASSER BIS 750°C

E.U. Franck, K.H. Dudziak and G. Coulon, University of Göttingen, Germany.
(To be presented in German). *

11:40 A3–6 SELF–DIFFUSION COEFFICIENTS OF CARBON DIOXIDE AT 1250 – 1700°K

G. Ember, J.R. Ferron and K. Wohl, University of Delaware, U.S.A.

12:00 A3–7 THE CARBON–HYDROGEN SYSTEM AT TEMPERATURES ABOVE 2500°C

J.M. Iwasyk and R.F. Baddour, E.I. du Pont de Nemours and Co. Inc., Wilmington, U.S.A.

MONDAY, AUGUST 7

Afternoon Session: GASEOUS STATES: FUNDAMENTAL STUDIES OF FLAMES OR PLASMAS APPLIED TO CHEMICAL AND METALLURGICAL PROCESSES.

Location: Moyse Hall, McGill University

Chairman: Dr. S.S. Penner, Guggeheim Jet Propulsion Center,

Co–Chairman: Prof. G. Pannetier, Paris, France. Pasadena, U.S.A.

2:00 A3–8 Sessional Lecture
POSSIBILITES DE CONTROLE DES PROPRIETES THERMODYNAMIQUES A L'AIDE DES CARACTERISTIQUES DES DETONATIONS

N. Manson, Faculté des Sciences, Poitiers, France.
(To be presented in French)

* Except where otherwise indicated, the papers will be presented in English.

3:00 A3–9 Sessional Lecture
IONISATION PROCESSES IN GASES AND THEIR APPLICATION TO ENERGY CONVERSION SYSTEMS

I. Fells, University of Sheffield, England.

4:00 Recess

4:10 A3–10 INFRA-RED SPECTROSCOPY OF HOT PLASMAS

R.H. Tourin, The Warner and Swasey Company, Flushing, N.Y., U.S.A.

4:30 A3–11 UNE METHODE POUR ETUDIER LA CINETIQUE DE CERTAINES COMBUSTIONS

F. Cabannes and P. Valentin, Faculté de Caen, France. (To be presented in French)

4:50 A3–12 DETERMINATION OF RATE CONSTANTS OF ELEMENTARY PROCESSES FROM FLAME VELOCITIES AS A FUNCTION OF TEMPERATURE, PRESSURE, AND MOLECULAR TRANSFER COEFFICIENTS

L.A. Lovachev, Academy of Sciences, Moscow, U.S.S.R.

TUESDAY, AUGUST 8

Morning Session: THERMODYNAMIC PROPERTIES: VAPOR PRESSURE DATA AND THE PROPERTIES OF VAPOURS (WITH EMPHASIS ON COMPOUNDS CONTAINING THREE KINDS OF ATOMS).

Location: Moyse Hall, McGill University

Chairman: Prof. F.D. Rossini, South Bend, Indiana, U.S.A.

Co-Chairman: Dr. C.W. Beckett, Washington, D.C., U.S.A.

9:00 A3–13 Sessional Lecture
TERNARY SPECIES AT HIGH TEMPERATURES

P.W. Gilles, University of Kansas, U.S.A.

10:00 A3–14 THE DISSOCIATION ENERGIES OF THE GASEOUS MONOXIDES OF THE RARE EARTHS. THERMODYNAMIC PROPERTIES OF SOME GASEOUS DIOXIDES

D. White, P. N. Walsh, H. W. Goldstein and D. F. Dever, The Ohio State University, Columbus, U. S. A.

10:20 Recess

10:30 A3–15 THE FREE ENERGY OF FORMATION OF SiC, TiC AND ZrC

G. [illegible] Vidale, General Electric Company, Philadelphia, U. S. A.

10:50 A3–16 THE VAPORIZATION OF LITHIUM AND SODIUM METABORATE

A. Buchler and J. B. Berkowitz–Mattuck, A. D. Little Inc., Cambridge, U. S. A.

11:10 A3–17 VAPORIZATION OF MAGNESIUM OXIDE AND ITS REACTION WITH ALUMINA

R. L. Altman and A. W. Searcy, University of California, Livermore, U. S. A.

11:30 A3–18 VAPOUR PRESSURES OF THE PLATINUM METALS

R. F. Hampson and R. F. Walker, National Bureau of Standards, Washington, U. S. A.

11:50 A3–19 THE ULTRAVIOLET BANDS OF MAGNESIUM HYDROXYDE AND OXIDE

L. Brewer and S. Trajmar, University of California, Berkeley, U. S. A.

TUESDAY, AUGUST 8

Afternoon Session: Two concurrent sessions will be held.

Session A: CONDENSED STATES: PREPARATION OF PURE AND SINGLE CRYSTAL PRODUCTS AT HIGH TEMPERATURES.

Location: Moyse Hall, McGill University.

Chairman: Prof. B. Chalmers, Cambridge, Massachusetts, U. S. A.

Co–Chairman: Prof. J. Bénard, Paris, France.

2:00 A3–20 Sessional Lecture
CHAUFFAGES ET OPERATIONS A HAUTES TEMPERATURES SANS CONTAMINATION

F. Trombe, Centre National de la Recherche Scientifique, Paris, France.
(To be presented in French)

3:00 A3–21 PREPARATION, STRUCTURE, AND ELECTRICAL PROPERTIES OF THE SINGLE CRYSTALLINE AB_2–TYPE SELENIDES AND TELLURIDES OF NIOBIUM, TANTALUM, MOLYBDENUM AND TUNGSTEN

L.H. Brixner, E.I. du Pont de Nemours and Company, Inc., Wilmington, U.S.A.

3:20 Recess

3:30 A3–22 CRYSTAL GROWTH OF SYNTHETIC FLUOR–PHLOGOPITE

T. Noda, S. Naka, S. Tsujimura and N. Daimon, University of Nagoya, Japan.

3:50 A3–23 EVIDENCE FOR THE EXISTENCE OF Si_2O_3

V.V. Dadape and J.L. Margrave, University of Wisconsin, U.S.A.

4:10 A3–24 EFFECTS OF VARIOUS ADDITIONS ON THE SYNTHESIS OF SILICON NITRIDE AND ON ITS POLYMORPHISM

H. Suzuki and T. Yamauchi, Tokyo Institute of Technology, Tokyo, Japan.

4:30 A3–25 THE SYNTHESIS OF CALCIUM TITANATE SINGLE CRYSTALS BY THE FLAME FUSION TECHNIQUE

L. Merker, National Lead Company, South Amboy, U.S.A.

4:50 A3–25A THE PHYSICO–CHEMICAL APPLICATIONS OF ELECTROMAGNETIC LEVITATION

A.E. Jenkins, University of New South Wales, Kensington, N.S.W. Australia

TUESDAY, AUGUST 8

Afternoon Sessions: See also preceding session.

Session B: THERMODYNAMIC PROPERTIES: VAPOUR PRESSURE DATA AND THE PROPERTIES OF VAPOURS (WITH EMPHASIS ON COMPOUNDS CONTAINING THREE KINDS OF ATOMS) – continued.

Location: Room 204, Engineering Building, McGill University.

Chairman: Prof. K. Schäfer, Heidelberg, Germany.

Co–Chairman: Prof. P.W. Gilles, Lawrence, Kansas, U.S.A.

3:00 A3–26 VAPOUR PRESSURES OF TUNGSTEN OXIDES

P.E. Blackburn, Westinghouse Electric Corporation, Pittsburgh, U.S.A.

3:20 A3–27 CONTRIBUTION TO THE THERMOCHEMISTRY OF CARBON MONOSULPHIDE

H. Schäfer and H. Wiedemeier, University of Münster, Germany.

3:40 A3–28 ON THE STABILITY OF SYMMETRIC DIATOMIC MOLECULES OF THE TRANSITION ELEMENTS

G. Verhaegen, F.E. Stafford, P. Goldfinger and M. Ackerman, Université Libre de Bruxelles, Brussels, Belgium.

4:00 Recess

4:10 A3–29 THE CALCULATION OF THERMODYNAMIC FUNCTIONS OF GASES IN A WIDE TEMPERATURE RANGE

L.V. Gurvich, Academy of Sciences, Moscow, U.S.S.R.

4:30 A3–30 HIGH–TEMPERATURE CHEMISTRY OF THE CHLORIDES OF THE PALLADIUM–GROUP METALS

W.E. Bell, U. Merten, K. Tagami and M.C. Garrison, General Atomic, Division of General Dynamics Corporation, San Diego, U.S.A.

4:50 A3–31 DOUBLE–OVEN EXPERIMENTS WITH LITHIUM HALIDES

J. Berkowitz, H. A. Tasman and W. A. Chupka, Argonne National Laboratory, Argonne, Ill., U. S. A.

WEDNESDAY, AUGUST 9

Afternoon Sessions: Two concurrent sessions will be held.

Session A: CONDENSED STATED: PRODUCTION OF, AND MEASUREMENTS AT HIGH TEMPERATURES, INCLUDING PYROMETRY.

Location: Moyse Hall, McGill University.

Chairman: Prof. L. M. Pidgeon, Toronto, Canada.

Co–Chairman: Dr. D. R. Lovejoy, Ottawa, Canada.

2:00 A3–32 Sessional Lecture
PRODUCTION AND MEASUREMENT OF HIGH TEMPERATURES
J. L. Margrave, University of Wisconsin, Madison, U. S. A.

3:00 A3–33 ADVANCES IN HIGH–TEMPERATURE IMAGING TECHNIQUES

P. E. Glaser and G. P. Ploetz, Arthur D. Little, Inc., Cambridge, U. S. A.

3:20 Recess

3:30 A3–34 MEASUREMENT AND APPLICATION OF HIGH HEAT FLUXES IN A SOLAR FURNACE

T. S. Laszlo, AVCO Research and Advanced Development Division, Wilmington, U. S. A.

3:50 A3–35 MESURE DES TEMPERATURES ET ANALYSE THERMIQUE DES SUBSTANCES TRAITEES AVEC LES FOURS SOLAIRES

M. Foex, Laboratoire de l'Energie Solaire, Mont Louis, Pyrénées Orientales, France.
(To be presented in French)

4:10 A3–36 OXIDE RESISTANCE FURNACE FOR LINEAR THERMAL EXPANSION MEASUREMENTS TO 1900°C

J. F. Bacon, R. D. Veltri and J. Y. Whittier, United Aircraft Corporation Research Laboratories, East Hartford, Conn., U. S. A.

4:30 A3–37 A 2700°C TUNGSTEN RESISTANCE FURNACE

J. F. Bacon, R. D. Veltri and J. Y. Whittier, United Aircraft Corporation Research Laboratories, East Hartford, Conn., U. S. A.

4:50 A3–38 DEVELOPMENT OF A HIGH–TEMPERATURE STAGE MICROSCOPE FOR FUSED SALTS INVESTIGATION UP TO 2300°C

A. Auriol, G. Hauser, and J. C. Wurm, Batelle Memorial Institute, Geneva, Switzerland.
(To be presented in French)

5:10 A3–39 THERMOCOUPLES FOR MEASURING URANIUM DIOXIDE FUEL TEMPERATURES IN–PILE

A. Harvey, Atomic Energy of Canada Limited, Chalk River, Canada.

WEDNESDAY, AUGUST 9

Afternoon Sessions: See also preceding session.

Session B: THERMODYNAMIC PROPERTIES: VAPOUR PRESSURE DATA AND THE PROPERTIES OF VAPOURS (WITH EMPHASIS ON COMPOUNDS CONTAINING THREE KINDS OF ATOMS) – continued.

Location: Room 204, Engineering Building, McGill University.

Chairman: Prof. I. N. Stranski, Berlin–Charlottenburg, Germany.

Co–Chairman: Prof. Leo Brewer, Berkeley, California, U. S. A.

3:00 A3–40 UBER DIE EINWIRKUNG VON WASSERDAMPF AUF OXYDE BEI HOHEREN TEMPERATUREN

O. Glemser and R. von Haeseler, University of Gottingen, Germany. (To be read by G. Gattow)
(To be presented in German)

3:20 A3–41 A TRANSPIRATION STUDY OF GASEOUS SPECIES IN THE BORON–OXYGEN–FLUORINE SYSTEM

D. L. Hildenbrand, L. P. Theard, and A. M. Saul, Aeronutronic Division of Ford Motor Company, Newport Beach, Calif., U. S. A.

3:40 A3–42 THE RATE OF VAPORIZATION OF ALUMINUM OXIDE

J. J. Diamond, R. F. Hampson and R. F. Walker, National Bureau of Standards, Washington, U. S. A.

4:00 Recess

4:10 A3–43 REACTION OF GRAPHITE WITH HYDROGEN: HEAT OF FORMATION OF THE METHYLENE RADICAL

W. A. Chupka, D. J. Meschi and J. Berkowitz, Argonne National Laboratory, Argonne, Ill., U. S. A.

4:30 A3–44 THE MEASUREMENT OF OSMOTIC COEFFICIENTS IN THE TEMPERATURE RANGE 100°C TO 280°C

J. H. de Nordwall and P. J. Jones, Atomic Energy Research Establishment, Harwell, England.

THURSDAY, AUGUST 10

Morning Sessions: Two concurrent sessions will be held.

Session A: CONDENSED STATES: PHASE EQUILIBRIA AND REACTIONS AT HIGH TEMPERATURES.

Location: Moyse Hall, McGill University.

Chairman: Prof. G. Chaudron, Paris, France.

Co–Chairman: Prof. J. White, Sheffield, England.

9:00 A3–45 THE NATURE OF MICROPHASES IN Ce $Cd_{\sim 4.5}$ SOLID SOLUTION

J. F. Lemons and G. R. B. Elliott, University of California, Los Alamos, N. Mex., U. S. A.

9:20 A3–46 STUDIES ON SOME INTERSTITIAL PHASES OF OXYGEN OR NITROGEN AND TITANIUM, ZIRCONIUM, HAFNIUM OR VANADIUM

S. Westman, B. Holmberg, C. Nordmark, T. Dagerhamn and A. Magneli, University of Stockholm, Sweden.

9:40 A3–47 DIAGRAMMES DE PHASES FORMES PAR LE SULFURE D'YTTRIUM AVEC LES SULFURES MS DES ELEMENTS BIVALENTS

J. Flahaut, L. Domange and M. Patrie, University of Paris, France.
(To be presented in French)

10:00 A3–48 SOLID- AND GAS-PHASE REACTIONS IN A TANTALUM CARBIDE INCANDESCENT LIGHT SOURCE

D. P. Cooper, Jr., G. R. Bird and L. Brewer, Polaroid Corporation, Cambridge, U. S. A.

10:20 Recess

10:30 A3–49 OXIDATION KINETICS IN THE MOLYBDENUM–SILICON SYSTEM IN THE 1000° – 2000°C TEMPERATURE RANGE

J. B. Berkowitz-Mattuck, A. D. Little, Inc., Cambridge, U. S. A.

10:50 A3–50 LEGIERUNGEN DES PLATINS MIT UNEDLEN METALLEN EINE NEUE METHODE ZU IHRER DARSTELLUNG

W. Klemm, University of Münster, Germany.
(To be presented in German)

11:10 A3–51 Sessional Lecture

CRYSTAL STRUCTURE AND STABILITY OF REFRACTORY PHASES

H. Nowotny, University of Vienna, Austria.

THURSDAY, AUGUST 10

Morning Session: See also preceding session.

Session B: THERMODYNAMIC PROPERTIES: CALORIMETRY AND HEATS OF REACTION

Location: Room 204, Engineering Building, McGill University.

Chairman: Prof. H. A. Skinner, Manchester, England.

Co–Chairman: Dr. W. A. Chupka, Argonne, Illinois, U. S. A.

9:00 A3–52 THE REACTION OF FERRIC CHLORIDE WITH SODIUM AND POTASSIUM CHLORIDES

C.M. Cook, Jr. and W.E. Dunn, Jr., E.I. du Pont de Nemours and Company, Inc., Wilmington, U.S.A.

9:20 A3–53 CALORIMETRIC HEATS OF MIXING IN BINARY LIQUID SYSTEMS OF SODIUM AND POTASSIUM WITH B–METALS

F.E. Wittig and T. Kleinsteuber, University of Munich, Germany.

9:40 A3–54 THE THERMODYNAMIC PROPERTIES OF COLUMBIUM AND CERIUM OXIDES

J.I. Gerassimov, V.I. Lavrentev, F.A. Kuznetsev and T.N. Rezuhina, Lomonossov University, Moscow, U.S.S.R.

10:00 A3–55 STUDY OF THE THERMODYNAMIC PROPERTIES OF THE SYSTEM IRON–PLATINUM

S. Mundiath and J.I. Gerassimov, Lomonossov University, Moscow, U.S.S.R.

THURSDAY, AUGUST 10

Afternoon Sessions: Two concurrent sessions will be held.

Session A: THERMODYNAMIC PROPERTIES: THERMODYNAMICS OF FUSED SALTS, ESPECIALLY METAL – FUSED SALT SYSTEMS.

Location: Moyse Hall, McGill University.

Chairman: Dr. A.R. vanDyken, U.S.A.E.C., Maryland, U.S.A.

Co–Chairman: Prof. J.I. Gerassimov, Moscow, U.S.S.R.

2:00 A3–56 Sessional Lecture
THERMODYNAMICS AND STRUCTURE OF FUSED SALTS

H. Flood, Norwegian Institute of Technology, Trondheim Norway.

3:00 A3–57 THE NATURE OF CHEMICAL BONDING IN FUSED ALKALI HALIDE – METAL SYSTEMS

K.S. Pitzer, University of California, Berkeley, U.S.A.

3:20 Recess

3:30 A3–58 THE ACTIVITY OF Bi IN MOLTEN Bi–$BiCL_3$ SOLUTIONS

D. Cubicciotti and R. Stringham, Stanford Research Institute, Menlo Park, Calif., U.S.A.

3:50 A3–59 DIAGRAMMATIC REPRESENTATION OF THE THERMODYNAMICS OF METAL – FUSED CHLORIDE SYSTEMS

R. Littlewood, Tube Investments Research Laboratories, Hinxton Hall, Saffron Walden, Essex, England.

4:10 A3–60 AN ELECTROCHEMICAL STUDY OF BISMUTH IN MOLTEN BISMUTH HALIDES

L.E. Topol, S.J. Yosim, and R.A. Osteryoung, Atomics International, Division of North American Aviation, Inc, Canoga Park, Calif., U.S.A.

4:30 A3–61 ACTIVITIES AND VAPOUR PHASE CONSTITUTION IN THE MOLTEN SALT SYSTEM KCl–$MgCl_2$

E.E. Schrier and H.M. Clark, Rensselaer Polytechnic Institute, Troy, U.S.A.

4:50 A3–62 THERMOCHEMISTRY OF PRECIPITATION AND 'LIQUID STRUCTURE' IN MOLTEN NITRATES

J. Jordan and E.J. Billingham, Jr., Pennsylvania State University, U.S.A.

THURSDAY, AUGUST 10

Afternoon Sessions: See also preceding session.

Session B: CONDENSED STATES: PHASE EQUILIBRIA AND REACTIONS AT HIGH TEMPERATURES – continued.

Location: Room 204, Engineering Building, McGill University.

Chairman: Dr. J.S. Anderson, Teddington, Middlesex, England.

Co–Chairman: Prof. J.L. Margrave, Madison, Wisconsin, U.S.A.

3:00 A3–63 PHASES NON–STOECHIMETRIQUES ET THERMODYNAMIQUES

M. Laffitte, Université d'Aix–Marseille, France.
(To be presented in French)

3:20 A3–64 ROLE OF GASEOUS SPECIES AND DEFECT STRUCTURES IN DETERMINING PHASE EQUILIBRIA

R. J. Ackermann, R. J. Thorn and G. H. Winslow, Argonne National Laboratory, Argonne, Ill., U. S. A.

3:40 A3–65 SUR LA FORMATION DE DIFFERENTS ETATS ORDONNES DANS DES PHASES NON–STOECHIOMETRIQUES REFRACTAIRES

R. Collongues, J. Lefèvre, M. Perez y Jorba and F. Queyroux, Centre National de la Recherche Scientifique, Vitry–sur–Seine, France.

4:00 Recess

4:10 A3–66 REACTIONS BETWEEN β-SPODUMENE AND SUBSTANCES ISOSTRUCTURAL WITH SILICA: I: PHASE EQUILIBRIA IN THE SYSTEM β-SPODUMENE–$AlPO_4$

M. Krishna Murthy, Ontaria Research Foundation, Toronto, Canada

4:30 A3–67 REACTIONS IN THE SYSTEM Si–B–O

H. F. Rizzo, M. P. Davis and W. R. Foster, Wright–Patterson Air Force Base, Ohio, U. S. A.

4:50 A3–68 HETEROGENEOUS REACTIONS INVOLVING OXIDATION AND REDUCTION AT HIGH TEMPERATURES AND PRESSURES.

H. P. Eugster, D. R. Wones and A. C. Turnock, Carnegie Institution of Washington, U. S. A.

5:10 A3–69 RECHERCHES SUR LE SYSTEME CaO–MgO–wustite

V. Cirilli and A. Burdese, Politecnico di Torino, Italy. (To be presented in French)

FRIDAY, AUGUST 11

Morning Sessions: Two concurrent sessions will be held.

Session A: THERMODYNAMIC PROPERTIES: THERMODYNAMICS OF FUSED SALTS, ESPECIALLY METAL–FUSED SALT SYSTEMS – continued.

Location: Moyse Hall, McGill University.
Chairman: Prof. H. Flood, Trondheim, Norway.
Co–Chairman: Prof. K. S. Pitzer, Berkeley, California, U. S. A.

9:00 A3–70 Sessional Lecture
THE TEMPERATURE SCALE ABOVE 1000°C

D.R. Lovejoy, National Research Council, Ottawa, Canada

10:00 A3–71 LES PROPRIETES THERMODYNAMIQUES D'EXCES DES MELANGES BINAIRES DES SELS FONDUS

I.G. Murgulescu and S. Sternbeg, l'Institutede Chimie de l'Academie de la R.P. Roumaine, Bucharest, Roumania.

10:20 Recess

10:30 A3–72 CALORIMETRY IN LIQUID THALLIUM NITRATE – ALKALI NITRATE MIXTURES

O.J. Kleppa and L.S. Hersh, University of Chicago, U.S.A.

10:50 A3–73 IMMISCIBILITY OF SODIUM BORATE AND SODIUM HALIDE IN THE MOLTEN STATE

B.L. Dunicz and R.C. Scheidt, U.S. Naval Radiological Defense Laboratory, San Francisco, U.S.A.

11:10 A3–74 DEPOLYMERIZATION OF POLYANIONS BY REACTION OF MOLTEN SALTS WITH THE ATMOSPHERE

C.F. Callis, J.R. van Wazer and J.S. Metcalf, Monsanto Chemical Company, St. Louis, Mo, U.S.A.

11:30 A3–75 SOLUBILITY OF METAL OXIDES IN MOLTEN SODIUM CHLORIDE: THE FIRST TRANSITION SERIES

K.H. Stern, National Bureau of Standards, Wash., U.S.A.

11:50 A3–76 ELEKTROCHEMISCHE UNTERSUCHUNG GESCHMOLZENER BORATE UND PHOSPHATE

Ju. K. Delimarski, W.N. Andreewa, K.M. Bojko, G.D. Nasarenko and T.N. Kapsowa, Institute of Inorganic Chemistry, Kiev, U.S.S.R.
(To be presented in German)

FRIDAY, AUGUST 11

Morning Sessions: See also proceding session.

Session B: CONDENSED STATES: PHASE EQUILIBRIA AND REACTIONS AT HIGH TEMPERATURES – continued.

Location: Room 204, Engineering Building, McGill University.

Chairman: Prof. H. Nowotny, University of Vienna, Austria.

Co–Chairman: Dr. H. F. McMurdie, Washington, D. C., U. S. A.

10:00 A3–77 SYSTEMS REQUIRING ATMOSPHERIC CONTROL: SYSTEMS CONTAINING FeO AND Cr_2O_3

J. White, University of Sheffield, England.

10:20 A3–78 THE SYSTEM IRON OXIDE – MAGANESE OXIDE IN AIR

A. Muan and S. Somiya, The Pennsylvania State Univ., U. S. A.

10:40 A3–79 UBER DAS VERHALTEN VON EISENOXYDEN BEI HOHEREN TEMPERATUREN

H. von Wartenberg, H. H. Weizenkorn, and O. Glemser, University of Gottingen, Germany.
(To be read by G. Gattow)
(To be presented in German)

11:00 Recess

11:10 A3–80 PHASE EQUILIBRIUM AND CRYSTAL CHEMICAL RELATIONSHIPS IN RARE–EARTH SYSTEMS

I. Warshaw and Rustum Roy, National Science Foundation, Washington, U. S. A.

11:30 A3–81 TUNGSTEN – YTTRIUM OXIDES

H. J. Borchardt, E. I. duPont de Nemours and Co., Inc., Wilmington, UlS. A.

11:50 A3–82 OXIDATION CHARACTERISTICS TO 2600°F OF SEVERAL MATERIALS EVALUATED FOR LEADING EDGES OF HYPERSONIC AIRCRAFT

J. M. Nowak, Bell Aerosystems Company, Buffalo, U. S. A.

FRIDAY, AUGUST 11

Afternoon Session: THERMODYNAMIC PROPERTIES: THERMODYNAMICS OF FUSED SALTS, ESPECIALLY METAL – FUSED SALT SYSTEMS – continued.

Location: Moyse Hall, McGill University.

Chairman: Prof. D. M. Newitt, London, England.

Co–Chairman: Prof. G. J. Janz, Troy, N. Y., U. S. A.

2:00 A3–83 THERMODYNAMIC STUDIES ON THE Tl–Bi LIQUID ALLOYS

K. Niwa, N. Shimoji and O. Nikun. Hokkaido University, Sapporo, Japan

2:20 A3–84 ACTIVITY COEFFICIENTS AND ASSOCIATION IN MOLTEN SALT SOLUTIONS

J. Braunstein, M. Blander, R. M. Lindgren and A. R. Alvarez Funes, Oak Ridge National Laboratory, Oak Ridge, Tenn., U. S. A.

2:40 A3–85 THE THERMODYNAMIC EVALUATION OF ACTIVITIES IN MOLTEN MIXTURES OF RECIPROCAL SALT SYSTEMS

K. Grjotheim, C. Krohn and J. M. Toguri, The Technical Institute of Norway, Trondheim, Norway.

3:00 Recess

3:10 A3–86 ACTIVITY COEFFICIENTS IN FUSED SALTS

D. G Hill, S. Woolner and A. R. Alvarez, Duke University, Durham, N. C., U. S. A.

3:30 A3–87 SELF–DIFFUSION IN MOLTEN SALT MIXTURES

R. B. Escue and G. Perkins, Jr., North Texas State College, Denton, Tex., U. S. A.

3:50 A3–88 THE MECHANISM OF SOLUTION OF ALUMINA IN THE ALUMINUM ELECTROLYTE

P. A. Foster, W. B. Frank and L. M. Foster, Aluminum Company of America, New Kensington, Pa., U. S. A.

4:10 A3–89 THE OSCILLOGRAPHIC INVESTIGATION OF THE ELECTROCHEMICAL KINETICS IN FUSED SALTS

A. V. Gorodisky, Academy of Science of the Ukrainian S. S. R., Kiev, U. S. S. R.

4:30 At the conclusion of the proceedings on the Friday afternoon, August 11th, 1961, the work of the Symposium will be terminated by Professor F. D. Rossini, Chairman of the Commission on Chemical Thermodynamics of the International Union of Pure and Applied Chemistry.

ABSTRACTS

of

PAPERS

presented at the

GAS STATE SESSIONS

FLAMES AUGMENTED BY ELECTRIC POWER

Bela Karlovitz

A new type of high temperature flame is described. This flame is formed by the combustion of fuel in a stream of air, or air enriched with oxygen, and by a super–imposed electrical discharge. The electrical power imput into the flame may be comparable to the heat released by the combustion, or it may exceed this heat several fold. Consequently the temperature of the flame may range from ordinary flame temperatures to the temperature of the electric arc.

Various geometrical configurations of electrically augmented flames are shown. The significant physical processes active in the flame are pointed out, and a simple theory of the flame is derived. Characteristics of the flame are calculated. A dimensionless characteristic number is derived which has to be kept below a critical value, for the establishment of the desired flame type. Numerical examples are given and it is shown that the electrical power input density into the flame can reach extraordinary values within the limitations set by this criterion.

The technically important features of the electrically augmented flame are enumerated, and potential applications are indicated.

Experimental flames are described, and results of measurements given.

SOME NEW MEASURING TECHNIQUES IN HIGH TEMPERATURE GASES

P. L. Blackshear and L. M. Fingerson

This paper describes a measuring technique that has been under study in the Combustion Laboratory of the Mechanical Engineering Department of the University of Minnesota for the past two years.

An anemometer consisting of a hollow, internally cooled, non-conductor has on its surface a thin film resistance element. The surface of the film is kept at constant temperature by an appropriately compensating power supply, and the resulting power requirement represents the heat flux from the electrically heated surface to the surroundings and to the internal coolant. This "heat flux probe" can be designed to operate at temperatures up to about 5,000° F. at atmospheric pressures and subsonic velocities. It is, in effect, a constant temperature hot wire anemometer that can be operated in flames. The heat flux to or from the film depends upon the mass flow per unit area approaching the sensing element, the enthalpy difference between the free stream and surface conditions, and the physical properties of the approaching stream. By placing the sensing element upstream of the throat of a sonic orifice, the approach mass flow has been linked to the other two properties of the stream. In the paper, representative measurements made in non-reacting, turbulent mixtures, chemically reacting high temperature gases, and electrically heated dissociated plasmas are described. A sketch of the heat flux probe and orifice is shown in the attached figure.

Discussion of Applications: The film probe has been used to study the effects of laminar transport properties in the mixing of a turbulent jet. In this case, cooling is not required. The uncooled probe is similar to the one shown in the figure, but is reduced in diameter with the removal of the cooling passages. The range of diffusion coefficients considered extend from those of relatively heavy smoke particles to helium in air. The mixing characteristic that is measured is the concentration intensity. This is the root-mean-square concentration fluctuation about the mean divided by the local mean concentration of the jet fluid.

In a jet of fixed geometry, the intensity is found to decrease as the molecular diffusion coefficient increases. In a second study, the heat flux probe is used to detect the flame temperature in a burning globule of flame generated by a spark intermittantly igniting a flowing stream. The measurements were made in an effort to explain anomolously low flame flobule growth rates.

In brief, the flame globules were found to expand at a rate that is lower by about 20% from the rate one would expect if the flame speed were the normal laminar flame speed and the internal density were that expected of an adiabatic reaction. The anomaly could be explained if the temperature were found to be lower than theoretical. This was not the case. The anomaly persists, however, the temperature determinations which agree with steady-state flame temperatures make an interesting demonstration of the aspirating heat flux probe's utility in measuring temperature fluctuations in high temperature gases. The probe used in this application is the one shown in the figure. A third application hinges on the use of the heat flux probe in an electrically heated plasma jet. This work is being done in cooperation with the Heat Transfer Laboratory at the University of Minnesota. For this work, a short mixing section was inserted upstream of the sensing element of the aspirating probe shown in the figure and a metered coolant was injected into the gas stream sampled. Because the scale of the coolant jets in the mixing section is small, the time response of the mixing process is still such that fluctuations in plasma enthalpy in the neighborhood of 1000 cycles/second can be followed. This work is currently in progress and the remarks concerning it describe the present status.

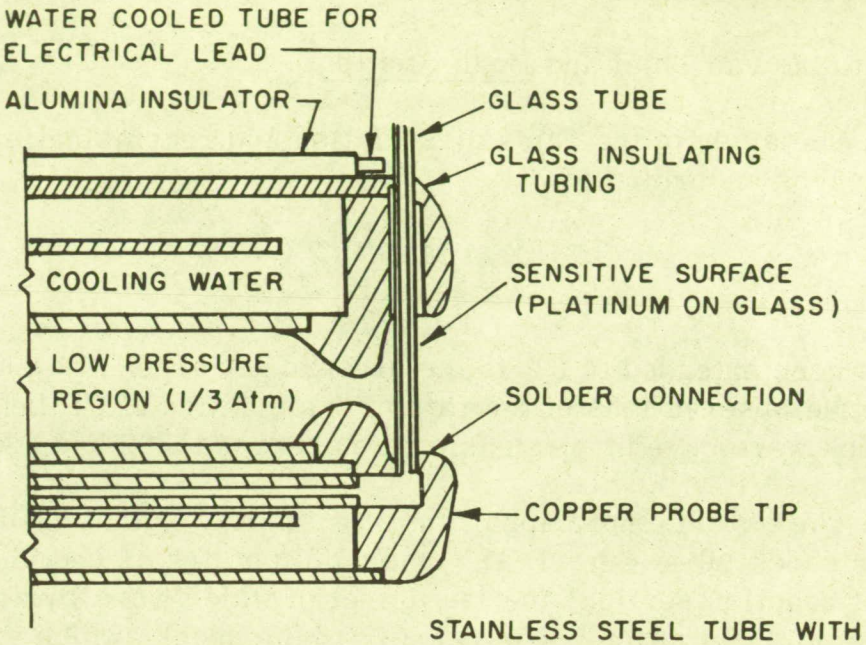

ASPIRATING HEAT FLUX PROBE

SHOCK WAVES IN CHEMICAL KINETICS: THE DISSOCIATION OF MOLECULAR CHLORINE

Matthias van Thiel and Doyle Britton

The study of the rates dissociation and recombination of the halogens according to

$$X_2 + M \underset{k_R}{\overset{k_D}{\rightleftharpoons}} 2X + M \qquad (1)$$

has been extended to Cl_2 in the presence of argon. (1) Spectrophotometric observations of the rate of dissociation of Cl_2 behind a shock wave gave measureable rates between 1800 and 2600° K.

The experimental apparatus was similar to that used previously. The shock tube, 4 in. I. D., had an 8 foot driver section and a 16 foot reaction section, the last 8 feet of which were Pyrex pipe for ease in observation. The velocity of the shock, which was used as athermometer, was measured between two stations 40 cm. apart near the downstream end. The shock itself could be observed at two stations 10 cm. downstream from the timing stations. Spectrophotometric observations were made using monochromatic light (from narrow band pass filters) at several wave lengths. If the light source was left off emission could be observed rather than the absorption of the Cl_2 molecules.

As a preliminary to the kinetic observations the extinction coefficient of Cl_2 as a function of temperature was determined at 385 mμ, from the initial rise in the light absorption at the shock front. The experimental values, with a scatter of about 10% from the smoothed curve, were about 10% lower than the values which would be predicted from low temperature data by the theory of Sulzer and Wieland (2). This according to equation (1) radiation recombination according to

$$2Cl \rightarrow Cl_2 + h\upsilon \qquad (2)$$

took place with emission being sufficiently great at the experimental wave lengths that it was necessary to correct the spectrophotometric trace, which gave the sum of the transmitted light and the emitted light, for the emission in order to calculate the Cl_2 concentration correctly.

This emission was also of interest in its own right and was studied at several wave lengths, 385 mμ, 410 mμ, 460 mμ, and 510mμ. The rate of emission was observed to increase as the atom concentration increased and was consistent with equation (2). If the rate of emission was divided by square of the calculated atom concentration, an effective rate constant for emission could be determined at each experimental temperature at each wave length. From the change in this apparent rate constant with temperature an activation energy for the emission process could be calculated for each wave length. By comparison of these activation energies with the known potential curves for ground state and excited Cl_2 molecules, it appeared likely that the emission was due to Cl_2 molecules in the repulsive part of the ${}^3\pi_{O^+{}_u}$ state, a slightly bonding state arising from the recombination of a ground state ${}^2P_{3/2}$ atom and an excited (881 cm^{-1})${}^2P_{3/2}$ atom. This interpretation is made uncertain by the lack of information available about the ${}^3\pi_{1_u}$ excited molecular state which might also contribute.

After correcting for the emission as discussed above the rate of association was measured in both 5% Cl_2–95% Ar and 10% Cl_2 –90% Ar mixtures. Four series of about ten shocks each were run, two series at each concentration. Generally speaking, the apparent rate constant in the 10% mixtures were higher than in the 5% mixtures; this could reasonably be attributed to greater efficiency of Cl_2 molecules as third bodies for the recombination and dissociation processes. However, the agreement between the two series at 10% were much poorer than the internal agreement of each of the series separately, likewise for the two 5% series. This discrepancy cannot be explained reasonably and greatly increases the uncertainly of the results which are summarized below.

Although the manufacturer indicated that the Cl_2 was 99.5% pure, an infrared examination showed up to 10% CO_2 present. After purification by a crude distillation this was reduced, and the only known impurity in the mixtures was CO_2 in the amount shown in Table 1. For this to account for the discrepancy would require a fantastic efficiency of CO_2 as a third body. Since CO_2 is only about twice as efficient as Ar for the recombination of Br_2 and I_2, it seems unlikely it would be much better here. If the combined 5% results are compared with the combined 10% results, it would appear that the rate constants for argon as a third body are about

Mixture No.	$\%Cl_2$	$\%CO_2$	$\log k = A + B/T$ A	B
2	9.69	0.32	6.066	5140 ± 864
3	10.00	0.12	7.020	2534 ± 761
2 + 3			6.547	3692 ± 787
5	4.94	0.06	7.122	2256 ± 345
6	5.03	0.01	7.447	1198 ± 741
5 + 6			7.082	2206 ± 474

half the apparent values and that the Cl_2 is perhaps 20–60 times more efficient. In view of the known results with Br_2 it is unlikely that the Cl_2 is this much more efficient, and this apparent result must be attributed to the large scatter in the experimental points. The rate constant for the recombination of Cl in the presence of Ar is slightly lower than that which would be extrapolated for the known rate constants for the recombination of Br. This is reasonable since any interaction between an Ar atom and the halogen atom, which would be the first step toward recombination, would be stronger for Br than for Cl.

References

1. See for example, D. Britton, N. Davidson, W. Gehman, and G. Schott, J. Chem. Phys. 25, 804 (1956) for work on I_2, and D. Britton, J. Phys. Chem. 64, 742 (1960) for work on Br_2.

2. P. Sulzer and K. Wieland, Helv. Phys. Acta 25, 653 (1952).

3. H. B. Palmer, J. Chem. Phys. 26, 648 (1957).

FAST REACTIONS IN ADIABATICALLY COMPRESSED GASES

W. Jost, A. Martinengo, and H. Gg. Wagner

The method of rapid adiabatic compression has been further developed for the investigation of fast gas reactions.

In order to exclude appreciable reaction occurring during the compression phase, the piston speed must be kept sufficiently high, especially during the last phase of compression. This requires a combination of a high piston speed and a very sudden stop, involving extreme strain of the moving parts.

It further was necessary to work without lubricants, if traces of impurities in the gas phase were to be kept out.

The compression apparatus thus developed consists of a light-metal piston with teflon rings, appropriately shaped and mounted, running in a steel cylinder. The compression piston was connected to a second piston which moved in a wider cylinder, and was driven by compressed air. At the end of its path the momentum of the moving parts was transferred to a second mass, supported by soft springs, (machine I) or by the air (machine II), and the piston was stopped over a distance of the order of 0.1 mm.

Compression and stopping equipment on the one hand, reaction cylinder and pressure recording device (capacity pick-up and oscilloscope) on the other hand were supported by two different foundations, separated by vibration absorbing material. Not even traces of the vibrations in the first equipment could be detected in the pressure records.

Reactions times between 10^{-3} and 10^{-1} secs. were accessible (if corrections were applied for reaction during compression, or if the second phase of two-stage reactions was of interest, times of 10^{-4} secs. were accessible). Temperatures at the end of compression could be varied between 300 and 1000° K, pressures between 0.5 and 40 atm., with piston speeds up to 20 m/sec. It was not reasonable to further increase the piston speed because the deceleration would have required longer distances. Pressure records with air showed a sharp kink between the compression phase and the final, constant-pressure phase, without recognizable transition.

In addition to pressure records spectroscopic investigations by means of glass or quartz windows in the reaction chamber were possible. Finally, a special device was built, in order to release the gas mixtures after measured time intervals. The samples, thus taken, could be analyzed by infrared spectroscopy or gas chromatography. Conventional chemical analysis should also be possible.

A number of hydrocarbons in mixture with air have been investigated which react after a certain induction time. Depending on conditions (temperature, pressure, composition) they may exhibit a one or two-stage ignition reaction. In the latter case one can define individual induction times t_1 and t_2 for each stage of the reaction and a total delay time (t_t) as the sum of t_1 and t_2. The first induction period increases with increasing fuel concentration. t_2 increases with decreasing fuel concentration. The total delay is determined by t_1, on the fuel rich side and by t_2 for lean mixtures, its minimum lies on the lean side for the investigated n-paraffins and near the stochiometric value for iso-octane. Increase in oxygen content (above that of the air) or addition of tetra-ethyl-lead do not affect the first reaction stage. Addition of small amounts of peroxides (10^{-3} Vol.-%) shortens the first induction period without observable influence on t_2. Addition of acetaldehyde has - less pronounced - the inverse effect. Iso-paraffins exhibit quite similar results.

These observations have been extended to shorter induction times by shock-wave measurements which are well compatible with the results from adiabatic compression experiments. Though shock-wave experiments give less detailed information it is possible by combination of both methods to observe one type of reaction over a temperature range of about 1000° K.

It was possible to measure reaction rates in hydrogen-air mixtures in machine II, described above, uninfluenced by wall effects. Wall temperatures are low (not above 150°C), diffusion depths during the induction times under consideration not above the order of 1 mm.

The induction periods are well reproducible in the region of 800 - 900° K and pressures between 1 and 25 at. For a constant temperature the observed induction times increase very rapidly with decreasing pressure ($t \sim 1/p$). This permits one to define a "Third Explosion Limit" within this region by extrapolating these values to infinite induction times.

At lower pressures (0.5 – 1 at) and temperatures of about 900° K, this "limit" agrees sufficiently well with the "Second Limit" investigated by other authors. Further experiments are being performed to investigate the influence of water–vapour, oxygen content (above that of air) and addition of H_2O_2 under conditions of adiabatic compression.

In preliminary experiments the behaviour of CS_2 – mixtures at temperatures of about 550° K and 10 at was observed. The results are similar to those obtained in static experiments at low pressure. The induction times decrease very rapidly with decreasing concentration of CS_2. Even at very low CS_2 – concentrations in air (1 Vol.–%) a further decrease of fuel concentration tends to shorten the induction period. The temperature dependence of the reaction rate seems to be more pronounced in very lean than in rich mixtures.

IONISATION VON HF UND NH_3 IN KOMPRIMIERTEM WASSERDAMPF BIS 750° C.

E. U. Franck, K. H. Dudziak, and G. Coulon

Wird Wasserdampf bei überkritischen Temperaturen auf eine Dichte von mehr als etwa o, 2 g/cm ^{3} komprimiert, so wirkt er als elektrolytisches Lösungsmittel. Messungen der elektro–lytischen Leitfähigkeit haben gezeigt, daβ NaCl(1), KCl (2, 3) und ebenso die übrigen Alkalichloride (4) in dem komprimierten Dampf teilweise der völlig in Ionen dissozieren konnen. Gleiches gilt auch für NaF (4) KOH (5) und HCl (5). In Lösungen von CO_2 und SiO_2 in Wasser bei 6oo° C und Drucken bis zu 1500 Bar lieβ sich keine elektrolytische Leitfahigkeit nachweisen, obgleich Konzentrationen des Gelösten bis zu mehreren Molprozent gewahlt wurden.

Aus den gemessenen Leitfähigkeitswerten wurden Dissoziations–konstanten K der gelosten Verbindungen in überkritischem Wasser errechnet. Fur KCl ergibt sich z. B. bei 600° C und Wasserdichten von 0, 3 bzw. 0, 7 g/cm^3 K=8, 3 · 10^{-6} bzw. 4, 3 . 10^{-3} mol/l. Bei konstanter Dichte ist die Temperaturabhängigkeit der Dissoziations konstanten negativ. Die übrigen Alkalichloride und auch NaF und KOH verhalten sich ähnlich. Die K–Werte fur HCl zwischen 400 und 750° C sind um ein bis zwei Größenordnungen kleiner.

Auf Grund des Dissoziationsverhaltens des HCl und einiger zusatzlicher Annahmen wurde die Berechnung der Dissoziationskonstante reinen Wassers für Temperaturen zwischen 300 und 800° C unternommen. Es ergibt sich (5)

$$\log K(H_2O) = -\frac{20500}{4,57T} + 9,0\log\rho - 4,4$$

Darin ist ρ die Wasserdichte in g/cm^3. Bei konstanter Dichte $\rho = 1$ erhält man danach für die mittlere Dissoziationsenergie bzw. Dissoziationsentropie des Wassers in diesem Temperaturbereich $\Delta E = 20,5$ kcal/mol und $\Delta S = 20$ cal/grad. mol. Dieser Gleichung entsprechend sollte die mit der Dissoziation verbundene Volumänderung bei konstanter Dichte von 1 g/cm^3 mit steigender Temperatur abnehmen von $-23,4$ cm^3/mol bei 25° C (Owen und Brinkley (6)) auf $-13,5$ und $-9,7$ cm^3/mol bei 400 und 800° C (ca. 7000 und ca. 14000 Bar). Diese Abschätzung von K (H_2O) wird im wesentlichen durch Stosswellenmessungen von David und Hamann (7) bestätigt. Im Gegensatz zum Verhalten aller bisher untersuchten in überkritischem Wasser gelösten Verbindungen nimmt die Dissoziationskonstante des Wassers selbst ausser mit der Dichte auch mit ansteigender Temperatur zu. Das bedeutet, dass hydrolytische Reaktionen bei hohen Temperaturen stark begünstigt werden.

Um solche Hydrolysen zu untersuchen, ist es wünschenswert, die Ionen-Dissoziation mässig starker Elektrolyte bei hohen Temperaturen kennenzulernen. Deshalb wurde die Leitfähigkeit von HF (4) und von NH^3 (8) in Wasser bis zu 750° C und maximal 2500 Bar gemessen. Das NH_3 ist das erste untersuchte Beispiel einer Anhydrobase in diesem Bereich. Ausserdem lassen sich überkritische Ammoniak-Wasser-Lösungen in grösseren Konzentrationen herstellen, ohne dass Phasentrennung oder übermässige Korrosion zu befürchten ist. Heisse $HF-H_2O$-Lösungen sind zudem für manche pneumatolytischen mineralbildende Prozesse von Bedeutung.

Das Prinzip der Messanordnung wurde bereits beschrieben. Ein zylinderförmiger, starkwandiger Autoklav aus einer hochwarmfesten Co-Cr-Ni-Fe-Legierung* diente als Messgefäss.

---

* ATS 112 der deutschen Edelstahlerke, Krefeld

Seine Pt–Ir–Auskleidung ist die eine Elektrode. Die Gegenelektrode ist an einem Pt–Ir–Schaft zentrisch eingeführt und durch ein langes, enges Rohr aus gesintertem Korund isoliert. Die Messlösung wird entweder im Autolaven durch Aufheizen auf dem gewünschten Druck gebracht oder mittels einer Pumpe aus rostfreiem Stahl in dem erhitzten Messautoklaven gepresst. Die Korrosion der HF–Lösungen an den nicht mit Platin ausgekleideten Teilen der Apparatur war grösser als bei den früher untersuchten Salz– und HCl–Löungen. Der Molenbruch des HF konnte aber nicht über $1,8 \cdot 10^{-4}$ gesteigert werden. Die Leitfähigkeitswerte waren in diesem Fall nur auf 5–10% genau bestimmbar. Die Korrosion der NH_3 – Lösungen war vergleichweise unerheblich. Daher konnte in einigen Bereichen noch mit einem NH_3 Molenbruch von $1,8 \cdot 10^{-2}$ (entsprechend 1 m–Lösungen unter Normalbedingungen) gearbeitet werden. Die HF–Messungen wurden durch Messungen mit NaF– und NaCl–Losungen untersucht, um Aufschlusse uber die Beweglichkeit der F^- – bzw. NH_4^+ – Ionen zu bekommen.

Zur Auswertung der Messungen, d.h. zur Ermittlung von Dissoziationsgraden und Dissoziationskonstanten ist die Kenntnis der Aequivalentleitfähigkeit bei unendlicher Verdunnung, nötig.

Es ist nicht möglich, die überkritischen Lösungen bis zur volligen Ionisierung des HF und NH_3 zu verdünnen. Daher konnten die Λ_0–Werte zunächst nur berechnet werden unter Verwendung der früher ermittelten (5) Ionenbewlichkeiten für hydratisierte H^+ und OH^- Ionen im komprimierten Dampf. Die Beweglichkeit der F^- – bzw. NH_4^+ Ionen wurden ähnlich denen der Cl^- und K^+ Ionen eingesetzt. Dies scheint hier zunächst erlaubt, da die fruheren Untersuchungen (2,4) gezeigt haben, dass die Bewglichkeiten der einwertigen Ionen in der überkritischen Phase allgemein sehr ahnlich werden.

In den obengenannten früheren Arbeiten waren abgeschätzte Viskositätswerte des Wassers ausführlich benutz worden. Messungen der Wasserviskosität bis zu 750° C und Drucken von 2500 Bar standen bisher nicht zur Verfügung. Es wurde auf verschiedene Weise versucht, Enskog – Ansätze (9) für die Dichteabhängigkeit der Viskosität und Diffusion zur Darstellung der Viskosität des Wassers in diesem Bereich zu verwenden.

Es zeigte sich jedoch, dass das den Enskog–Gleichungen zugrunde liegende Modell starrer Kugeln nicht realistisch genug ist. Arbeiten zur Messung der Viskosität des Wassers bei hohen Dichten sind in Angriff genommen.

Bei der weiteren Auswertung wurden die interionischen Wechselwirkungen wie früher (3) nach dem Verfahren von Shedlovsky berücksichtigt.

Tabelle

Dissoziationskonstanten K des HF in überkritischem Wasser der Dichte ρ (g/cm^3).

Zum Vergleich K–Werte fur KCl und HCl.

(K=a(Kation)· a(Anion)/a(Molekül))

	t°C	$\rho = 0,3$	$\rho = 0,5$	$\rho = 0,7$
HF	450	$3,5 \times 10^{-9}$	$2,3 \times 10^{-7}$	$7,0 \times 10^{-6}$
	550	$1,9 \times 10^{-9}$	$3,7 \times 10^{-8}$	$1,9 \times 10^{-6}$
	650	$8,6 \times 10^{-10}$	$2,1 \times 10^{-8}$	$1,1 \times 10^{-6}$
HCl	550	$2,3 \times 10^{-6}$	$4,6 \times 10^{-5}$	$2,0 \times 10^{-3}$
KCl	550	$4,8 \times 10^{-6}$	$2,1 \times 10^{-3}$	$8,8 \times 10^{-2}$

Die Tabelle zeigt Dissozationskonstanten des HF im überkritischen Wasser; zum Vergleich darunter Werte für HCl und KCl. Die Konstanten für HF sind etwa 2 Grössenanordnungen niedriger als die des HCl. Aus der Temperaturabhängigkeit der K–Werte ergibt sich eine mittlere Dissoziationsenergie $\Delta E = -12$Kcal/mol. Das Diagramm zeigt Messwerte der Aequivalentleitfähigkeit von überkritischen NH_3–Wasser–Lösungen. Die Temperaturabhängigkeit bei konstanter Dichte ist wesentlich geringer als bei den früher untersuchten Verbindungen. Oberhalb von 500° C scheint die Temperaturabhängigkeit sogar positiv zu sein. Dieser Befund muss mit einer veränderten Messanordnung überprüft werden. Vorläufige Berechnungen ergeben formal für die Ionisationskonstante der Reaktion $NH_3 + H_2O \; NH_4^+ + OH^-$ z. B. bei 640° C und Gesamtdichten von 0,35 und 0,59 g/cm^3 (entsprechend 1050 und 2220 Bar) $K = 3,8 \times 10^{-9}$ und $1,6 \times 10^{-7}$ mol/l. Bei 450° C und Gesamtdichten von 0,58 und 0,68 g/cm^3 (entsprechend 830 und 1320 Bar) erhält man $9,2 \times 10^{-8}$ und $5,1 \times 10^{-7}$ mol/l.

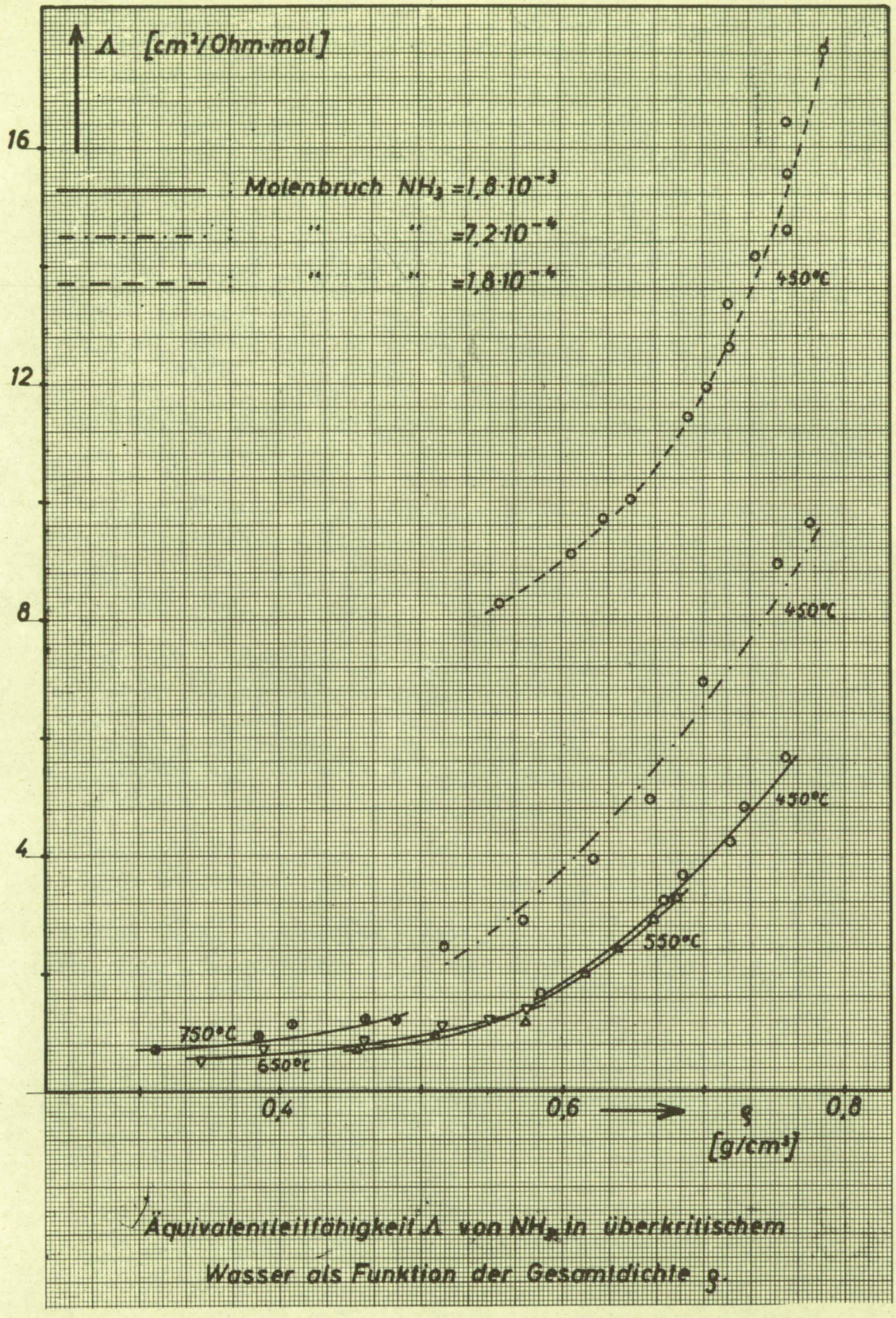

Äquivalentleitfähigkeit Λ von NH_3 in überkritischem Wasser als Funktion der Gesamtdichte ρ.

Literaturverzeichnis

1. L. K. Fogo, S. W. Benson, C. S. Copeland
J. Chem.Physics, 22, 200, 212 (1954)

2. E. U. Franck
Zeitschrift für Physikalische Chemie, N. F. 8, 92, (1956)

3. E. U. Franck
Zeitschrift für Physikalische Chemie, N. F. 8, 107 (1956)

4. K. H. Dudziak
"Elektrolytische Dissoziation von Alkalichloriden und Fluorwasserstoff in überkritischem Wasserdampf".
Diplomarbeit, Göttingen, 1959.

5. E. U. Franck,
Zeitschrift für Physikalische Chmie, N. F. 8, 192 (1956)

6. R. Owen, S. Brinkley
Chem. Rev. 29, 461, (1941)

7. David, H. G., S. D. Hamann
Trans. Far. Soc. 55, 72 (1959)

8. G. Coulon
"Elektrolytische Leitfähigkeit von Ammoniak in überkritischem Wasserdampf".

9. Vgl. I. O. Hirschfelder, C. F. Curtis u. R. B. Bird
"Molecular Theory of Gases and Liquids"
New York, 1954, Wiley and Sons.

SELF–DIFFUSION COEFFICIENTS OF CARBON DIOXIDE AT 1250 – 1700° K

G. Ember, J. R. Ferron, and K. Wohl

This paper presents the first results of a program involving measurement of transport properties of gases at flame temperatures. Gas diffusivities have heretofore been measured at temperatures above 1000° C in only one instance (1). The present measurements of self–diffusivity of carbon dioxide at 1250 – 1700° K, make it possible for the first time to test carefully the accuracy of theoretical methods for estimating diffusivities at high temperatures, conditions under which theory should begin to lack validity.

A flow method, similar in principle to that used at lower temperatures by Walker and Westenberg (2) and previously, for turbulent diffusivity measurements by Woertz and Sherwood (3), was employed in the experiments. Tracer gas, consisting of radioactive $C^{14}O_2$ mixed with ordinary CO_2, was injected continuously into a laminar stream of essentially pure carbon dioxide. The spreading by diffusion of the tracer was observable by measuring the decay of radioactivity axially from the point of injection. The slope of a plot of reciprocal $C^{14}O_2$ concentration versus distance from the point of injection yielded the diffusion coefficient. Temperature and flow rates were held constant during experiments.

The hot, laminar stream of CO_2 was provided by the combustion products from a flat carbon monoxide – oxygen flame, stabilized on a water–cooled, porous bronze plug. This method of heating the gases allows one to work at higher temperatures using ordinary construction materials than is possible when, using the flow method, one heats the gas stream by external means and then makes its velocity profile uniform with suitable devices. The method also permits one to use higher temperatures than would be readily feasible with a Loschmidt cell, where heat must be transferred to the diffusing gases through the walls of the cell and where it is necessary to maintain isothermal conditions over a large region.

---

* This research was sponsored by Project Squid, which is supported by the US Office of Naval Research under contract Nonr 1858 (25) NR – 098 – 038

The hot stream from the flame rose through a cylindrical alumina chamber with electrically–heated walls which ensured that the region of measurement was isothermal. Gas samples were taken continously through a platinum–rhodium capillary tube, cooled and then passed through a sandwich–type radiation detector cell operated in the proportional range. The detector signal was observed on a combined ratemeter–scaler. Rather elaborate precautions were taken to dilute the gases to a safe radiation level before discharging them to the atmosphere. Temperatures were measured with three thermocouples, two of them in fixed positions within the diffusion chamber and the third attached to the sampling probe and free to be moved with the probe by a three–dimensional positioning device.

Performance of the apparatus was tested by measuring self–diffusivity of CO_2 at room temperature (without flame) and at high temperatures by measuring binary diffusivities in the $CO_2 - N_2$ system. Good agreement with literature data was obtained in both cases.

Self–diffusivity data for the high–temperature range are shown in the diagram. The points marked A represent experimental results. The lower curve (C) shows diffusivities calculated by the Chapman – Enskog theory using a Lennard–Jones 12–6 potential. The force constants used are temperature–dependent values obtained form viscosity data (4). Curve C is about 40 % lower than the points of A. The middle curve (B) represents the same calculated diffusivities but corrected now for the non–spherical character of the CO_2 molecule after the theory of Curtiss and Co–workers (5). (We have assumed that Curtiss' theory, which actually applies to a rigid spherocylinder, can be used in the first approximation for a Lennard–Jones molecule with a somewhat cylindrical shape.)

The quite striking improvement of the agreement between calculated and observed values (to within 12%) which one obtains after taking non–sphericity into account illustrates the relatively large effect of non–sphercicity on diffusivity compared to that on viscosity. It appears, however, that further improvement of the calculated diffusivities might be possible with force constants determined from diffusivities as well as from viscosities.

The method of Buckingham (6) was used first to obtain a single set of force constants (independent of temperature) from viscosity data (194 – 1500° K) and diffusivity data (300 – 1700° K),

the respective non-sphericity effects being ignored. These force constants gave calculated diffusivities within 1.5% of the observed values, but the discrepancy for viscosity was about 30%.

Following a theoretically sounder procedure for evaluating the force constants, the experimental data were first corrected for non-sphericity using the factors of Curtiss. The numbers thus obtained would be expected to be better represented by a Lennard-Jones potential than the original data. Buckingham's method was then applied, yielding a single set of parameters for the temperature range 200-1700° K (σ = 3.55 Angstroms, ϵ/k = 355° K). These parameters gave calculated diffusivities and viscosities within 15% of the experimental values over the entire temperature range. In order to obtain better agreement than this, one would need a non-sphericity correction which is more accurate for the CO_2 molecule. This would probably by temperature-dependent.

One can conclude that, for carbon dioxide at least, non-sphericity should be accounted for in calculating diffusivities at high temperatures but perhaps not in calculating viscosities. Such a correction makes it possible to eliminate or at least significantly decrease deviations which otherwise would require temperature-dependent force constants and/or different sets of parameters for calculating different transport properties.

Notes: (1) Klibanov, Kamenetsky, and Pomerantsev, J. Tech. Phys., USSR, 12, 14 (1942)

(2) Walker and Westenberg, J. Chem. Phys. 32, 436 (1960); 29, 1139, 1147 (1958)

(3) Woertz and Sherwood, Ind. Eng. Chem., 31, 1034 (1939)

(4) Hirschfelder, Curtiss, and Bird, Molecular Theory of Liquids and Gases, John Wiley and Sons, New York; 1954.

(5) C. F. Curtiss, et al, J. Chem. Phys. 27, 1643 (1959); 26, 1257 (1958); 25, 1619 (1957); 24, 225 (1956)

(6) R. A. Buckingham, Proc. Roy. Soc., 168A, 264 (1938)

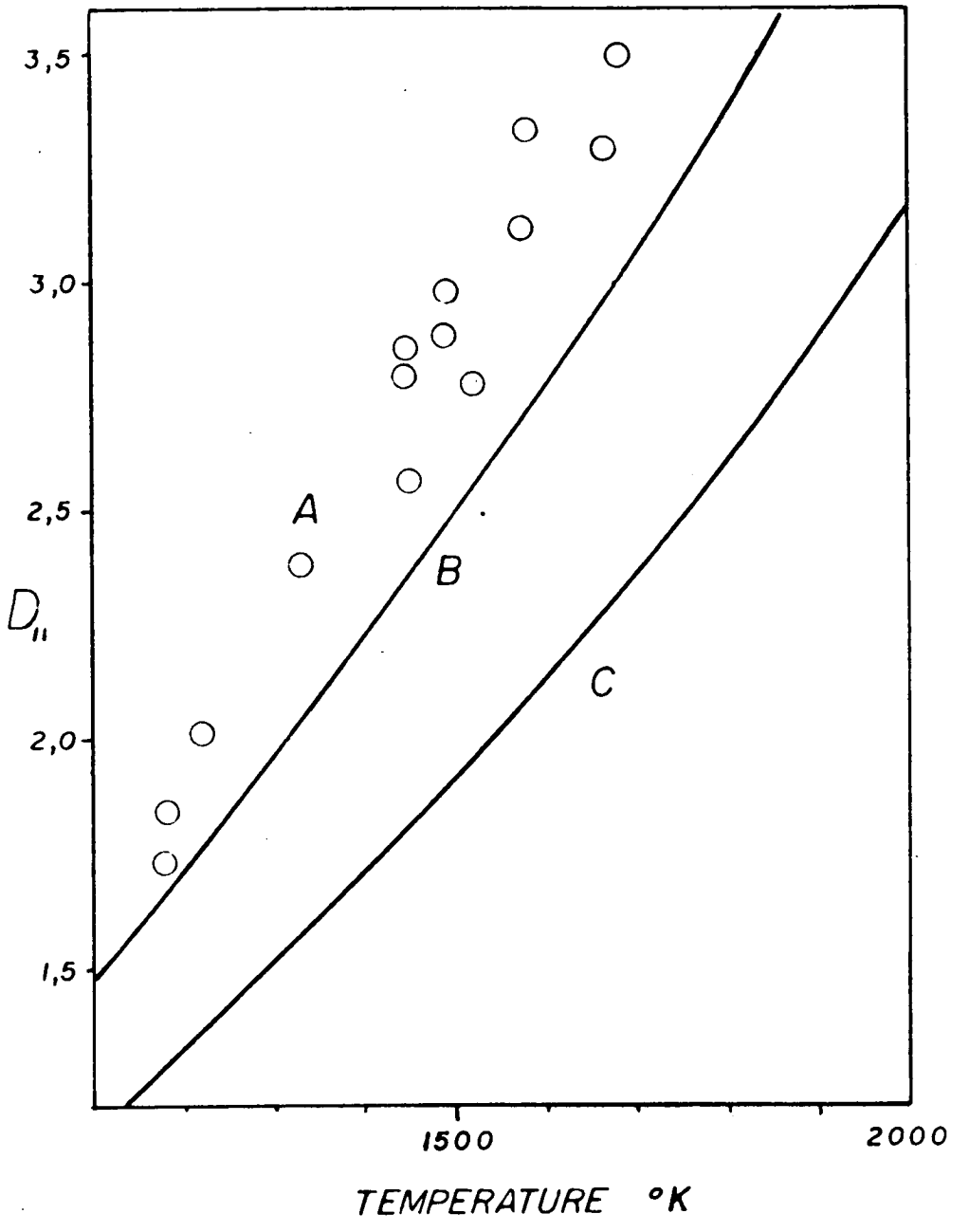

Diagram for "Self-Diffusion Coefficients of Carbon Dioxide at 1250 - 1700 °K" , by G. Ember, J.R. Ferron and K. Wohl.

THE CARBON–HYDROGEN SYSTEM AT TEMPERATURES ABOVE 2500° C.*

John M. Iwasyk and R. F. Baddour

Introduction: In the last five years activity in high temperature chemistry has increased markedly as evidenced by the twofold increase in publications, but no commercial high temperature (i.e. above 2300° C) gas phase process exists in the United States today (1, 2). There are several reasons for this situation, but the most basic reason is the lack of fundamental high temperature data and techniques for obtaining this data.

The over–all objective of this thesis was to obtain a fundamental picture of the chemistry of the carbon–hydrogen system above 2500° C. by solving the following problems:

A. The design and fabrication of a high temperature reactor which could attain and sustain temperatures of 8000° K. for periods up to ten minutes.

B. A detailed chemical analysis of species in the product stream at various reactor conditions.

C. The development of expressions which would characterize the reactor and predict the product composition for various operating conditions.

Procedure: Figure 1 shows the details of a high intensity carbon arc reactor which successfully reacted carbon vapor and hydrogen. The reaction products were sampled with a water–cooled probe and analyzed by means of mass spectrography and gas chromatography. The effects of arc power input, gas flow rate, probe diameter, probe position, diluent content in the feed gas, and reactant ratio (H_2/C) upon reaction gas composition were studied.

---

* Ph. D. Thesis, Chemical Engineering Dept., Massachusetts Institute of Technology

Results and Conclusions: Previous literature reports have failed to consider both the effect of carbon vapor and the existence of C_2H upon the thermodynamic equilibrium composition for the C + H_2 system above 2500° C. (3, 4). Figure 2 is the thermodynamic diagram which takes these two effects into account between 2500° K. and 4500° K. at 1 atm. Figure 2 also shows that the maximum concentration of hydrocarbon species occurs near the sublimation point, and the important species in the hot reaction gas are C_2H_2, C_2H_1, H, H_2, C_S, C_1, C_2, and C_3.

If upon quenching, the following reactions are assumed to occur in the quench probe:

$$C_2H + H \longrightarrow C_2H_2 \qquad (1)$$

$$2H \longrightarrow H_2 \qquad (2)$$

then Figure 3 shows the acetylene content in the quenched gas as a function of the temperature of the hot equilibrium gas mixture entering the quench probe. It is noted that acetylene content reaches a maximum of 34% at 1 atm. and a decrease in pressure increases acetylene content in the quenched gas below the sublimation temperature of 3750° K. Above the sublimation temperature an increase in pressure will raise acetylene content in the quenched gas.

Figure 4 represents the case where reaction (1) is assumed not to occur or that C_2H is not present in the hot equilibrium mixture. Acetylene content in the quenched gas reaches a maximum of 14% and a decrease in pressure reduces acetylene content below the sublimation temperature at 1 atm.

Experimental evidence for the existence of C_2H and reaction (1) is shown in Figures 5 and 6. In figure 5 acetylene concentrations in the quenched gas are greater than 14% and in Figure 6 an increase in diluent content (i.e. corresponds to a decrease in pressure) increases the acetylene content. Figure 5 also shows that low H_2/C ratio and high arc power inputs give the highest C_2H_2 contents, which is in accordance with theoretical considerations. If perfect mixing, equilibrium conditions, and perfect quench are assumed to hold for the hot reaction gas entering the probe, then the 18.6% acetylene concentration sample actually entered the probe at 3470°K.

Sample probe inner diameter and inlet position played an important part in quenched gas composition. Figure 7 shows the effect of probe diameter on acetylene content in the quenched gas. It is noted that the smaller probes reduced acetylene content for a given reactor condition which suggests that the probe walls may increase the rate of reaction (2) with respect to reaction (1) which would decrease C_2H_2 content. Figure 8 shows the drop in acetylene content with an increase in sampling distance from the anode face. This is due to gas mixtures entering the probe at lower temperatures.

Figures 9 and 10 present evidence for the cause of C_2H_2 which should not appear in the quenched gas if a thermodynamic equilibrium mixture is sampled and perfectly quenched. Figure 9 shows that position has a large effect on ethylene content in the quenched product gas. This suggests that the cathode walls promote the hydrogenation of acetylene.

In all cases studied experimentally, acetylene was the major reaction product. Ethylene in amounts up to 1 1/4 vol. per cent was present in certain cases, along with traces of diacetylene, vinyl-acetylene, methane, and benzene.

Literature Cited

(1) Margrave, J. L., "Annual Review of Physical Chemistry", 10, 457 (1959)

(2) Hiester, N., "High Temperature Technology", Symposium at Alismar, California, October, 1959, sponsored by Stanford Research Institute.

(3) Plooster, M. N. and Reed, T. B., Journal of Chem. Phys. 31, pp. 66–72, July, 1959.

(4) Kroepelin, H. and Neuman, K. K., "ASME Symposium Proceedings on Thermophysical Properties", McGraw–Hill Inc., New York (1959)

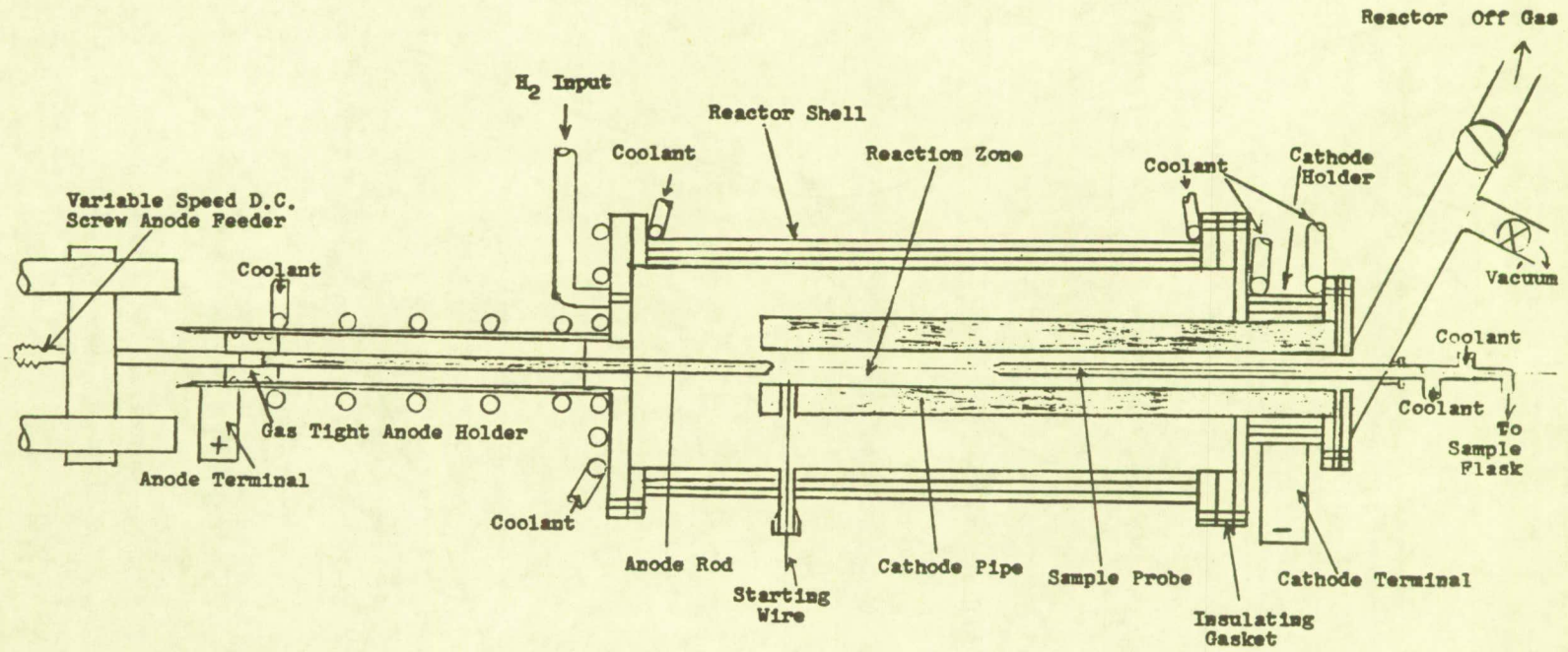

Figure 1 Series XXI High Intensity Arc Reactor, Scale ½" = 1"

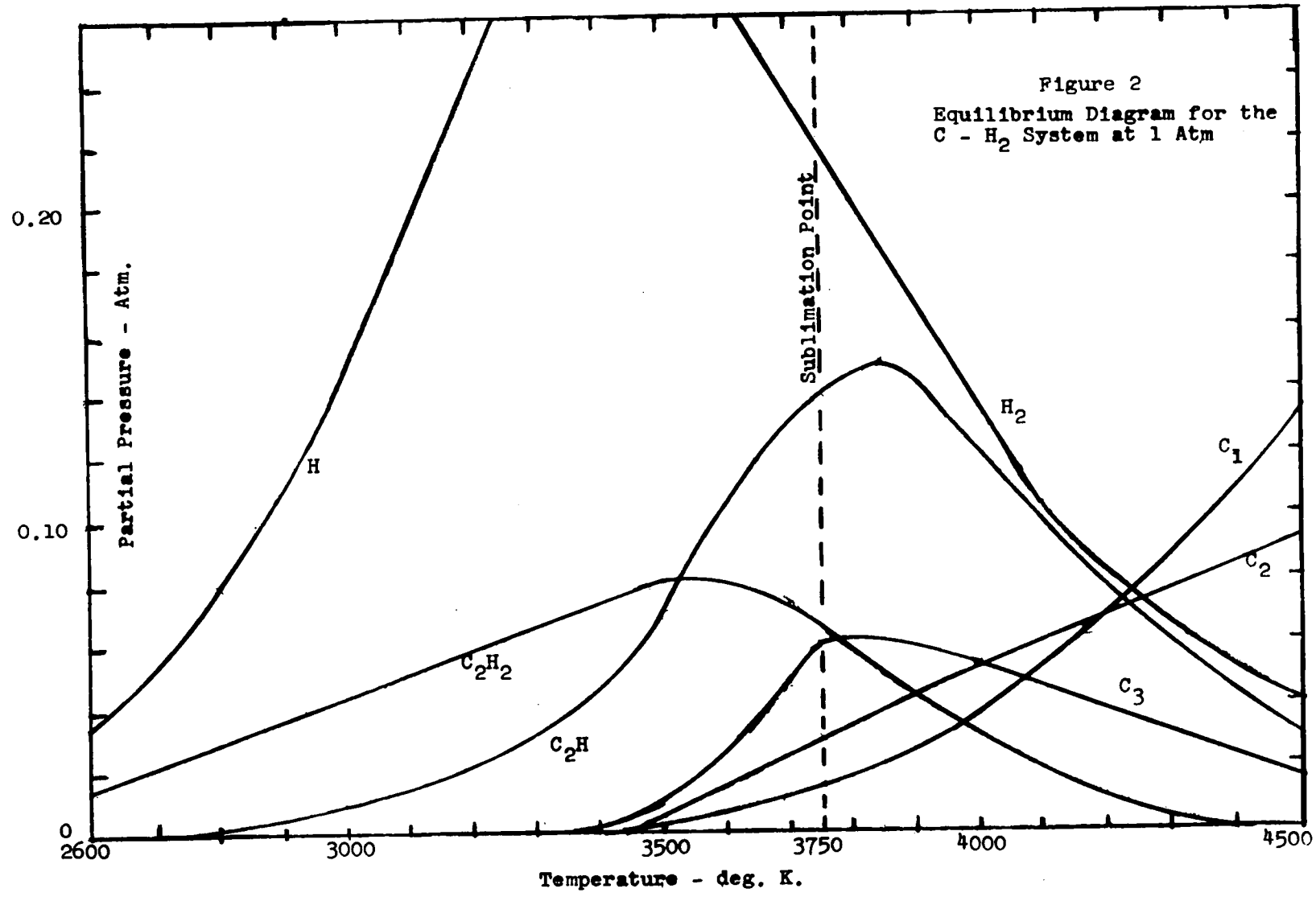
Figure 2
Equilibrium Diagram for the
C - H_2 System at 1 Atm
Sublimation Point
Partial Pressure - Atm.
0.20
0.10
0
H
H_2
C_1
C_2
C_2H_2
C_2H
C_3
2600
3000
3500
3750
4000
4500
Temperature - deg. K.

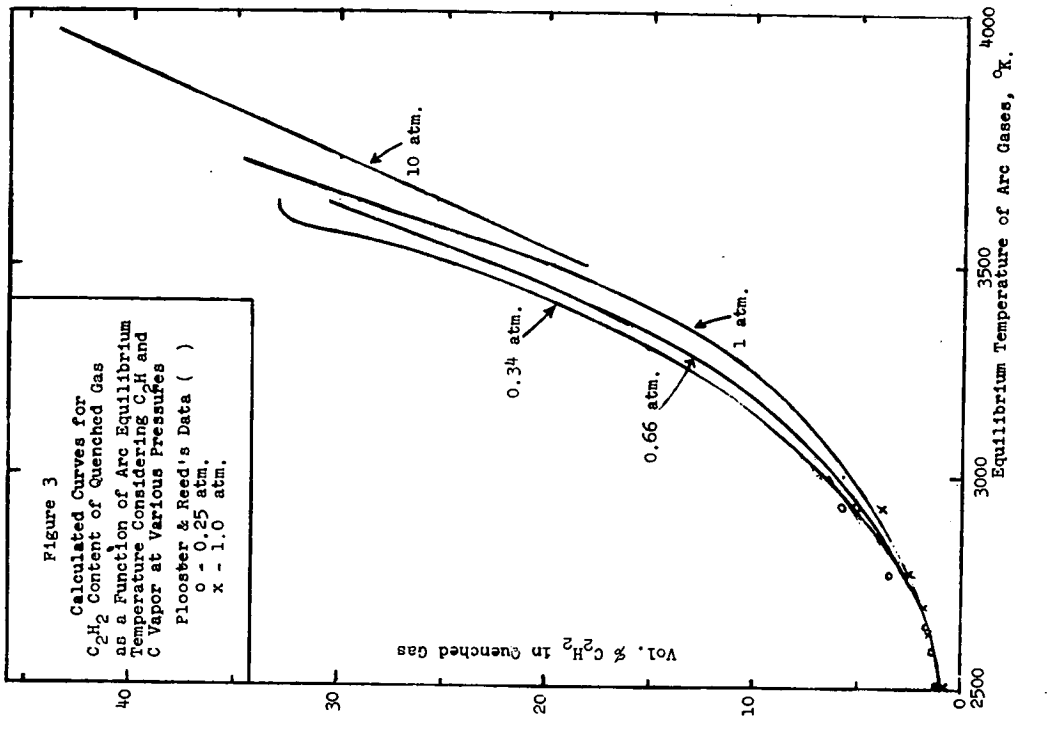
Figure 3
Calculated Curves for
C_2H_2 Content of Quenched Gas
as a Function of Arc Equilibrium
Temperature Considering C,H and
C Vapor at Various Pressures
Plooster & Reed's Data ( )
o - 0.25 atm.
x - 1.0 atm.
Vol. % C_2H_2 in Quenched Gas
Equilibrium Temperature of Arc Gases, °K.
10 atm.
0.34 atm.
1 atm.
0.66 atm.

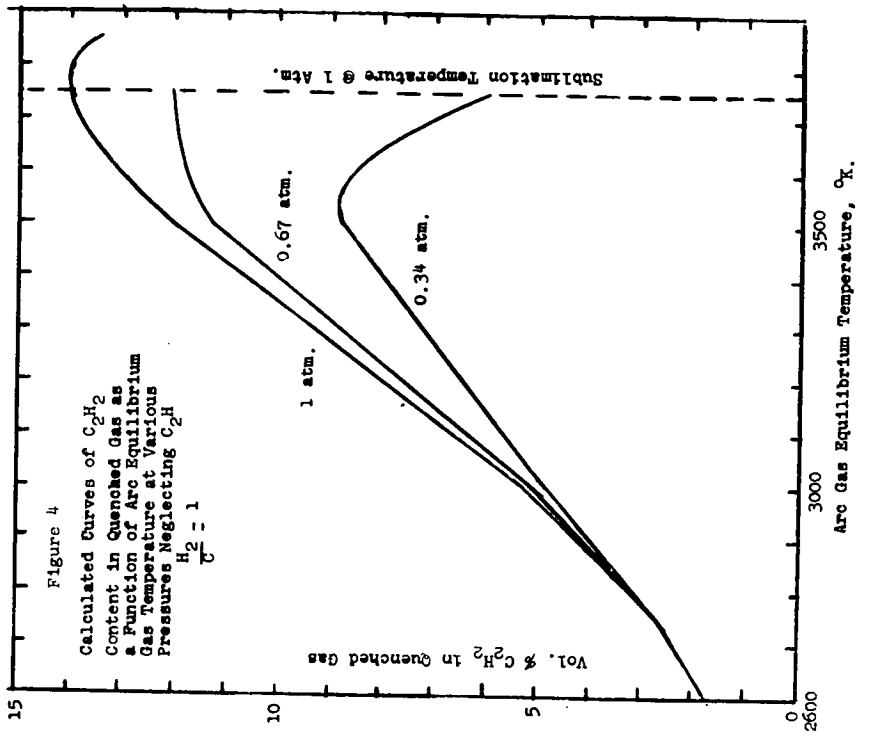
Figure 4
Calculated Curves of C_2H_2
Content in Quenched Gas as
a Function of Arc Equilibrium
Gas Temperature at Various
Pressures Neglecting C_2H
$\frac{H_2}{C} = 1$
Vol. % C_2H_2 in Quenched Gas
Arc Gas Equilibrium Temperature, °K.
Sublimation Temperature @ 1 Atm.
0.67 atm.
1 atm.
0.34 atm.

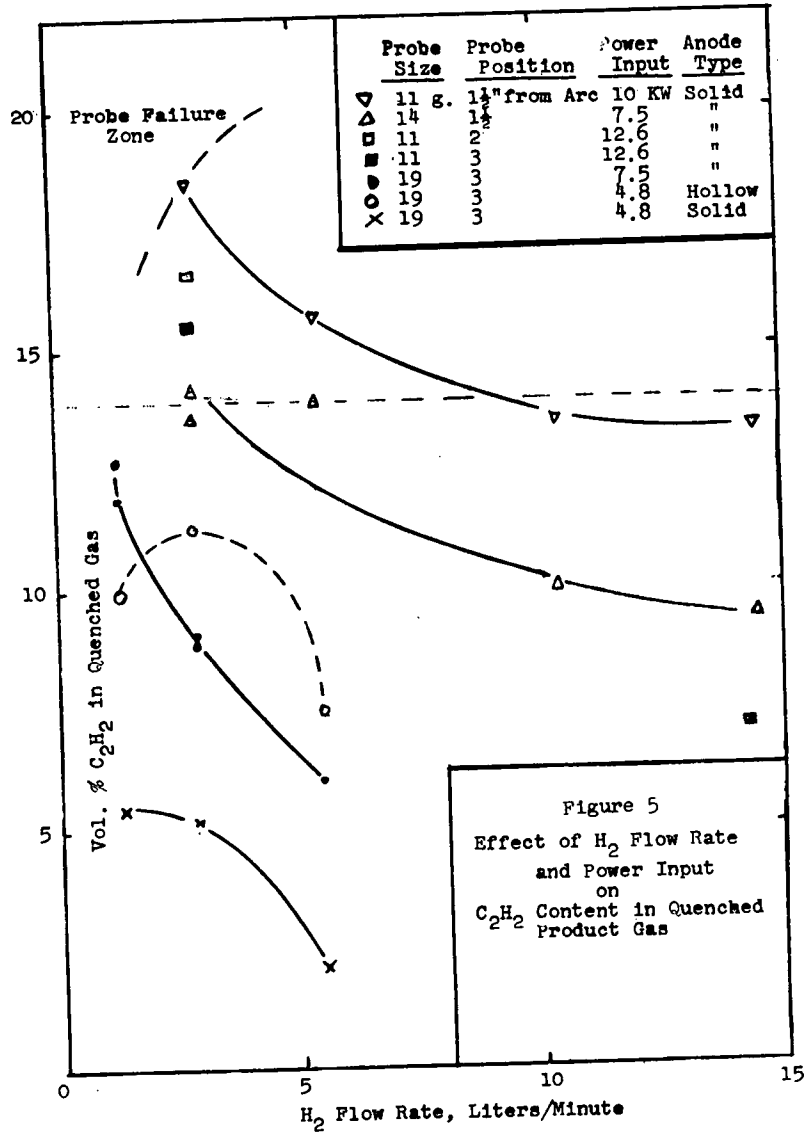

Figure 5
Effect of H_2 Flow Rate and Power Input on C_2H_2 Content in Quenched Product Gas

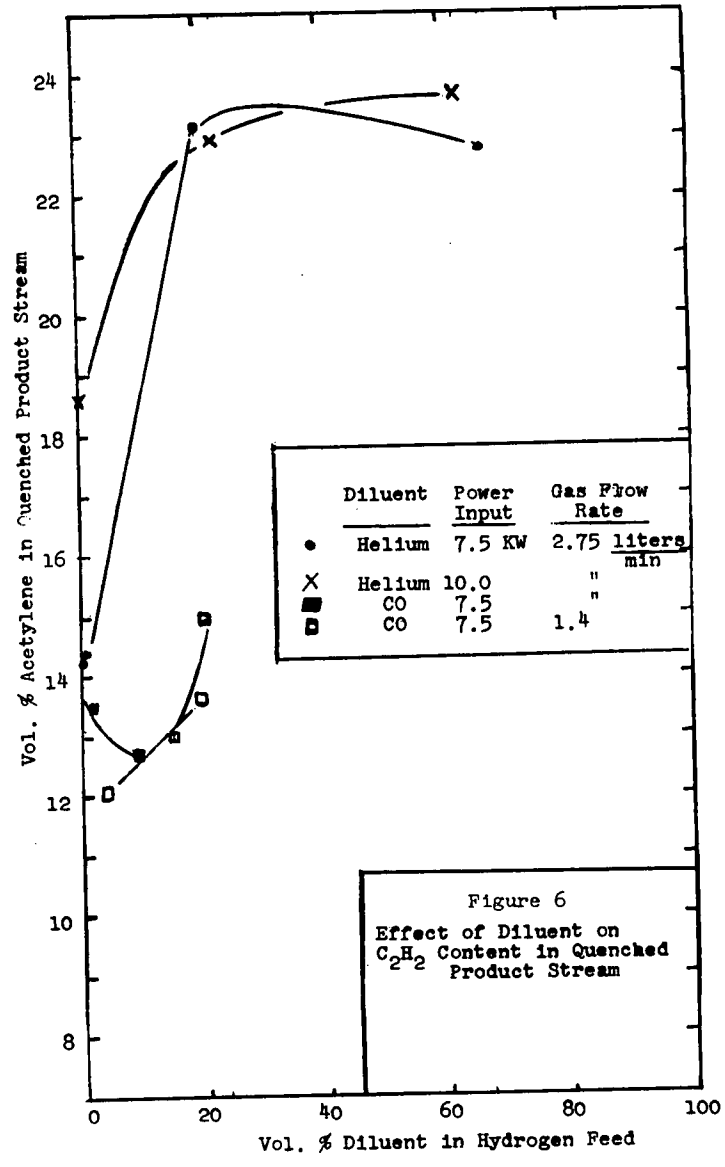

Figure 6
Effect of Diluent on C_2H_2 Content in Quenched Product Stream

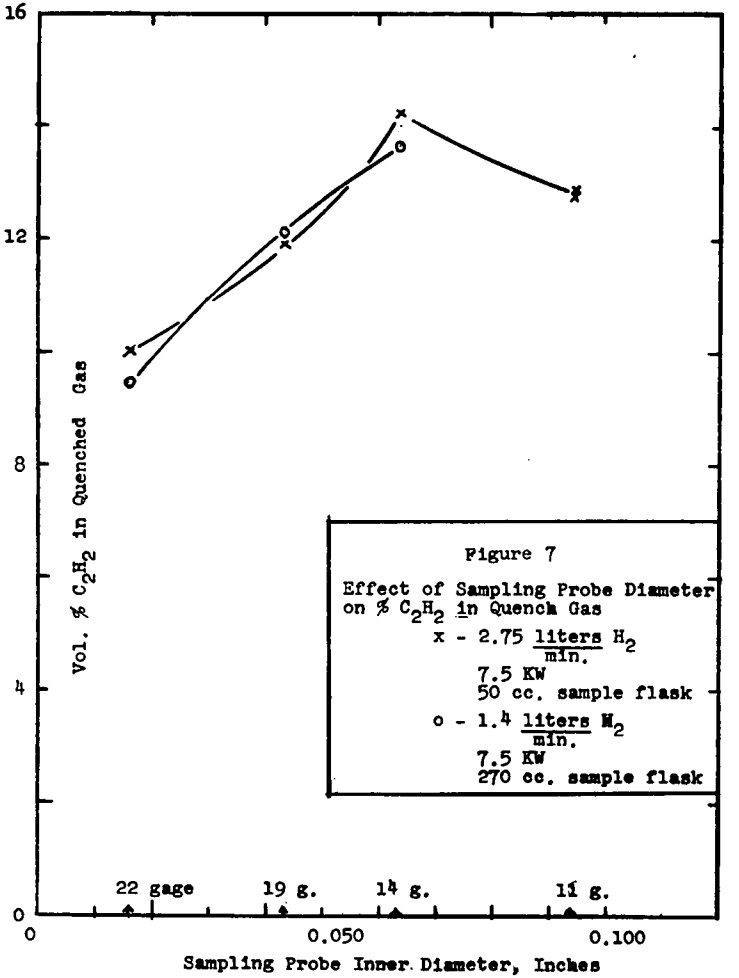

Figure 7

Effect of Sampling Probe Diameter on % C_2H_2 in Quench Gas

x - 2.75 $\frac{\text{liters } H_2}{\text{min.}}$
7.5 KW
50 cc. sample flask

o - 1.4 $\frac{\text{liters } H_2}{\text{min.}}$
7.5 KW
270 cc. sample flask

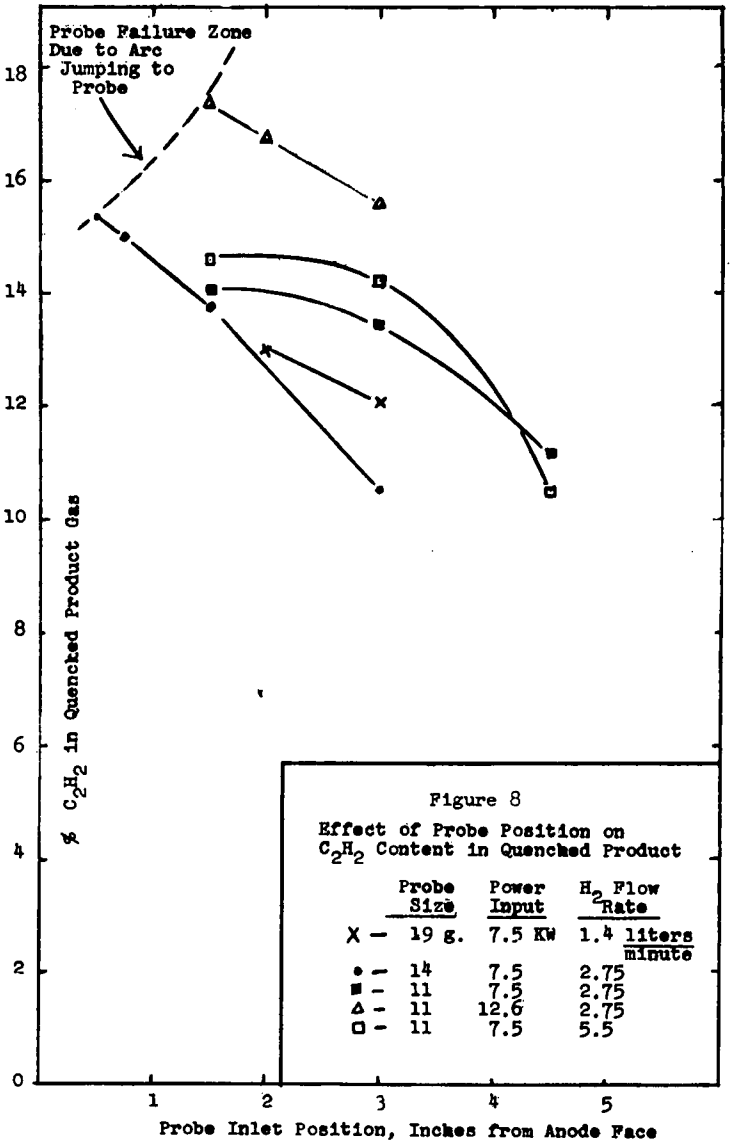

Figure 8

Effect of Probe Position on C_2H_2 Content in Quenched Product

	Probe Size	Power Input	H_2 Flow Rate
X —	19 g.	7.5 KW	1.4 $\frac{\text{liters}}{\text{minute}}$
• —	14	7.5	2.75
■ —	11	7.5	2.75
△ —	11	12.6	2.75
□ —	11	7.5	5.5

Figure 9

Effect of Sample Probe Diameter on C_2H_4 in Quenched Gas

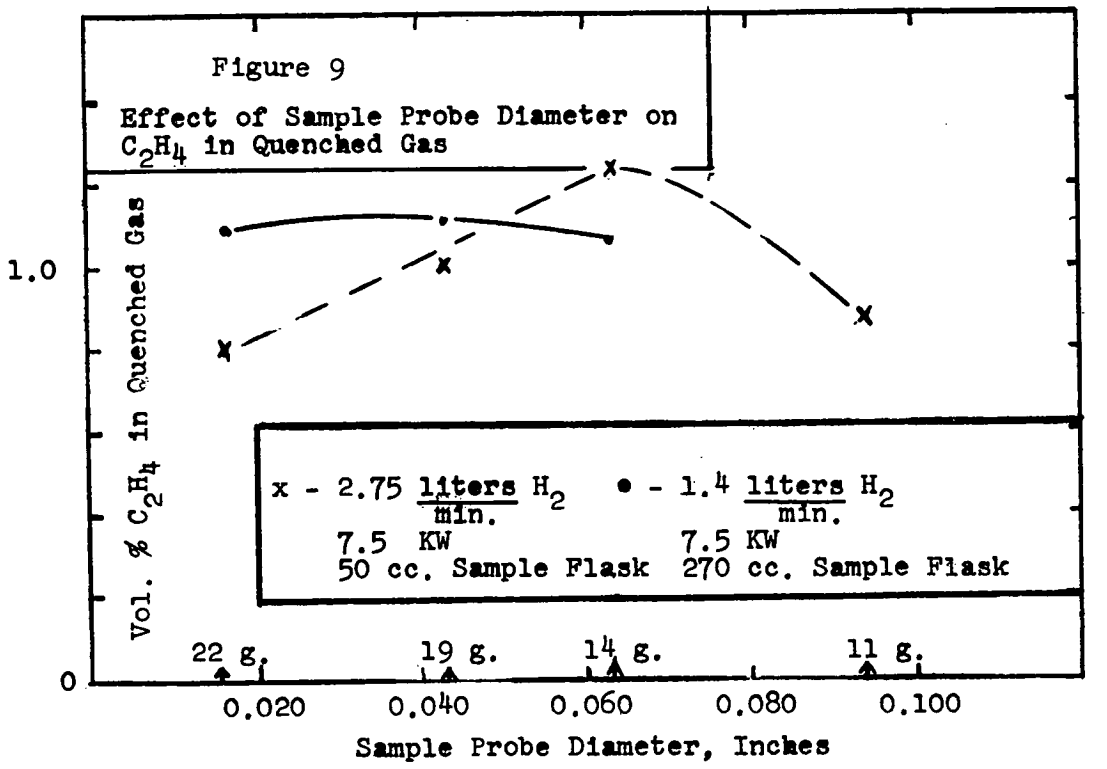

Figure 10

Effect of Sample Probe Position on C_2H_4 Content in Quenched Gas

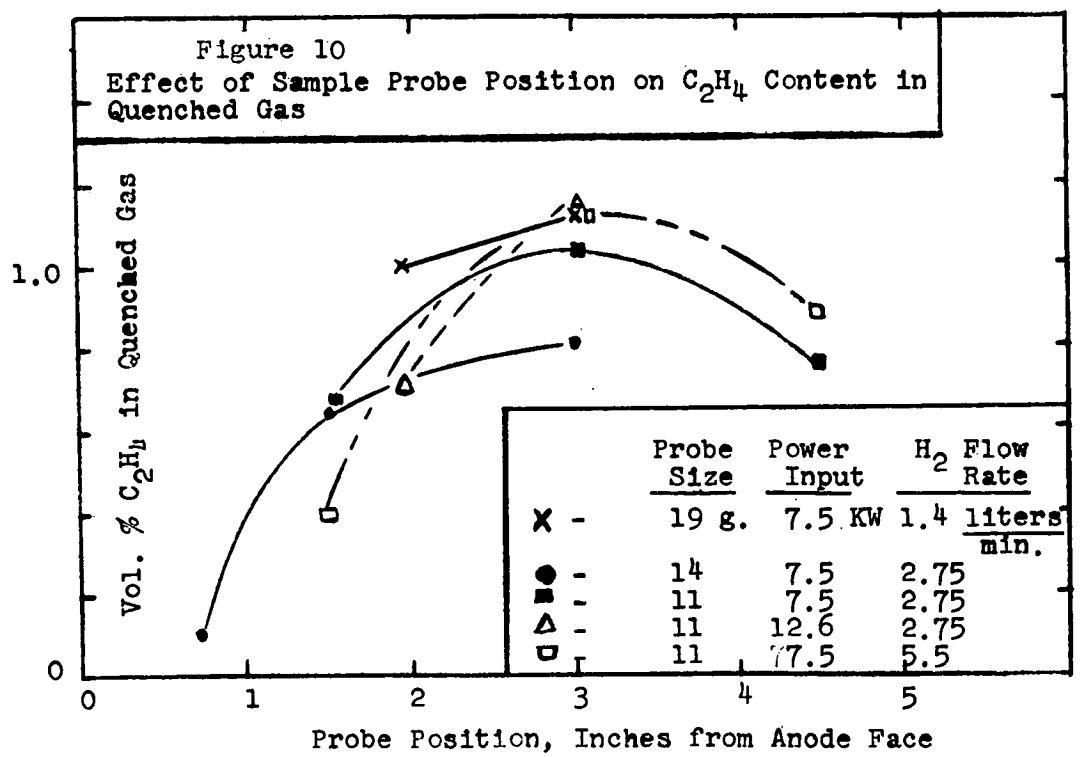

POSSIBILITES DE CONTROLE DES PROPRIETES THERMODYNAMIQUES A L'AIDE DES CARACTERISTIQUES DES DETONATIONS.

N. Manson

La comparaison des célérités des détonations observées et calculées à l'aide de la théorie de Chapman-Jouquet, permet d'obtenir comme l'ont montré de nombreux travaux portant sur les mélanges gazeux et explosifs condensés, des renseignements instructifs concernant certaines chaleurs de dissociation et des paramètres figurant dans les équations d'état des gaz à très haute pression et température elevee. Son emploi en tant que méthode de contrôle des grandeurs thermodynamiques pose toutefois un certain nombre de problèmes qui sont mis en évidence et discutés an examinant, plus particulièrement, dans le cas des mélanges explosifs gazeux:

a) les conditions dans lesquelles les détonations stables sont observées et leurs caractéristiques mesurées (notamment la célérité qui est la seule caractéristique qui peut etre actuellement déterminée avec grande précision: 0,1 – 0,2%)

b) dans quelle mesure la théorie peut être considérée comme vérifiée, compte tenu de la possibilité de prendre éventuellement en considération le fait que les produits de la détonation n'obéissent pas tout à fait a la loi des gaz parfaits;

3) les conditions d'emploi et l'aide que la méthode dite inverse est susceptible d'apporter.

IONISATION PROCESSES IN GASES AND THEIR APPLICATION TO ENERGY CONVERSION SYSTEMS

I. Fells

Ionisation phenomena occuring in gases have been known and investigated for many years. Recent advances in applied science such as the development of high intensity combustion systems, plasma technology and magneto–hydrodynamics have stimulated research into the processes of ion formation and recombination in gases. Ion beam techniques linked with mass spectroscopy, microwave attenuation measurements and shock tubes, magnetically driven and otherwise, are some of the newer research tools which have been developed to assist in the elucidation of ionisation processes. The many different ions which have now been detected in combustion systems indicate the complex nature of the kinetic processes leading to their formation: at the same time a certain uniformity in the relative abundance of the ions detected in many different systems suggests the possibility of some underlying basic processes. Further knowledge of these processes should assist in the difficult search for conditions which will increase the ion concentrations in flames and increase the efficiency of energy conversion systems involving principles such as magnetic braking of a partially ionised fluid or charge separation in a gaseous plasma.

INFRARED SPECTROSCOPY OF HOT PLASMAS*

Richard H. Tourin

A research program has been undertaken to measure infrared emission and absorption spectra of hot plasma streams. These measurements are useful for identifying chemical species in a plasma, in the study of energy transfer in plasmas, and for determination of plasma temperatures. Measurements have been made of the infrared spectra of nitrogen, argon, and helium plasmajet flames, with various admixtures, at 1 atm pressure.

The plasmajet used in this work is of the axial flow, gas-stabilized type. Energy is supplied to the gas by a D. C. arc of up to 24 KW input. The arc is struck between a solid cylindrical tungsten anode and the inside surface of a concentric hollow copper cylinder. The copper cathode is water-cooled; it also serves as primary nozzle. The primary gas stream flows through the annulus between the two electrodes, and emerges from the nozzle opening at a velocity of 30 to 100 meters/sec. The nozzle diameter is 3/16 inch; the plasmajet flame averages about 3/8 inch in diameter and 3 inches in length at 1 atm pressure. A secondary nozzle is used for seeding the primary gas stream with various materials.

The plasmajet flame is located at the focus of an infrared optical system, as shown in Fig. 1. For measuring flame absorption, radiation from the globar G is modulated by chopper Ch_1 and focused at the center of the plasma flame by mirrors M_1 and M_2. Both the flame and the globar image are then imaged on the entrance slit of the infrared monochromator, by mirrors M_3 and M_4. Since the globar radiation is modulated, while the flame radiation is not, the flame acts only as an absorber; the steady signal due to radiation emitted by the flame is filtered out by the AC amplifier. For measuring emission of the plasma flame, radiation of the globar is blocked off, and chopper 2 is used to modulate the plasmajet emission. With this system, emission or absorption spectra of the flame can be scanned continuously, and emission or absorption at a selected wavelength can be recorded as a function of time.

---

* Supported in part by the U. S. Air Force through Aeronautical Research Laboratories, Wright-Patterson Air Force Base, Ohio.

A blackbody source is used to calibrate the system for energy and temperature determinations.

The plasmajet torch is mounted on a carriage which can be moved in three rectangular co-ordinates. This permits focusing different regions of the flame on the monochromator slit, by which means the temperature and radiation of the plasmajet flame can be mapped.

Spectra of nitrogen, argon, and helium plasma-jets have been measured in the spectral range 0.57μ. Numerous spectral lines and bands have been observed. Temperatures of flames can be determined from their infrared emission and absorption at selected wavelengths (1). Figure 2 shows helium plasmajet temperatures determined from the infrared emission and absorption of helium at 4.05μ. Similar results were obtained for argon, using a wavelength of 4.015μ.

The nitrogen plasmajet is optically thin at all wavelengths. When an image of the nitrogen plasma-jet is reflected back upon the flame itself, the resultant spectrum has double the intensity of the flame alone, showing that absorption in the flame is negligible. For this reason the radiant heat transfer from the nitrogen plasmajet is also negligible. The nitrogen plasmajet can be made to radiate by seeding it with an infrared absorbing gas, such as CO_2. Figure 3 shows some effects of seeding a nitrogen plasmajet with CO_2. The emissivity is increased by seeding. This results in increased emission of radiation from the flame. However, the temperature is greatly reduced compared to the pure nitrogen plasmajet, because of the energy lost in heating the CO_2 gas. The temperature continues to fall as the concentration of seeding gas is increased, and consequently there is no further increase in radiant emission after the concentration of CO_2 reaches 35%.

Reference

1) R. H. Tourin and M. Grossman, Combustion and Flame 2, 330 (1958).

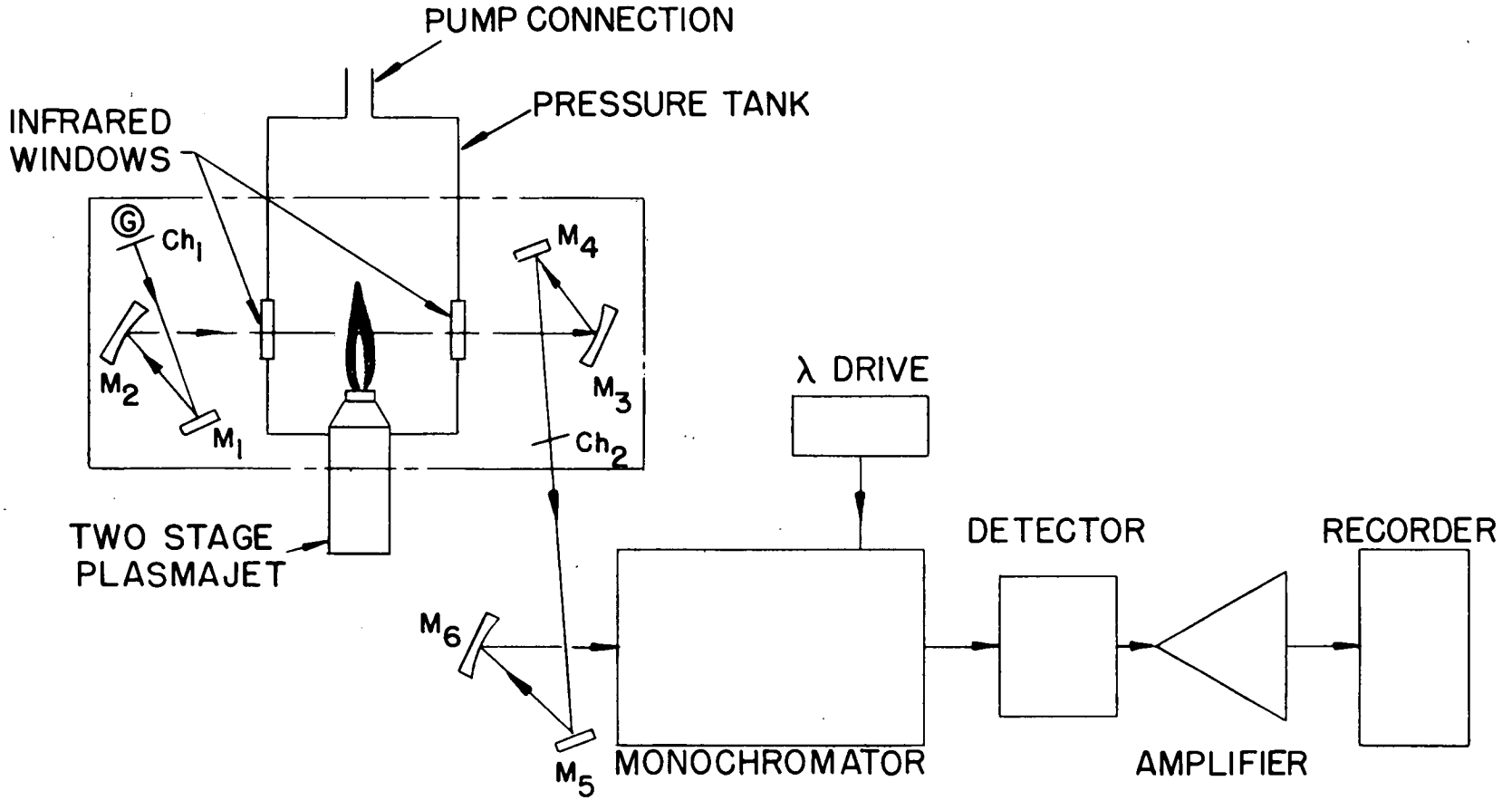

Fig. 1. Schematic diagram of setup for measurement of infrared emission and absorption of hot plasma streams.

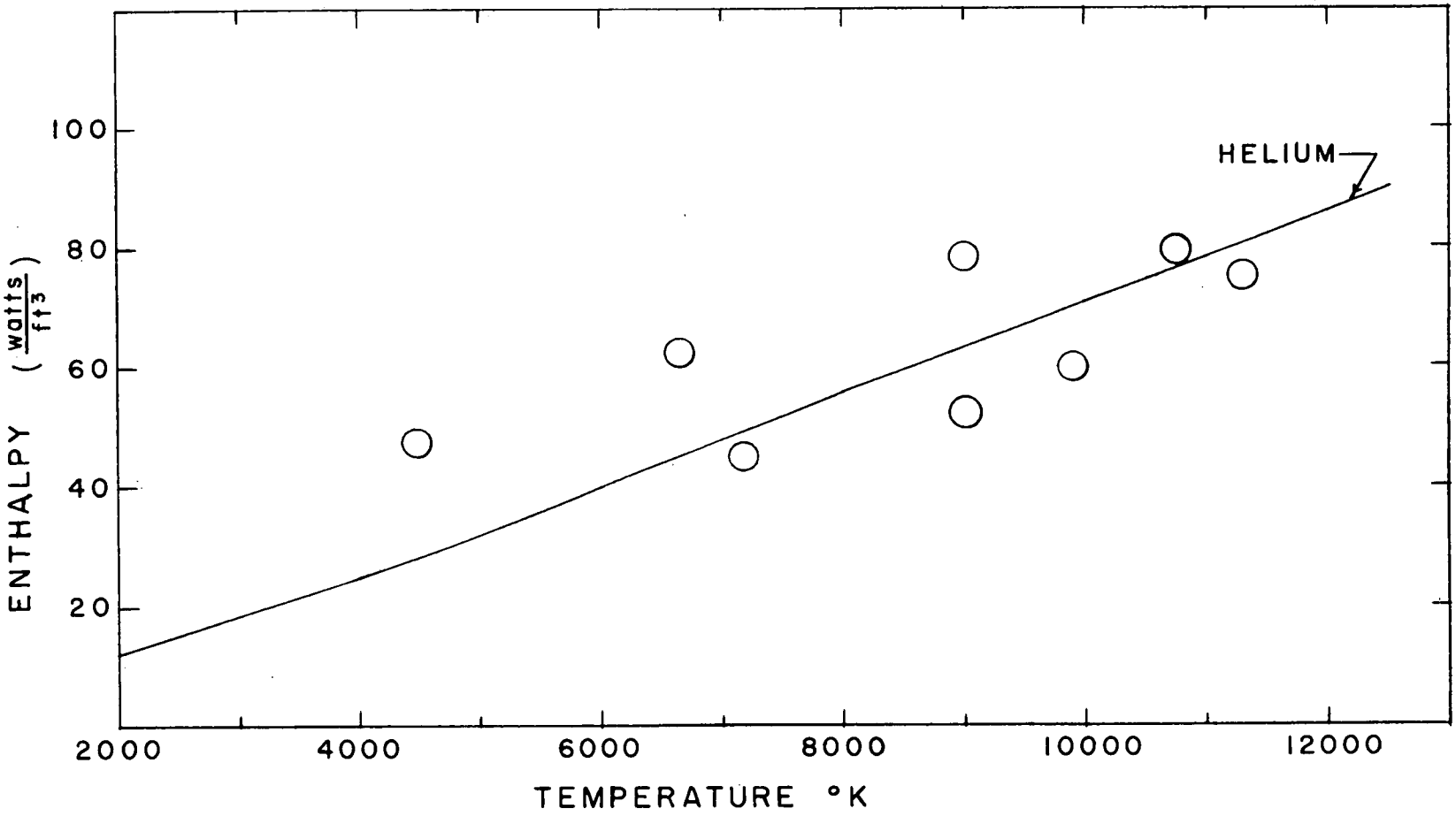

Fig. 2. Helium plasma temperatures measured by the infrared monochromatic method. The experimental points are compared to a plot of calculated gas enthalpy versus temperature.

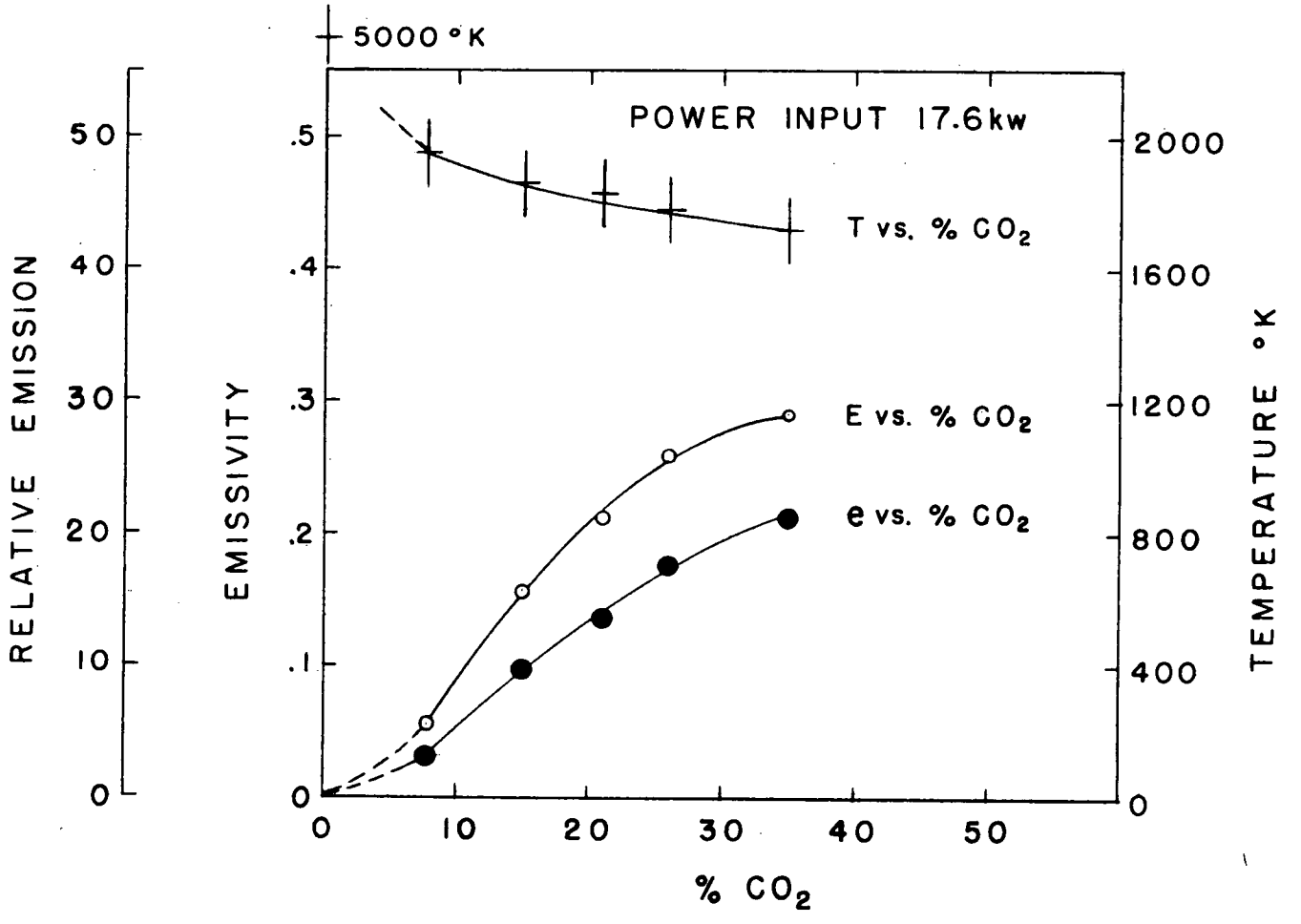

Fig. 3. Effects of seeding a nitrogen plasma with CO_2. The infrared emission E, emissivity e, and temperature T, of the plasma flame at 4.40–μ are plotted vs. % CO_2 in the flame. The energy radiated from the plasmajet is increased by seeding with CO_2, but the temperature falls, because energy is consumed to heat the CO_2 gas.

UNE METHODE POUR ETUDIER LA CINETIQUE DE CERTAINES COMBUSTIONS

F. Cabannes et P. Valentin

Certaines combustions dans les flammes en phase gazeuse, ou entre phases gazeuse et solide, font intervenir des phénomènes de diffusion; et il est important de fixer leur rôle dans le cinétique de ces combustions.

Pour aborder ce problème, l'on a étudié la combustion de l'hydrogène dans l'air, puis celle du méthane dans l'air au voisinage d'une paroi solide chauffee entre 100 et 1400° C (200° F à 2.500°). Dans une petite soufflerie on place dans un écouldment laminaire du mélange combustible, une plaque plane parallele à l'écoulement, et l'on détermine a l'intérieure de la couche limite, qui se développe le long de la plaque, les répartitions de vitesse, de température et de concentration des gaz combustibles et brûlés.

Nous reproduisons les courbes de concentration d'hydrogène et de methane obtenues en explorant la couche limite lors de la combustion de ces gaz dans l'air au voisinage d'une surface de platine chauffée. L'on porte en fonction de la distance y à la plaque, le rapport de la concentration (àcette distance), à la concentration en dehors de la couche limite.

Combustion de l'hydrogène: On distinque très aisément la combustion catalytique en surface (gradient de concentration non nul sur la plaque, Courbe 1 et 2), et la combustion normale en phase homogène, lorsque la température dépasse environ 800° C (1,500° F), (Courbes 2, 3, 4). Cette dernière combustion n'est pas influencée par la nature de la plaque (platine nu ou recouvert d'alumine). La combustion en surface est totale dès 100° C (200° F), mais l'influence de la combustion catalytique diminue vers 800° C (1,500° F) (Courbe 2), et devient nulle vers 900° C (1,700° F) (Courbe 3).

L'étude comparative des Courbes de vitesse, température et concentration, montre que dans toute la couche limite la diffusion, perpendiculairement à l'écouldment, joue un rôle prépondérant.

Combustion de l'hydrogène

Δ	$u_o = 6.5$ m/s	$T_p = 500°C$	$C_o = 0.028$
+	"	$T_p = 880°C$	$C_o = 0.052$
o	"	$T_p = 920°C$	$C_o = 0.052$
X	"	$T_p = 1000°C$	$C_o = 0.052$

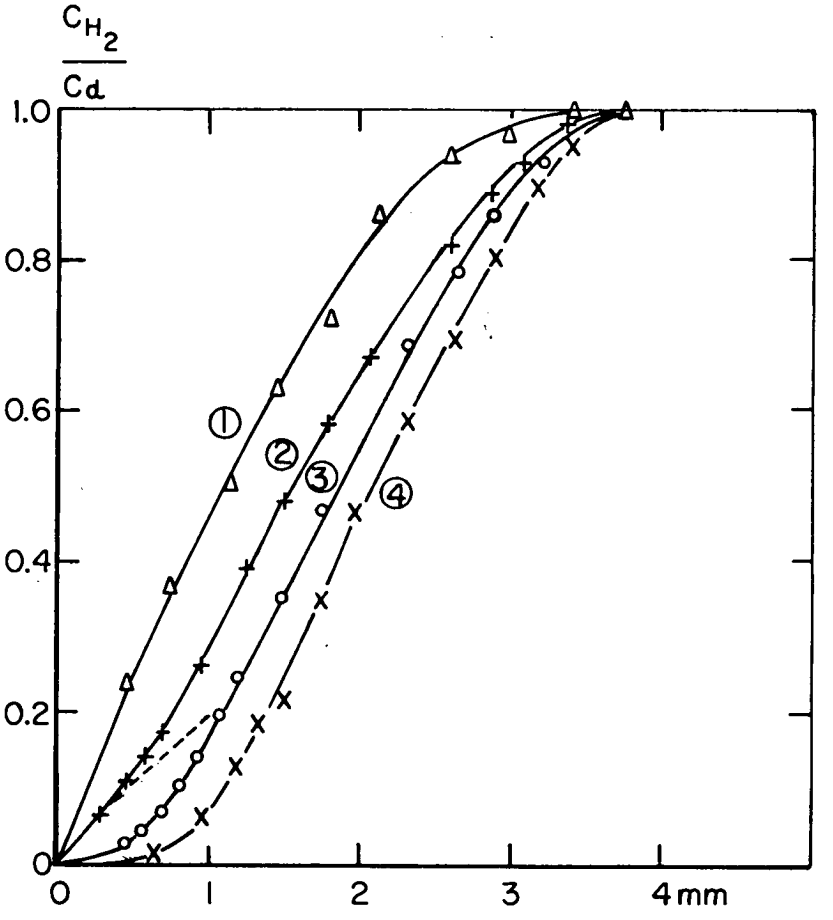

Combustion du méthane ($C_0 = 0.04$)

□ $u_0 = 8.2$ m/s $T_p = 1180°C$ (Plaque recouverte d'alumine)

\+ $u_0 = F$ m/s $T_p = 800°C$

o " $T_p = 1100°C$

x " $T_p = 1250°C$

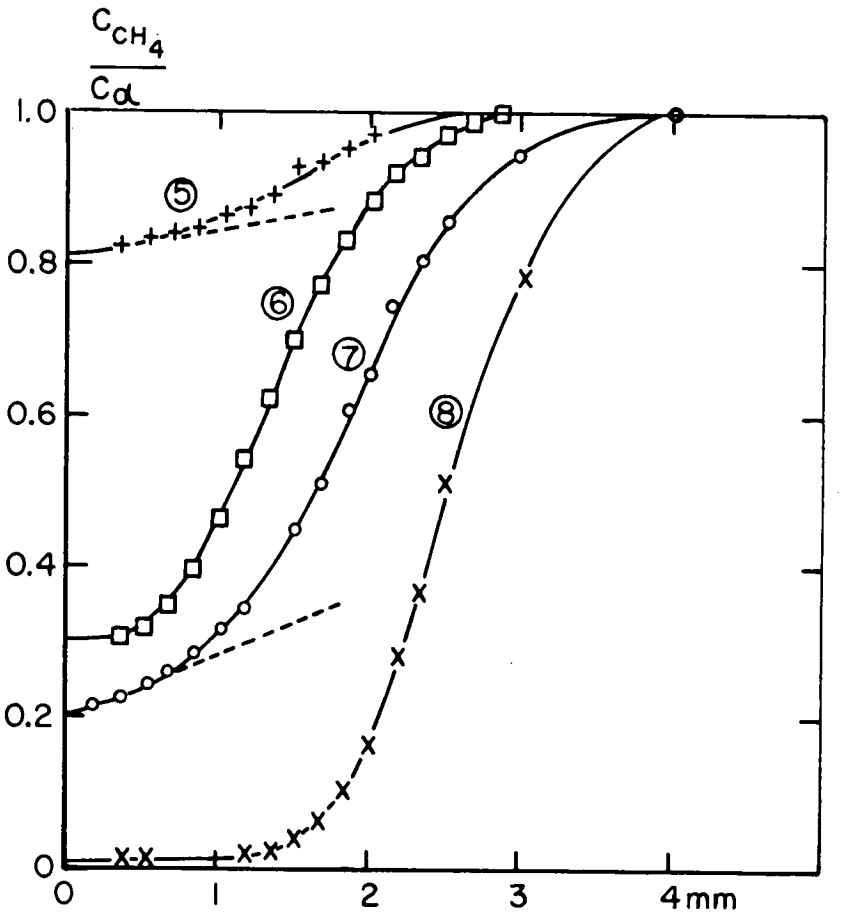

Les équations relativement simples de l'écoulement laminaire permettent d'expliquer les résultats observés, et d'évaluer les vitesses de réactions en surface et en phase homogène (la première n'étant limitée que par la diffusion de l'hydrogène). La combustion en phase homogène met en jeu une énergie d'activation E = 30 à 40 K cal à 900° C (1700° F).

Combustion du Methane: On distingue trois modes de combustions du méthane dans l'air au voisinage d'une plaque de platine; la combustion catalytique de surface est incomplète, on l'observe entre 600° C et 1300° C environ (1100° F – 2300° F), elle n'est pas importante car moins de 10% du méthane qui brûle, brûle en surface dans les conditions les plus favorables (Courbe 7).

L'importance de la combustion en phase homogène dépend de la nature de la plaque (Courbes 6, 7), on met ainsi en évidence une combustion catalytique en phase homogène, due probablement aux produits d'évaporation du platine. Avec une surface ne possédant pas d'activité catalytique, on observe seulement la combustion normale d'origine thermique.

Conclusions: L'exploration de la couche limite laminaire, dans des conditions expérimentales favorables, fournit de précieux renseignements sur la combustion de certains gaz comme l'hydrogène et le méthane, les mécanismes de ces combustions, les influences de certains facteurs, tels que la température, la composition du mélange combustible, l'activité catalytique de la paroi, l'importance des différents types de réactions (catalytique ou non), et dans certains cas, les valeurs des vitesses de réaction.

Ces renseignements, en particulier les vitesses de réactions, sont obtenus dans un domaine de température ou l'on a très peu de résultats: 800 à 1.300° C (1.500 à 2.300° F) et complètent la connaissance que l'on a, par ailleurs de la combustion lente, et de la combustion dans les flammes, de ces gaz.

DETERMINATION OF RATE CONSTANTS OF ELEMENTARY PROCESSES FROM FLAME VELOCITIES AS FUNCTIONS OF TEMPERATURE, PRESSURE AND MOLECULAR TRANSFER COEFFICIENTS

L. A. Lovachev

In a series of investigations the author has obtained approximate analytical relations connecting the flame velocity with initial and final parameters of gas mixtures and with functions of elementary process rates. A paper submitted to the 8th Symposium on Combustion dealt with laminar flame features as a function of the chain reaction mechanism.

Theoretical treatment has shown markedly different dependences of flame velocities on temperature, pressure, and transfer coefficients for branched and unbranched systems. This may be a key to establishing the type of the reaction responsible for the chemical process in the given mixture. By correlation of these dependences with flame velocities as functions of initial substance concentrations, it is possible to find out what elementary processes are limiting the course of the reaction. Pre-exponential factors and activation energy constants of limiting elementary processes may then be found.

The rate constant of process $H + O_2 \longrightarrow OH + O$ in hydrogen/oxygen and hydrogen/air mixtures, and the constant of quadratic chain termination in three-body collisions were established from flame velocities as functions of the combustion temperature and molecular transfer coefficients, respectively.

Analytical relations for flame velocities permit explanation of a number of facts obtained when treating experimental data on chain reactions in flames by the thermal theory equations. The reaction orders with respect to initial substances determined in this way appear to be zero, fractions, and variables. This does not correspond to actual reaction orders, but is accounted for by relations between constants of elementary processes and concentrations of initial, intermediary and final products, as well as by temperature and molecular transfer coefficients. Thus the reaction orders obtained by the thermal theory equations depend on these variables and parameters, and this shows both the complexity of chemical processes in flame, and the impossibility of describing them by means of simple molecular

reactions.

Determination of overall reaction orders from flame velocities as a function of pressure, making use of the thermal theory equations, gives fractional and varying values. Since these values are not predetermined but obtained from experimental functions, the thermal theory equations turn out to be empirical or semi-empirical. The fractions and variables are due to the application of equations derived for simple molecular reactions to chain reactions in flames. As shown by the author's paper submitted to the 8th Symposium, very different dependences of flame velocities on pressure are accounted for by chain reaction pecularities, and they may be derived from the analytical relations for flame velocities, without resorting to fractional or varying reaction orders.

With flames involving unbranched chains the slope in the plot of flame velocity against negative combustion temperature will be determined not only by activation energies for elementary process constants, but also by the heats of formation of active centres. Thus, since the "effective" activation energy obtained from thermal theory equations for flames involving unbranched chains depends mainly on heats of formation of active centres, it will not be a characteristic of the burning mixture. For flames involving branched chains the "effective activation energy will depend mainly on the activation energy for branching, and the "effective" activation energy value may change two-fold, depending upon the temperature with which the rate function of heat emission is associated.

As shown by analysis of theoretical relations for flame velocities in branched and unbranched systems, the dependences of flame velocities on heat conduction and on active centre diffusion coefficients are different for different types of chain reactions and are not consistent with functions obtained according to thermal theories. In other words, wrong allowances are made for molecular transfer coefficients when using thermal theory equations. Thus in treating experimental values for flame velocities as a function of the combustion temperature, the "effective" constant of the overall process appears to be a certain quantity depending on initial, intermediate, and final concentrations of reactants, on heats of active centre formation, and active centre diffusion coefficients, as well as on the temperature related to the rate function of the overall reaction. Consequently, an "effective" rate constant of this kind will not be a kinetic characteristic of the burning mixture.

ABSTRACTS

of

PAPERS

presented at the

THERMODYNAMICS SESSIONS

TERNARY SPECIES AT HIGH TEMPERATURES

Paul W. Gilles

Unusual ternary species can be prepared at high temperatures by three kinds of evaporation reactions. In one of these, a solid reacts with a gas producing a different gas as in the reaction,

$$Ta_2O_5(s) + 3\ TaCl_5(g) = 5\ TaOCl_3(g). \qquad (1)$$

The second is the reaction of two condensed phases to form gases as in the reaction,

$$3\ BeO(s) + W(s) = BeWO_3(g) + 2\ Be(g). \qquad (2)$$

The third is the simple sublimation of a ternary substance such as the reaction,

$$UOS(s) = UOS(g). \qquad (3)$$

All three of these types of reactions involve vaporization processes, and it is therefore important to examine the features of vaporization processes.

The study of a vaporization process serves to establish the nature and energetics of chemical binding in the gaseous state; to establish the nature of high temperature reactions; to measure the thermodynamic properties of solids, liquids and gases; to study the kinetics of high temperature reactions; and to prepare new substances. Many of the data required for the testing of chemical binding come from high temperature vaporization studies.

Usually the study of a vaporization process proceeds through five stages: (1) the net reaction is established, (2) the gaseous species are identified, (3) the vapor pressure is measured; (4) the kinetics of the evaporation process may be measured, and (5) finally the detailed mechanism of the vaporization process can be established. Most of our present studies in connection with vaporization processes are in the first three stages.

There are several techniques that may be employed in establishing the net reactions of a vaporization process.

Among these are x-ray diffraction and chemical analysis of the residual substances, mass balance observations, the variation of transport with the pressure of carrying gas in transpiration experiments, and direct identification of the gaseous species.

The most satisfactory method of identifying the gaseous species involves the use of the mass spectrometer. An unambiguous establishment of the molecular weight can be made and the pressure of a particular species can be followed as a function of time or temperature of the evaporating source. Other less direct methods for establishing the vapor species in complicated systems involve the use of a velocity selector and molecular beam apparatus, the use of a torsion effusion method, the use of spectroscopic apparatus, and the use of a transpiration technique.

A ternary gaseous substance can be produced by vaporization in a one-component or in a multi-component system. For example, the vaporization of UOS(s) to produce UOS(g) occurs in a one component system. The reaction of Ta_2O_5 with $TaCl_5$ to form $TaOCl_3$ occurs in a two component system, and the reaction between MgF_2 and B_2O_3 producing OBF(g) and MgB_2O_4 occurs in a three component system.

In equilibrium studies, the number and nature of the condensed phases establish the variance of the system in accordance with the phase law. Thus, in a one component system, the pressure of each species is fixed at constant temperature. In a two component system the pressure is fixed at constant temperature only (a) if there are two condensed phases, or (b) if the vapor and a single condensed phase have the same composition, or (c) if the composition of a single condensed phase is fixed. In a three component system the pressure is fixed at a given temperature only (a) if there are three condensed phases present, or (b) if the composition of one of two condensed phases is fixed, or (c) if two composition variables for a single condensed phase are fixed.

The chemical equation for the net reaction must indicate the phases that are present in the new system. For example, in a one compoent system the reaction is reaction (3). In the two component case the reaction is reaction (1). In the three component case the reaction is,

$$MgF_2(s) + 2\ B_2O_3(l) = 2\ OBF(g) + MgB_2O_4(s). \qquad (4)$$

In each of these cases a sufficient number of condensed phases is present so that the pressure is fixed at a given temperature.

The number of components in a chemical system is not necessarily the number of ingredients. Fox example, as is well known, $CaC0_3$ forms a two component system. The number of components can be ascertained after some of the chemistry of the system is known. For example, the two ingredients MgF_2 and B_20_3 form a three component system because of the occurrence of reaction (4).

The pressures of the gaseous substances produced are measured by various techniques. In the lowest pressure regions the Knudsen and Langmuier techniques are appropriate. Frequently the sensitivity of these methods can be increased by using a mass spectrometer, radiochemical techniques, or microchemical analytical techniques. At higher pressures, the transpiration method is appropriate.

Entropies and heats of formation of gaseous substances can be obtained from vaporization data if sufficient data are available for the condensed phases. In complex systems, such data may not be available. The resultant entropies of the gaseous molecules can be compared for reasonablemess with those empirically calculated.

The structures of high temperature ternary species are much more difficult to obtain. Adequate theory is lacking for the calculation of reliable structures. Spectroscopic methods are about the only useful ones. Studies on HOBO(g) have been made with infrared spectrometers, and it is conceivable that microwave spectrometers can be used for certain high temperature species.

If the structures are adequately known, then, of course, the thermodynamic functions can be calculated from the usual statistical thermodynamic formulas. On the other hand, if the structures are not available, then certain empirical entropy calculations may give approximate values.

Most of the ternary gaseous species that are known are hydroxides, and the ones that have been discovered recently usually arise by reactions similar to reaction (1), for example,

$$Li_2O(s) + H_2O(g) = 2\ LiOH(g). \qquad (5)$$

The ones so found are $Zn(OH)_2$, LiOH, MgOH, $WO_2(OH)_2$, and $Be(OH)_2$.

Of the next greatest abundance are the oxyhalides such as TiOCl, $TaOCl_3$, $MoOCl_2$, and BOF. Miscellaneous ternary species are $LiAlF_4$, LiBaO, $WO_x(BeO)_y$, and GeSiC.

The methods of preparing these substances and some of their properties are described.

THE DISSOCIATION ENERGIES OF THE GASEOUS MONOXIDES OF THE RARE EARTHS: THERMODYNAMIC PROPERTIES OF SOME GASEOUS DIOXIDES

D. White, P. N. Walsh, H. W. Goldstein, and D. F. Dever

The dissociation energies of the stable gaseous monoxides in the lanthanide series have been determined. Two types of experiments have been employed in these investigations which are as follows:

(a) Knudsen effusion studies of the solid sesquioxides in the temperature range 1800 to 2600° K, coupled with x-ray investigation of the quenched condensed phase and mass spectrometric determination of the composition of the vapor phase.

(b) Mass spectrometric investigation of the thermodynamic properties of the isomolecular gaseous oxygen exchange reactions of the type

$$M_a(g) + M_bO(g) \rightleftharpoons M_b(g) + M_aO(g)$$

where M_a and M_b refer to particular rare earths in the Lanthanide series. It is obvious that in the type of reaction shown above the mass spectrometric results lead directly to the difference in dissociation energies of the two gaseous monoxides involved if the variation of the equilibrium constant with temperature is measured. Further, to an excellent approximation, the absolute value of the equilibrium constant can be determined.

It is shown that the dissociation energies derived from both sets of experiments are consistent provided that the ground state multiplicity and electronic excitations of the gaseous monoxides are taken into account in the calculations from the Knudsen effusion experiments. Although there is no information concerning these multiplicities or excitations in the available literature, the entropy association with these can be computed from the measured thermodynamic properties of the isomolecular reactions mentioned above.

The mass spectrometric investigations in both sets of experiments (a) and (b) were performed with a Bendix-time of flight spectrometer.

The utility of this time of flight instrument in precise thermodynamic investigations at elevated temperatures is demonstrated. With certain precautions one can achieve a sensitivity resolution and precision comparable to what has been observed with focusing type instruments employed in high temperature investigations.

The thermodynamic properties of the gaseous dioxides $CeO_2(g)$, $PrO_2(g)$, and $TbO_2(g)$ have also been determined. There are the only stable dioxides which have been identified to date in the lanthanide series. As in the case of the gaseous monoxides, the dioxides have been investigated by both the Knudsen effusion and mass spectrometric technique. The calculated heat associated with the dissociation of these oxides to the atoms suggests that the metal–oxygen bonding energy does not change appreciably as one goes from the monoxide to the dioxide. It would seem that all the dioxides of the lanthanide series would be stable under suitable oxidizing conditions.

Some interesting correlations appear in the trend of the dissociation energies of the gaseous monoxides with atomic number of the rare earth metal in the compound. The dissociation energy decreases as one goes from Lanthanum to Europium and abruptly rises at Gadolinium. From Gadolinium to Lutetium the dissociation energy again decreases with atomic heat of sublimation of the rare earth metals with atomic number. This leads to the observation that the heat of formation of the gaseous monoxides are nearly independent of atomic number. These correlations will be discussed.

THE FREE ENERGY OF FORMATION OF SiC, TiC, AND ZrC

Guido L. Vidale

A new method of measuring the vapor density of gaseous species is described, and its usefulness for measuring vapor pressures and free energies of formation of compounds at elevated temperatures is demonstrated.

The main advantages of this method are its high selectivity of the precise species being measured, its applicability at temperatures as high as 3000° C and at partial pressures as low as 10^{-9} atmospheres, and the relative assurance that the vapor under investigation is in chemical equilibrium with some condensed phase.

The vapor under investigation is contained in a cylindrical cell inside an isothermal furnace, and an optical beam is passed through small holes at both ends of the cell. This beam consists of the radiation from a hollow cathode discharge tube operated at liquid nitrogen temperature through which is passed a rapid flow of argon carrier gas. The hollow cathode cup is lined with the element whose vapor density is being determined, so that the resonance lines of this element are fairly intense.

After passing through the hot vapor, this beam is introduced into a monochromator, and the absorption of a given resonance line by the hot vapor is measured. Under the conditions of this investigation, the half-width of the line generated in the hollow cathode source has been shown to be considerably narrower than the half-width of the absorption line contour of the hot vapor in the furnace. Therefore, the value of I/I_0 can be related directly to the atom density when the oscillator strength of the line is known. Corrections must be made, however, for the hyperfine structure of the line, and for the effect of Doppler and pressure broadening on the absorption coefficient at the center of the line.

In order to avoid measuring the light radiated from the walls and from the hot gas in the furnace, the radiation from the source is chopped before entering the cell, and the output of the measuring photomultiplier is phase-locked to the chopper.

A partial pressure of 5–20 cm. of inert gas must be maintained in a furnace to prevent the vapor in the cell from diffusing too rapidly through the apertures at the ends of the cell. A sharp drop-off in the furnace tube temperature at the ends of the cell must also be created to keep the density of the vaporized species low outside the cell. Convection currents which might lead to excessive transport of vapor out of the cell must also be avoided. Meeting these requirements, while also keeping the cell temperature as uniform as possible, is perhaps the most difficult thing to accomplish, since uncertainties in the path length are probably the most serious source of error in this method.

Several furnaces have been used in these studies. At temperatures lower than 1000° C, a nichrome wound tube furnace provided with a vacuum tight silica tube may be used.

For temperatures between 1000 and 1800° C and in an oxidizing atmosphere, a platinum–rhodium wound furnace having an alundum chamber and quartz window has been used. The cell used was made of platinum. In both these furnaces, temperature measurements could be made conveniently using thermocouples. At temperatures higher than 1800 and in the absence of oxygen, a resistive carbon tube furnace has been used. In this case, the cell is also made of graphite, and temperature measurements are made with an optical pyrometer.

In order to establish the accuracy of this method, the vapor pressure of sodium over sodium metal was measured using the sodium D line. In this case, the value of the oscillator strength, and the effect of the various line contour corrections can be established exactly. The excellent agreement between the measured pressure and the accurately known vapor pressure of sodium confirms the accuracy of the technique. An analysis of errors shows that an uncertainty of 15–20% may be encountered in these vapor pressure measurements, although the sodium results have a considerably smaller error.

The vapor pressure of metal atoms over the invariant system metal carbide plus graphite are being measured using this method. SiC, TiC, and ZrC have been studied, and the free energy of formation of these compounds has been calculated. The temperatures at which the Si 2516 A, Ti 3371 A, and Zr 3601 A lines are 50% absorbed by the equilibrium vapor over the respective metal and the carbide phases have been measured. Then, making use of the known heat of vaporization of the metal, the ratio of the equilibrium pressure over the metal and over the carbide at the same temperature has been calculated from the experimental data. The free energy of formation of the carbide is then easily calculated.

Although some corrections had to be applied for pressure and Doppler broadening, the importance of these corrections is much smaller than had been the case for sodium, and no previous information of the value of the oscillator strengths was needed. This greater accuracy was due to using the absorption measurements of the metal atom, rather than relying exclusively on a calculated absorption coefficient. Most of the errors which might have been present in the determination of the vapor pressure of sodium, therefore, tended to cancel in the case of the carbides.

Acknowledgment: This work was performed under Contract No. AF 33(616)-6841, U. S. Air Force, Wright Air Development Division and under Contract No. AF 04(647)-269, U. S. Air Force, Ballistic Missiles Division.

THE VAPORIZATION OF LITHIUM AND SODIUM METABORATE *

Alfred Buchler and J. B. Berkowitz-Mattuck

The vaporization of lithium and sodium metaborate and of some related boron compounds has been studied by means of the technique developed by Inghram, Chupka and their associates in which a mass spectrometer is used to determine the composition of the vapors effusing from a Knudsen cell containing the material to be studied. The principal vapor species at the temperatures of the experiments were found to be the monomers, $LiBO_2$ and $NaBO_2$. Significant amounts of dimer and very small amounts of trimer were also observed. The instrument used in this work was a 60°, 12"-radius direction-focussing mass spectrometer constructed by Nuclide Analysis Associates, State College, Pennsylvania, from designs by Professor M. G. Ingrham. Both tungsten and molybdenum Knudsen cells 12 mm in diameter, 40 mm high and having 1 mm diameter effusion holes were used to produce beams of neutral molecules. Sixty-volt electrons were used to produce ions which were accelerated through a 2800 volt field, mass analyzed and detected by a 16-stage electron multiplier followed by a vibrating reed electrometer. The Knudsen cells were heated by radiation and, at higher temperatures by electron bombardment from a tungsten filament. Temperatures were measured with a platinum-platinum-10% rhodium thermocouple inserted in the bottom of the Knudsen cell. The samples used in the experiments were obtained by the dehydration under vacuum of $LiBO_2 . 2H_2O$ (Lithium Corporation of America) and $Na_2B_2O_4 . 8H_2O$ (Fisher Scientific Company).

The mass spectrum of lithium metaborate vapor was obtained at temperatures between 750° and 920° C. Satisfactory agreement was obtained between experiments in tungsten and molybdenum cells.

---

*This work was supported by the U. S. Army Office of Ordinance Research with funds provided under the Advance Research Projects Agency Program.

The ions observed were Li^+, $LiBO_2^+$, $Li_2BO_2^+$ and $Li_3(BO_2)_2^+$, with a relative abundance of the order of 0.3 : 1 : 0.2 : 0.001. The fragmentation pattern of lithium metaborate thus resembles that of the alkali halides as reported by Berkowitz and Chupka and Porter and Schoonmaker. In accordance with the latter work, the ionization and fragmentation reactions may be written as follows:

$$LiBO_2 + e \longrightarrow LiBO_2^+ + 2e \quad (1)$$

$$LiBO_2 + e \longrightarrow Li^+ + BO_2 + 2e \quad (2)$$

$$Li_2(BO_2)_2 + e \longrightarrow Li_2BO_2^+ + BO_2 + 2e \quad (3)$$

$$Li_3(BO_3)_3 + e \longrightarrow Li_3(BO_2)_2^+ + BO_2 + 2e \quad (4)$$

The assumption that the lithium ions observed are produced in reaction (2) is supported by the observations that the appearance potential of Li^+ is of the order of 1 volt higher than that of $LiBO_2^+$, and that the $Li^+/LiBO_2^+$ ratio remains constant over a 500-fold range of pressure.

Sodium metaborate was studied between 620° and 830° C. The ions observed were Na^+, $NaBO_2^+$, $Na_2BO_2^+$ and $Na_3(BO_2)_2^+$. In contrast to the case of lithium metaborate, however, Na^+ was the most abundant species observed, the $Na^+/NaBO_2^+$ ratio being of the order of 2. Also, the $Na_2BO_2^+/NaBO_2^+$ ratio varied with the crucible material, being 0.4 in the case of tungsten and 0.1 in the case of molybdenum. Finally, the appearance potential of Na^+ was found to be 5.5 volts compared to a 10 volt appearance potential for $NaBO_2^+$. A low appearance potential for sodium ions has been reported by Berkowitz and Chupka in the mass spectrum of sodium fluoride; applied to the present case, their arguments would suggest the reaction:

$$NaBO_2 + e \longrightarrow Na^+ + BO_2^- + e \quad (5)$$

as the source of the sodium ions. This reaction, however, is expected to have a low cross-section, and container effects cannot be ruled out at this time. It is expected that experiments in platinum-lined crucibles will yield more reliable values for the heats of sublimation of lithium and sodium metaborate monomers and dimers than are available at present. Nevertheless, close resemblance of the alkali metaborates to the alkali halides may be taken as established, a resemblance which suggests the structure:

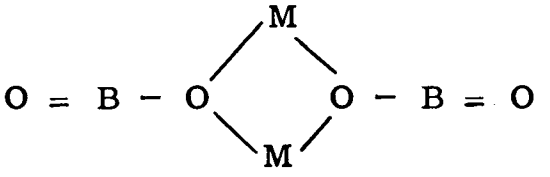

M = Na, Li

for the dimeric species in analogy to the recently established bridged structure of lithium halide dimers. This conclusion is also supported by infrared spectroscopic work on sodium metaborate vapor now in progress in this laboratory.

It is of interest to observe that the vapor of metaboric acid, HBO_2, studied by Berkowitz, Chupka and Meschi, and that of boron oxyfluoride, BOF, studied by White, Walsh, and Sommer and in this laboratory, each consists only of monomer and trimer, the latter presumably having the formula

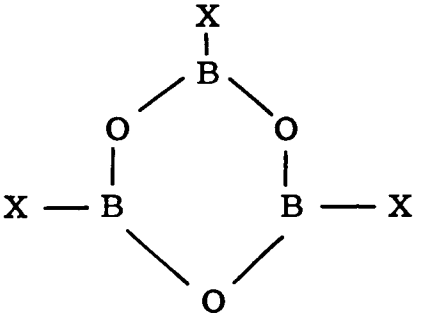

X = OH, F

No fragmentation was reported in the case of metaboric acid, while the case of boron oxyfluoride trimer the principal fragment ion is $B_3O_3F_2^+$, the B_3O_3 ring remaining intact. In the alkali metaborates, on the other hand, there appears to be no tendency to form six-membered B_3O_3 rings.

and

$$Na_2B_4O_7\ (s) \longrightarrow 2NaBO_2\ (g) + B_2O_3(s) \quad (6)$$

$$Na_2B_4O_7\ (s) \longrightarrow Na_2B_4O_7\ (g) \quad (7)$$

The mass spectrum observed was very complex. It contained Na^+, $NaBO_2^+$, $Na_2BO_2^+$, observed in the evaporation of sodium metaborate, as well as $B_2O_3^+$ and $B_2O_2^+$, known from the mass spectrum of B_2O_3 vapor. In addition, however, the ions $NaBO^+$, Na_2B^+, and BO_2^+ were observed; the molecular antecedents have not yet been identified. Nevertheless, the presence of species containing sodium–boron–sodium bridges is strongly suggested.

We should like to thank Mr. James L. Stauffer for his enthusiastic assistance with these experiments.

VAPORIZATION OF MAGNESIUM OXIDE AND ITS REACTION WITH ALUMINA

Robert L. Altman and Alan W. Searcy

The vaporization of MgO from 1800 to 2100° K was investigated by the Knudsen effusion technique. Alumina effusion cells containing crystalline MgO and surrounded by a tungsten susceptor were heated inductively for periods up to 9 hours. The magnesium partial pressures obtained from the experimental weight-loss results by application of the Knudsen equation are shown as circles in Fig. 1. The P_{Mg} expected by consideration of the vaporization processes

$$MgO\ (s) \longrightarrow Mg\ (g) + 1/2\ O_2\ (g),$$

$$MgO\ (s) \longrightarrow Mg\ (g) + O\ (g),$$

is shown by the line. The weight-loss results in this temperature range indicate that molecular species such as gaseous MgO are of minor importance in the vaporization of magnesia.

These results were confirmed by transpiration experiments with argon and oxygen passed over crystalline MgO at 2030° K. The weight loss with pure oxygen indicated that the partial pressure of gaseous MgO was less than 3×10^{-8} atm while similar passage of argon gave a P_{Mg} of 1×10^{-6} atm, which is close to the equilibrium value under these conditions.

The gaseous species in the vaporization of MgO also reacted with the alumina Knudsen cell to form magnesium aluminate (spinel). As this spinel would be expected to have a lower magnesium partial pressure than crystalline MgO, some Knudsen effusion runs with the spinel have been made. The results are shown as crosses in Fig. 1.

Chemical analysis showed that the alumina content of the spinel increased upon heating, as would be indicated by the reaction

$$MgAl_2O_4\ (s) \longrightarrow Al_2O_3\ (s) + Mg\ (g) + (1-2x)\ O_2\ (g)\ 2\ (x)\ O\ (g).$$

However, x-ray powder patterns failed to reveal any of the characteristic lines of Al_2O_3. It appears that the alumina produced upon heating the spinel dissolved in the excess magnesium aluminate, further decreasing the activity of the magnesium vapor. We found that the lowest vapor pressure results contained the greatest excess of alumina in the residue. The weight loss obtained in the runs yielding nearly stoichiometric $MgAl_2O_4$ indicates that the heat of formation of this spinel from the respective oxides is close to zero.

We have also observed that alumina crucibles lose weight when heated above 1800° K. Our weight-loss results agree closely with the mass spectroscopic investigation of this vaporization process.

Our Knudsen effusion and transpiration experiments with magnesia indicate that the dissociation energy of gaseous MgO is significantly less than the values of about 100 kcal/mole obtained by flame intensity studies.

Lagerqvist and Uhler have made a rotational analysis of the lowest $^1\Sigma^* - {}^1\Sigma^* - {}^1\pi$ transitions of gaseous MgO. We have applied these results to the extensive band-head data of Mahanti to obtain additional vibrational levels. A least-squares fit to the vibrational data so obtained gave the spectroscopic constants and dissociation energies shown in Table 1.:

State	T_o	W_o	W_oX_o	D_o
	cm^{-1}			kcal /mole
$^1\Sigma$		778.84	5.12	85
$^1\pi$	3503.24	660.91	4.29	73
$^1\Sigma^*$	20003.32	817.80	4.00	119

The dissociation energy was obtained with the equation

$$D_o = W_o^{2/4}\ W_oX_o.$$

Adding the electronic energy, T_o, to the dissociation energy of the $^1\pi$ state, we see that the energies of the dissociated atoms of both the $^1\Sigma$ and the $^1\pi$ states are within several kilocalories of each other. If both of these states dissociate to the same atoms, this allows us to estimate the dissociation energy of the $^1\Sigma$ state as about 84 kcal/mole.

The heat of sublimation of gaseous MgO, ΔH_o°, can be obtained from this dissociation energy estimate by means of a thermochemical cycle, from which

$$\Delta H_o^\circ + D_o^\circ (MgO) = 238 \text{ kcal/mole} + E ,$$

where E is the excitation energy of the dissociation products above ground-state Mg and O atoms.

Applying $-(F_T^\circ - H_o^\circ)/T$ data for both gaseous and crystalline MgO to our transpiration vapor pressure results, we obtain a ΔH_o° of about 153 ± 3 kcal/mole. This value indicated that the $^1\Sigma$ state dissociates to ground state atoms, i.e.,

$$MgO\ (^1\Sigma) \longrightarrow Mg(^1s) + O\ (^3P).$$

In conclusion, our experimental data support the earlier findings of the mass spectrographic investigation of the vaporization of MgO carried out by Inghram and Porter.

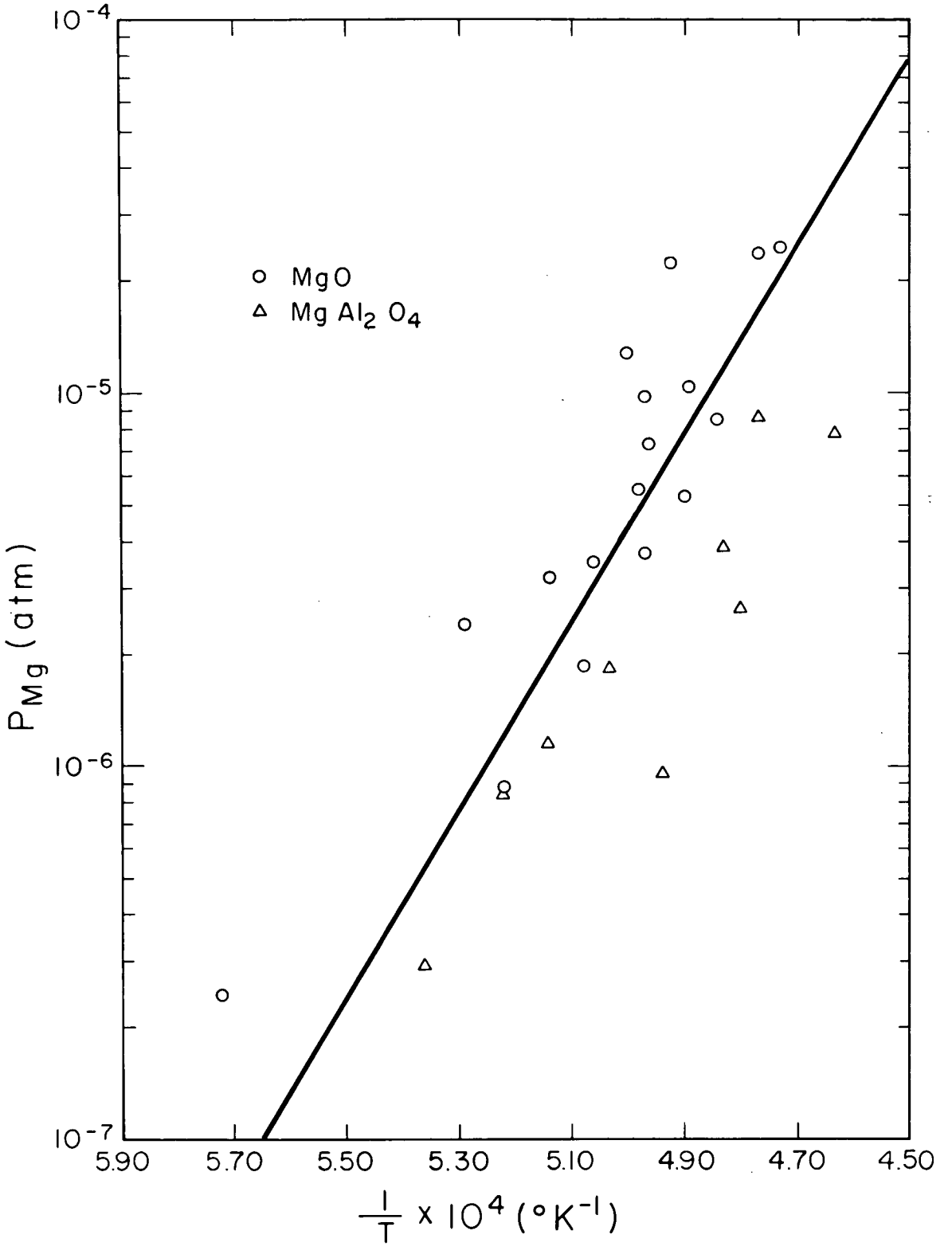

Fig. 1. Vapor pressure of MgO and $MgAl_2O_4$.

VAPOR PRESSURES OF THE PLATINUM METALS

R. F. Hampson and R. F. Walker

The experimental technique used to determine the vapor pressure of Pt, Ir, Rh, and Pd was based on the method of Langmuir. Measurements of the rates of vaporization of the substances (m) were related to the equilibrium vapor pressures (p) in accordance with the equation:

$$P = \frac{m}{\alpha} \left(\frac{2\pi RT}{M}\right)^{1/2}$$

A value of unity was adopted for the coefficient of vaporization, α, and it was assumed that the appropriate value for the molecular weight of the vapor species, M, was that of the monomeric species.

The rates of vaporization were measured in situ, by suspending the samples into a water-cooled, glass chamber from an equi-arm, quartz beam microbalance. The microbalance had a sensitivity of about one microgram. Samples of known surface area were heated by direct induction, using a water-cooled, copper concentrator to obtain efficient, uniform heating, Each sample consisted of a short rod, 0.75 ins. long x 0.085 ins. dia. A short length of wire of the same substance was used to attach the sample to a balance suspension which consisted of a chain of 0.010 dia. sapphire rods. The balance and furnace chamber was kept evacuated to pressures in the 2×10^{-6} to 8×10^{-5} mm. Hg. with a liquid-nitrogen-trapped, oil-diffusion-pump.

Brightness temperatures of the samples were measured by sighting with an optical pyrometer at 75° to the surface normal. With Pt, Ir, Rh observed surface temperatures were converted to true temperatures using literature values for the normal spectral emissivities and correcting for the non-normal sighting. With Pd an approximately black-body hole was drilled in the sample at the angle of sighting, yielding observed temperatures which were within -1 to -3° of true temperatures. The nominal temperature of each measurement was maintained to within $\pm$ 5° K or better.

The balance was used as a deflection instrument, deflections of its beam being directly proportional to changes in weight. Interaction of the rf induction field with the sample prevented the balance being read continuously.

The balance was, therefore, read before and after each run at high temperature. Very rapid heating and cooling of the samples was possible; hence, errors arising from the weight loss of the sample during heating and cooling were small. For each sample, the duration of the runs (excluding heating and cooling periods) was increased from about 1 minute at the highest temperatures to about 2 or 3 hours at the lowest temperatures, to yield weight losses of about 100 micrograms.

Heats of sublimation at 298° K, ΔH_v° (298), were calculated from the vapor pressures with the aid of tabulated free energy functions. The least-squares lines for the vapor pressure data, the heats of sublimation, and the normal boiling points obtained were as follows:

1) Platinum.

$$\text{Log } P_{atm} = 6.761 - \frac{27,575}{T}. \quad (1916 - 2042^\circ \text{ K})$$

$$\Delta H_v^\circ \text{ (298)} = 134.9 \pm 1.0 \text{ kcal/mole}$$

$$\text{B.P.} = 4100 \pm 100^\circ \text{ K}$$

2) Iridium.

$$\text{Log } P_{atm} = 7.139 - \frac{33,337}{T}. \quad (1986 - 2260^\circ \text{ K})$$

$$\Delta H_v^\circ \text{ (298)} = 159.9 \pm 2.0$$

$$\text{B.P.} = 4700 \pm 100^\circ \text{ K}$$

3) Rhodium.

$$\text{Log } P_{atm} = 6.894 - \frac{27,276}{T}. \quad (1709 - 2075^\circ \text{ K})$$

$$\Delta H_v^\circ \text{ (298)} = 132.5 \pm 2.0$$

$$\text{B.P.} = 4000 \pm 100^\circ \text{ K.}$$

More complete data on Pd will be presented together with data on other platinum metals. The calculated vapor pressures and least-squares lines for platinum, iridium, and rhodium are shown in Figures 1-3, respectively. The data of Jones, Langmiur, and Mackay; and Dreger and Margrave are also compared with the present measurements of the vapor pressure of platinum in Figure 1.

Simultaneously with the present investigation, the vapor pressure of the substances have been measured by other laboratories using different approaches to the experimental problems involved. The body of data will be discusses against the background of the techniques with the aim of focussing attention on some possible significant differences in the results obtained by the different laboratories.

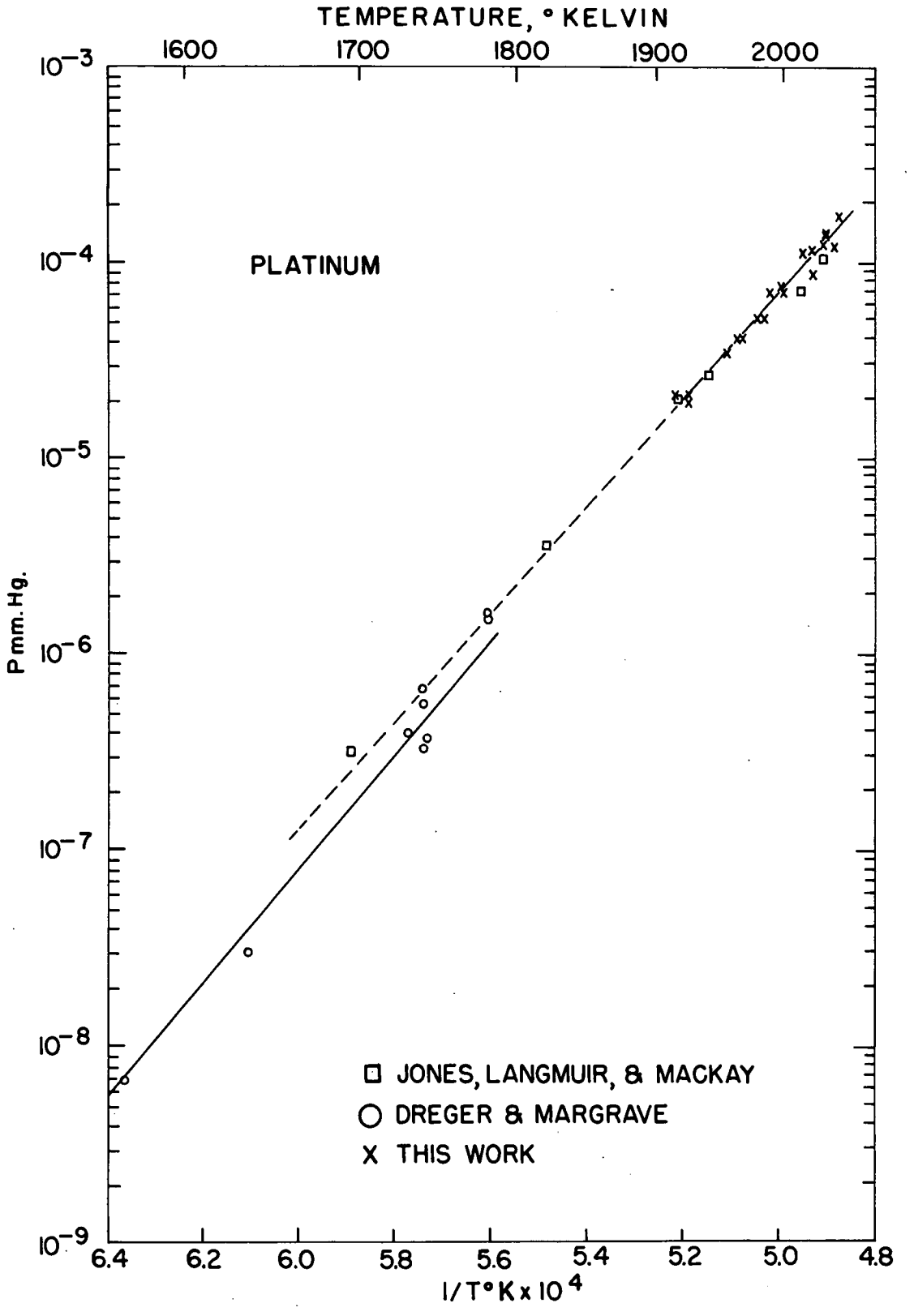
TEMPERATURE, ° KELVIN
1600
1700
1800
1900
2000
PLATINUM
P mm. Hg.
10^{-3}
10^{-4}
10^{-5}
10^{-6}
10^{-7}
10^{-8}
10^{-9}
6.4
6.2
6.0
5.8
5.6
5.4
5.2
5.0
4.8
1/T°K x 10^4
JONES, LANGMUIR, & MACKAY
DREGER & MARGRAVE
THIS WORK

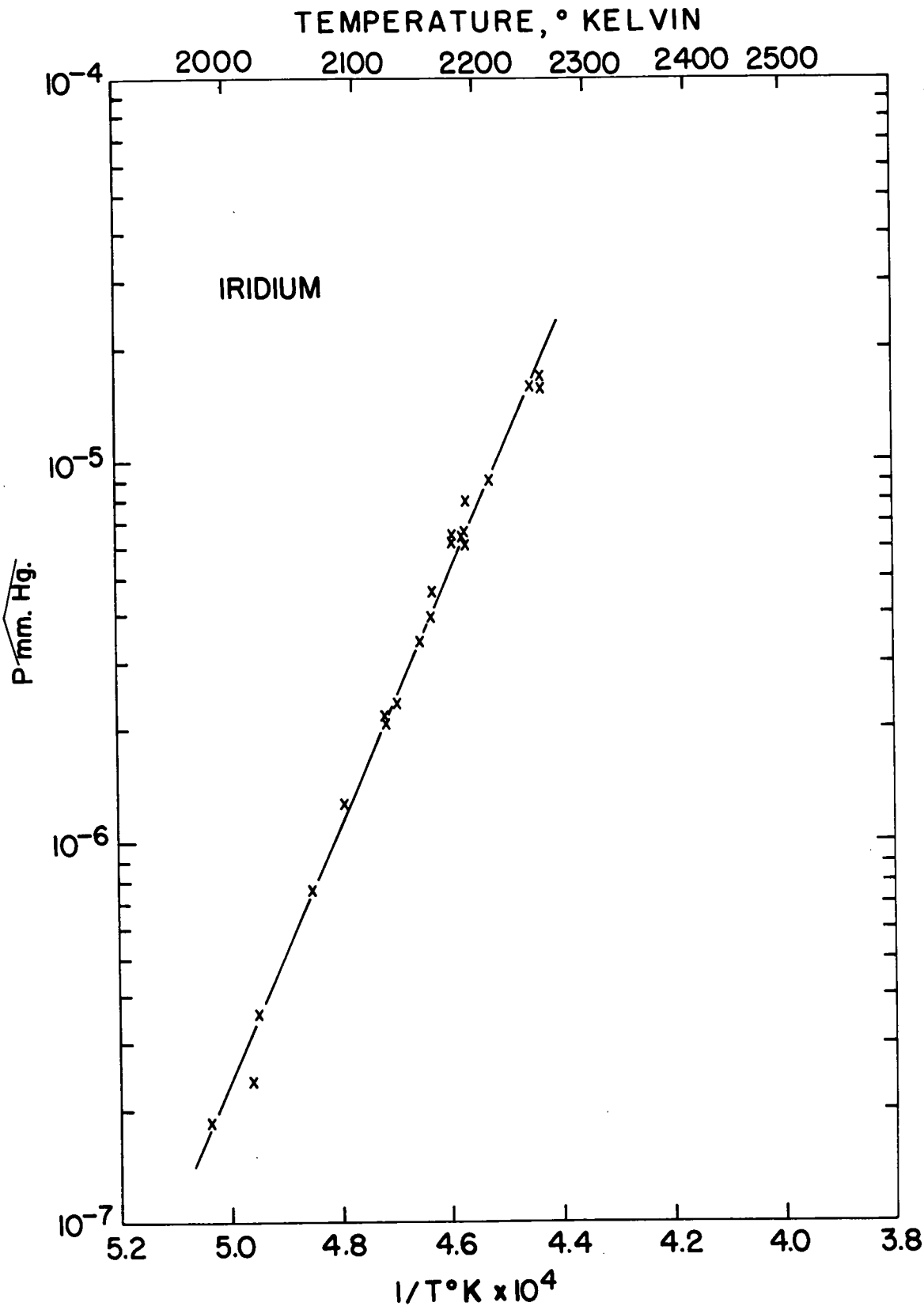
TEMPERATURE, ° KELVIN
2000
2100
2200
2300
2400
2500
IRIDIUM
P mm. Hg.
10⁻⁴
10⁻⁵
10⁻⁶
10⁻⁷
5.2
5.0
4.8
4.6
4.4
4.2
4.0
3.8
1/T°K x 10⁴

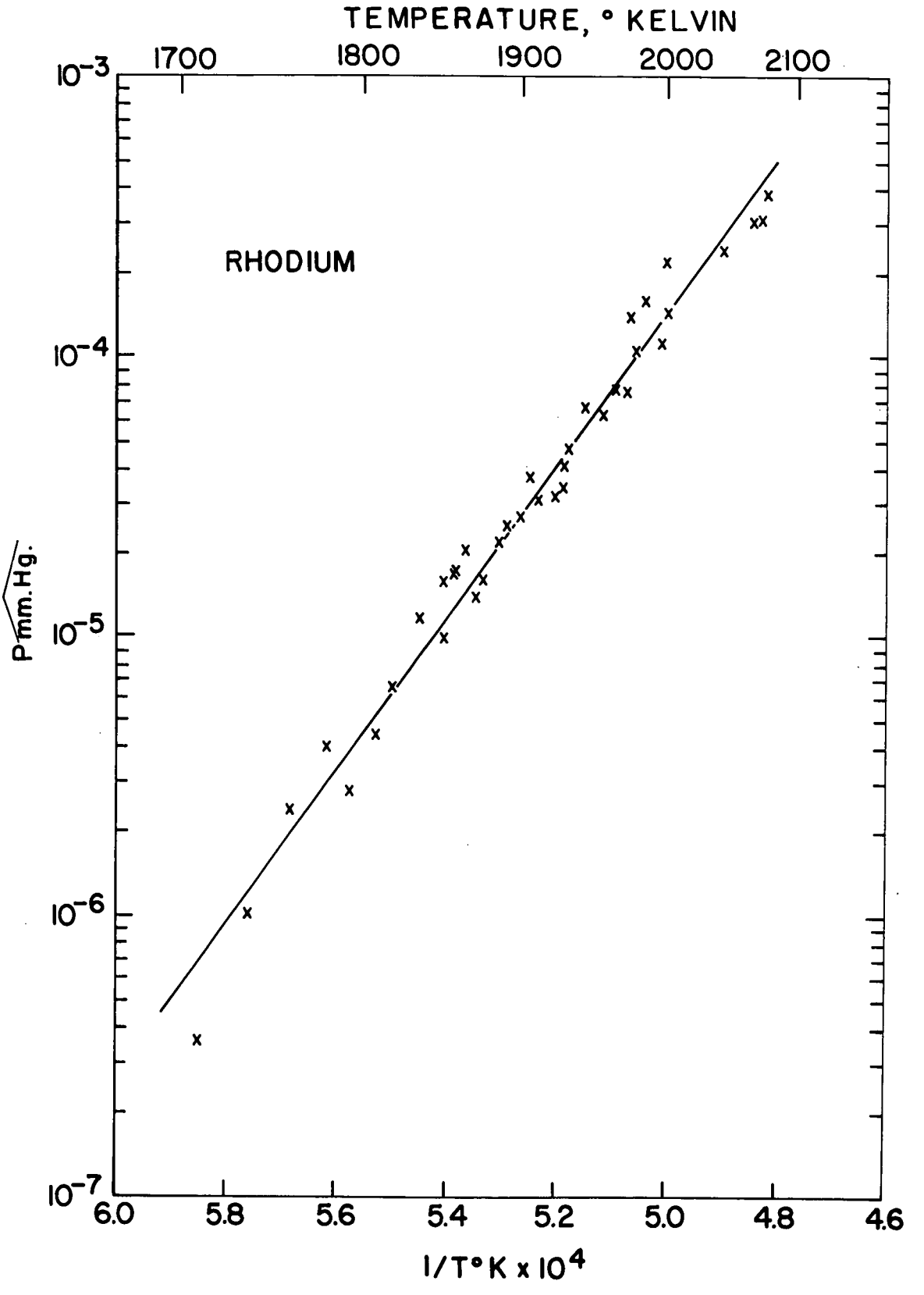
TEMPERATURE, ° KELVIN
1700
1800
1900
2000
2100
RHODIUM
P mm.Hg.
10-3
10-4
10-5
10-6
10-7
6.0
5.8
5.6
5.4
5.2
5.0
4.8
4.6
1/T°K x 10^4

THE ULTRAVIOLET BANDS OF MAGNESIUM HYDROXIDE AND OXIDE

Leo Brewer and Sandor Trajmar

In spite of the importance of MgO as a refractory material the vaporization processes of MgO are still not firmly established (1). High temperature vapors containing magnesium characteristically show a number of spectral bands in emission or absorption. A number of these bands have been analyzed (2, 3, 4) and have been shown to be due to the diatomic molecule MgO. A rather complex band system around 3800 A has not been capable of analysis in the past (5), and there are indications (5, 6) that the band is due to a mixture of two band systems, one associated with MgOH, and the other with some oxide of Mg.

In the present work, the bands have been studied in the King furnace and in a vacuum arc with elimination of water and hydrogen which are normally present and with addition of hydrogen, argon, oxygen, and water. The intensity changes were compared with the intensity changes of the known MgO and MgH bands.

The results show that the band system is indeed a composite of two separate systems. One of these virtually disappears along with disappearance of the MgH bands if water and hydrogen are minimized. Upon addition of hydrogen to MgO, this hydroxide band shows roughly the square root dependence of intensity upon hydrogen pressure expected for MgOH. Comparison of the hydroxide spectra with the known MgO bands has shown that they vary together when the magnesium oxide activity is varied. (6, 7) Thus there is good support for the formula MgOH.

When hydrogen and water are minimized, the remaining bands are still quite complex. The intensity of these bands varies together with the intensity of the known MgO bands. The difficulty of complete elimination of the interfering hydroxide bands makes it difficult to obtain sufficiently accurate measurements to distinguish between a band system of Mg_2O_2 or a triplet band of MgO which might have similar complexity.

Table 1

The Most Prominent Hydroxide Bands in the Furnace Spectrum

Wave length in A	Degr.	Wave length in A	Degr.
3660.1	V	3783.36	V
3676.0	V	3784.52	V
3684.06	V	3792.78	V
3686.4	V	3797.44	V
3695.09	V	3802.40	M
3703.25	V	3808.82	V
3704.09	V	3810.17	V
3707.9	V	3819.23	V
3708.80	V	3834.80	M
3709.34	M	3845.08	M
3719.60	V	3846.93	M
3724.8	M	3848.56	M
3731.76	V	3849.68	V
3732.37	M	3854.9	V
3742.19	M	3859.7	V
3747.07	M	3876.82	V
3751.34	M	3880.16	V
3759.37	M	3882.5	V
3770.63	V	3901.16	V
3772.9	M	3914.64	M
3782.0	V	3919.1	V
		3936.2	V

Letters V and M indicate that the bands are degraded towards violet or have only headless maximum.

Table 2

The Most Prominent Oxide Bands Observed in Vacuum Arc

Wave length in A	Degr.	Wave length in A	Degr.
3639.45	M	3790.96	R(?)

Table 2
(Con't.)

3672.11	R	3798.24	R
3674.77	R	3798.36	R
3677.63	R	3804.16	R
3680.92	R	3804.31	R
3684.46	R	3805.28	R
3695.98	M	3810.30	R
3698.53	R	3815.70	R
3720.66	V	3817.53	R
3720.96	V	3821.51	R
3721.40	V	3824.4	V
3724.9	V	3854.80	M
3766.10	R	3855.21	R
3771.80	R	3859.54	V
3772.33	R	3874.19	M
3777.40	R	3887.12	R
3777.81	R	3895.47	M
3782.65	R	3902.60	M
3784.20	R	3906.82	R
3788.47	R	3911.38	R
		3916.39	R

R, V, and M mean: degraded to red, violet, or headless maximum.

Most of the bands listed by Gaydon and Pesic (5) have been confirmed by the present work and are listed in Tables 1 and 2. The group of oxide bands between 3639.45 and 3724.9 A and the group between 3824.4 and 3916.39 A are especially complex and indistinct with degradation in either direction while the group between 3766.10 and 3821.51 A has more of the character of a diatomic spectrum. Thus it is possible that the spectral region contains bands of three species, e.g., MgOH, MgO, and Mg_2O_2. It is hoped that it might be possible to analyze photographs of the oxide spectrum under hydrogen free conditions using the 21 foot spectrograph.

References

1. L. Brewer and A. W. Searcy, Am. Rev. of Phys. Chem. 7, 259(1956).

2. P. C. Mahanti, Ind. J. Phys. 9, 455 (1935).

3. R. F. Barrow and D. V. Crawford, Proc. Phys. Soc, London 57, 12 (1945).

4. A. Lagerquist and V. Uhler, Arkiv. för Fysik 1, 459 (1949).

5. A. G. Gaydon and D. Pesic, Proc. Phys. Soc. A 73, 244 (1959).

6. E. M. Bulewicz and T. M. Sugden, Trans. Far. Soc. 55, 720 (1959).

7. L. Brewer and R. Porter, J. Chem. Phys. 22, 1867 (1954).

VAPOR PRESSURES OF TUNGSTEN OXIDES

P. E. Blackburn

Although there have been several studies regarding the vaporization of tungsten trioxide and one concerned with tungsten dioxide, there are no data available on the vaporization of the other oxides. In addition there are discrepancies among the various authors' calculated heats and entropies of sublimation for the vapor pressure over WO_3. The thermal values calculated for WO_2 vaporization do not coincide with literature values for solid dioxide and trioxide. The subject of this research covers the pressures over the four tungsten oxides, the related thermal values, and the high temperature phase diagram of the tungsten–oxygen system.

In these studies vapor pressures were measured by determining effusion rates from a Knudsen cell or evaporation from a surface (the Langmuir method). Under both conditions the rates were found by measuring the weight change of the sample with time, using either a quartz beam balance or a quartz helix sealed inside a vacuum system. The reproducibility of these balances varied between 0.2 and 30 μg.

A resistance furnace controlled to $\pm$ 0.5° C was used for lower temperature measurements. At higher temperatures an induction furnace heated a thick walled molybdenum susceptor in which the sample was heated by radiation. The heavy walls (~ .27") were necessary to shield the sample from the magnetic field within the induction coil.

Results: The vapor pressure over WO_3 was measured between 1040 and 1260° K by the Langmuir method using a pellet of WO_3 fused by arc melting in an argon atmosphere. Pressures determined from this sample varied between 2×10^{-12} and 5×10^{-8} atm. After a number of measurements were made using the pellet the rate of evaporation dropped by a factor of 10. The remaining determinations yielded lower pressures. When the fused sample was oxidized to $WO_{3.00}$, it was found that the mean composition of the reduced sample was $WO_{2.990}$. Vapor pressures of the fused sample after oxidation were the same as those before the pressure drop was observed. The oxygen loss of the sample is believed to have occurred during the arc melting process when the sample was at least 500° hotter than it was during the vapor pressure experiments.

At the melting point, the oxygen dissociation pressure is greater than 10^{-2} mm. The large drop in pressure is believed to be due to surface depletion of WO_3.

Effusion measurements over WO_3 using a platinum Knudsen cell between 1180 and 1510° K were made in the pressure range of 3×10^{-9} to 2×10^{-4} atm. In all cases the gas phase was assumed to consist of W_3O_9 molecules, the predominate species found by Berkowitz, Chupka, and Inghram. Other gas species are also present, but only the relative concentration of W_4O_{12} has been precisely measured. The slope and intercept of the Van't Hoff curve computed by least squares gives a heat of sublimation of 123.6 ± 1.9 kcal/mole of W_3O_9 and an entropy of sublimation of 65.5 ± 1.0 eu/mole of W_3O_9 computed at the 9.5% confidence level. It is estimated that the other gas species whose concentrations are not known may increase the total uncertainties in the heat of sublimation to ± 5 kcal and in the entropy to ± 2.6 e.u. Table 1 compares literature values with those determined here for the vaporization of WO_3 to W_3O_9.

Table 1
Heat and Entropy of Vaporization of WO_3

Author	Temperature Range °K	ΔH_T kcal/mole of W_3O_9	ΔS_T e.u./mole of W_3O_9	ΔF_{1350} kcal/mole
Ueno	1343–1393	112.6±3	58.4	33.8
Berkowitz et al	1340–1460	130 ± 5	69.5	36.2
Blackburn et al	1314–1581	108 ± 15	54.1	35.0
This Research	1035–1506	123.6±5	65.5	35.2

It is believed that the values found here have considerable reliability due to the wide temperature and pressure range covered in this research.

There was excellent agreement between the pressures measured by Knudsen and by Langmuir methods. The two sets of data give a WO_3 evaporation coefficient lying between 0.72 and 1.0 where the range is calculated at the 95% confidence level.

This uncertainty, a function of internal consistency, may be compared to the corresponding reproducibility for the pressure measurements of 12%.

Vapor pressures as a function of oxide composition were determined by reducing WO_3 to a lower composition and then measuring the rate of effusion at constant temperature. Since it was established by Blackburn et al that the lower oxides vaporize by disproportionation to $(WO_3)_n(g)$ and the next lower solid phase, the pressure could be measured while the solid phase changed continuously. The composition of the solid phase was determined from the equation:

$$a\ WO_{3-x}(s) = \frac{b}{n}\ (WO_3)_n(g) + c\ WO_{3-y}\ (s)$$

where a, $\frac{b}{n}$, and c are the number of moles of each oxide, x is the gram-atoms of oxygen per mole removed from WO_3 during the hydrogen reduction, (3-y) is the oxygen-tungsten ratio of the solid phase after removing $\frac{b}{n}$ moles of $(WO_3)_n$, and n is the degree of polymerization in the gas phase. In this study n has been assumed to be 3 over all solid phases.

The pressures were measured between 1450 and 1630° K and from $WO_{2.95}$ to $WO_{1.7}$. The phase limits of the tungsten-oxygen system were determined from the degree of change in vapor pressure with tungsten enrichment of the solid phase. The metal rich end of the two phase regions exhibited a gradual decrease in oxide pressure as vapor was removed so that these end points were difficult to determine precisely. Table II presents the phase limits found with measurements at six temperatures.

Although there was no direct determination of the homogeniety range of WO_3, comparison of vapor pressures over WO_3 with the pressures measured at $WO_{2.95}$ indicate that WO_3 must have a very narrow homogeneity range.

The vapor pressures over the two phase regions, studied using a platinum Knudsen cell were employed to calculate the thermal values for vaporization, again assuming W_3O_9 to be the gas species. Since the dioxide disproportionates to trioxide gas and tungsten metal, the possibility exists that the tungsten might dissolve in the platinum,

resulting in a trioxide pressure in equilibrium with dissolved tungsten rather than tungsten alone.

Table II
Phase limits of Tungsten Oxides
1480 to 1630°K

Phase	Oxygen–Tungsten Ratios
WO_3	limits not detected
$W_{20}O_{58}$	2.94 – 2.88
$W_{18}O_{49}$	2.74 – 2.70
WO_2	2.02 – 1.98

Vapor pressures over WO_2 + W were measured in a tungsten cell as well as in the platinum cell. Results using the tungsten cell were about 30% lower than the measurements made in the platinum cell. This difference may be compared to a standard deviation of 10% for the pressures determined in the tungsten cell. The vapor pressure of platinum at these temperatures, is too low to account for the difference between these two measurements. A least squares fit to the data gives the thermal values shown in Table III where the heats of vaporization for $W_{18}O_{49}$ and $W_{20}O_{58}$ have been adjusted to conform with those for WO_2 and WO_3.

These values are consistent with the available thermal data for the solid phases.

During the tungsten oxide phase limit measurements, it was found that experiments made at temperatures below 1200 and 1250° C failed to give results consistent with those at higher temperatures. The principal difference was the absence of definite single phase and two phase regions. Instead the pressure, as a function of oxide concentration, changed continuously through the experiment. It is believed that disagreement between this work and that done on WO_2 by Blackburn et al is due to the latter's attempt to measure pressures at temperatures where the solid phase does not readily approach equilibrium.

Table III
Thermal Values for Vaporization of Tungsten Oxides

Reaction	ΔH_{1500} kcal/mole of W_3O_9	ΔS_{1500} eu/mole of W_3O_9
$\frac{9}{2} WO_2(s) \quad W_3O_9(g) + \frac{3}{2}W(s)$	146.4 ± 9.2	72.9
$\frac{3}{13}W_{18}O_{49}(s) \quad W_3O_9(g) + \frac{15}{13}WO_2(s)$	129.9 ± 6.1	64.8
$\frac{15}{64}W_{20}O_{58}(s) \quad W_3O_9(g) + \frac{3}{32}W_{18}O_{49}(s)$	125.9 ± 10.3	65.0

The pressure drop observed during the Langmuir measurements on $WO_{2.99}$ may be due to the lack of solid phase equilbrium at lower temperatures, as mentioned above. The lower pressure is about 30 % of that calculated over $W_{20}O_{58}$, suggesting an evaporation coefficient for this phase of 0.3. However, the probable absence of solid phase equilibrium does not permit definite conclusions about the observed decrease in vapor pressure. Analysis of the diminution in pressure below that over stoichiometric WO_3 indicated that the pressure drop does not involve a diffusion mechanism.

CONTRIBUTION TO THE THERMOCHEMISTRY OF CARBON MONOSULFIDE

H. Schäfer and H. Wiedemeier

According to spectroscopic measurements the existence of carbon monosulfide CS in explosions of CS_2–O_2 mixtures, in the photolysis of CS_2 and in high frequency discharges in a CS_2 atmosphere is well confirmed. The reactions as

$$CS_2(g) + C(s) = 2\ CS(g),$$

and

$$MeS(s) + C(s) = CS(g) + Me(g),$$

(Me = metal) are appropriate systems for investigations by which one can derive the enthalpy of formation of carbon monosulfide.

Effusion measurements with MnS and carbon in graphite crucibles led to a more accurate value for ΔH (CS, 298).

Reaction of CS_2 with C filaments at high temperatures: By means of the reaction:

$$CS_2(g) + C(s) = 2\ CS(g),$$

one can describe a transport of carbon. The application of C filaments as carbon that could be heated by an electric current allows one to follow the reaction by current measurements.

At about 1500° C one can assume the following equilbrium condition at the glowing filament:

(1) $CS_2(g) + C(s) = 2CS(g)$,

(2) $CS_2(g) = C(s) + S_2(g)$,

(3) $2\ CS_2(g) = 2\ CS(g) + S_2(g)$.

A change of total pressure will affect each reaction differently. At low pressures reaction (1) will be dominant, at higher pressures reaction (2). The cross-section of the filament becomes changed, its electrical resistance changes in the opposite direction. Reaction (3) represents the condition when the change of resistance is zero.

The data of this pressure inflection point, $p_{(CS_2)}$ and T, for which all three equations are valid, were found to be:

T(Start): 1773°K, $P(CS_2)$ (Start): 100mm = 0.13atm.

The total pressure at the filament is:

$$\Sigma p = P_{CS} + P_{CS_2} + P_{S_2} = 0.13\text{atm}.$$

Reaction (2) gives for 1773° K $P_{S_2}/P_{CS_2} = 0.24$. In combination with the relation for ΣP we get $P_{S_2} = 0.018$ atm and then $P_{CS_2} = 0.076$atm. Equation (3) finally gives $P_{CS} = 0.036$atm. On the basis of reaction (1) for which all data except $\Delta H(CS)$ are known one can now calculate the heat of formation of CS:

$$\Delta H(CS, 298) = 58 \pm 5 \text{ kcal}.$$

Evaporation experiments with mixtures of metal–sulfides and carbon:

For the investigation of the reaction between metal–sulfides and carbon known quantities of MgS, Cu_2S and MnS were heated in graphite crucibles to 1300–1400° C. From the total weight loss and the analytical determination of Me and S in the residue the atomic ratio of evaporated Me, S and C can be calculated. Without consideration of CS formation this ratio Me:S:C is calculable from known data for the following assumed reactions:

(1) $MeS(s) = Me(g) + {}^{1}/_{2}\ S_2(g)$,

(2) $S_2(g) = 2\ S(g)$,

(3) $CS_2(g) = C(s) + S_2(g)$.

The numbers are:

	MgS	Cu_2S	MnS	Remarks
°C	1300	1300	1400	
C:S	0.27	0.27	0.28	without CS formation
C:S	0.48	0.75	1.0	experimental results

The difference is due to a formation of CS according to

(4) $CS_2(g) + C(s) = 2CS(g)$.

The partial pressure of CS for reaction (4) is now calculable, and this leads to the only unknown datum for this equation:

with	MgS	Cu_2S
$\Delta H(CS, 298)$, kcal	64	59

Differences between these values are probably due to different, unknown volatilities of the sulfides to form gaseous molecules. With the result of the C–filament experiments the preliminary value is:

$$\Delta H(CS, 298) = 60 \pm 6 \text{kcal}$$

Determination of Equilibrium in the Mn–S–C system: For more exact investigations effusion measurements according to the Knudsen method have been carried out with MnS and C in graphite effusion cells. Before investigation the total system the volatility of MnS was determined by the same method in Mo crucibles at 1400° C. For three different states of MnS in the gas phase the mean values for ΣP over MnS(s) are at 1400°C:

State in gas–phase	Mn+S	$Mn+\frac{1}{2}S_2$	MnS
P (atm x 10^5)	1.63	1.41	1.15

These numbers are used later for the calculation of $\Delta H(CS)$.

For the investigation of the total system according to the reaction

$$MnS(s) + C(s) = CS(g) + Mn(g),$$

high vacuum and temperatures from 1300–1500°C were applied. The effusion orifice of the graphite cells were calibrated with zinc vapor.

From the observed weight losses, the experimental temperature and time one can calculate the equilibrium pressure ΣP of the considered reaction by means of the Knudsen formula. Since this is a reaction between solid phases, equilibrium conditions are reached when the weight losses and hence the pressure are independent of the starting amount of MnS and C. By a calculation of error it could be shown that the application of the mean molecular weight for Mn and CS in the Knudsen formula is less than 0.6 % and, therefore, within the general experimental error range of ± 1% of the value for $\Delta H(CS)$.

The entropies and C_P functions of all reactants of the investigated reaction are known. The equilibrium constant $K_P = P_{CS} \times P_{Mn}$ is calculable by means of ΣP. Therefore, using the third law method, one can solve this equation for the enthalpy of reaction:

$$\Delta H(CS(g), 298) = \Delta H(\text{reaction}, 298) - (\Delta H(Mn(g), 298) - \Delta H(MnS(s), 298)).$$

For the decisive difference $\Delta H(Mn) - \Delta H(MnS)$ two values are available: Data from the literature for $\Delta H(Mn(g), 298) = 68.34$kcal and $\Delta H(MnS(s), 298) = 49.49$kcal give the value 117.8 kcal.

The evaluation of our measurements of the MnS decomposition according to the equation:

$MnS(s) = Mn(g) + {}^{1}/2\ S_2(g)$ in Mo crucibles gives 123.9kcal for this difference.

During all investigations in the MnS–C–system, the evaporation ratio of C:S was always found to be 1:1 within the experimental error. The literature data for Mn(g) and MnS(s) are in contradiction to these observations. The experimental results force one to the assumption that those data have to be corrected.

Combining the experimental value with $\Delta H(react., 298) = 178.6kcal$ for the CS reaction, one obtains:

$$\Delta H(CS(g), 298) = 54.7kcal,$$

while the literature data for Mn(g) and MnS(s) give:

$$\Delta H(CS(g), 298) = 60.7kcal.$$

Since at the present it is not decided which value for the $\Delta H(Mn) - \Delta H(MnS)$ term is the more reliable one, the mean value is ued for further calculations:

$$\Delta H(CS(g), 298) = 58 \pm 3\ kcal.$$

A greater accuracy should be obtainable by means of further measurements with MnS in Mo crucibles.

From the dissociation energy of CS by A. G. Gaydon ($7.2 \pm$ lev) one can calculate for the heat of formation of CS:

$$\Delta H(CS, 298) = 59 \pm 23kcal.$$

With the value for $\Delta H(CS, 298) = 58 \pm 3kcal$ and strictly on the basis of experimental results of C. J. B. Fincham and R. A. Bergman (Journal of Metals, 690 (1951)), who investigated the equilibrium conditions between diluted solutions of sulfur in carbon saturated liquid iron and gas mixtures of Ar and CS_2, an approximate value for the enthalpy of formation of the HS molecule could be calculated:

$$\Delta H(HS, 298) = 15kcal.$$

Finally, investigations of desulfurization of carbide melts by R. Juza and K. Bunzen (Z. anorg. allg. Chemie 298, 334 (1958)) could be interpreted in agreement with experimental results of Juza and Bunzen that the sulfur evaporates as CS.

ON THE STABILITY OF SYMMETRIC DIATOMIC MOLECULES OF THE TRANSITION ELEMENTS

G. Verhaegen, F. E. Stafford, P. Goldfinger, and M. Ackerman

In the last decade mass spectrometry has made possible the identification and the determination of the dissociation energies of many symmetric diatomic molecules (1). At first the existence of these molecules may have been surprising. Today, it leads us to believe that all the elements, apart from noble gases, form diatomic molecules. No symmetric diatomic molecules of the transition elements have yet been found. The aim of the present work is to predict the conditions under which these molecules might be observed.

In order to define these conditions it is necessary to estimate not only the dissociation energies of these molecules, but also their free energy functions. It is useful to represent their "chemical stability" by the free energy change for the principal net reaction:

$$\Delta F^\circ_T = -RT\ln p_X/p_{X_2} = D^\circ_o - \Delta H^\circ_{o\,(vap)} - T\left[(fef)_{Xg} + (fef)_{Xs} - (fef)_{X_{2g}}\right]^\circ_T$$

$$= \Delta H^\circ_{o\,(vap)}\,(1-\alpha)/\alpha - T(\Delta fef)^\circ_T \qquad (1)$$

where p is the saturated vapor pressure, D°_o the dissociation energy of X_2 gas, $\Delta H^\circ_{o\,(vap)}$ the enthalpy of vaporization of X, $fef = -(F^\circ_T - H^\circ_o)/T$, the free energy function, and α is defined as $\Delta H^\circ_o(vap)/D^\circ_o$.

A few years ago, Pauling (2) observed that $\alpha \approx 1.5$ for alkali metals. This relationship can be extended. Figure I. shows α vs. atomic number for all elements for which data are available. The elements seem to fall in three distinct classes: $\alpha \approx 1.2$ to 2.0 for the elements of groups I_A, I_B, III_B, IV_B with the electron structures s^1, s^2p^1, s^2p^2; $\alpha \geq 5$ for groups II_A and II_B with structures s^2, $d^{10}s^2$; and finally $\alpha = 0.5 - 1.0$ for groups V_B, VI_B, VII_B which include all the familiar molecules formed from atoms with the structures s^2p^3, s^2p^4, s^2p^5. The first two classes listed above, with $\alpha > 1$ are the high temperature molecules.

The concentration of molecules in the saturated vapor increases with increasing temperature. We note that in each class α varies by hardly 50% while D_o° (kcal/mole) varies by about a factor of 10: from 10.8 (Cs_2) to 140 (C_2), from 22 (At_2) or 35.5 (I_2) to 225 (N_2), and from 1.4 (Hg_2) to 15.6 (Be_2).

It is interesting to remark that ΔH_o° and D_o° have a quite irregular sequence in group I_B (Cu, Ag, Au) but $\alpha = 1.8 \pm 0.1$ remains constant.

The transition elements can be divided into three groups according to their electronic structures: six elements, Cr, Nb, Mo, Ru, Rh, and Pt have a half full s sub-shell (s^1d^{n-1}) ; Pd has a full d sub-shell (d^n) ; and the others have a full s sub-shell (s^2d^{n-2}) ; n represents the number of electrons in the outermost shell.

Applying the above correlation between α and electronic structure to the transition elements, we expect $\alpha \approx 2$ for the six elements with the $d^{n-1}s^1$ configuration and $\alpha > 5$ for the others.

To complete the information required to predict the experimental conditions necessary for the observation of these molecules, we have calculated their free energy functions. Although these calculations include estimates of electronic states, vibration frequencies and interatomic distances, this does not impair the significance of the results. (3)

By mass spectrometry one can observe concentrations of X_2 in X as small as 10^{-4}. Thus among the six metals with α presumably equal to 2 (s^1d^{n-1}) Cr_2 should be observable at about 1850° K with $P_{Cr} = 2.10^{-4}$ atm. The other five should be observed at about 3000° K with vapor pressures between 10^{-3} and 10^{-2} atm. Reliable measurements are difficult to obtain under such conditions. However, we have tried to surmount these difficulties and have succeeded in finding the limits $D_o^\circ(Cr_2) < 40$ and $D_o^\circ(Pd_2) < 35$ kcal/mole.

Using another method we have calculated values of $D_o^\circ(Cr_2)$ and $D_o^\circ(Pd_2)$. Inserting our recent values of $D_o^\circ(AuPd) = 35$ and $D_o^\circ(AuCr) = 51$ kcal/mole in the empirical formula (4).

$$D^{\circ}_{o}(XY) - \tfrac{1}{2}\left[D^{\circ}_{o}(X_2) + D^{\circ}_{o}(Y_2)\right] = (X_X - X_Y)^2 \qquad (2)$$

where X represents Pauling's electronegativity we calculate $D^{\circ}_{o}(Cr_2)=38$ and $D^{\circ}_{o}(Pd_2) = 17$ kcal/mole. These results give $\alpha_{Cr} \approx 2.5$ and $\alpha_{Pd} \approx 5$ and seem to confirm our correlation with α.

It might be worthwhile noting here a relationship existing between the electronic states and enthalpies of sublimation of the transition elements: that is $\Delta H^{\circ}_{o}(X) = A - B \Sigma \epsilon (X)$, where $\Delta H^{\circ}_{o}(X)$ is the enthalpy of sublimation of X, $\epsilon(X)$, the energy of the first excited electronic levels of X (d^n, $d^{n-1}s^1$, $d^{n-2}s^1p^1$) and A and B parameters constant throughout a given period. Figure II shows the measured and calculated values of $\Delta H^{\circ}_{o}(X)$ from Ca to Zn; for this period A = 181 kcal/mole and B = 0.5. As one can notice both curves coincide very well especially for the maximum (V) and the minimum (Mn). Other values* of A (206 and 250 kcal/mole) have been found for the following two periods. This might mean that in their crystals, all the transition elements are in the same promotional state due to a contribution of the levels d^n, $d^{n-1}s^1$, $d^{n-2}s^2$ and $d^{n-2}s^1p^1$, and that the heat of sublimation to this promotional state is constant for each period.

---

* The electronic levels in the 2d and 3d transition element series are not so well known, therefore the correlation is less definite.

References.

(1) M. G. Inghram et J. Drowart, Mass Spectrometry Applied to High Temperature Chemistry, in High Temperature Rechnology, Proceedings of a Symposium, Asilomar, Calif. McGraw – Hill (1960).

(2) L. Pauling Phys. Rev. 54, 899 (1938).

(3) M. Ackerman, P. Goldfinger, F. E. Stafford, G. Verhaegen (to be published.)

(4) L. Pauling, The Nature of the Chemical Bond, Cornell University Press, Ithaca, N. Y. (1960).

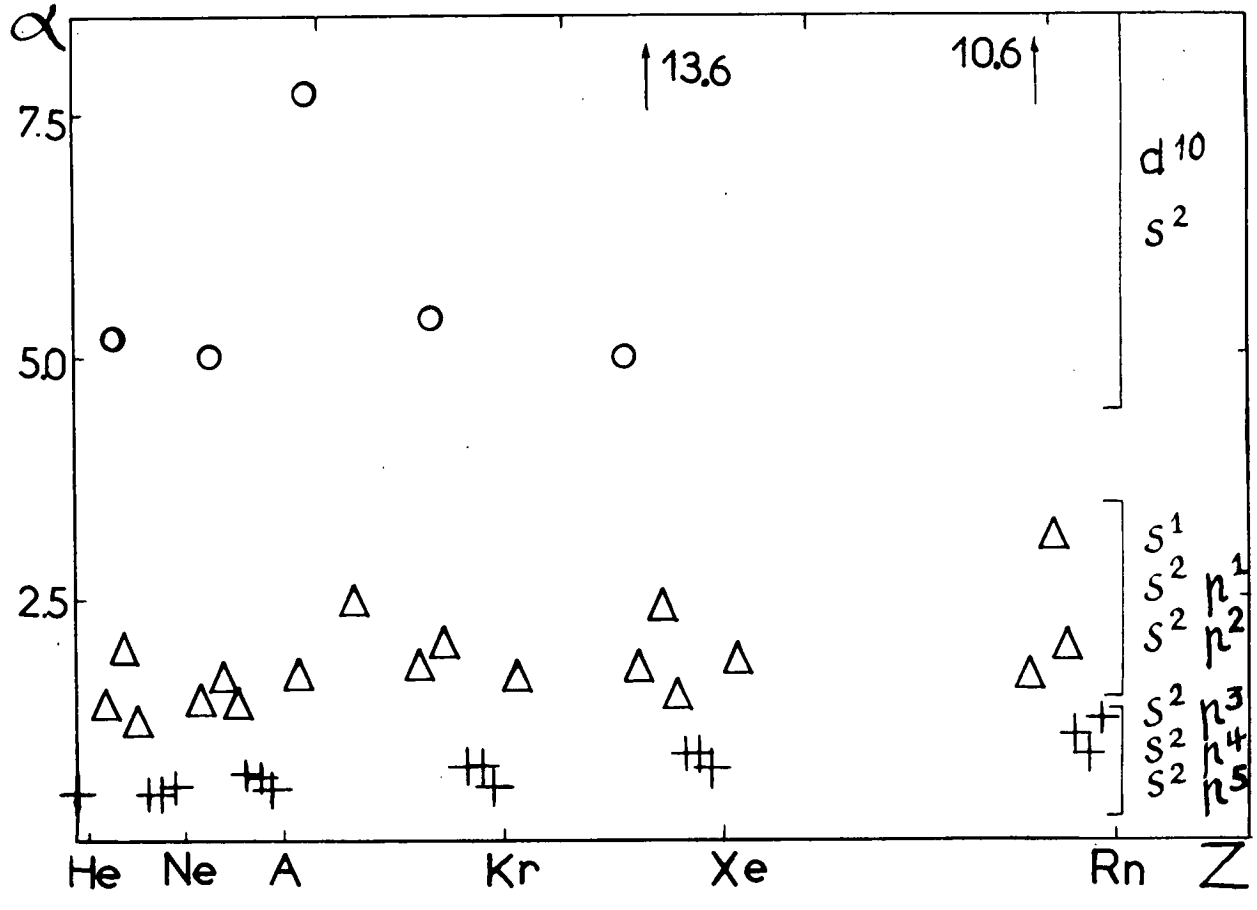

Fig. I. $\alpha = \Delta H^{\circ}_{\circ(vap)} D^{\circ}_{\circ}$ vs. Z, where $\Delta H^{\circ}_{\circ(vap)}$ is the enthalpy of sublimation of the monoatomic species $D^{\circ}_{\circ}$ is the energy of dissociation of the symmetric diatomic molecule and Z the atomic number. Crosses (X) indicate elements for which $\alpha = 0.5 - 1.0$, triangles (Δ) those for which $\alpha \geq 5$ and circles (O) those for which $\alpha = 1.5 - 2.0$. The structures of the outer electronic shells of the atoms are indicated on the right-hand side of the figure.

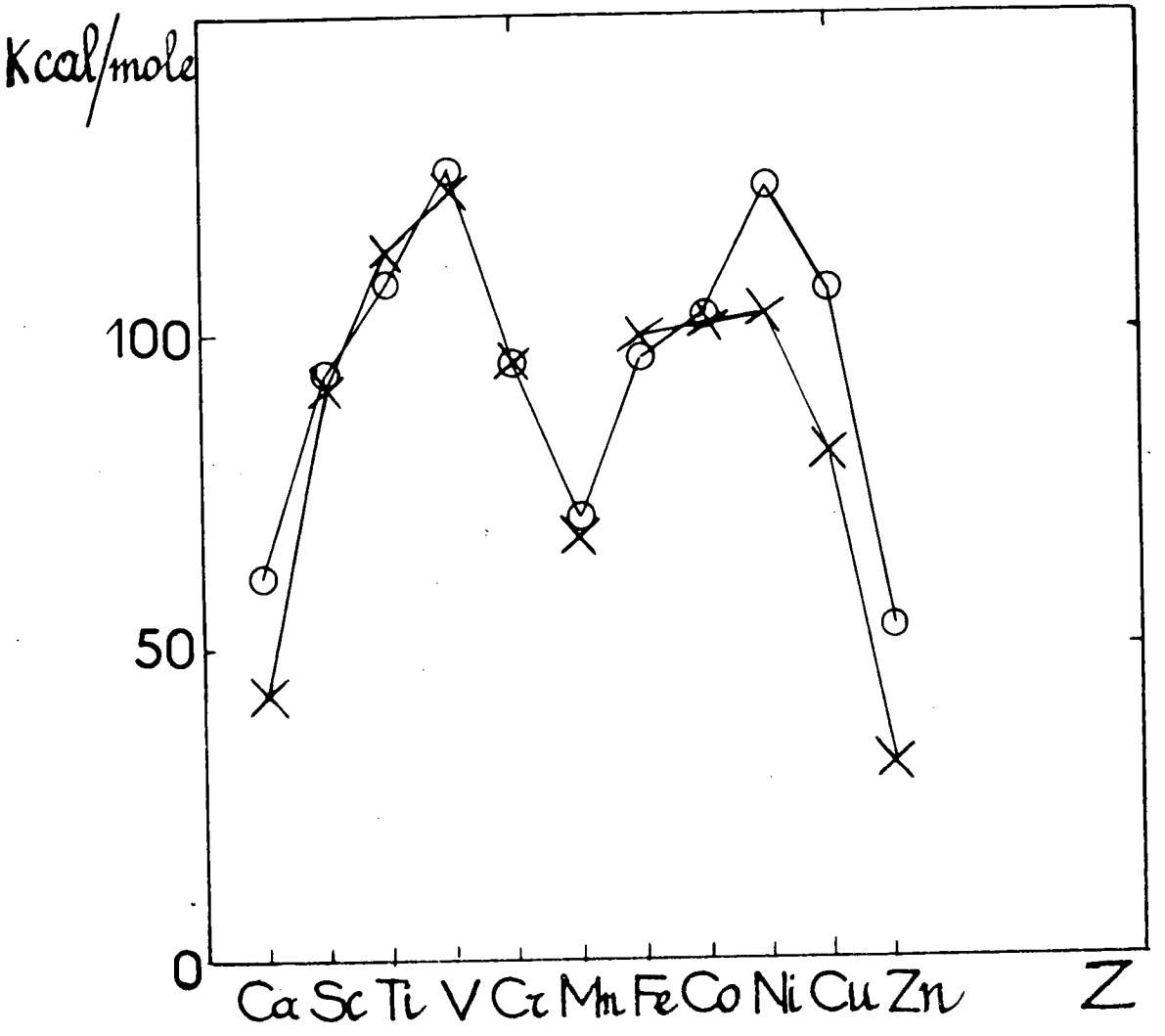

Fig II.

Measured (X) and calculated (O) enthalpies of sublimation, in kcal/mole for the elements ranging from Ca to Zn. ΔH°_{o} (vap)$_{calc.}$ = 181 − 0.5 $\Sigma\varepsilon$(X) kcal; ε(X) is the excitation energy to the lowest d^n, $d^{n-1}s^1$, $d^{n-2}s^2$, $d^{n-2}s^1p^1$ levels of the atom.

THE CALCULATION OF THERMODYNAMIC FUNCTIONS OF GASES IN WIDE TEMPERATURE RANGE

L. V. Gurvich

Thermodynamic functions of 335 gases in ideal state are tabulated in the handbook, "Thermodynamic Properties of Individual Substances", being published in the U.S.S.R. (for 22 gases in the range 293.15 – 20,000; for others 293.15 – 6,000°K). All these functions were calculated by the authors of the book.

The calculations of thermodynamic functions of monoatomic gases up to 20,000° K as well as of those with low ionization potentials (e.g. alkali and alkali–earth metals) were made with limitation of the partition functions according to the principal quantum number. All levels with $n \leq n_{max}$, including those unobserved in the spectra, were taken into account. Thermodynamic functions for 12 diatomic gases were calculated by direct summation over electronic, vibrational and rotational levels up to maximum quantum numbers v and j. For other diatomic gases calculations were made by the method of Gordon and Barnes, taking into account the following corrections: limitation of number of the rotational levels, existence of the excited electronic states and splitting of the rotational levels of the molecules in some electronic states. An obvious advantage of the Gordon–Barnes method mainly for the calculations at high temperature was demonstrated by comparing the date obtained by this method and that of Mayer and Geppert–Mayer.

For 13 simple polyatomic gases the calculations were made by the Gordon method, for others by approximation the rigid rotator – harmonic oscillator. The excited electronic states, centrifugical distortion of the molecules and other effects were taken into account.

The errors of the calculated values of thermodynamic functions of all gases were estimated. The coefficients in equation like

$$S^{\circ}_{T} = s \cdot \ln x + \sum_{n=-2}^{n=7} s_n \cdot x^n \qquad (x = T \cdot 10^{-4})$$

approximating with great accuracy the values of the thermodynamic functions from 293.15 to 6,000° K were found.

HIGH–TEMPERATURE CHEMISTRY OF THE CHLORIDES OF THE PALLADIUM–GROUP METALS*

Wayne E. Bell, Ulrich Merten, K. Tagami, and M. C. Garrison

The high–temperature chemistry of the chlorides of the palladium–group metals has been studied over the temperature range from 500° to 1500° C and over the chlorine pressure range of 0.1 to 1 atm.

Procedure: Condensed phases were identified using chemical analysis, thermal analysis, and X–ray techniques. Vapor pressures were determined by the transpiration method. Dissociation pressures were measured using both static and dynamic (transpiration) methods.

Vapor species were identified by studying the effect of chlorine pressure on vapor pressure. In this method of identifying vapor species, the equilibria

$$xM(s) + \frac{Y}{2} Cl_2 = M_x Cl_y\ (g) \qquad (1)$$

$$xMCl_z\ (s \text{ or } l) + \frac{Y - zx}{2}\ Cl_2 = M_x Cl_y\ (g) \qquad (2)$$

are studied in a temperature range where the condensed chloride, solid or liquid MCl_z, is stable over a portion of the chlorine pressure range. From the equilibrium constant for reaction (1) is obtained

$$\log P_{M_xCl_y} = \frac{Y}{2} \log P_{Cl_2} + \log K.$$

A similar expression is obtained for reaction (2), and y/2 and $(\frac{y - zx}{2})$ are evaluated from a $\log P_{M_xCl_y}$ versus $\log P_{Cl_2}$ plot. Since z is, in general, already known from other studies, x may then be evaluated.

---

* This work was supported under Contract AT(04–3) – 164 with the U. S. Atomic Energy Commission.

At higher temperatures, where condensed chlorides are unstable, this technique can be used only to determine y.

RESULTS

Ruthenium. The condensed chloride phase was studied and the results show that solid $RuCl_3$ is the only stable condensed chloride in the temperature range and chlorine pressure range studied. The dissociation pressure of the chloride was measured over the range 650° to 839° C. A log p vs. $\frac{1}{T}$ plot of the data yields at the mean temperature (1020° K) $\Delta H°_{1020} = -57.2 \pm 1.0$ kcal/mole and $\Delta S°_{1020} = -50.9 \pm 1.0$ e.u. for $Ru(s) + 3/2\ Cl_2 = RuCl_3(s)$. The dissociation pressure is calculated to be 1 atm. at 853° C.

The effect of chlorine pressure on vapor pressure was studied and the results indicate that $RuCl_3(g)$ and $RuCl_4(g)$ are the important vapor species. The trichloride vapor species was identified from the data obtained at temperatures where $RuCl_3(s)$ is unstable; therefore, the number of metal atoms in the vapor species can not be established from the data. The value is assumed to be one.

Vapor pressures were measured as a function of temperature. The data show that $RuCl_4(g)$ is the important vapor species over $RuCl_3(s)$ under the conditions studied. At 853° C and 1 atm chlorine pressure, $RuCl_4(g)$ reaches a maximum partial pressure of 0.065 atm. Above 853° C, where Ru(s) is the stable condensed phase at 1 atm chlorine pressure, the partial pressure of $RuCl_4(g)$ decreases with increasing temperature. At 900° C, $RuCl_3(g)$ becomes the important vapor species, and at 1500° C and 1 atm chlorine pressure it has a partial pressure of 0.16 atm. The temperature dependence data yield $\Delta H°_{1400} = +8.2 \pm 2.0$ kcal/mole and $\Delta S°_{1400} = +1.0 \pm 2.0$ e. u. for $Ru(s) + 3/2\ Cl_2 = RuCl_3(g)$; and $\Delta H°_{1400} = 24.6 \pm 3.0$ kcal/mole and $\Delta S°_{1400} = -27.2 \pm 3.0$ e. u. for $Ru(s) + 2\ Cl_2 = RuCl_4(g)$.

Rhodium. Results show that solid $RhCl_3$ is the only stable condensed chloride under the conditions studied. The dissociation pressure of the chloride was measured over the range 720° to 956° C and the data yield $\Delta H°_{1100} = -67.2 \pm 2.0$ kcal/mole and $\Delta S°_{1100} = -53.9 \pm 2.0$ e.u. for $Rh(s) + \frac{3}{2}\ Cl_2 = RhCl_3(s)$. The dissociation pressure reaches 1 atm at 974° C.

Chlorine pressure dependence data indicate that $RhCl_3(g)$ is the gaseous species of importance. Temperature dependence data show that the partial pressure of $RhCl_3(g)$ is 2.1×10^{-2} atm at 1500°C and 1 atm chlorine pressure. Below 974° C, where $RhCl_3(s)$ is the condensed phase, the partial pressure of $RhCl_3(g)$ falls off rapidly with decreasing temperature, and at 800°C and 1 atm chlorine pressure it has a partial pressure of 1.5×10^{-5} atm. The data yield $\Delta H^\circ_{1500} = +17.1 \pm 2.0$ kcal/mole and $\Delta S^\circ_{1500} = +1.9 \pm 2.0$ e.u. for $Rh(s) + \frac{3}{2} Cl_2 = RhCl_3(g)$.

Palladium. Results show that the only stable solid chloride of palladium is $PdCl_2$. The compound melts at 680° C. The solubility of palladium in $PdCl_2(l)$ is small near the melting point of the compound, but increases with temperature. Dissociation pressures were measured over the range 517° to 958° C. A log p vs. $\frac{1}{T}$ plot of the data shows a slight break at 674° C, the eutectic temperature. From the slope of the curve below the break are calculated $\Delta H^\circ_{947} = -38.6 \pm 1.0$ kcal/mole and $\Delta S^\circ_{947} = -32.6 \pm 1.0$ e.u. for $Pd(s) + Cl_2 = PdCl_2(s)$. From the change in slope at the break, the heat of fusion of $PdCl_2(s)$ is calculated to be 4.4 ± 2.0 kcal/mole. At 980° C, the liquid chloride in equilibrium with palladium contains 61 atom–% chlorine and has a dissociation pressure of 1 atm.

Studies of the effect of chlorine pressure on vapor pressure show that the important gaseous species under the conditions of the investigation are $PdCl_2$ and Pd_5Cl_{10}, a gaseous polymer. The data do not exclude the possibility of contributions from other species such as Pd_4Cl_8 and Pd_6Cl_{12}. The number of metal atoms in the dichloride vapor species is assumed to be one. The existence of a gaseous polymer is not entirely unexpected since $PdCl_2(s)$ is known to exist in a polymerlike crystal structure.

The partial pressures of $Pd_5Cl_{10}(g)$ and $PdCl_2(g)$ were measured as a function of temperature. At 1 atm chlorine pressure, the partial pressure of $Pd_5Cl_{10}(g)$ reaches a maximum of 1.2×10^{-2} atm at 859° C. Above 850° C, the partial pressure of $Pd_5Cl_{10}(g)$ begins to decrease with increasing temperature as a result of the increasing solubility of palladium in the liquid chloride. Above 980° C, where Pd(s) is the stable condensed phase, the partial pressure of $Pd_5Cl_{10}(g)$ decreases rapidly with increasing temperature and $PdCl_2(g)$ becomes the main gaseous species.

At 1506° C and at 1 atm chlorine pressure, the partial pressure of $PdCl_2(g)$ is 0.1 atm. The temperature dependence data yield $\Delta H^\circ_{1573} = +27.9 \pm 2.0$ kcal/mole and $\Delta S^\circ_{1573} = +11.1 \pm 2.0$ eu for $Pd(s) + Cl_2 = PdCl_2(g)$; and $\Delta H^\circ_{953} = +47.3 \pm 2.0$ kcal/mole and $\Delta S^\circ_{953} = +38.6 \pm 2.0$ e.u. for $5PdCl_2(s) = Pd_5Cl_{10}(g)$.

DOUBLE OVER EXPERIMENTS WITH LITHIUM HALIDES

J. Berkowitz, H. A. Tasman, and W. A. Chupka

In virtually all of the applications of the mass spectrometer for the determination of high temperature properties, one or more of the following assumptions have been made:

1) A measured ion peak corresponds to a specific molecular progenitor.
2) The cross section for ionization of a molecule by electrons is the sum of the cross sections of its component atoms. (Addivity Rule).
3) When a Knudsen cell is combined with a mass spectrometer, the partial pressure of a given molecular species within the cell is related to its ion intensity by the relation

$$P_i = k_i I_i T, \qquad (1)$$

where k_i is a constant depending upon the species involved and the geometric arrangement of the ion source, but independent of the pressure and temperature of the Knudsen cell.

These assumptions have been tested for each of the lithium halides, by use of a specially designed double-over. Milne (1) had previously suggested the use of a double over for measuring relative ionization cross sections. In Milne's scheme, the sample is loaded into one chamber, its vapor flows into the other chamber via a connection channel and the vapor is subsequently superheated in the latter chamber. His analysis then assumes that the pressure in both chambers is the same, i.e., that viscous flow pervades and the major impedance to flow is the effusion hole. Experimentally, this constrains flow through the effusion orifice to the molecular domain and simultaneously, flow through the connecting channel to the viscous region. This constraint limits the range of pressure variation to less than one order of magnitude and consequently severely affects the accuracy which can be obtained.

An alternative to the "constant pressure" double over described above, which permits a wider pressure variation, is the "constant source" double-oven. (See Fig. 1) In this arrangement a frit of sintered metal is interposed in the channel between the two ovens.

In one experimental arrangement a pressure ratio across the frit of 30 was readily attained. This effect, together with a temperature difference between the ovens of 300° C, increases the operating range considerably. Since (asshown below) the calculations involve a difference of two numbers (Δ), it is essential that the statistical error of measurement be smaller than Δ in order to arrive at a significant result. For a given statistical error, the experiment becomes meaningful only when the operating range is broad enough to provide Δ about three times this error. Hence, the wider operating range actually makes the experiment possible.

The system described above may be used for determining relative ionization cross sections when the following assumptions are closely approximated:

1) The net mass flow of particles through the frit is constant when the temperature of the upstream oven and the temperature of the frit are held constant.

2) The partial pressure (P_i) of a molecular species in the downstream oven is related to its corresponding ion current (I_i) as measured in the mass spectrometer by relation (1), where T is the absolute temperature and K_i is specific to each molecular species because it incorporates the probability of ionization.

3) The vapor consists predominantly of two species, say monomer and dimer.

Consider now two consecutive experiments in which the upstream oven temperature is kept constant but the downstream oven temperature is varied. Because of the constant mass flow condition, it follows that

$$\frac{P'_M}{\sqrt{T'}} + \frac{\sqrt{2}P'_D}{\sqrt{T'}} = \frac{P''_M}{\sqrt{T''}} + \frac{\sqrt{2}P''_D}{\sqrt{T''}} \qquad (2)$$

where the subscripts signify monomer and dimer, and the superscripts differentiate the two experiments.

Combining equations (1) and (2) yields

$$\frac{k_M}{k_D} = \frac{\sqrt{2}\,(I''_D\sqrt{T''} - I'_D\sqrt{T'})}{I'_M\sqrt{T'} - I''_M\sqrt{T''}} \qquad (3)$$

which is the inverse ratio of the corresponding ionization cross sections. The expression may be readily be generalized for more than two species, nullifying assumption (3), but the experimental demands inherent in the form of the final result require drastic improvement in the precision of measurement.

In applying Eg. (3) to a specific system, one must inquire into the kind of cross sections being investigated. For example, the saturated lithium halide vapors have been shown to consist of monomer, dimer, trimer, and tetramer in measurable quantities. (2) The electron impact ionization process can lead to dissociative as well as primary ionization. Hence, several ion peaks observed in a mass spectrometer can have contributions from more than one of the polymeric species. In identifying a particular ion peak with a partial pressure of vapor, as in Eq. (1), one must be careful to ascertain what fraction of that peak is to be attributed to the specific polymeric molecular progenitor. When one has elicited these various contributions, one has determined the fragmentation pattern of each molecule upon electron impact. For the purpose of this paper, the ion currents I_i in Eq. (3) are to be interpreted as the summation of all ions originating from a particular molecular species. Hence, Eq. (3) will yield the total ionization cross sections.

The identical double-oven apparatus described above can be utilized to determine fragmentation patterns. (3) Although the following discussion may readily be generalized, we restrict the problem again to monomer and dimer species. The procedure then is to perform two consecutive experiments in which the downstream oven temperature is kept constant, and the upstream temperature varied. This assures that the equilibrium constant describing the monomer-dimer equilibrium in the downstream oven will remain unchanged. Utilizing this condition and the assumption of Eq. (1), Gorochov (3) has shown that

$$c = \frac{I''_{M,D} - \sqrt{n}\, I'_{M,D}}{I'_D\,(n - \sqrt{n})}$$

where $I_{M,D}$ is an ion peak that has contributions from monomer and dimer molecules

I_D is an ion peak that can be definitely attributed to dimer species alone

c is a number by which I_D must be multiplied to determine the contribution to $I_{M,D}$

$n = \frac{I''_D}{I'_D}$ is the ratio of dimer ion intensities under the two experimental conditions.

It should be noted that the fortuitous existence of I_D ions is a further assumption in this development.

For both types of double-oven experiments, meaningful results depend upon achieving a significant difference between two numbers, i.e., a difference several times larger than the uncertainity in measurement. In practice, this requires measuring ion intensities to a precision of 1%, and producing large shifts in monomer: dimer ratios. The presence of other molecular species also tends to confuse the result. The presence of an I_D-type ion is also necessary.

The lithium halides have been selected for this study, largely because dimer and monomer have been shown to be of comparable intensity, and higher species appear to be of minor importance. (2), (4) Assuming, then, that only monomer and dimer comprise the vapor, the experimental results yield fragmentation patterns shown in Table I.

Table I

	M^+/MX^+	M^+/M_2X^+	MX^+/M_2X^+
LiF	(4.5)	0.13_8	0.001
LiCl	0.30	0.12_5	0.03
LiBr	0.46	0.13	0.06_6
LiI	0.16	0.21	0.06

It has previously been shown (2) that the ion M_2X^+ satisfies the requirements of an I_D-type, i.e.,

$$M_2X_2 + \bar{e} \rightarrow M_2X^+ + X + 2\bar{e} \qquad (5)$$

Monomer molecules cannot give rise to M_2X^+, and larger molecular species are not abundant enough to affect the result. The monomer fragmentation pattern for LiF given in Table I is of dubious value, because the experimental values in this instance display a dependence upon temperature and/or pressure, which violates the assumption of Eq. (1).

In Table II are shown the experimental results based on Eq. (3). Also shown in this table is a set of cross section ratios based upon comparison of ion intensities observed in this study with molecular ratios determined by Kusch and co-workers, (4)(5) using a velocity-selecting molecular beam device. A third method, based upon totally evaporating a known weight of sample in the mass spectrometer, is currently being investigated.

Table II

	k_M/k_D based on Eq. (3)	k_M/k_D cf. with Kusch, et. al. (4), (5)
LiF	2.82 2.42	3.15
LiCl	1.20 1.10	0.83
LiBr	1.42	1.84
LiI	1.04	—

In the case of LiF, evidence was obtained for substantial kinetic energy in the Li^+ fragment ion, which seriously affects the efficiency of collection of this ion in the mass spectrometer. From column 1 of Table II, the other lithium halides provide evidence for a dimer: monomer cross section ratio between 1 and 2, indicating that the Additivity Rule is not satisfied.

The relatively poor agreement between columns 1 and 2 may be due to poor detection efficiency in the molecular beam velocity–selector experiments. The surface ionization detector used in the latter investigation is not as efficient for lithium halides as it is for the other alkali halides. (4)

The double–oven arrangement can also provide more precise energies of dimerization by minimizing the confusion due to fragmentation. One can study the equilibrium as a function of temperature, maintaining the dimer intensity (and hence its possible contribution to a monomer peak) at a low level. A typical graph of this type is shown in Fig. 2. The dimerization energies obtained are reported below.

LiF: $\Delta H = 61.4 \pm 1$ kcal/mole, LiCl: $\Delta H = 49.1 \pm 1.5$ kcal/mole and LiI: $\Delta H = 37.9 \pm 2$ kcal/mole.

References

1. T. A. Milne, J. Chem. Phys. 28, 717 (1958).

2. J. Berkowitz and W. A. Chupka, J. Chem Phys. 29, 653 (1958).

3. L. N. Gorochov, Vestnik Moskovskovo Universiteta 6, 231 (1958).

4. R. C. Miller and P. Kusch, J. Chem. Phys. 25, 860 (1956); 27, 981 (1957).

5. M. Eisenstadt, G. M. Rothberg, and P. Kusch, J. Chem. Phys. 29, 797 (1958).

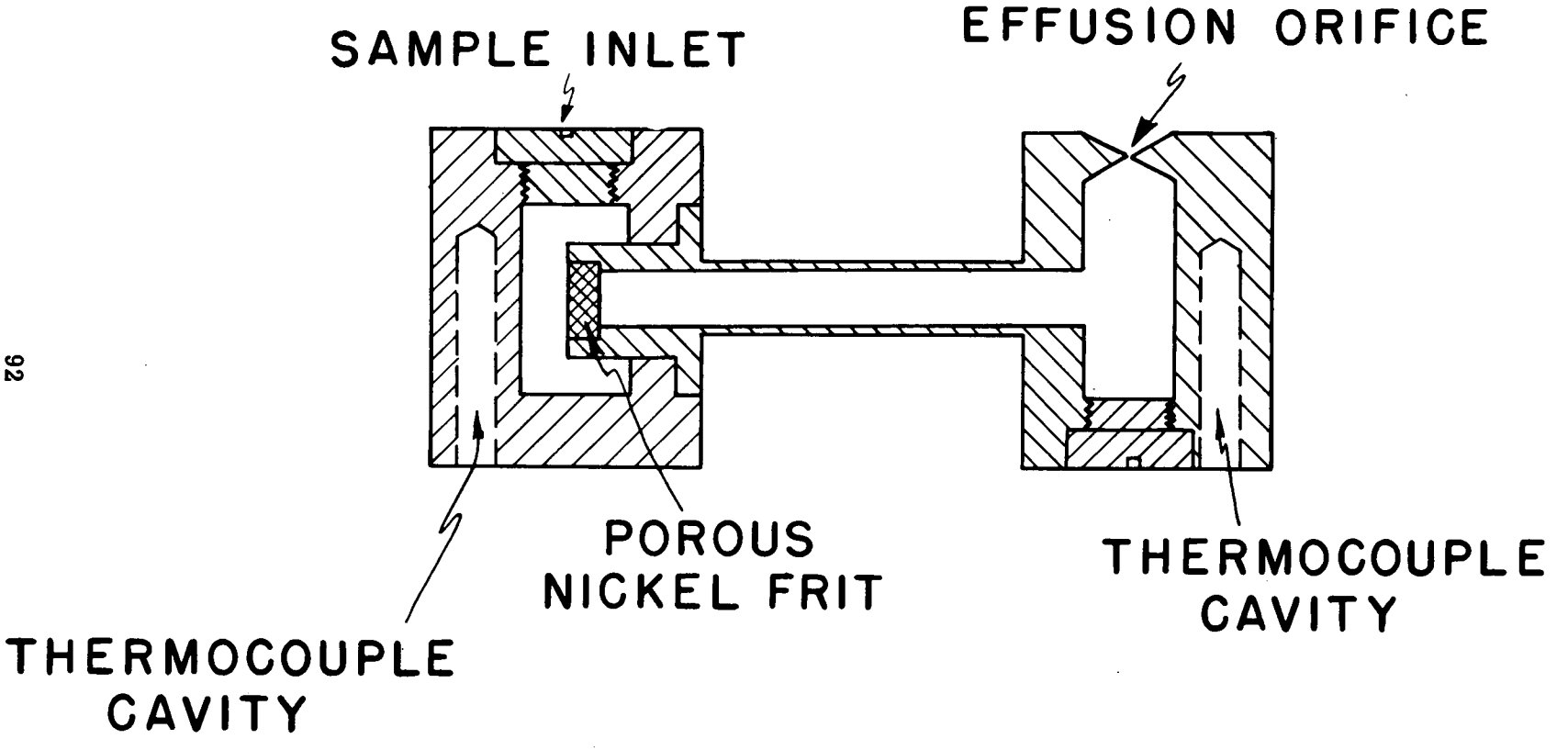

FIGURE I

DOUBLE OVEN APPARATUS

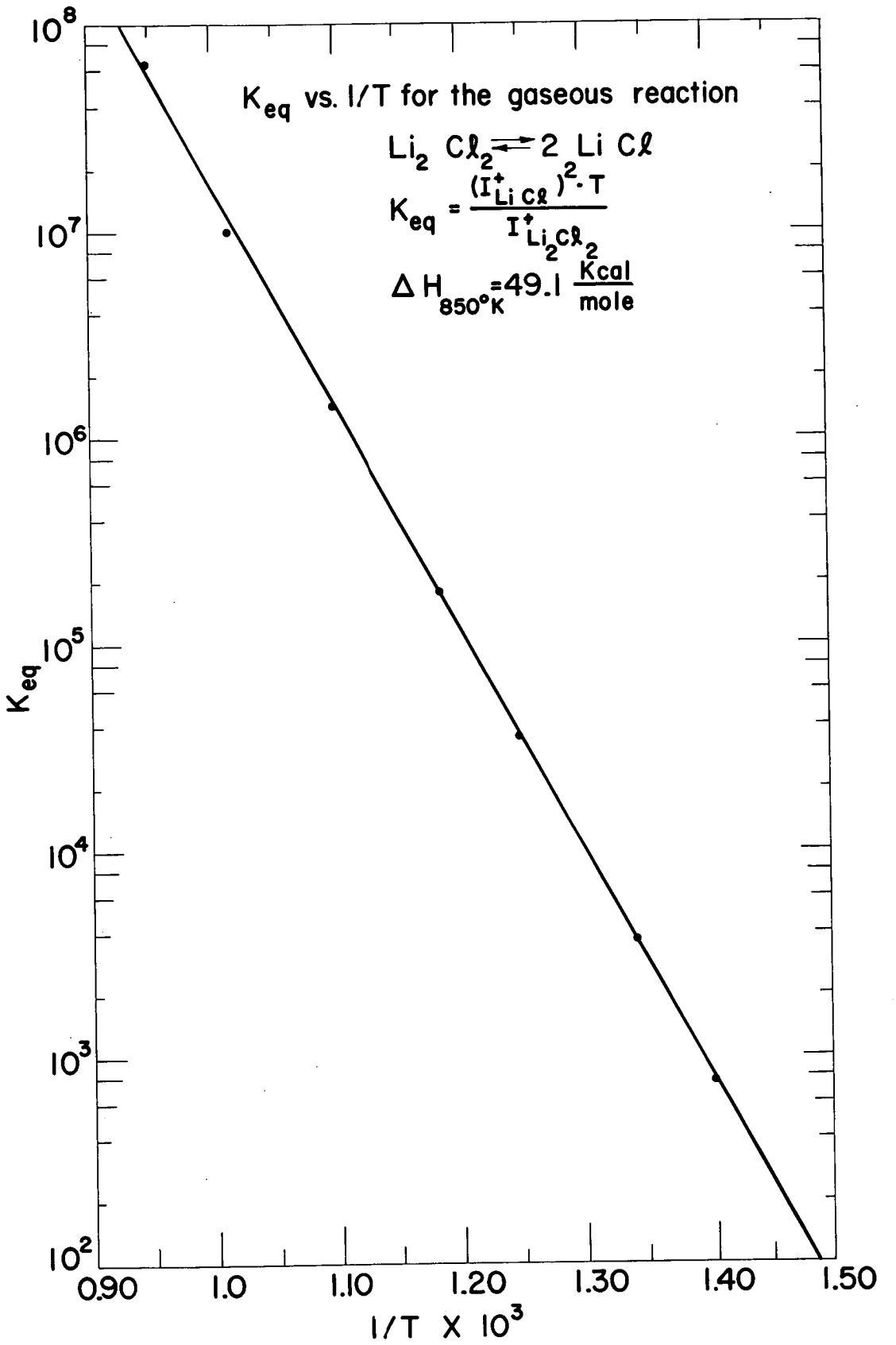
K_{eq} vs. 1/T for the gaseous reaction
$Li_2 Cl_2 \rightleftharpoons 2\ Li\ Cl$
$K_{eq} = \frac{(I^+_{Li\,Cl})^2 \cdot T}{I^+_{Li_2Cl_2}}$
$\Delta H_{850°K} = 49.1 \frac{Kcal}{mole}$
10^8
10^7
10^6
10^5
10^4
10^3
10^2
K_{eq}
0.90
1.0
1.10
1.20
1.30
1.40
1.50
1/T X 10^3

Figure 2.

UBER DIE EINWIRKUNG VON WASSERDAMPF AUF OXYDE BEI ERHOHTEN TEMPERATUREN

O. Glemser and R. von Haeseler

Die Oxyde WO_3, MoO_3 and TeO_2 zeigen in Gegenwart von Wasserdampf eine höhere Flüchtigkeit als sie ihren Gleichgewichtsdampfdrucken entspricht. Untersucht man diesen Effekt mit der Mitführungsmetho de unter Variation des Wasserdampfpartialdrucks im Trägergas, so erhalt man bei konstanter Temperatur eine lineare Abhängigkeit de transportierten Substanz Δm von p_{H_2O}. Da es sich um Gleichgewichtsmessungen handelt, sind die ermittelten Geraden nur so zu deuten, dass ihr Wert für $p_{H_2O} = 0$ dem Dampfdruck des oxyds entspricht, während der Anstieg mit p_{H_2O} auf die Bildung einer Verbindung zwischen oxyd und Wasser zurückzuführen ist, die beim Abkuhlen wieder in ihre Ausgangskomponenten zerfällt. Aus dem Experiment geht hervor, dass jeweils ein Molekül Wasser mit dem Bodenkorper reagiert. Demnach sind folgende Reaktionen möglich:

(1) $(MeO_x) + (H_2O) \rightleftharpoons (MeO_{x-1}\ (OH)_2)$

(2) $2(MeO_x) + (H_2O) \rightleftharpoons (Me_2O_{2x-1}\ (OH)_2)$

(3) $3(MeO_x) + (H_2O) \rightleftharpoons (Me_3O_{3x-1}\ (OH)_2)$ usw.

Diese Reaktionen können aus dem Experiment nicht voneinander unterschieden werden, weil nur eine Änderung in der Steigung der Gerad verbunden ist, diese aber erst durch Beziehung auf eines dieser Gleichgewichte ermittelt werden kann. Die formulierung des Reaktionsproduktes als gasförmiges Hydroxyd wird im folgenden durch die thermochemischen Daten belegt.

1) $WO_3 + H_2O$
Unter der Annahme, dass nur Reaktion (1) vorliegt, wurden die Gleichgewichtskonstanten für 5 verschiedene Temperaturen im Bereich von 900 – 1100° C ermittelt zu

$K_p(900°C) = 4.7 \times 10^{-4}$ $K_p(950°C) = 9.3 \times 10^{-4}$

$K_p(1000°C) = 1.7 \times 10^{-3}$ $K_p(1050°C) = 3.3 \times 10^{-3}$

$K_p(1100°C) = 5.5 \times 10^{-3}$

Für die Reaktionsenthalpie und -entropie erhält man

$\Delta H_T = 39.9$ Kcal/Mol.

$\Delta S_T = 18.8$ Cl/Mol.

Bei Berücksichtigung des Verdampfungsgleichgewichts des Oxyds lässt sich die homogene Reaktion (alle Partner gasförmig) berechnen.

Da nur die Daten der Reaktion $3WO_3 = (WO_3)_3$ bekannt sind, erhält man unter Verwendung der heterogenen Gleichung (3) für das Gleichgewicht

$$(WO_3)_3 + (H_2O) \rightleftharpoons (W_3O_3\,(OH)_2)$$

eine Reaktionsenthalpie von $\Delta H^\circ_T = 68.1$ Kcal/Mol.
und eine Reaktionsentropie von $\Delta S^\circ_T = -37.5$ Cl/Mol.

Findet bei der Reaktion eine Depolymerisation statt, so ist diese Warmetönung noch in Rechnung zu stellen, d.h., man erhält für ΔH°_T einen noch grösseren negativen Wert. Damit kann als Reaktionsprodukt nur ein gasförmiges Hydroxyd mit echten Bindungen vorliegen.

2.) $MoO_3 + H_2O$

In Temperaturbereich von 600 – 690°C wurden folgende Gleichgewichtskonstanten für (1) bestimmt:

$K_p(600°C) = 3.95 \times 10^{-4}$ $K_p(630°C) = 8.09 \times 10^{-4}$

$K_p(660°C) = 1.39 \times 10^{-3}$ $K_p(690°C) = 2.62 \times 10^{-3}$

Für die Temperaturabhängigkeit gilt $\log K_p = -\frac{7731}{T} + 5.45$

Die Reaktionsenthalpie beträgt $\Delta H_T = 35.3$ Kcal/Mol.

die Reaktionsentropie $\Delta S_T = 24.9$ Cl/Mol.

Für die homogene Reaktion $(MoO_3)_3 + (H_2O) = (Mo_3O_8(OH)_2)$

folgt $\Delta H^\circ_T = -47.9$ Kcal/Mol, ΔS°_T 47.0 Cl/Mol.

Es handelt sich demnach auch hier um ein gasförmiges Hydroxyd.

3.) $TeO_2 + H_2O$

Bei diesem Oxyd konnte der Effekt der höheren Flüchtigkeit in Wasserdampf erstmalig beobachtet werden. Im Temperaturberich von 600 – 700°C wurden die Gleichgewichtsknostanten erhalten zu

$K_p(600°C) = 6.7 \times 10^{-5}$ $K_p(650°C) = 1.7 \times 10^{-4}$

$K_p(700°C) = 4.2 \times 10^{-4}$

Für die heterogene Reaktion ergibt sich

$$\log K_p = -\frac{7920}{T} + 4.11$$

Uber die Clausius–Clapeyron'sche Beziehung berechnet man die Reaktionsenthalpie zu $\Delta H_T = 33.4$ Kcal/Mol.

die Reaktionsentropie zu $\Delta S_T = 18.8$ Cl/Mol.

Da in der Gasphase über TeO_2 nur monomere Moleküle nachgewiesen sind, erhält man hier über $TeO_2 \rightleftharpoons (TeO_2)$ unter Verwendung von (1) die Daten für die homogene Reaktion

$$(TeO_2) + (H_2O) \rightleftharpoons (TeO(OH)_2)$$

zu $\Delta H^{\circ}_{T} = -21.6$ Kcal/Mol.

und $\Delta S^{\circ}_{T} = -18.1$ Cl/Mol.

Damit ist auch die Existenz eines gasförmigen Tellurhydroxyds hinreichend belegt.

Die vorliegenden Versuche konnten nur bis zu einem Wasserdampfdruck von einer Atmosphäre durchgefuhrt werden. Es wäre interessant festzustellen, wie sich die Verhältnisse mit weiterer Drucksteigerung ändern. Auf diese Weise kann zur Deutung der Löslichkeit von Oxyden im hyperkritischen Gebiet beigetragen werden. Es ist anzunehem, dass mit steigendem Druck auch solche Reaktionen einsetzen, die stärker als linear vom Wasserdampfdruck abhängen, d.h., es werden Verbindungen gebildet, die mehr als zwei Hydroxylgruppen im Molekül enthalten. Eine für diese Messungen geeignete Apparatur Wird gegenwärtig gebaut.

A TRANSPIRATION STUDY OF GASEOUS SPECIES IN THE BORON–OXYGEN–FLUORINE SYSTEM

D. L. Hildenbrand, L. P. Theard, and A. M. Saul

There is at present very little available information regarding the properties or even the existence of gaseous metal oxyhalides. Bond energy considerations, however, indicate that certain oxyhalides may be important species in metal oxide–halide systems at high temperatures. The enthalpy change, although unfavorable, can often be offset by the increase in entropy accompanying the formation of oxyhalide, particularly in cases involving the reaction of a gaseous halide with a condensed oxide. It is necessary, therefore, to establish the thermodynamic properties of the oxyhalides before reliable equilibrium calculations can be made for metal oxide–halide systems at high temperatures. This paper presents results of a study of the oxyfluorides of boron.

Initial studies indicated that boric oxide samples experienced appreciable weight losses when exposed to a stream of gaseous boron trifluoride at temperatures of 500 to 800° K. These temperatures are far too low to account for the weight loss on the basis of direct vaporization of boric oxide. The reaction has been investigated in more detail by the transpiration method in order to obtain quantitation information about the reaction products.

Experimental: An all–metal flow system was used in which a platinum boat containing the boric oxide sample was placed between two close–fitting nickel plugs within a one inch I. D. nickel transpiration tube. The annular space between each plug and the tube was sufficiently small so that the plugs served as effective heat shields and barriers to diffusion. In addition, the upstream plug aided in preheating the flow gas. The temperature within the reaction zone was measured with a calibrated platinum, platinum–rhodium thermocouple which was suspended directly above the sample boat, and it could be maintained constant within 2° by automatic control of the power input to a Kanthal–wound resistance furnace surrounding the transpiration tube. Flow rates were measured with meters which were separately calibrated for each of the flow gases used by discharge into a gas buret.

In all cases, the extent of reaction was determined from sample weight loss measurements. In operation, the weighed sample boat was inserted into the transpiration tube, which had been previously flushed with boron trifluoride, and the metered flow of gas was started. At the termination of a run, the sample was removed, cooled in a desiccator and then weighed on an analytical balance in a dry box. A few check measurements of the vapor pressure of zinc chloride, using argon as the flow gas, gave close agreement with established literature values, indicating the operation to be satisfactory.

Results: In interpreting the results of a transpiration experiment, it must be established over what range of flow rates the flow gas is saturated with the gaseous reaction product and to what extent the result is influenced by diffusion transport. It can be shown that at sufficiently high flow rates, diffusion effects will become unimportant and that k, the mass transport of gaseous product per unit time can be expressed as

$$k = \frac{PMv}{RT} \qquad (1)$$

where P, M and T are the partial pressure, molecular weight and temperature of the vapor, R is the gas constant and v is the gas flow rate. Over the range in which saturation is achieved without interference from diffusion, equation (1) requires that the ratio k/v be essentially constant. Table I shows the constancy of k'/v at boron trifluoride flow rates below about 6 cm^3/min as measured at 800° K, indicating that saturation is attained in this range.

Table I

v cm^3/min	$k'/v \times 10^3$ g/cm^3	v cm^3/min	$k'/v \times 10^3$ g/cm^3
2.5	0.60	4.3	.60
3.1	.61	4.8	.56
3.7	.58	6.5	.52
4.0	.50	6.7	.51
4.0	.58	8.0	.44
4.0	. .54	11.8	.41

For convenience, the rate of boric oxide weight loss, k', has been substituted for k, since the two are directly proportional. Furthermore, a plot of k' versus v can be extrapolated through the origin, as is also required by equation (1).

Flow rate studies at other temperatures have given the same results. At flow rates above about 6 cm^3/min, the residence time of flow gas is apparently too short for equilibrium to be attained.

The most probable course of reaction is

$$x\ BF_3(g) + y\ B_2O_3(l) = (BF_3)_x \cdot (B_2O_3)y(g) \qquad (2)$$

All measurements were made on glassy or liquid boric oxide, and analysis of the residual B_2O_3 after extended exposure to BF_3 in the flow tube showed no change in purity. The stoichiometric coefficient x has been determined from studies of the rate of B_2O_3 weight loss at various BF_3 pressures, since it can be shown that the partial pressure of gaseous product (or k'/v) is proportional to the pressure of BF_3 raised to the power x, if ideal gas behavior and unit activity for B_2O_3 are assumed. Table II shows that the ratio of k'/v to BF_3 pressure is essentially constant over the range 0.2 to 1.0 atmosphere at 595 and 800°K, so that x is equal to one.

Table II

595°K		800°K	
P_{BF_3} atm	$\frac{k'/vx10^3}{P_{BF_3}}$ $g/cm.^3 atm$	P_{BF_3} atm	$\frac{k'/vx10^3}{P_{BF_3}}$ $g/cm.^3 atm$
0.35	0.24	0.20	0.57
.53	0.27	.37	.47
1.00	0.30	.52	.50
		.58	.46
		1.00	.56

The BF_3 pressure was varied by dilution with argon. Attempts to vary the activity of B_2O_3 in order to determine y have been thus far unsuccessful, but the small choice of suitable structures and analogy with work on the B–O–H system strongly indicate that y is equal to one and that the gaseous product is the molecule $(OBF)_3$.

The rate of weight loss has been determined at ten temperatures over the range 600 to 1100°K, using BF_3 flow rates of 4 to 5 cm^3/min. From the weight loss data, equilibrium constants have been calculated for reaction (2), assuming x and y are equal to one. A plot of log K versus 1/T is shown in Figure I.

The rate of weight loss has been determined at ten temperatures over the range 600 to 1100°K, using BF_3 flow rates of 4 to 5 cm^3/min. From the weight loss data, equilibrium constants have been calculated for reaction (2), assuming x and y are equal to one. A plot of log K versus 1/T is shown in Figure I. From the slope of this plot, the heat of reaction (2) is derived as 2.9 kcal. at 850°K, indicating the reaction to be almost thermoneutral. An entropy of 121.3 cal/deg mole at 850°K is derived for $(OBF)_3(g)$ from the free energy equation and the entropies of BF_3 and B_2O_3. By analogy with other substituted boroxoles, the most plausible structure for $(OBF)_3$ would seem to be a planar symmetric six-membered ring of alternate boron and oxygen atoms, with a fluorine atom bound to each boron. Such a structure is compatible with the derived entropy if the entropy of cyclization of the hypothetical monomer OBF is assumed to be comparable to the established analagous values for an number of hydrocarbons. From estimated thermal functions and the available thermal properties of B_2O_3 and BF_3, the heat of formation of $(OBF)_3(g)$ at 298°K is derived as −566 kcal/mole.

Acknowledgment: This work has been supported by the Advanced Research Projects Agency and the U. S. Navy Bureau of Weapons under Contract No. rd 17980, Task 3.

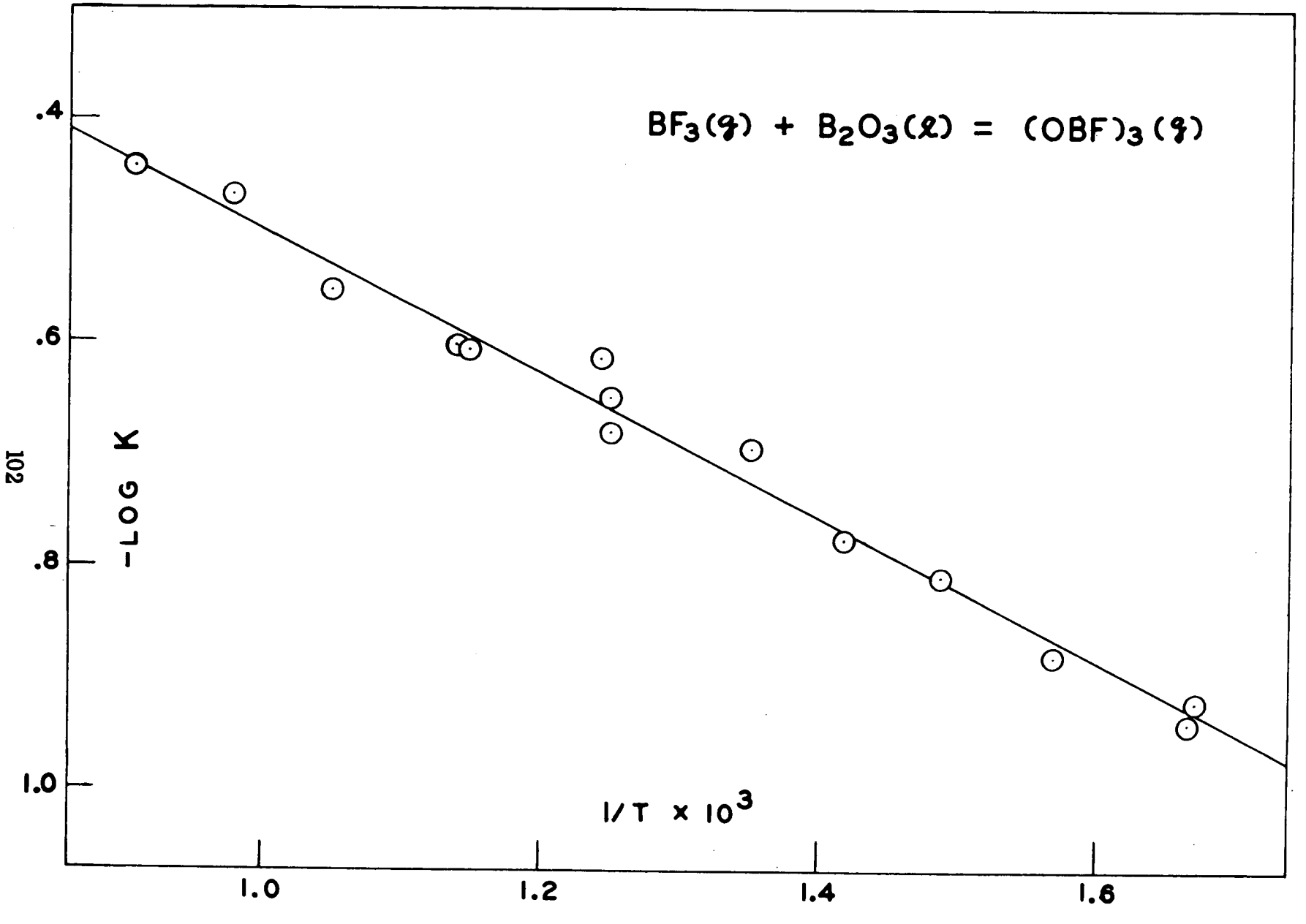

FIGURE 1

THE RATE OF VAPORIZATION OF ALUMINUM OXIDE

J. J. Diamond, R. F. Hampson, and R. F. Walker

In another paper presented at this Symposium a microbalance technique for measuring the rate of vaporization of platinum metals is described. Adaption of this technique to the study of ceramics is complicated by the need to introduce a metal heating element. The complications arise because the heating element is liable to react with the sample at high temperature, and to interfere with the free evaporation if it partially encloses the sample. It is not possible to predict the quantitative significance of these factors without prior experiment.

Using rf induction heating the apparent rate of vaporization of crystalline samples of aluminum oxide has been measured by enclosing the sample with platinum, tungsten, molybdenum, and graphite susceptors, and also by enclosing a tungsten susceptor within the sample. Details of the design of the apparatus and of the special techniques used to prepare the samples are presented. Data on the rate of vaporization under these experimental conditions is given, and is interpreted in terms of the quantitative effect of the factors discussed above.

The problems arising from the presence of a metal heating element can be eliminated by using image furnace techniques. These techniques introduce severe problems of temperature measurement, however; additional problems arise from the uncertainity of the surface area, the uniformity of the temperature, and the weight–loss determinations. A solar furnace and an arc–image furnace have been used to measure the rate of vaporization of alumina *in vacuo* and in the presence of foreign gases. Full details of the experimental techniques are given, together with an evaluation of the problems and uncertainities involved in the particular approaches. Data on the rates of vaporization of solid and liquid alumina is presented, together with estimates of the coefficients of vaporization.

In parallel with the foregoing measurements, determinations of the vapor species involved are being made with a mass spectrometer. Combination of these determinations with the rate measurements and estimates of vaporization coefficients yields thermodynamic data on the vaporization processes, viz., vapor pressures and heats of vaporization.

REACTION OF GRAPHITE WITH HYDROGEN. HEAT OF FORMATION OF THE METHYLENE RADICAL

William A. Chupka, David J. Meschi, and Joseph Berkowitz

A graphite–lined Knudsen cell equipped with a gas–inlet lead was used to study the reaction of hydrogen with graphite. The major purpose of the study was to determine the heat of formation of CH_2, the methylene free radical.

In order to obtain equilibrium conditions the graphite liner was built with a system of baffles which increased the reaction time and the reactive surface area. The pressure of hydrogen in the cell could be estimated by measuring the pressure at the inlet to the cell and applying corrections for the conductance and temperature of the cell, the effects of dissociation, etc. Uncertainties in these corrections introduced an uncertainty of about a factor of two in the pressure. The hydrogen pressure was kept in the range 0.1 – 1.0 mm. and the temperature of the cell was raised as high as 2600° K.

The vapor effusing from the cell was bombarded by electrons of controlled energy and the resulting ions analyzed by a mass spectrometer. The vapor was found to consist predominantly of carbon and hydrogen atoms and molecules and acetylene. Small amounts of C_2H, CH, CH_2, and CH_3 were also detected. In order to investigate these radicals it was necessary to use electron voltages just a few volts above their ionization potentials. This procedure insured that the ions observed were parent ions and were not produced by fragmentation. The partial pressures of CH, CH_2, and CH_3 were estimated by comparison of their parent ion intensities with that of C^+ produced from C atoms since the atomic carbon partial pressure is accurately known as a function of temperature. The partial pressures of CH and CH_3 so determined were in fair agreement with those calculated from available thermochemical data. The measured partial pressure of CH_2 was combined with estimated thermodynamic functions calculated on the basis of a linear molecule with triplet ground state. Interatomic distances were those found by Herzberg and Shoosmith and vibrational frequencies were those listed by Mulligan and Pimentel. The $\Delta H°$ of formation at 298° K was calculated to be 80.0 kcal/mole for CH_2 gas. In these experiments with hydrogen, the intensities of the free radicals were too low to allow any useful measurement of the temperature dependence of the equilibrium constant.

Many attempts were made to approach equilibrium from another direction, namely by pyrolysis of various organic compounds. The compounds used were CH_4, CH_3I, CH_2I_2, C_2H_4, $CH_3CO\,CH_3$ and a few mixtures of these. In all cases, complete equilibrium with respect to decomposition to carbon and hydrogen was never reached as evidenced by much too large partial pressures of the free radicals and parent compounds. However in all cases the disproportionation reaction $2CH_2 \rightarrow CH + CH_3$ appeared to reach equilibrium since the equilibrium constant in all cases but one had a value of about 3.0 which was also roughly the value observed in the experiments with hydrogen. This value was about the same for all cases but that of acetone in spite of the fact that the relative amounts of the various radicals varied greatly from one compound to another. The temperature coefficient of the equilibrium constant was practically zero except for acetone in which case the temperature coefficient was anomalously high. Excepting the case of acetone, both the absolute value of the equilibrium constant and its temperature coefficient gave independently values of about 2.0 kcal/mole for the heat of the reaction and thus a value of about 86 kcal/mole for the heat of formation of CH_2.

The reliability of experimental data and the thermodynamic functions employed were examined and the value 82 ± 8 kcal/mole was chosen for the heat of formation of CH_2 at 298° K.

THE MEASUREMENT OF OSMOTIC COEFFICIENTS IN THE TEMPERATURE RANGE 100° C TO 280° C

H. J. de Nordwall and P. J. Jones

Introduction: Until recently studies of the thermodynamics of electrolyte solutions at temperatures above 25° C have taken the form either of painstaking investigations at temperatures up to 100° C for a very small number of salts, or of rather crude vapour pressure measurements on saturated solutions over a wide temperature range. This temperature range has recently been extended to 275° C for hydrochloric acid by e.m.f. measurement. Other investigations by this method will no doubt follow, but wide application of the technique is restricted by the lack of suitable electrodes. However, any absolute measurements of osmotic coefficients can in principle be supplemented by isopiestic comparisons, which have now been made up to 100° C.

We have attempted to design an apparatus to determine the absolute values of the osmotic coefficients of a large number of salts over a wide temperature range by the measurement of vapour pressure lowering. Though it is difficult to achieve high accuracy in ϕ by this method, it has the advantage of almost universal application.

Method and Apparatus: The vapour pressure difference (Δp) to be expected between the solvent and the solutions over the temperature range 100° C to 289° C will vary from ~ 1 cm of mercury to several atmospheres for concentrations ranging from 0.5 molal upwards.

The principle we have used to determine Δp is to translate wet steam pressures into dry nitrogen pressures for both solution and solvent separately using diaphragms, which form parts of condensers, as null balance detectors. The two nitrogen pressures are then compared using a mercury manometer.

The solutions are contained in iridium–platinum cells, whose tops form the thin flexible diaphragm. Changes in capacity of the diaphragm condensers are measured with an A.C. bridge which also supplies signals to control the nitrogen pressure in the cell containers. Each cell is contained in a separate compartment, which fits into an autoclave which hangs in an oil bath thermostat. Temperature difference between the two cells affect the osmotic coefficient by less than 0.01%.

The mercury manometer is a steel U–tube. Meniscus displacement is measured using moveable differential transformers, whose output passes through a sharp maximum when the meniscus passes the central coil. A glass manometer is used at lower pressures and a compound manometer is used for large pressure differences. The uncertainty in the measurement of Δp with the steel manometer is $\mp$ 0.35 mm.

The condenser capacities corresponding to unloaded cell diaphragms are determined at the beginning of each experiment with the apparatus assembled and at 100° C. A solution boiling point apparatus is coupled to each cell compartment so that the pressure over the boiling solution is the same as that in the cell compartment. This pressure is then slowly changed until the temperature of the boiling solution is identical with that of the autoclave, when the pressure in the cell compartment must be equal to the vapour pressure of the liquid in the cell. The capacity bridge is then balanced. The autoclave temperature is measured with a platinum resistance thermometer. In conjunction with steam tables this provides a check on the measured solvent vapour pressure, which is measured at the same time as Δp, with a dead weight piston gauge.

The advantages of this method are:

(1) Corrosive solutions are confined to small parts which can be made from previous metals.

(2) Electrical insulation is made easier by using capacity as the indicating property.

(3) The sensitivity of the null detector is independent of pressure and of Δp, and different differential gauges can be used to measure Δp without dismantling the apparatus.

The precision limiting factor is the accuracy with which the vapour pressures can be balanced by nitrogen. This is a function of the overall sensitivity of the diaphragm motion sensing condenser and the capacity bridge and of the accuracy with which the effect of temperature on the 'zero' capacity of the condenser can be estimated. The overall sensitivity of the condensers varies between 1 μA/mm of mercury pressure difference and 5 μA/mm, so that the balance point can be determined to better than $\mp$ 0.1 mm.

However, the precision with which the temperature coefficient of capacity can be estimated corresponds to a standard deviation of ~1 mm of mercury in terms of pressure.

An overall error of less than 1.5 mm of mercury in Δp can therefore be expected. The 1 mm error in pressure balancing determines the lower concentration limit of the solutions.

Results: Corrections need to be applied to observed molalities and vapour pressures before ϕ, the osmotic coefficient, can be calculated. Allowance is made for the changes in molality of the solution due to solvent vaporization, the non-ideality of steam as a gas and the variation of vapour pressure with the pressure on the liquid phase. The ratio of the fugacities of the solvent and the solution is calculated for the condition where the pressure in both liquid phases is the saturation vapour pressure of the solvent at the temperature of the experiment. Values of ϕ for ~2 m sodium chloride calculated from mean values of $\Delta p/p_0$ for groups of points at similar temperatures are shown in Fig. 1. The standard deviation of the experimental $\Delta p/p_0$ values from the best plot of $\Delta p/p_0$ against temperature is $\mp$ 0.0008 corresponding to $\mp$ 1.1%. Data for 2 molal sodium chloride at lower temperatures are quoted from the literature for reference. Our smoothed points can be seen to lie on a ϕ versus temperature curve which is a reasonable continuation of the curve for 2 m sodium chloride from 0°C to 100°C. At the time of this abstract going to press ϕ had only been measured at this single concentration, but we intend to present further results at the Congress.

Further experiments to determine ϕ from 100° C to 280° C over the concentration range 1 – 5 molal are in progress. Modifications to the diaphragm condenser design to increase accuracy are being made.

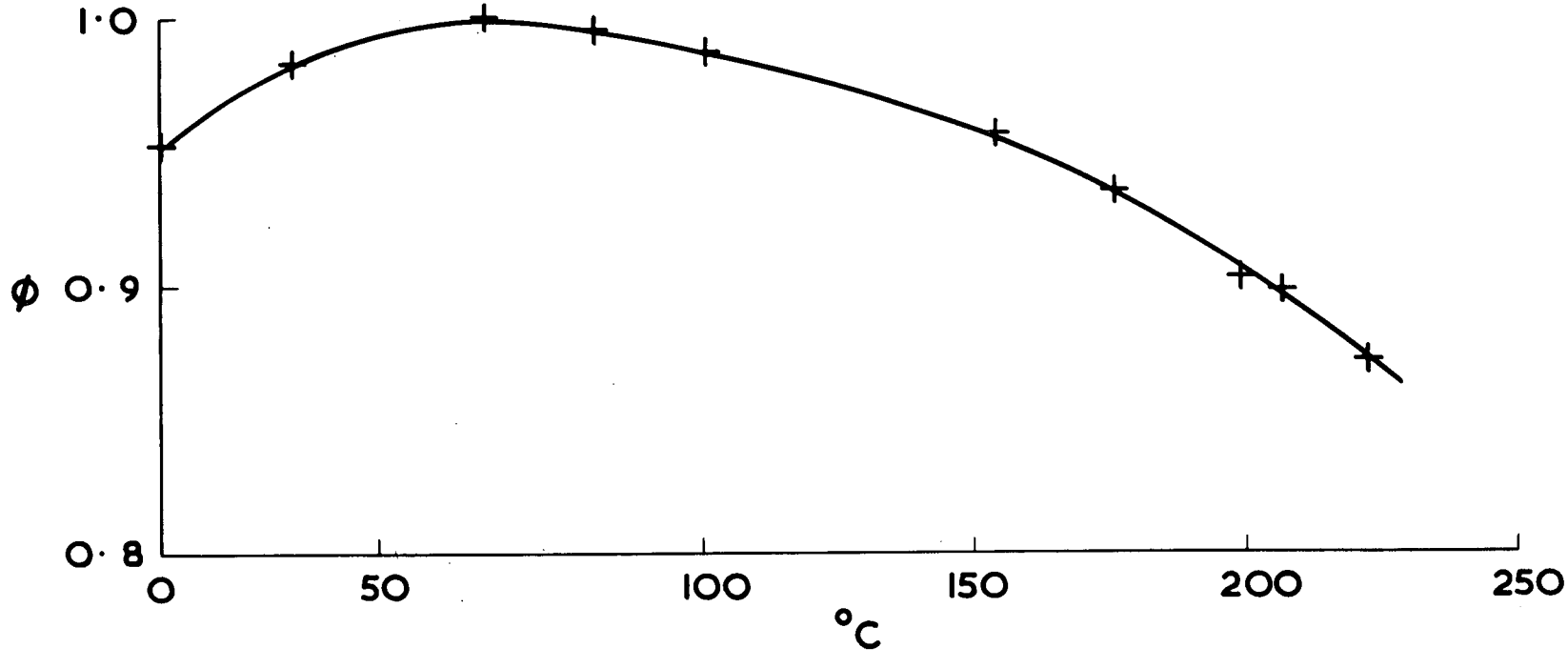

FIG. 1. OSMOTIC COEFFICIENT OF 2 MOLAL SODIUM CHLORIDE AS A FUNCTION OF TEMPERATURE.

THE REACTION OF FERRIC CHLORIDE WITH SODIUM AND POTASSIUM CHLORIDES.

C.M. Cook, Jr. and W.E. Dunn, Jr.

It is well known that the volatility of ferric chloride is profoundly reduced, even at elevated temperatures, by addition of NaCl. Earlier workers have noted this vapor pressure reduction but, being unable to isolate a complex compound and observing that the $FeCl_3$–NaCl phase diagram appeared to contain but one eutectic, concluded that no compound is formed between sodium and ferric chlorides. However, a detailed study of the $FeCl_3$–NaCl and $FeCl_3$–KCl systems shows that the decrease in ferric chloride activity in fact does result from the reaction between $FeCl_3$ and MCl to give $MFeCl_4$. The complex compound, $MFeCl_4$, is stable in solid, molten, and vapor states.

The existence of $NaFeCl_4(c)$ is indicated by the liquid–solid phase diagram of the system $FeCl_3$–NaCl. The compound $NaFeCl_4$ melts congruently at 163°C. with the two eutectics occurring quite near to the melting point, at $X_{NaCl} = 0.48$, 157°C., and at $X_{NaCl} = 0.51$, 162°C. In the system $FeCl_3$–KCl the compound $KFeCl_4$ melts congruently at 249°C., the eutectics being at $X_{KCl} = 0.45$, 206°C., and $X_{KCl} = 0.52$, 242°C.

X–ray diffraction photographs from powdered mixtures of $FeCl_3$ and MCl which have been previously melted show a complicated pattern of lines that is presumably due to $MFeCl_4$. In the case of those mixtures where $MCl/FeCl_3 \geq$ unity the pattern of alkali chloride is also present; where $MCl/FeCl_3 <$ unity the MCl pattern disappears and the ferric chloride pattern can be detected.

The enthalpy change for the reaction

$$MCl(c) + FeCl_3(c) = MFeCl_4(c) \qquad (1)$$

was determined by measurements of the heats of solution in 6 N. HCl of $MFeCl_4(c)$, MCl(c) and $FeCl_3(c)$. As in the case with many complex compounds the sodium complex salt forms from its parent salts with less energy than its potassium analog. For $NaFeCl_4$, $\Delta H(1) = -0.8$ kcal./mole; for $KFeCl_4$, $\Delta H(1) = -7.2$ kcal./mole.

The heat capacities and heats of fusion of $NaFeCl_4$ and $KFeCl_4$ were measured with a drop calorimeter, values of the heats of fusion being 4.39 kcal./mole and 3.85 kcal./mole, respectively.

The existence of $MFeCl_4$ in the melt is evidenced by the composition and temperature dependence of ferric chloride vapor pressure above MCl–$FeCl_3$ mixtures. At constant temperature, as NaCl is added to liquid $FeCl_3$ the vapor pressure falls in a steep titration–like curve to nearly zero at 50 mole % NaCl. As the NaCl concentration rises from 45 to 50 mole % the ferric chloride pressure drops by 2 $^1/_2$ orders of magnitude, behavior which is consistent with the nearly quantitative formation of $NaFeCl_4$ in the melt. The small pressure of $FeCl_3$ present at elevated temperature above melts containing more than 50 mole % MCl varies with melt composition according to the equilibrium

$$MCl(soln.) + FeCl_3(v) = MFeCl_4(soln.). \qquad (2)$$

At 1000°K., $K_{(2)}^{-1} = 13$ mm Hg if M = Na, and $K_{(2)}^{-1} = 2.6$ mm Hg if M = K.

The vapor pressure of ferric chloride above MCl–$FeCl_3$ melts of constant composition varies with temperature according to

$$\ln P_{FeCl_3}^{t} = A + BT^{-1} \qquad (3)$$

Where $P_{FeCl_3}^{t} = P_{FeCl_3} + 2\,P_{FeCl_3}$ is a combined pressure of ferric chloride monomer and dimer. The slope, B, in Expression (3) can be regarded as 1/R times the heat of solution of ferric chloride vapor in the melt. For melts containing more than 50 mole % $FeCl_3$ the $\ln P_{FeCl_3}^{t}$ vs. T^{-1} curves are approximately parallel to that of pure liquid ferric chloride. Thus in $FeCl_3$–rich melts the heat of solution of $FeCl_3^t$ is about the heat of condensation, and no apparent reaction of $FeCl_3$ with solvent is taking place. If the melts are made rich in MCl, however, the slopes of $\ln P_{FeCl_3}^{t}$ vs. T^{-1} curves become markedly steeper showing that in these melts the ferric chloride vapor is reacting exothermically with the excess MCl. The enthalpy of Reaction (2) is calculated from the slopes of the ferric chloride pressure–temperature curves to be ca. −30 kcal./mole for M = Na, and ca. −36 kcal./mole for M = K.

The compound $MFeCl_4$ appears to be somewhat volatile. Appreciable quantities of sodium or potassium–containing vapors are observed above $MFeCl_4$–containing melts at temperatures as low as 600°C. The vapor phase above certain MCl–rich melts contains Fe(III)/M(I) atom ratios considerable less than 2, but Fe(III)/M(I) ratios less than unity have not been observed. Accordingly, it appears reasonable that the alkali atoms are present in the vapor as $MFeCl_{4(v)}$. the analogous gaseous $NaAlCl_4$ and $LiAlF_4$ are already known.

The vapor pressures of pure $NaFeCl_{4(l)}$ and $KFeCl_{4(l)}$ are found to be

$$\text{Log } P_{NaFeCl_4,} \text{ (mm Hg)} = 7.496 - 5.904\ T^{-1},\ 750°K. \leq T \leq 1100°K.$$

$$\text{Log } P_{KFeCl_4,} \text{ (mm Hg)} = 5.657 - 4.517\ T^{-1},\ 850°K. \leq T \leq 1100°K.$$

The vapor pressures of ferric chloride and of the volatile $MFeCl_4$ compound were determined by a transpiration method. The melt was contained in a Vycor flask immersed in a solder bath. A slow, metered stream of Cl_2 was preheated, passed through the melt, filtered through SiO_2 wool to remove mechanically–entrained droplets, and brought into a removable condenser in which the $FeCl_3$ and $MFeCl_4$ were cooled and collected. The moles Fe(III) and moles M(I) per mole of Cl_2 gas were determined by analysis, and from this the vapor pressures were calculated. It was assumed in this calculation that $MFeCl_4$ was monomeric.

CALORIMETRIC HEATS OF MIXING IN BINARY LIQUID SYSTEMS OF SODIUM AND POTASSIUM WITH B–METALS.

F. E. Wittig and T. Kleinsteuber

Since 1953 we have pursued a program on the behavior of heats of mixing in binary liquid alloy systems with reference to the position of the metals in the periodic table. This program comprises:

1. a thorough study of new and efficient calorimetric methods at temperatures up to 600° (with F. Huber and W. Schmatz), between 600° and 1100° (with E. Gehring) and now between 1000° and 1600°C.
2. a systematic study of heats of mixing in binary liquid alloy systems of metals melting below 1000°C.

3. a systematic discussion of results in terms of position of both metals in the periodic table and kind of chemical bond.

At present 45 systems with Ag, Mg, Zn, Cd, Hg, Al, In, Tl, Sn, Pb, Sb and Bi have been studied and some empirical rules for the behavior of binary systems of B–metals derived. So called ξ–functions according $H^M = \xi . x . (1-x)$ are computed by least square methods. Starting with one metal as steady A–component, the ξ –function of any binary combination with all other metals as B–component is put into the periodic table according to the position of the second B–component. In any combination of a B–metal with all other B–Metals we can state the following rules:

1. We always get the same pattern, when taking the B–component from the 4., 5. or 6. Period.
2. The most negative values always occur in the period of the first A–component.
3. Shifting from the period of the A–component to the next always results in a shift to more positive values (about 8 kj/g–At).
4. The A–A–System, e.g. Zn–Zn, may be considered as Zero–level. Combining with rule 3 any system with components from the same group should give positive heats of mixing. This holds for Zn–Cd, Zn–Hg, Al–In, (most probably for Al–Ga and Al–Tl), Sn–Pb and Sb–Bi, but not for Hg–Cd, owing to additional bond energies.
5. Within one period the III–V and very probably the II–VI are most negative. The IV–IV–systems exhibit a maximum in a trough.
6. The periodic tables of ξ –functions follow the same pattern, when taking the A–component from the same group with exception of rule 2 and 3.

After rule 2 the most negative combinations are always obtained by taking the second B–component from the same period, e.g. Cd–In, Cd–Sn, and Cd–Sb, or Hg–Tl, Hg–Pb, and Hg–Bi. Comparing periods of those Minimum–Systems the most negative is obtained in the 6th period, when the A–component is from group II, III or IV. In group V the reverse happens, probably due to the transition from metals to metalloids. The rules for the behavior of heats of mixing can be applied to the phase diagrams as well. Marked deviations from regular behavior occur in the same way in other properties as the magnetic susceptibility, the excess volume and viscosity. This may be considered as evidence, that our rules depend on a certain bond mechanism controling a limited region of the periodic system.

On crossing the borders of such regions some of those rules may become invalid and other rules may perhaps become preponderant. In further pursue of our work we consider the behavior of liquid systems of B–metals with metals from group Ia and IIa, starting with Sodium, Potassium and Magnesium. In this way we are trying to study the increasing influence of differences in electronegativity. With B–metals only small changes of electronegativity occur between 1, 2 and 1, 5, and differences are perhaps not significant, but with Mg, Na and K values are dropping below 1, 0 , and we are expecting an increasing contribution from ionic bonds, most certainly when crossing the Zintl–boundary between gourp IIIb and IVb.

Until now the systems of Sodium with Cd, Hg, In, Tl, Sn, Pb and Bi and of Potassium with Hg and Tl were studied by mixing the liquid metals at temperatures between 110°C and 500°C under purified Argon in the high–temperature–calorimeter of Wittig and Schmatz. Work will be continued on any other reasonable system of Potassium and Magnesium. Results are stated by smoothed ξ –functions in Table I. Integral and partial heats of mixing can be derived from ξ –functions with simple computations outlined in previous work (e. g. Z. physik. Chemie, NF, 21, 47; 1959, Z. Metallkunde, 51, 226; (1960). In Fig. I we present the curves of ξ –functions in the periodic table according to the position of the second B–component in group II, III, IV, and V, and the 5th or 6th period. Unfortunately some trouble occured in the system Na–Bi, owing to a very violent reaction resulting in splashing and evaporation of metals at 500°. Until now results are somewhat erratic in the system. Of course our work is not advanced enough to give a thorough and comprehensive discussion of the behavior of this kind of liquid phases, but there are some points of interest worth mentioning. With Sodium we get the same pattern in period 5 and 6 (Rule 1) and a shift to Potassium is not likely to change very much . (Rule 6). Rule 2 and 4 cannot be discussed with present results, but rule 5 is in accord with decreasing values going from group II to V. The shift to more positive values when going from period 5 to 6, suggested by rule 3, is not confirmed. This seems to indicate, that misfit energies are not so important in view of higher bond energies and much more negative heats of mixing. This point will become clearer, when more results will become available, but there seems to be a crossing of curves in period 5 and 6 going from group IV, to V, as mentioned before, discussing the Minimum–Systems of B–metals, where the influence of misfit–energies is minimized by taking the components from the same period.

Another interesting point is the break in the curve at 20 at–% Sn or Pb after crossing the Zintl–boundary, resulting in a step in the partial heats of mixing. The concentration of 20–%t.–% strongly suggest a peculiar high bond energy, when 4 Atoms Na share their 4 electrons with 1 atom of Sn or Pb, in accord with opinions advanced by Wagner, (Systems Ag–Te and Ag–S), and with our recent results in the System Ag–Sn.

Table I

Na –Cd	$\xi = -6240_{\circ} \exp 2,06.x + 6240 - 1800.x$		400°
Na –Hg	$\xi = -480.000/(1-x)$	$0,0 < x < 0,2$	110°
	$\xi = -735.000/x$	$0,68 < x < 1,0$	
Na –In	$\xi = -152.000 - 59600.x + + 45500.x^2$		500°
Na –Tl	$\xi = -32600 - 48600.x + 47400.x^2$		350°
Na –Sn	$\xi = -71.100 + 26.100.x - 600.000.x^2$	$0,0 < x < 0,2$	500°
	$\xi = -134.000 + 320.000_{\circ}x - 503.500.x^2$	$0,2 < x < 0,43$	
	$\xi = -122_{\circ}000 + 92.000.x$	$0,61 < x < 1,0$	
Na –Pb	$\xi = -64_{\circ}700\ x\ 10.200.x$	$0,0 < x < 0,2$	430°
	$\xi = -100_{\circ}600 + 79.730.x - 17.850.x^2$	$0,2 < x < 1,0$	
Na –Bi	$\xi = -21.000/(1-x)$	$0,0 < x < 0,04$	500°
	$\xi = -211_{\circ}000 + 179.000.x$	$0,5 < x < 1,0$	
	$\xi = -808.000 + 1636.000.x - 912.000.x^2$	$0,7 < x < 1,0$	280°
K –Hg	$\xi = -38.900/(1-x)$	$0,0 < x < 0,25$	110°
	$\xi = -80.600/x$	$0,9 < x < 1,0$	
K –Tl	$\xi = -15.500 - 53_{\circ}900.x$	$0,0 < x < 0,6$	350°
	$\xi = -50.000 + 7.500.x$	$0,6 < x < 1,0$	

ξ in j/g – At; x,conc. of second component in at–%.

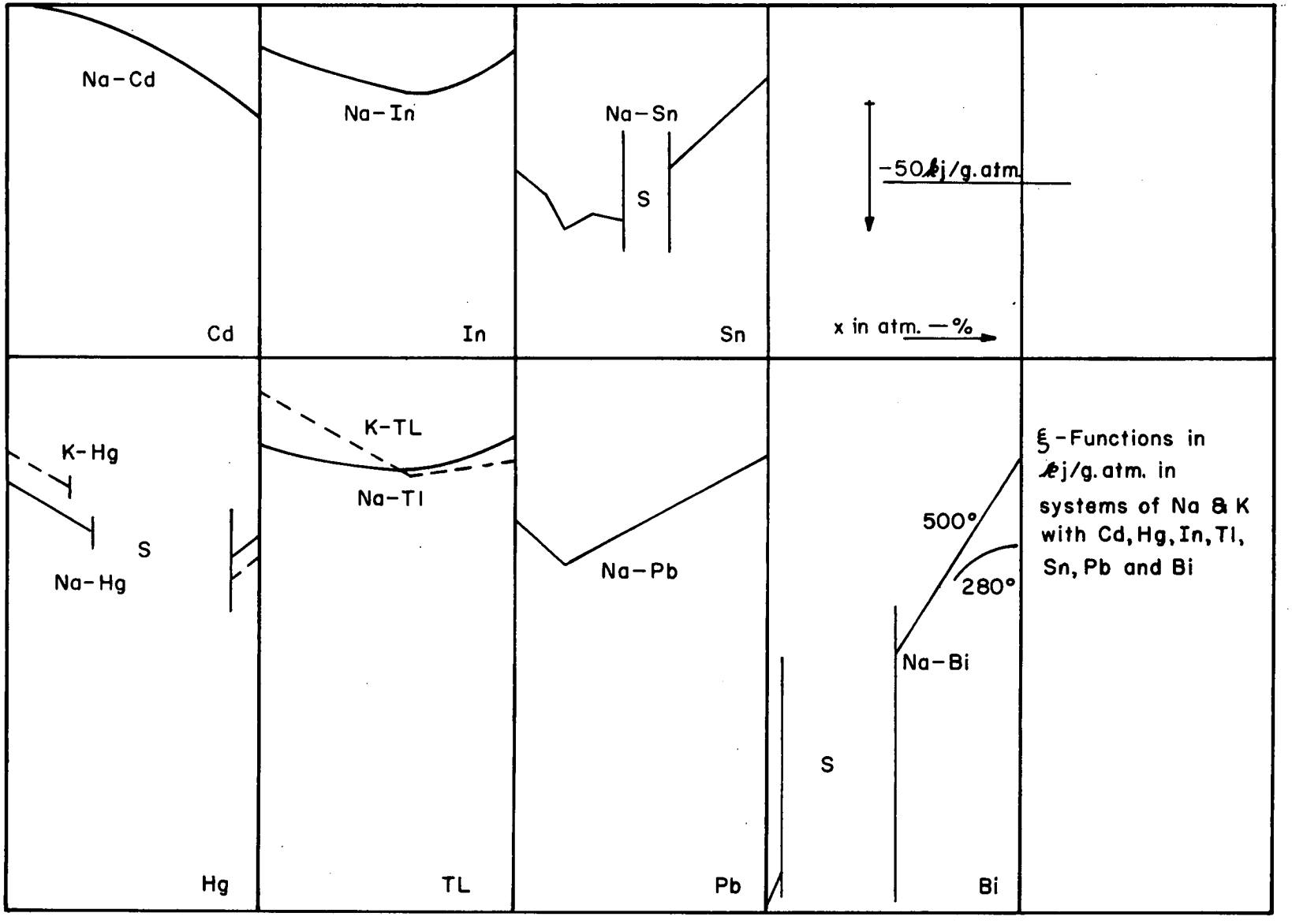
Na-Cd
Cd
Na-In
In
Na-Sn
S
Sn
-50 kj/g.atm.
x in atm. — %
K-Hg
S
Na-Hg
Hg
K-TL
Na-Tl
TL
Na-Pb
Pb
500°
280°
Na-Bi
S
Bi
ξ-Functions in kj/g.atm. in systems of Na & K with Cd, Hg, In, Tl, Sn, Pb and Bi

THE THERMODYNAMIC PROPERTIES OF NIOBIUM AND CERIUM OXIDES.

Y.I. Gerassimov, V.I. Lavrentev, F.A. Kuznetsev, T.N. Rezuhina.

Equilibrium reduction of niobium pentoxide to niobium oxide has been investigated and cells including the lower niobium oxide and metallic niobium have been studied (1)

The equilibrium of the oxides of niobium with hydrogen in the temperature interval of 1200–1550°C has been studied by the circulation method in the apparatus described in (2). The sample under study in the form of a tablet was placed in a molybdenum furnace of short circuit type in a platinum boat in such a way that the contact of the tablet with platinum was minimum. The gross chemical composition of the reduction products was determined by the increase in weight upon heating them in air up to Nb_2O_5. The phase composition was determined by the X-ray method. Two reduction reactions were investigated.

$$2.5NbO_{2.4} + H_2 \longrightarrow 2.5NbO_2 + H_2O \quad \ldots\ldots\ldots (1)$$

$$NbO_2 + H_2 \longrightarrow NbO + H_2O \quad \ldots\ldots\ldots (2)$$

The logarithms of the equilibrium constant at different temperatures for reactions (1) and (2) are given (with an accuracy of $\pm$ 0.3% by the following equations.

$$\lg K_{pI} = -\frac{15050}{4.575T} + 1.3306 \qquad (1207 - 1400°C)$$

$$\lg K_{pII} = -\frac{29490}{4.575T} + 1.334 \qquad (1400 - 1500°C)$$

From this $\Delta G°_{I}(cal) = 15050 - 6.087T$

$\Delta G°_{II}(cal) = 29490 - 6.10T$ (I cal = 4.1840 abs. Joules)

Combining reactions I and II with the reaction of the formation of water vapour,

$$H_2 + 1/2O_2 \longrightarrow H_2O \quad \ldots\ldots\ldots (3)$$

the isobaric potential of which according to Chipman[3] is expressed by the equation

$$\Delta G^\circ_{III}(cal) = -59251 + 2.006T\lg T - 7.5\times10^{-5}T^2 + 4.08\times10^{5}T^{-1} + 6.8085T,$$

and using data from literature for the heat capacities of niobium dioxide and niobium oxide[4] and of oxygen[5], ΔG°_{IV} (accordingly ΔH°_{IV}) and ΔG°_{V} (accordingly ΔH°_{V}) of the formation of $NbO_{2.4}$ and NbO_2 according to the reactions:

$$NbO_2 + 1/2O_2 \longrightarrow NbO_{2.4} \quad \ldots\ldots\ldots (ly)$$

$$Nbo + 1/2O_2 \longrightarrow NbO_2 \quad \ldots\ldots\ldots (y)$$

can be calculated.

$$\Delta G^\circ_{IV} = -26450 + 8.60T\lg T - 0.859\times10^{-3}T^2 + 1.642 + 1\,0^{5}T^{1} - 20.55T \quad (T > 1040^\circ C)$$

$$\Delta G^\circ_{IV} = -29050 - 6.60T\lg T + 2.219\times10^{-3}T^2 + 0.431\times10^{5}T^{-1} + 24.71T \quad (298 - 1040^\circ C)$$

$$\Delta G^\circ_{V} = -98100 - 16.36T\lg T + 1.240\times10^{-3}T^2 - 0.861\times10^{5}T^{-1} + 75.68T \quad (T > 1040^\circ C)$$

$$\Delta G^\circ_{V} = -95500 - 1.165T\lg T - 1.839\times10^{-3}T^2 + 0.35\times10^{5}T^{1} + 30.42T \quad (298 - 1040^\circ C)$$

From these equations at 298.2°K $\Delta G^\circ_{IV} = -26.2$ Kcal, $\Delta H^\circ_{IV} = -28.1$ Kcal, $\Delta S^\circ_{IV} = -6.36$ e.u. $\Delta G^\circ_{V} = -87.3$ Kcal, $\Delta H^\circ_{V} = -94.95$ Kcal, $\Delta S^\circ_{V} = -25.6$ e.u.

In the calculation for $NbO_{2.4}$ the heat capacity of $NbO_{2.4}$ was taken as $C_p = 19.2 + 1.77\times10^{-3}T - 3.659\times10^{5}T^2$ under the assumption that the heat capacity of $NbO_{2.4}$ changed with temperature in the same way as that for $NbO^*_{2.5}$ and that for $NbO_{2.5}$, C_{p298} is equal to 1.56 cal/gm-mol.

*Reference 4

In the composition region from $NbO_{2.4}$ to $NbO_{2.5}$ the value of the equilibrium constant $K_p = P_{H_2O} / P_{H_2}$ quickly increases and so could not be measured with sufficient accuracy in our apparatus. Therefore, this part of the isotherm was estimated by linear extrapolation.

For the reaction of the formation of Nb_2O_5 from NbO_2, $2NbO_2 + 1/2O_2 \longrightarrow Nb_2O_5$ ..... (VI)

linearly extrapolating from $NbO_{2.4}$ to $NbO_{2.5}$ we obtain at 298.2°K;

$\Delta H^\circ_{VI} = -70.25$ Kcal; $\Delta G^\circ_{VI} = -65.5$ Kcal; $\Delta S^\circ_{VI} = -15.9$ e.u.

We could not carry out the equilibrium reduction of niobium oxides to metallic niobium with hydrogen. Therefore, the method of electromotive force with solid electrolytes was used for the determination of the thermodynamic properties of the lower niobium oxide NbO.

Measurement of the E.M.F. of the cell

$$Pt \mid Fe, Fe_{0.95}O \mid \text{Solid electrolyte} \mid Nb, NbO \mid Pt \quad \ldots\ldots\ldots\ldots (A)$$

was carried out in the temperature interval of 841–1073°C. The solid electrolyte and both the electrodes, consisting of a mixture of the metal and its oxide in equilibrium with each other, were prepared in the form of tablets. Measurement of E.M.F. was conducted in vacuum in the apparatus described in (6). Mixed crystals of thorium dioxide and lanthanum oxide, possessing pure oxygen ion conductivity were used as the solid electrolyte. The equilibrium E.M.F. values of the cell (A) arise from the change in the isobaric potential ($\Delta G^\circ_{VII} = -2FE_A$) of the reaction

$$Fe_{0.95}O + Nb \longrightarrow NbO + 0.95Fe \quad \ldots\ldots\ldots\ldots (VII)$$

The maximum deviation of the experimental values from the linear dependence of the E.M.F. with temperature does not exceed $\pm$ 0.008V which constitutes nearly 1.2% of the measured value. The experimental values in the temperature interval under study can be expressed (with an accuracy of $\pm$ 0.7%) by the equation

$$\Delta G^\circ_{VII} = -34500 + 3.15T$$

It can be calculated that for the formation of NbO according to the reaction

$Nb + 1/2O_2 \longrightarrow NbO$ ..... (VIII)

ΔG°_{VIII} is equal to $-98450-0.564TlgT-0.63x10^{-3}T^2-0.08x10^5T^{-1}+22.10T$ (298–1346),

using ΔG°_T of the reactions $FeO + CO \longrightarrow Fe + CO_2$ (6) and $CO + 1/2O_2 \longrightarrow CO_2$ (7) and the temperature dependence of the heat capacity for NbO_2 according to (4) and for NbO according to (3).

From this at 298.2°K: $\Delta G^\circ_{VIII} = -92.4$ Kcal;

$\Delta H^\circ_{VIII} = -98.4$ Kcal; $\Delta S^\circ_{VIII} = -20.2$ e.u.

Combining reactions (V) and (VIII) it can be calculated $\Delta G^\circ_{VIII} = -350+15.80TlgT-1.87x10^{-3}T^2+0.781x10^5T^{-1}-53.58T$ (T 1040°C)

for the reaction $Nb+NbO_2 \longrightarrow 2NbO$ ..... (VIII)′

The direct measurement of the isobaric potential of this reaction ($\Delta G^\circ_{VIII'} = 2FE_b$) was carried out in the cell (b).

Pt | NbO, NbO_2 | Solid electrolyte | Nb, NbO | Pt ..... (b)

The following values were obtained for $\Delta G^\circ_{VIII'}$:

T°C	950	1003
ΔG calculated (cal)	−8950	−9090
ΔG experimental (cal)	−8900	−9090

Combining reactions (y), (yI) and (yIII) it can be calculated that at 298.2° K, $\Delta H^\circ_{IX} = -456.0$, Kcal; $\Delta G^\circ_{IX} = -424.9$ Kcal; $\Delta S^\circ_{IX} = -107.4$ e.u.

$\Delta H^\circ_X = -193.3$ Kcal; $\Delta G^\circ_X = -179.7$ Kcal; $\Delta S^\circ_X = -45.8$ e.u.

for the formation of Nb_2O_5 and NbO_2 respectively from their elements according to the reactions $2Nb + 5/2O_2 \longrightarrow Nb_2O_5$ ..... (IX)

and $Nb + O_2 \longrightarrow NbO_2$ ..... (X)

According to a plan for a systematic study of the thermodynamic properties of rare earth oxides the following subjects were studied; heat of formation of the sesquioxide of cerium Ce_2O_3 (9), heat capacities of oxides CeO_2 (10), Ce_2O_3 (11) and Pr_2O_3.

Ce_2O_3 obtained by the reduction of CeO_2 in a stream of highly purified hydrogen is stable in air at room temperatures. This permits the determination of the heat of the reaction

$$Ce_2O_3 + 1/2O_2 \longrightarrow 2CeO_2 \quad \ldots\ldots\ldots (XI)$$

In the calorimetric bomb by the ordinary method it was found that $(\Delta H_{289})_{XI}$ for this reaction is equal to -85.43 ± 0.26 Kcal. The Ce_2O_3 used in this work had the normal hexagonal structure.

Heat capacities of CeO_2, Ce_2O_3 and Pr_2O_3 were measured by the method of mixing in the massive metallic calorimeter. The sample under study CeO_2 was placed in a platinum ampoule, samples Ce_2O_3 and Pr_2O_3 in sealed evacuated quartz ampoules, provided with platinum covers.

The true molar heat capacities of the oxides under study were calculated from the values of the average heat capacities.

CeO_2 $C_p = 14.59 + 4.895 \times 10^{-3} T$ (0.2% 608–1171°K)

Ce_2O_3 $C_p = 23.31 + 1.265 \times 10^{-2} T$ (0.5% 578–1116°K)

Pr_2O_3 $C_p = 23.73 + 1.251 \times 10^{-2} T$ (0.5% 712–1126°K)

Using data from literature for standard heats of formation of CeO_2 (12), Pr_2O_3 and Pr_6O_{11} (13), and for heat capacities of Pr_6O_{11} (14), metallic Ce and Pr (15), oxygen (5) we obtain for reactions XII–XVII:

$$Ce + O_2 \longrightarrow CeO_2 \quad \ldots\ldots\ldots (XIII)$$
$$2Ce + 3/2O_2 \longrightarrow Ce_2O_3 \quad \ldots\ldots\ldots (XIV)$$
$$2Pr + 3/2O_2 \longrightarrow Pr_2O_3 \quad \ldots\ldots\ldots (XV)$$
$$Pr_2O_3 + 1/3O_2 \rightarrow 1/3Pr_6O_{11} \quad \ldots\ldots (XVI)$$
$$2Pr + 11/6O_2 \rightarrow 1/3Pr_6O_{11} \quad \ldots\ldots\ldots (XVII)$$

$(\Delta H^\circ_T)_{XII} = -85500+1.74T-1.49\times10^{-3}T^2-0.94\times10^{3}T^{-1}$

$(\Delta H^\circ_T)_{XIII} = -259800+0.62T+0.31\times10^{-3}T^2-1.88\times T^{-1}$

$(\Delta H^\circ_T)_{XIV} = -434000-0.49T+2.13\times10^{-3}T^2-2.82\times10^{5}T^{-1}$

$(\Delta H^\circ_T)_{XV} = -437000+0.33T, 2.86.10^{-3}T^2-2.82\times10^{-5}T^2$

$(\Delta H^\circ_T)_{XVI} = -19440 +5.27T-1.845\times10^{-3}T^2 -0.627\times10^{5}T^{-1}$

$(\Delta H^\circ_T)_{XVII} = -456550+5.60T+0.935\times10^{-3}T^2-0.0692\times10^{5}T^{-1}$

LITERATURE CITED

1. Lavrentev, V.I., Gerassimov, Y.I. and Rezuhina, T.H. 1961: Dokl. Acad. Sci. 6; 136.
2. Zharkova, L.A., Lavrentev, V.I., Gerassimov, Y.I., Rezuhina, T.N. and Simanov, Y.P. 1960: Dokl. Acad. Sci. (USSR), 134; 872.
3. Chipman, J. 1934: Trans. Am. Soc. Metals 22; 385.
4. Geld, P.V. and Kusenko, F.G. 1960: Izvestia Acad. Sci. (USSR) 2; 79.
5. Kelley, K.K. 1949; U.S. Bur. Mines, Bull. 476.
6. Rezuhina, T.N., Lavrentev, V.I., Levitsky, A.V. and Kuznetsev, F.A. 1961: Zhurnal Fiz. Khim. (In press).
7. Darken, L.S. and Garry, R.W. 1945: J. Am. Chem. Soc. 67: 1938.
8. Peters, H., and Mobius, H.H. 1958: Z. Phys. Chem. 209; 298.
9. Kuznetsov, F.A., and Rezuhina, T.H., and Golubenko, A.N. 1960: Zhurnal Fiz. Khim. 34 (9).
10. Kuznetsov, F.A. and Rezuhina, T.H., and Golubenko, A.N. 1960:
11. ——— and ——— 1960: Ibid. (35 (In press).
12. Haber, E. and Holley, C. 1953: J. Am. Chem. Soc. 75: 5645.
13. Stubblefield, C.T. 1953: Ibid. 78; 3018.
14. Beomeke, S.O. and Ziegler, W.J. 1951. Ibid. 73: 5099.
15. Stull, D.R. and Sinke, G.C. 1956: Thermodynamic properties of the elements. NY.

A STUDY OF THE THERMODYNAMIC PROPERTIES OF THE SYSTEM IRON–PLATINUM.

S. Mundiath, J.I. Gerassimov

Iron is known to form a continuous series of solid solutions with platinum. Superlattice structures for Fe_3Pt (19–33 atomic percent), FePt and $FePt_3$ (72–77 atomic percent) have been reported by several authors and have been investigated by X–ray and other methods. A study of the thermodynamic properties of this system was considered important from the view of understanding the nature of ordering reactions. We intend to make this study a systematic investigation of the thermodynamic properties, endeavoring to cast some light on the factors that promote the formation of supper–lattices, on the nature of the transition itself and the critical temperature of the transition. With this in view the electromotive force developed by the cells:

$$Fe \mid Fe^{++} - (CaCl_2,\ NaCl) \mid Fe_mPt_n$$

$$Fe,\ FeO \mid O^{--}(ZrO_2,\ CaO) \mid Fe_mPt_n - FeO$$

was studied as a function of temperature and alloy composition between 550 and 1000°C.

The results obtained were used for the calculation of partial free energy and heat of solution of one gram–atom of iron in alloys of various compositions. Likewise were calculated integral thermodynamic quantities for the formation of alloys of different compositions from pure metals. A negative deviation from the laws of ideal solutions is observed.

THERMODYNAMICS AND STRUCTURE OF FUSED SALTS

H. Flood

Introduction: "Structure" in relation to liquids ordinarily implies short range order–disorder, (including deviations from random distribution of the structural units), coordination number, distances and finally also the type of the bonding forces.

Any statistical description gives only a more or less crude picture of the "true" structure. Our main interest in fact is to derive the simplest possible model which is able to account for the physical chemical properties of molten salts.

Thermodynamic experimental data can tell, in principle only if a proposes structure is a possibility or not, but frequently it will be unable to decide which one of several structures is correct, or if a particular structure is the only one possible.

Important also is to keep in mind Hildebrand's warning than an insufficient model may still fit the activity (ΔG) data well, however, much more serious disagreement will be evident when applied to ΔS and ΔH data.

The entropy S in particular is the bridge between thermodynamics and structure.

S determined by thermodynamical methods can be considered as the sum of two contributions, the first expressing the ability of thermal movements of the structural units (vibrational, rotational or translatoric entropy), the second associated with the structural configuration in mixtures of different units (entropy of mixing).

The review is divided into three parts:

a) one component melts, dealing with the entropy effects of the vibrational type.

b) mixtures of salt melts with one common ion

c) mixtures of salt melts without common ions, dealing with entropies of mixing.

One Component System: Two thermodynamic quantities mainly relate the liquid structure to the structure of the solid substance, viz. ΔS_f (the entropy of fusion) and ΔV_f (The change of volume by the melting process). These are related by the Clausius–Clapeyron equation:

$$\Delta V_f = dT_f/dp \; \Delta S_f$$

Unfortunately, most of the older data on ΔS_f and ΔV_f quoted in the literature must be used critically. Recent data on ΔS_f (Bredig et al.) and ΔV_f (Sauerwald et al.) on the alkali halides have simplified the empirical picture. If ΔS_f is plotted against $\Delta V_f/V_f$ (or V_s) all the data except the Li–halides appear to assemble on one curve. The data support the impression that variations in ΔS_f and ΔV_f may be related chiefly to the solid phase. Similar features are also apparent when considering the more incomplete ΔS_f data of compounds of the type MX_2.

Attention is also called to the results of thermal expansion of alkali halides. These show that fusion occurs at a "corresponding" temperature, when both the relative thermal expansion and the vibrational energy have reached a certain limit – nearly the same for all the halides, (compare also the constancy in the ratio T_f/T_b, T_b – Boiling Point).

The above considerations indicate that the structure of molten salts might be of more general type, less differentiated, than the structures of the solids.

Salt Mixtures with a Common Ion: The majority of binary salt mixtures with common ions are known to show negative heat of formation, quite opposite from the formation of solid solutions.

The endothermic formation of solid solutions (of ions of different size) is qualitatively explained by the loss in lattice energy due to the change in the nearest neighbor distances.

The negative ΔH_{mix} in the liquid solutions are in agreement with the picture of a change in the second nearest neighbor distances.

Considering this effect only in mixing $M_I X$ and $M_{II} X$

$$\Delta H_{mix} \simeq N_{M_I} (1 - N_{M_{II}}) \left(\frac{d_1 - d_2}{d_1 - d_2}\right)^2$$

when d_1 and d_2 are the interionic distances characteristics for the two pure components.

Kleppa has shown recently that this formula is in excellent agreement with his calorimetric measured heats of mixing of alkali nitrates, as far as the variation of ΔH_{mix} with the interionic distances is concerned.

However, recent (unpublished) data of Toguri et al from exchange equilibria in bromide–chloride–salt mixtures show increasing negative deviations from ideality in the sequence

Li– Na – K

which is opposite from the second nearest neighbor considerations.

Hence, it seems evident that endothermic packing effects contribute essentially to the heat of mixing, as the pure components (normally) should give a better packing than the mixed state.

Ideal or regular mixtures are expected when

$$|\Delta H| < z\ RT$$

(z = coordination number), deviations when $|\Delta H| \geq z\ RT$, in extreme cases resulting in either immiscibility or formation of ordered $M_I \cdot \cdot \cdot \cdot M_{II} \cdot \cdot \cdot \cdot M_I$ structures in the melt, corresponding formally to formation of a complex compound $M_I(M_{II}X_2)$

(Examples: $KCl + MgCl_2(FeCl_2) \rightarrow K_2MgCl_4(K_2FeCl_4)$,

$NaF + AlF_3 \rightarrow Na_3AlF_6$ or $NaAlF_4$).

The entropy of mixing of components of different volumes is thoroughly discussed in connection with molecular mixtures, compare for instance the theory of the athermal mixtures.

Very little is known concerning the volume effect in ionic systems.

Mixtures of Alk ($CrO^{-2} - Cr_2O_7^{-2}$), however, shows weak positive deviations from ideality, which is strictly the opposite of athermal monomer–dimer mixtures. Furthermore liquidus lines in calcium–boro–silicate mixtures can be calculated from the simple model of ideal mixtures of ortho, pyro and 3–meric meta ions.

This indicates that volume effects are of less importance in the more open structures of the molten salts.

Another important question, still unsatisfactorily answered, is the entropy effects arising from differences in the charge of the mixed ions, whether a divalent cation should be treated as occupying one (Temkin model) or two sites of a monovalent cation. In the latter case a further question is whether the empty sites always are in neighbor positions of the divalent ions, or if they are randomly distributed in the cationic positions in the melt.

Only few systems investigated offer information regarding these questions. In some cases ($AgCl–PbCl_2$, $Na_2CO_3 - CaCO_3$) the Temkin model seems to be favoured, but systems are known ($CaF_2 - CaO$, $FeO–Fe_2O_3$) where models of defect structures might be favourable.

From the liquidus curve of binary SiO_2–phase diagrams interesting conclusions can be drawn regarding the structure of acid silicate systems (Førland).

Salt Mixtures witnout a common Ion: The review deals with models based on ideal and regular Temkin mixtures and deviations from the Temkin distribution.

The question of their applicability is still far from completely answered, but a few scattered tests indicate that the models based on nearest neighbor interactions are too simple to explain the order of magnitude of deviations from ideality, even in systems so simple as alkali halide mixtures.

THE NATURE OF CHEMICAL BONDING IN FUSED ALKALI HALIDE–METAL SYSTEMS

Kenneth S. Pitzer

In a series of difficult experiments Bredig and his collaborators (1) have measured the properties of the mixed alkali metal–halide liquid systems. These systems are of particular interest from a chemical bonding viewpoint, since there seems to be no possibility of a sub–valence state for the alkali metals. Consequently, they truly represent a transitional region between typical ionic (non–metallic) bonding and metallic bonding.

In preparation for discussion of solutions, calculations are presented for the pure metals to show the degree to which the metallic state is more stable than a hypothetical ionic state based on the positive ions and electrons locallized in cavities. These cavities containing single electrons are essentially like F–centers and the calculations of Tibbs (2) and others (3) were used to guide the choice of reasonable parameters. These calculations are for the solid metals, since more complete data are there available, and the NaCl structure is used which would be equivalent to a face–centered cubic metal. The usual structure for the actual metals is body–centered cubic, but the face–centered structure also occurs at practically the same energy. From the molal volume and the positive ion radius (Pauling) the radius of the available spherical cavity is calculated. It is assumed that the electron spends 70 % of the time within the cavity volume which is taken as that of the sphere touching the positive ions increased in radius to include half of the additional empty space. Some overlap of electron orbitals is permitted in view of the probability that at least half of the neighboring electrons will have antiparallel spin. The exact choice of parameters is not essential; these values are reasonable in view of Tibbs (2) results. The usual Madelung formula is used for the electrostatic lattice energy and the quantum mechanical formula for the energy of a particle in a spherical box for the electron in the cavity. The results show the real metal to be of lower energy than the hypothetical ionic crystal by 21 kcal/mole for Li, 18 for Na, 10 for K, and 9 for Rb and Cs.

Solid alkali halides dissolve small amounts of additional metal and it is well known that the positive ions occupy regular lattice sites while the electrons occupy otherwise vacant negative ion sites.

The latter are called F–centers. There seems to be every reason to believe that the basic structure is similar in fused systems but the metal solubility is much larger and the cavities with electrons need not be the same size as the negative ions. Studies of mixed fused alkali halides (4) show only moderate deviation from Raoult's law, hence ions of differing size must be able to mix without serious geometrical difficulty. Consequently, we would expect the heat of solution of the hypothetical ionic metal in the salt to be small. The heat of solution of the real metal should, therefore, be approximated by the excess energy of the hypothetical ionic metal over that of the real metal. In the liquid state these excessive energies may be expected to be si milar to, but somewhat smaller than those for the solids in view of the expansion on melting, etc.

Johnson and Bredig (5) have shown that their results for the potassium systems clearly indicate a dimerization equilibrium for the solute metal in the composition range 1 to 4%. The freezing point data for KCl are consistent with an equilibrium in which associated pairs have an energy 4 to 5 kcal/mole lower than the monomeric species. The data for other systems (1, 5) are consistent with similar dimerization equilibria. It seems unlikely that these dimeric species are similar in detail to the gaseous diatomic molecules of alkali metals. However, the calculations of Tibbs (2) and others (3) for F–centers show that the wave functions for electrons in cavities extend substantially outside the cavity as defined by the surrounding positive ions. Thus, if two such electron–cavities are on adjacent negative ion sites, their wave functions overlap, and the combined state for antiparallel spin will be stabilized appreciably. This energy of dimerization may be estimated from the F–center wave functions. (2, 3) In the outer region this function for NaCl is similar to a hydrogen–atom–like function for for a dielectric constant of 2.33 which is n^2 for NaCl. The energy of interaction is estimated from the bond energy curve for H_2 at R = $3.2a_o$ (the Cl–Cl distance divided by 2.33) but with the energy divided by the factor $(2.33)^2$ as required for this theory. The result is 6 kcal/mole which compares reasonably with the observed energy of dissociation in KCl of 4 to 5 kcal.

Several systems allow approximate calculations of the activity coefficient of the metal in dilute solution relative to the pure metal as a standard state.

From potassium vapor equilibrium at 1173° K Johnson and Bredig (5) report $\gamma = 13$ in KCl. The sodium iodide system shows two liquid phases, each quite dilute, over an extended temperature range. By assuming $\gamma = 1$ in the metal rich phase, γ is found to be 53 at 934° K and 43 at 975° K in the salt rich phase which is approximately 2% metal. These values correspond to only a small excess entropy and a heat of solution of the metal of 9 kcal/mole. Similar calculations for sodium chloride yield $\gamma \cong 30$ near 1130°K and $\Delta H \cong 12$ kcal/mole. If ideal entropy is assumed for potassium in potassium chloride, the γ value yields $\Delta H = 6$ kcal. These values range from 1/2 to 2/3 of the estimates based on the calculations for the solid metal. Conversion to the liquid state might account for most of the difference and details of the ionic model for the metal could be adjusted within the reasonable range to improve agreement. Such refinements are not justified at this stage but the general model is seen to be consistent with the observed properties.

Solutions of liquid metal containing a little salt cons titute a different problem. Here the solvent is in a metallic state, and the halide ions may be taken as foreign particles in the electron gas comprising the valence electrons of the metal. The energy of such a system is being calculated and preliminary results are encouraging. The results will be combined with the heats of fusion of the salts and compared with the experimental heat of solution values.

This research was carried out under the auspicies of the U. S. Atomic Energy Commission.

References

1. M. A. Bredig and J. W. Johnson, J. Phys. Chem., 64, (1960) and earlier papers there cited.

2. S. R. Tibbs, Trans. Faraday Soc., 35, 1471 (1939).

3. D. L. Dexter, Phys. Rev., 98, 244 (1954); J. A. Krumhansl, ibid, 93, 245 (1954); and papers there cited.

4. E. Aukrust, et al., Ann. N. Y. Acad. Sci., 79, 830 (1960) R. P. Tastogi and K. T. Varma, Trans. Faraday Soc., 53, 1165 (1957).

5. J. W. Johnson and M. A. Bredig, J. Phys. Chem., 62, 604 (1958).

THE ACTIVITY OF Bi IN MOLTEN Bi–$BiCl_3$ SOLUTIONS

D. Cubicciotti and R. Stringham

The present measurements of the activity of Bi in solution in molten $BiCl_3$ were undertaken to help characterize the state of the dissolved metal. Earlier determinations of the activity of $BiCl_3$ in these melts showed positive deviations from Raoult's law, in general, and a short range of conformity to Raoult's law for low Bi concentrations. The data were not sufficiently precise, however, to derive the activity of the Bi compound in the dilute range.

In the method chosen to determine the Bi activities, the liquid Bi – $BiCl_3$ mixture was equilibrated with a gaseous mixture of H_2 – HCl and gas composition was determined with a mass spectrometer. The $BiCl_3$ was distilled twice under a stream of dry N_2 into the equilibration bulb. The molten $BiCl_3$ was then treated with dry HCl several times to convert any oxide to H_2O, which was removed when the HCl was removed. About 0.1 per cent of the $BiCl_3$ was reduced to Bi with a measured amount of pure, dry H_2. The system was allowed to react and a small sample of the gas was removed for analysis. When the gas composition remained constant over a number of hours, it was felt that equilibrium had been reached. The analysis of the gas sample was performed by freezing out the HCl at liquid N_2 temperatures and determining the amount of H_2 with a mass spectrometer. The composition of the liquid phase was determined by a mass balance on the amount of $BiCl_3$ initially and the total amount of H_2 used to reduce it. To date (February, 1961) results have been obtained at several compositions from 0.1 to 0.7 mole per cent Bi in $BiCl_3$ at three temperatures (270°, 335°, and 380°C). These will be extended and by August it is expected that the entire range of compositions of one liquid phase in that temperature region will have been examined.

The equilibrium H_2 – HCl pressures can be related to the activity of the Bi component of the melt in the following way. Without assuming any detailed state for the dissolved Bi, it is possible to consider the Bi – $BiCl_3$ melt as a two component system with components Bi and $BiCl_3$. (At this point it would be equally valid to have assumed any other reasonable pair of components such as BiCl and $BiCl_3$ or $BiCl_2$ and $BiCl_3$ etc.) Then for discussions of the thermodynamic properties one can calculate the activity of the component Bi (even if later arguments show the state of the dissolved Bi to be quite different.)

Then the activity of the Bi component can be obtained from the equilibrium:

$$3/2\ H_2\ (g) + BiCl_3\ (\text{in melt}) = 3\ HCl\ (g) + Bi\ (\text{in melt})$$

The equilibrium constant for this reaction is given by:

$$K = \frac{p^3(HCl)}{p^{3/2}(H_2)} \times \frac{a(Bi)}{a(BiCl_3)}$$

In dilute solutions the activity of the Bi in the melt is proportional to the ratio $\frac{p^{3/2}(H_2)}{p^3(HCl)}$ because the activity of $BiCl_3$ is not seriously different from unity.

Once the activity of Bi is known as a function of concentration, then it can be compared with the functional variation expected from the various models proposed for these solutions. In particular for the dilute range of Bi concentrations Henry's law should apply and the activity should be a linear function of concentration. It was found that a plot of $\frac{p^{3/2}(H_2)}{p^3(HCl)}$ versus mole fraction of Bi was a straight line over the range of concentrations studied to date (0.1 to 0.7 per cent Bi) and through the origin. This dependence is what would be expected for monatomically dispersed Bi. Plots of the data as $\frac{p^{4/2}(H_2)}{p^4(HCl)}$ and $\frac{p^{2/2}(H_2)}{p^2(HCl)}$ could also be fit by straight lines (although there was some curvature to the points), however, neither of these lines passed through the origin. Straight lines through the origin. would be found with these functions if Bi_2Cl_2 or BiCl were the state of the dissolved Bi. Thus these two species fit the observed data less well than monatomically dispersed Bi.

This research was supported by the Research Division of the U. S. Atomic Energy Commission.

DIAGRAMMATIC REPRESENTATION OF THE THERMODYNAMICS OF METAL–FUSED CHLORIDE SYSTEMS

R. Littlewood

The thermodynamics of metal–fused chloride systems is more complicated than appears at first sight, especially when reactions involving impurities, particularly anionic impurities, are taken into consideration. In such cases, the presentation of thermodynamic data in diagram form has definite advantages, particularly when what is required is a general appreciation of the effect on the system of a variety of different conditions. The diagrams of Pourbaix (1) have been notably successful in the analogous field of metal–agueous solutions where Pourbaix plots equilibrium potential of the system against pH and his diagrams divide themselves into regions of stability of different solid phases (compounds of the metal in question).

In the fused salt field, it is also possible to express free energies as equilibrium potentials and there are a number of possible functions of composition which can be used as the second variable. In previous work, we have already used several types of diagram to describe the thermodynamics of metallic corrosion in fused chlorides (2), but in the present paper, we shall be concerned with diagrams employing only one particular composition variable, namely the activity of oxide ion in the melt expressed in terms of its negative logarithm, pO^{2-}. The resulting E–pO^{2-} diagrams have been found particularly useful when considering systems involving oxides, or oxygen, in contact with fused chlorides and in practice, this covers all conditions under which fused chlorides are normally used.

The properties of $E - pO^{2-}$ diagrams for metal–fused chloride systems have much in common with those E–pH diagrams for metal–agueous systems and as an example of their utility, the paper shows how in particular, E–pO^{2-} diagrams can be applied to metal extraction processes involving chlorides. The main advance here is that the method offers a rational approach to the problem of predicting impurity levels in the products of such processes. The impurity levels are obtainable directly from the diagrams and represent the highest product purity that could be obtained from the particular process under ideal conditions.

In electrowinning processes using fused chlorides as a solvent,

the main impurities in the metal product are traces of metal produced by reduction of the chloride solvent, and oxygen, which can seldom be completely eliminated from these processes. Oxygen is particularly important in the case of refractory metals such as Ti or Zr. It is shown how E–pO^{2-} diagrams can be used to predict the level of oxygen and of metallic impurities in the metal product under a given set of conditions of bath composition, cathode potential, etc. The treatment can be extended to cover any other metallic impurities present in the feed materials, either as metals or as chlorides. The diagrams can also be used to estimate the effect on product purity of changes either in the mode of operation of the process (e.g. concentration of metal chloride in the bath, cathode potential) or in the fused chloride used as solvent (e.g. change from KCl as solvent to LiCl).

E–pO^{2-} diagrams are equally applicable to processes involving reduction of metal chlorides with base metals, and once again, the levels of impurities in the product can be predicted directly from the diagrams. As an example, some of the relative advantages and disadvantages of sodium over magnesium as reducing agents for $TiCl_4$ in the production of titanium are discussed in terms of E–pO^{2-} diagrams.

The applicability of E–pO^{2-} diagrams to corrosion reactions in fused chlorides and the calculation of solubility products of oxides in fused chlorides are considered: LiCl, KCl, NaCl, and $MgCl_2$.

References

L. M.J.N. Pourbaix, "Thermodynamique des Solutions Aqueuses Diluées", English translation by J.N. Agar, Arnold, London 1949.

2. C. Edeleanu and R. Littlewood, Electrochimica Acta, 3, 195 (1960).

ELECTROCHEMICAL STUDY OF BISMUTH IN MOLTEN BISMUTH HALIDES

L. E. Topol, S. J. Yosim, and R. A. Osteryoung

E.M.F., polarographic, and chronopotentiometric measurements have been carried out on molten systems of the type

$$c/Bi(N_1),\ BiX_3(l-N_1)//BiX_3(l-N_2),\ Bi(N_2)/C \text{ or } W$$

where the N's denote mole fractions and the X's are either chloride or bromide. Generally, a three-compartment borosilicate glass cell, blanketed by argon, was used, the compartments being separated by glass frits or by asbestos fibers sealed through glass. One compartment with a weighed amount of Bi metal added initially to give a mole fraction, N_1, dissolved in the $BiX_3(I-N_1)$ served as a reference half-cell. A graphite rod served as the inert electrode. A second compartment contained a similar graphite electrode for the e.m.f. indicator electrode and two tungsten microelectrodes for polarographic and chronopotentiometric measurements. The third compartment contained a tungsten spiral which served as an anode in the coulometric electrolysis in which Bi was introduced into the center compartment by reduction of Bi^{+3}.

The useful voltage span obtained polarographically was about 0.8 volts in the chloride melt and about 0.6 volts in the bromide melt. In all cases, after Bi was added a polarographic wave was obtained indicating the oxidation of a soluble entity. The limiting current increased in direct proportion to the amount of Bi coulometrically introduced up to a Bi mole fraction of about 0.002. As the current-voltage curves crossed the voltage axis at maximum slope without any observable break, it was concluded that the electrode process is reversible. By measuring the effect of temperature on the limiting current in both halides, an estimate of approximately 6 kcalories was made for the activation energy for the presumed diffusion limited process. A log plot analysis of the polarographic waves was not conclusive, in that $\bar{n}$ values of 1.5 – 1.8 were obtained. Chronopotentiometric experiments in the Bi–$BiBr_3$ system also appear to substantiate the existence of a soluble entity which is oxidized in an apparently reversible manner at the tungsten electrode.

E.M.F. vs. log Q (equivalents of electricity passed in the coulometric generation) plots were made from the experimental E.M.F.–Q

data determined at temperatures between 238 and 350° C. In addition, cells containing 75% $BiCl_3$ – 25% $AlCl_3$ and 70% $BiCl_3$ – 30% KCl were also run to investigate effects of changes of acidity in the system. The experimental plots for each temperature are very similar and result in initially straight lines which undergo a rather sharp change in slope at fairly low metal concentrations. Typical experimental plots are shown in Figure 1 for the Bi–$BiCl_3$ system. The region of initial slope persisted to a higher added Bi concentration the higher the temperature. The initial slopes obtained from the plots at all temperatures correspond to an apparent Nernst $\underline{n}$ of 2; $\underline{n}$'s of 6 or 8, depending on the temperature, are calculated from the apparently linear region beyond the curvature. In virtually every case the first points, i.e., those at very low bismuth additions, fall below the line of $n = 2$ slope. This is attributed to the presence of some Bi in the initially "pure" BiX_3 due to a slight decomposition on melting and thus the true concentration of bismuth was greater by a small amount than that added coulometrically. The original concentration of bismuth was determined for each cell by measuring the polarographic limiting current as a function of Bi metal added and extrapolating to zero current. This yielded a Q of about 20–30 microequivalents/35 gms. BiX_3, or a mole fraction as Bi of about 8×10^{-5}. The correction increased the range where linearity of the initial ($n = 2$) plots occured, and also changed the slopes, in the case of Bi–$BiCl_3$ for example, from $2.28 \pm .12$ to 2.05 ± 0.10.

The Nernst $\underline{n}$ of 2 was taken to indicate the presence of Bi^+, arising as a result of a net reaction which may be indicated as either

$$Bi^{+3} + 2e \longrightarrow Bi^+ \qquad (1)\ \text{(coulometric addition)}$$

or

$$2Bi + Bi^{+3} \longrightarrow 3Bi^+ \qquad (2)\ \text{(direct addition of Bi)}$$

In any event, the potential determining couple at the low concentration is considered to be the $Bi^+ - Bi^{+3}$ couple.

The large change in slope in the e.m.f. v. log Q plots may be ascribed to a departure of the system from Henry's law behavior, with the deviation, α, represented as

$$\alpha = \text{antilog}\left((E_{ideal} - E_{exptl.})/(2.3RT/2F) \right) \qquad (3)$$

where

$$E_{ideal} = E_{reference} - \frac{2.3RT}{2F} \log N_{Bi^+} \qquad (4)$$

or, from equation (2)

$$E_{ideal} = E_{reference} - \frac{2,3RT}{2F} \log 3/2\ N_{Bi} \quad (5)$$

and

$$E_{expt.} = E_{reference} - \frac{2,3RT}{2F} \log 3/2\ N_{Bi}\ \alpha \quad (6)$$

However, spectroscopic evidence (1) indicates the presence of two bismuth species as a result of the dissolution of Bi in $BiCl_3$. Thus, an alternate interpretation consists of the possible formation of a second, lower-valent Bi species, e.g., a Bi^+ polymer. By considering α to be the fraction of Bi metal reacting with BiX_3 to form BiX and $(1 - \alpha)$ the fraction forming other species, it is shown that the shape of an α vs. log N_{Bi} plot for dilute solutions depends only on the species involved, i.e., on the reaction

$$y\ BiX \rightleftharpoons Bi_yX_y \quad (7)$$

and not on the numerical value of the equilibrium constant. Results of this analysis indicated a tetramer, Bi_4X_4, to be the most probable higher order species formed. Calculations of K for reaction (7) were carried out and an example of the results for tetramers, as well as trimers and pentamers, for a Bi–$BiCl_3$ run at 325° C is given in Table I. From the results of runs at various temperatures, the equilibrium constant for the formation of Bi_4Cl_4 from BiCl was deduced to be

$$\log K = \frac{(4.49 \pm 0.54) \times 10^3}{T,\ °K} - 1.93 \pm 0.95 \quad (8)$$

The effect of added acidity ($AlCl_3$) is to increase the stability of BiCl, while added base, (KCl), decreases its apparent stability relative to polymer formation.

The results in the Bi–$BiBr_3$ system are similar to those of the chloride system in that the data again indicate a species BiBr which polymerizes to a tetramer. In the bromide case the K for reaction (7) was smaller by about 10^2 than for the Bi–$BiCl_3$ system. This is also consistent with the experimentally determined longer range of stability of BiBr compared to BiCl.

The behavior of concnetrated $BiBiX_3$ solutions was examined, and a decrease in the apparent n value at higher concentrations (above 10 mole per cent Bi) relative to the apparent n values for the lower concentrations of Bi may be explained on the basis of activity effects.

Reference

1) C. R. Boston, G. P. Smith, Annual Progress Report, Metallurgy Division, Oak Ridge National Laboratory, ORNL-2988, pp. 9–16 (July, 1960).

Table I

Typical Variation of K with Composition for the Reaction

$$y\ BiCl = Bi_y Cl_y$$

$N_{Bi} 10^2$	K_N at 325°C		
	y = 3	y = 4	y = 5
0.308	2.98×10^3	5.54×10^5	$(10.97) \times 10^7$
.471	3.47	4.80	7.08
.716	4.69	5.28	6.35
1.03	5.11	4.83	4.86
1.35	5.89	5.05	4.62
1.88	7.23	5.64	4.69
2.53	8.69	6.29	4.86
3.40	9.74	6.45	4.54
4.37	10.70	6.58	4.30
5.90	9.67	5.09	2.85
7.63	11.58	5.79	3.07
Av. K_N:	$(7.25 \pm 3.02) \times 10^3$	$(5.57 \pm 0.64) \times 10^5$	$(5.29 \pm 1.41) \times 10^7$

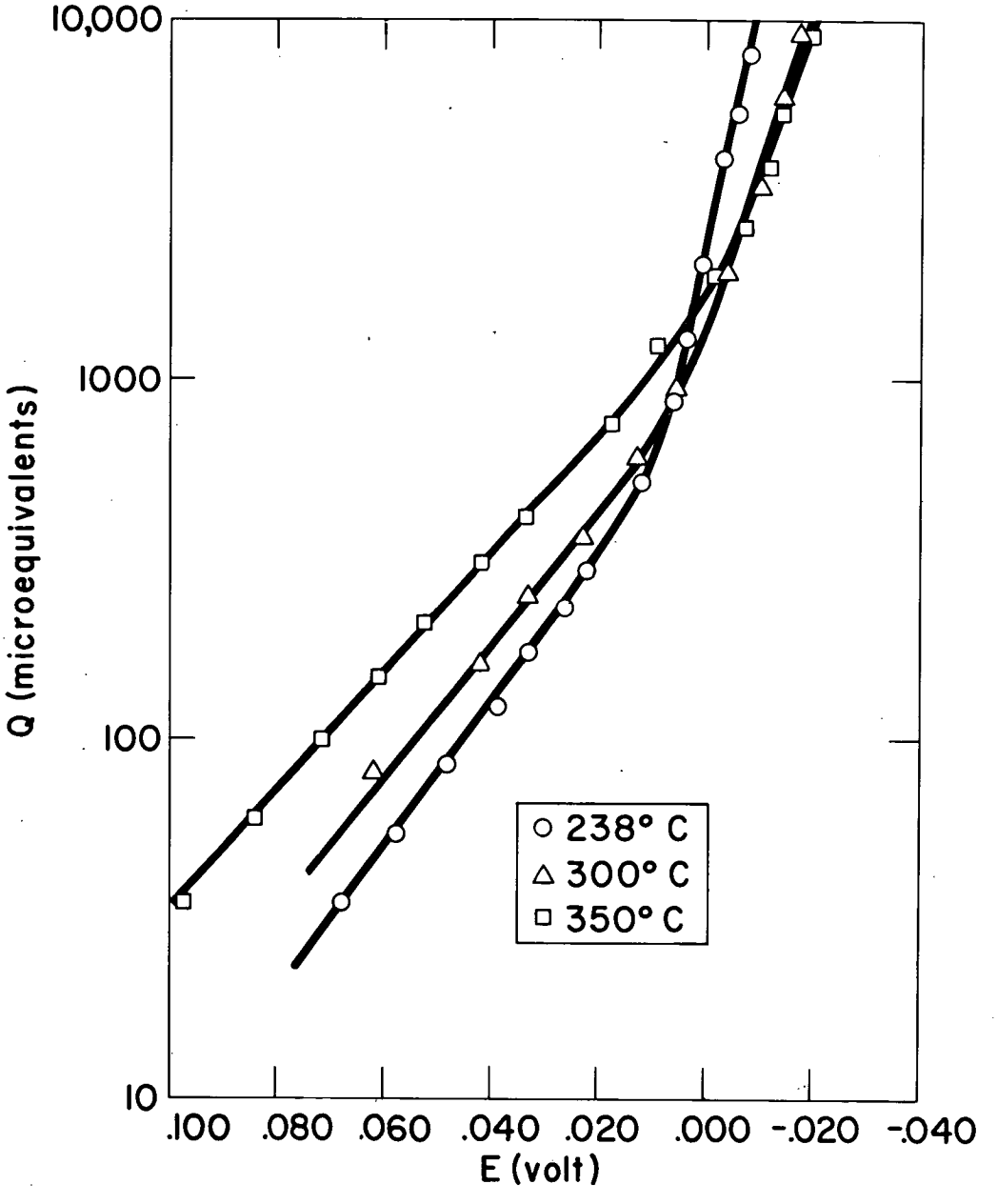

Fig. 1. Results for cells of the type: Bi(0.5 mole %), $BiCl_3$ ‖ $BiCl_3$, Bi (Q)

ACTIVITIES AND VAPOR PHASE CONSTITUTION IN THE MOLTEN SALT SYSTEM KCl – $MgCl_2$

Eugene E. Schrier and Herbert M. Clark

The vapor pressures of the pure molten salts KCl, $MgCl_2$, and CeCl have been determined in the temperature range 950 – 1100° C by the use of a boiling point technique. In this method, the temperature of boiling is determined, at a given inert gas pressure, as that temperature at which a halt is observed in the melt temperature while the furnace temperature continues to rise. Superheating was found to be unimportant in these measurements. Results for the alkali chlorides are in good agreement with previously reported values. The data for $MgCl_2$ differ considerably from the older work, but the value of the Trouton constant derived in the present investigation is more acceptable than that obtained previously.

The vapor pressures for twelve different mixtures of KCl and $MgCl_2$ covering the entire composition range have also been determined with the boiling point method at temperatures between 1000 – 1150° C. Plots of vapor pressure versus composition exhibit a strong minimum at all temperatures near the composition 66.7 mole % KCl – 33.3 mole % $MgCl_2$. The apparent heats of vaporization of the mixtures rise to a maximum at this composition.

Vapor analysis has been done on the same salts and mixtures using the transpiration method. These measurements are made by passing an inert gas over a salt sample at a known temperature. The salt vapor entrained by the carrier gas is condensed in a specially-designed portion of the apparatus. Diffusion and flow rate effects have been shown to be unimportant in the apparatus constructed for this investigation. The transpiration data for the pure salts may be combined with the boiling point measurements to yield the average molecular weight of the vapor. The following form of Dalton's Law has been found suitable for this calculation:

$$\bar{M}_i = \frac{W}{n_{c.g.}} \left[\frac{P_T}{P_B} - 1 \right] \qquad (1)$$

where:

$\bar{M}_i$ = the average molecular weight of salt vapor i at a given temperature

W = the weight in grams of the salt collected in a transpiration experiment

$n_{c.g.}$ = the number of moles of carrier gas used in the experiment

P_T = the total pressure of carrier gas and salt vapor present together in the transpiration cell during the experiment (mm)

P_B = the vapor pressure of salt i at the temperature of the of the experiments (mm).

Values of $\bar{M}$ for each salt in the temperature range 975 – 1100° C were relatively constant and were found to be as follows: KCl, 96.1; $MgCl_2$, 125; CsCl, 217. The monomer weights of the salts are 74.5, 95.2, and 168.7 respectively. Association into dimers is postulated for all the salts with the vapors of each consisting of approximately 25% dimer and 75% monomer. The mole fraction and partial pressure of each species were calculated from the average molecular weight. Equilibrium constants for dissociation of the dimer were found to be in reasonable agreement with those derived by other workers for the alkali chlorides. The heats and entropies of dimerization for KCl and CsCl differed from those for magnesium chloride indicating the effect of structural differences in the types of dimers for these systems.

Transpiration measurements made on various KCl – $MgCl_2$ mixtures indicated the presence of a mixed polymer in the vapor over these mixtures. The transpiration data obtained in these measurements was initially treated to yield apparent partial pressures for each salt, that is, partial pressures computed on the assumption that only monomers and dimers of the pure components exist in the vapor. The sum of these apparent partial pressures, the apparent total pressure, when plotted against the compostion at any given temperature in the range of the measurements, exceed the true vapor pressures of the mixtures, particularly in the middle composition range. A plot of the difference between the apparent total pressure and the true total vapor pressure versus composition effectively removes the dependence of the vapor pressure curves on liquid phase interactions. Such a plot then gives the shape of the vapor phase interactions as a function of liquid composition.

It is found that this difference curve rises to a maximum at liquid composition 54 mole % KCl, exactly that composition at which the number of formula weights of $MgCl_2$ equals the number of formula weights of KCl in the vapor as determined by analysis of the condensate obtained in the transpiration measurements. This result provides direct evidence for the existence of $KMgCl_3$ in the vapor, since it has been shown that the maximum yield in an equilibrium reaction is given when the reactants are initially present in stoichimetric proportions.

As a result of this finding, a model is postulated for the vapor over KCl – $MgCl_2$ mixtures which includes the mon omers and dimers of the pure salts and the compound $KMgCl_3$. Combination of the transpiration data with the boiling point measurements using the stoichimetric constraints provided by the model allows the calculation of the mole fractions and partial pressures of the components present in the vapor of the system. A criterion of the fit between the boiling point and transpiration data is developed which indicates that the two sets of measurements agree, within the limits of the model, to approximately 6%. This value falls within the experimental limits of combined data which is shown to be 8%. The nature of the deviations indicates, however, the possibility that the vapor phase model may be incomplete.

The partial pressure calculated for the monomers may be used to obtain activities for KCl and $MgCl_2$. Uncertainties in the data limit the calculation to values of the activities for $MgCl_2$ to the range of liquid compositions, 0 – 52.9 mole % KCl, and for KCl, to the liquid compositions 67.2 – 100 mole % KCl. The data are compared with experimental values obtained by other methods and with the model of Flood and Urnes for the system which postulates that the melt is made up of the ions, K^+, Mg^{++}, $MgCl_4^{--}$, and Cl^-. Activities calculated from this model on the assumption that the liquid is an ideal mixture of these ions compare favorable with those obtained in the present investigation. The following tables gives this comparison:

ACTIVITIES FOR $MgCl_2$

Composition (Mole % $MgCl_2$)	Experimentally Determined at 1125° C	Calculated Using Flood's Model
88.3	0.853	0.815
78.0	0.687	0.641
65.4	0.458	0.418
57.1	0.296	0.268
47.1	0.108	0.104

ACTIVITIES FOR KCl

Composition (Mole % KCl)	Experimentally Determined at 1125° C	Calculated Using Flood's Model
67.2	0.289	———
79.4	0.641	0.650
91.9	0.868	0.903

The agreement is seen to be good to 10% which appears reasonable when it is recalled that Flood's model has been used far above the temperatures for which it was originally designed.

THERMOCHEMISTRY OF PRECIPITATION AND LIQUID STRUCTURE IN MOLTEN MIXTURES

Joseph Jordan and E. J. Billingham, Jr.

The precipitation of silver chloride, silver bromide and silver iodide was studied in several fused salt solvents, viz., in pure molten sodium nitrate and pure potassium nitrate, as well as in eutectic melts of sodium–potassium nitrate and of lithium–potassium nitrate. "Thermometric titration curves" of dilute potassium halides (0.001 to 0.05 molal) with silver nitrate were recorded in an adiabatic calorimeter in which random temperature fluctuations were minimized to ± 0.001° C. The titrant was delivered by a remotely controlled automatic buret. Temperature changes were determined with the aid of a thermistor bridge which had a sensitivity of 0.0003° C. A typical titration curve is plotted in Figure 1. Reaction heats were determined from the temperature change occuring during the titration (C'C" in the figure) and solubility products calculated from the curvature of the titration curve in the vicinity of the end point. From these experimental data, the corresponding free energies and entropies of precipitation were evaluated in narrow temperature intervals (~ 1°C) in a range between 150° and 350° C. The results are shown in Table I.

The silver halides precipitated from the fused nitrate solvents as crystallive solid phases, having the usual 1:1 stoichiometry. The entropies of precipitation exhibited remarkable trends of behavior, which are illustrated in Figure 2. The entropy of precipitation of silver chloride was invariant in the various solvent melts and in the entire range of temperatures investigated. In contradistinction, entropy changes corresponding to the precipitation of AgBr and AgI varied extensively as a function of solvent and temperature. This behavior is accounted for by the combined effect of two factors, viz. :

a. the selective mobility of silver ion at elevated temperatures in crystals of silver bromide and silver iodide.

b. The properties inherent in the liquid structure of the fused salt solvents used in this study.

A model is proposed in which the molten salt solvent is visualized as consisting of closely packed lattice units. Inter–lattice vacua amount to less than 2% of the molar volume. Eighty percent of the lattice positions are occupied by anions or cations, and twenty percent are

vacant "holes". Electroneutrality is maintained throughout the melt. Solute cations and anions may occupy corresponding catonic and anionic vacancies, or interstitial positions, and may be subject to appreciable steric hindrance effects.

Table I – Thermodynamic Parameters of Precipitation Processes in Fused Nitrate Melts

Solid Phase	Temperature °C	$LiNO_3 - KNO_3$ Eutectic*			$NaNO_3 - KNO_3$ Equimolar melt			Pure $NaNO_3$			Pure KNO_3		
		ΔH°	ΔF°	ΔS°	ΔH°	ΔF°	ΔS°	ΔH°	ΔF°	ΔS°	ΔH°	ΔF°	ΔS°
AgCl	158	−19	−15	−9									
	250				−18	−13	−10						
	318	−20	−13	−12									
	350	−19	−13	−10				−18	−12	−10	−18	−12	−8
AgBr	158	−26	−18	−20									
	250				−24	−18	−12						
	318	−27	−16	−17	−22	−16	−9						
	350	−26	−17	−15				−19	−16	−5	−19	−16	−3
AgI	158	−32	−24	−18									
	250				−30	−23	−13						
	318	−35	−22	−22									
	350	−36	−23	−20				−27	−23	−7	−27	−23	−7

ΔF°, ΔH° in kcal/mole; ΔS° in cal/mole deg.

*43.1 mole % $LiNO_3$

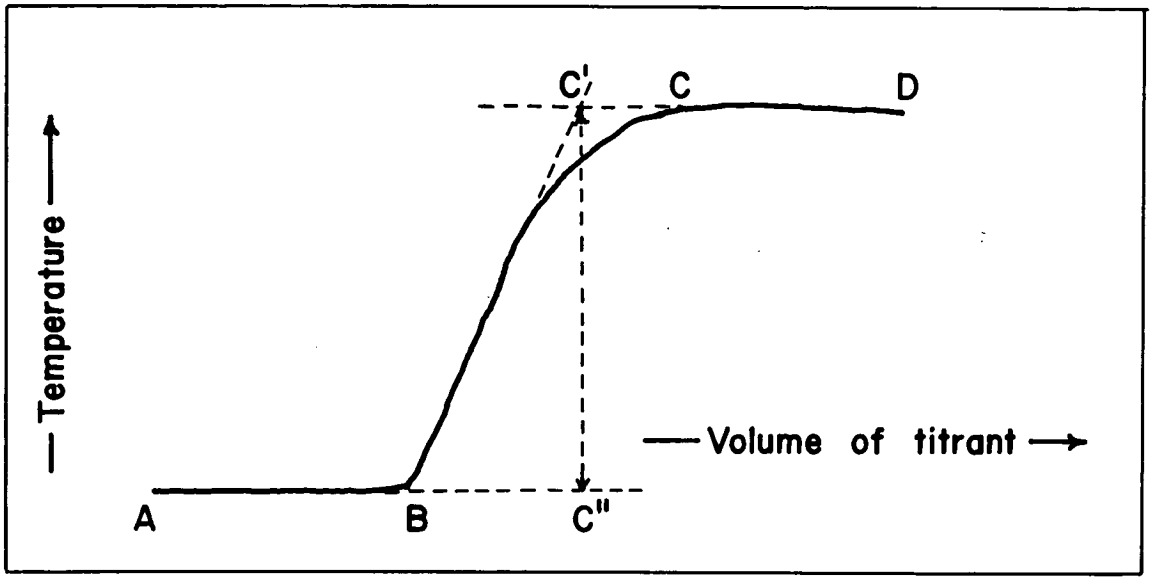

Figure 1 — Typical thermometric titration curve: 0.000115 molal KBr titrated with $AgNO_3$ in $NaNO_3$-KNO_3 eutectic at 250 °C

AB - Time-temperature blank prior to titration

B - Start of titration

CD - Excess reagent line

C' - Extrapolated end point

C'C'' - Temperature change corresponding to heat of reaction

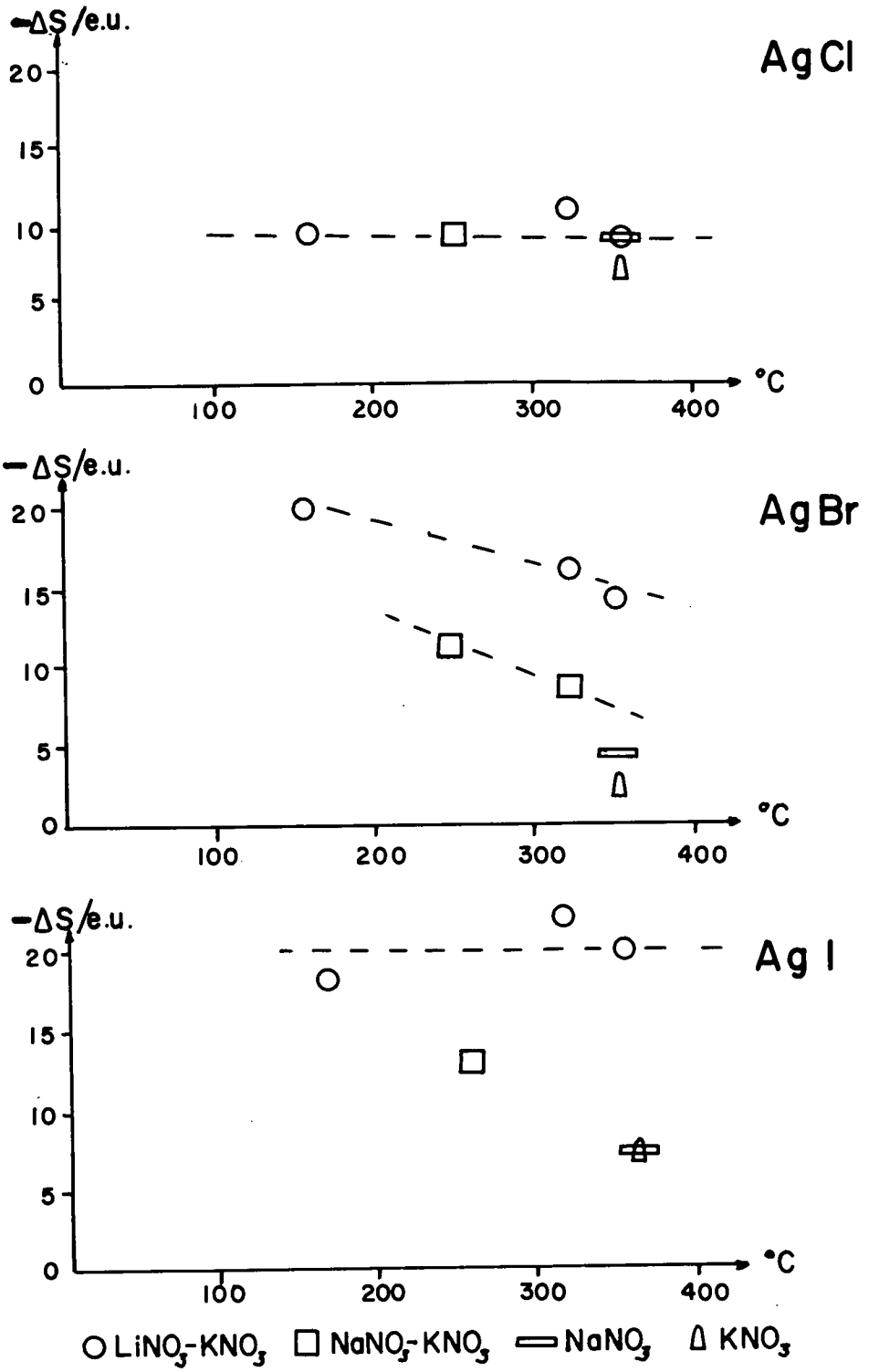

ENTROPIES OF PRECIPITATION
FIGURE 2

TEMPERATURE SCALES ABOVE 1000°C

D. R. Lovejoy

INTRODUCTION

Thermodynamics: The concept of temperature is introduced into thermodynamics by the Zeroth law – two bodies in thermal equilibrium with a third are in equilibrium with one another. Kelvin defined temperature by means of the second law; this implies a lower limit, the absolute zero, of temperature (which is unattainable according to the third law). The choice of 273.16 degrees as the water triple point temperature completes the definition of the Kelvin thermodynamic scale. Temperatures at present studied by physicists range from 10^{-6}°K to 10^{9} °K. From the point of view of thermodynamics, the temperature is a reciprocal integrating factor for heat.

Statistical Mechanics: Statistical mechanics deals with the underlying microscopic processes and from this point of view, temperature may be regarded as the breadth of a statistical distribution of energy. This is particularly illuminating in certain cases. Small particles at low enough temperatures may have too few quanta of energy to be described statistically, so that they must be treated from the point of view of fluctuation phenomena, and it is not possible to assign them a temperature. Again certain systems such as electron spins have a finite number of possible energy levels. These may be equally filled, corresponding to infinite temperatures or, as in maser action, have higher levels more filled than lower levels, corresponding to negative temperatures. Lastly, as in flames and hot gases, we may have different sub-systems with long relaxation times between them and with different temperatures assignable to each sub-system. A hot gas may have one molecular vibration energy temperature, another molecular translation energy temperature, yet another electron energy temperature, and so on.

THERMODYNAMIC SCALE

Gas Thermometry: The fundamental laws of gases are simple and well-known and the pressure volume relationship may be used as a thermometric parameter to realize the Kelvin temperature scale in the range from about 1 °K to 1500 °K.

Optical Pyrometry: For higher temperatures we have Planck's radiation law. Since accurate absolute measurements of radiant energy are not possible and since relative measurements are not as yet possible at the water triple point, it has been necessary to choose a high temperature fixed point determined by gas thermometry as the basis for relative radiant energy measurements. The solid–liquid equilibrium point of gold is usually chosen. Furthermore, an accurate knowledge of the second radiation constant, C_2, is required. The optical pyrometer type of instrument using essentially monochromatic radiation is the most accurate means of making the appropriate radiation measurements.

PRACTICAL SCALES

A large number of physical and chemical phenomena are available as thermometric parameters, and many of them offer far greater simplicity, convenience and precision than gas thermometry or optical pyrometry; for example vapour pressure, liquid in glass, electrical resistance and thermocouple thermometers. In particular, platinum wire resistance and Pt/Pt–10% Rh thermocouple thermometers are extremely reproducible not only in the case of each wire or couple, but as between different wires and couples, and they lend themselves to the measurement of temperature by interpolation between defined or measured points.

Based on these thermometers, and with appropriate interpolation formulae or tabulated functions, and with agreed values for fixed points, various practical temperature scales have been adopted. These scales are based on the degree Celsius, historically derived from the ice point at 0°C and the steam point at 100°C. The degree Celsius equals the degree Kelvin within very close limits.

The principal scales used or referred to in high temperature work are as follows:–

Washington Geophysical Laboratory Scale (GLS): The scale is defined using the Pt/Pt–10Rh thermocouple and a number of fixed points to about 1600°C.

International Temperature Scale (1927) (ITS 1927): The Pt/Pt–10Rh thermocouple subject to certain tests, which amount to purity checks, defines the scale from 660° C to 1063°C through a quadratic interpolation formula with constants determined by calibration at 630.5° C, the silver and gold point, both of which are given in the definition. Above 1063° C the scale is defined by means of monochromatic radiation using Wien's law and defined values of the gold point and C_2.

International Temperature Scale (1948) (ITS 1948): Is similar to ITS 1927 except for changes in the defined values of the silver point and C_2; the use of Planck's law instead of Wien's law; and the lowering to 630.5° C of the thermocouple defined range.

International Practical Temperature Scale (1960)(IPTS) Essentially the same as ITS 1948.

Thermodynamic Scale (TS)

COMPARISON OF SCALES

In Table I, experimental values of the gold and silver points are listed. The work of Moser, Otto, and Thomas is the most exhaustive to date and has been taken as the basis of the thermodynamic scale in this paper. Table II lists values of C_2. The 1927 and 1948 values were based on determinations of h/e (h, Planck's constant; e, electronic charge), while the last value depends on the most recent (and much more accurate) determinations of the atomic constants h, c (velocity of light), and k (Boltzmann's constant). Table III gives an indication of the maximum precision which has been attained near the gold point with the principal types of thermometer. The electrical noise thermometer is being developed in the hope of obtaining a gold point value independent of high temperature gas thermometry. For the same reason the optical pyrometer range is being extended downwards using photodetectors and infra–red wavelengths. The substitution of a photomultiplier for the eye in optical pyrometry is only just beginning, but should yield considerable advances in both precision and accuracy over a wide temperature range. For the remaining thermometers, the listed precision is probably close to the attainable limit.

Table IV compares a number of fixed points on the different scales including a "probable" Thermodynamics Scale (TS) based on 1064.7° C for the gold point and 1.43886 cm. deg. for C_2.

Figure 1 gives the difference between the ITS 1927 and the ITS 1948, and Figures 2 and 3 include curves showing the deviation between the probable TS and the IPTS.

ACCURACY OF REALIZATION

It should be emphasized that the accuracy of realization of a temperature scale is not the same thing as the precision or reproducibility of measurements, which is usually much higher. Also, the maximum accuracy can only be reached under favourable experimental conditions. For example, thermocouples are subject to contamination and to various electrical effects which may make illusory the apparent accuracy. Again, optical pyrometry may be limited in accuracy by the inadequacy of internal rheostats and calibrated scales in most commercial instruments, or by the source emissivity not being sufficiently well known.

In the event that the source is not a black body accurate optical pyrometer measurements may still be ade if the emissivity is known. In this case we speak of the luminance temperature, i. e. the temperature of a black body having the same luminance or brightness, and it is then necessary to specify the effective wavelength of the pyrometer.

Tungsten strip lamps make a highly reproducible secondary standard of luminance temperature in the range 800° C to 2200° C, as is shown by the results of seven optical pyrometer calibrations done at a number of points in this range by five national laboratories, see Table V. The accuracy of optical pyrometry has been the subject of careful analysis, the results of which are included in Figures 2 and 3. At higher temperatures, most of the error is due to the uncertainty in the effective wavelength used in calibrating the absorption filters, which in turn is due to the variation among individual observers' relative luminour efficiencies.

It can be shown that absorbing filters commonly in use may be calibrated at lower temperatures and used with confidence for optical pyrometer measurements at quite high temperatures. Since these calibrations are based on Wien's law, it is necessary to correct them to a Planck's law basis. This correction which is negligible below about 4000° C is shown in Figure 5.

Thermocouples are of great importance in precise high temperature measurement and Table VI summarizes the properties of some

of the more important couples. The listed uncertain ties are taken from manufacturers' data or published work and relate to deviation from standard reference tables. Greater accuracy may be obtained by calibrating individual thermocouples by optical pyrometry.

CONCLUSIONS

The use of photo–multiplier detectors in optical pyrometry should lead to improved scale accuracy because they make possible the use of prism monochromators or interference filters to define better the effective wavelength. At the same time further and better determinations of the gold point should make it possible to bring the practical scale into better agreement with the thermodynamic scale. Finally, improvements in thermocouple materials are constantly extending the range and precision of these instruments. In this connection, the development of a gas tight sheath for use above 1900° C, (the limit of re–crystallized alumina), or alternatively a technique for embedding thermocouples in a refractory would greatly improve their usefulness.

TABLE I

Gas Thermometer Determinations of the Gold and Silver Points

		t_{ag} °C	t_{au} °C	$t_{au} - t_{ag}$ gas thermometer deg.	$t_{au} - t_{ag}$ optical pyrometer deg.
Holborn and Day	1900	961.8	1063.8	102.0	102.3
Day and Gorman	1914	960.3	1062.7	102.4	102.1
Oishi, Awano and Mochizuki	1956	961.28	1063.69	102.41	102.3
Moser, Otto and Thomas	1958	962.16	1064.76	102.60	102.5
Gordov, Arjanov and Dijkov	1960	———	1064.54	———	———
ITS 1927	———	960.5	1063.0	———	———
ITS 1948 and IPTS	———	960.8	1063.0	———	———

TABLE II

Values of the Second Radiation Constant

	$C_2 = \frac{hc}{k}$ cm. deg.
ITS(1927)	1.432
ITS(I948) and IPTS	1.438
Atomic constants	1.43886

h = Planck's constant
c = velocity of light
k = Boltzmann's constant

$$\frac{J_t}{J_{tau}} = \frac{\exp\left[\frac{C_2}{\lambda(t_{au} + T_o)} - 1\right]}{\exp\left[\frac{C_2}{\lambda(t + T_o} - 1\right]}$$

J_t and J_{au} are the radiant energies per unit wavelength interval at wavelength λ, emitted per unit time by unit area of a black-body at the temperature t, and at the gold point t_{au} respectively and $t_o = 273.15$ deg

TABLE III

Precision of Measurement Near Gold Point

Noise thermometer	2	deg.
Visual optical pyrometer	0.1	deg.
Gas thermometer	0.1	deg.
Photo–multiplier pyrometer	0.01	deg.
Pt/Pt–10Rh thermocouple	0.02	deg./hour drift
Pt resistance thermometer	0.002	deg./hour drift

TABLE IV

High Temperature Fixed Points

(Relation between different scales and accuracy of realization.)

Fixed Point	GLS °C	ITS 1927 °C	ITS 1948 and IPTS °C	TS °C	σ
NaCl	800.4	800.4	800.8	801.4	0.1
Ag	–	960.5	960.8	962.1	0.1
Au	1062.6	1063.0	1063.0	1064.7	0.1
Cu *	–	1083	1083	1085	1
Li_2SiO_3	1201	1201	1201	1203	1
$CaMgSi_2O_6$ **	1391.5	1391.5	1389.9	1393	1
Ni	–	1455	1453	1456	1
Co	–	1494	1492	1495	1
$CaSiO_3$ **	1544	1550	1547	1550	1
Pd	1549.5	1555	1552	1555	1
Pt	–	1773	1769	1773	1
Rh	–	1966	1960	1964	3
Ir	–	2454	2443	2449	3
W	–	3407	3380	3389	20
C ($\lambda = 0.66\mu$)	–	3544	3514	3524	6

σ Standard deviation error of realization of fixed point on the scale.

N. B. 1. Ag, Au, Primary fixed points on the IPTS.

2. Cu, Ni, Co, Pd, Pt, Rh, Ir, W, secondary fixed points on the IPTS.

3. C sublimation point, luminance temperature, measured at positive crater of carbon arc for $\lambda = 0.66\mu$.

* reducing atm.
** diopside
*** Pseudowollastonite

TABLE V

Luminance–Temperature Current Calibrations for Two Secondary Standard Lamps at National Laboratories

Lamp No. 421 Amp.	NPL* °C	DAMG 1958 °C	NBS 1957 °C	NBS 1958 °C	NRC 1957 °C	NRC 1958 °C	PTB 1957 °C	Mean °C	Stand. Dev. °C
3.15	800	796	799	798	797	798	798	798	1.2
3.62	900	898	899	899	897	898	898	898	1.0
4.21	1000	1000	1000	1000	998	999	1000	1000	0.8
4.92	1101	1103	1102	1103	1102	1103	1103	1102	0.8
5.70	1201	1204	1202	1202	1201	1203	1203	1202	1.0
6.55	1301	1304	1301	1302	1301	1302	1303	1302	1.0
7.44	1401	1402	1400	1401	1402	1399	1401	1401	1.0
Lamp No. 242									
8.62	1271	1268	1269	1267	1269	1267	1267	1268	1.4
9.77	1423	1419	1420	1420	1419	1416	1420	1420	2.0
10.90	1553	1549	1548	1550	1549	1550	1550	1550	1.4
12.99	1764	1761	1750	1760	1762	1764	1763	1762	1.6
15.07	1953	1951	1951	1950	1952	1953	1953	1952	1.1
16.16	2050	2043	2044	2043	2043	2048	2048	2046	2.9
18.28	2218	2215	2217	2216	2218	2220	2219	2218	1.6

* The NPL listings are based on routine calibrations made in 1947 for lamp No. 242 and in 1951 for lamp No. 421.

TABLE VI

Data on High Temperature Thermocouples

Couple	Recommended Maximum Temperature		Uncertainty	Relative E.M.F.	Atmos.
Pt/Pt–10Rh	1400°C	(1769°C)	± 2°C	20 mV	VNO
Pt–6Rh/Pt–30Rh	1700	(1800)	10	16	VNO
Pt–20Rh/Pt–40Rh	1800	(1884)	10	5	VNO
Ir/Rh–40Ir	2000	(2300)	20	10	VNO
W/Ir	2100	(2400)	20	38	VN–
W/Re	2400	(3100)	50	18	VNR
W/W–26Re	2800	(3200)	50	34	VNR
Chromel P/ Alumel	1300		5	80	VNO
Platinel	1300		3	80	VNO
W/Mo	2600		50	5	VNR

V Can be used in vacuum
N Can be used in neutral atmosphere (He or A)
O Can be used in oxidizing atmosphere
R Can be used in reducing atmosphere

The bracketed maximum temperature is the melting point of the less refractory arm of the couple. Relative E.M.F. is E. M. F. at 2000°C or E.M.F. extrapolated to 2000°C if this is outside range of couple.

Uncertainty is maximum deviation to be expected from reference tables or among different wires, or among different batches of wire. The stability of most of the above thermo–couples is sufficient to permit the calibration of individual thermocouples to an accuracy determined by that of the calibrating thermocouple or pyrometer.

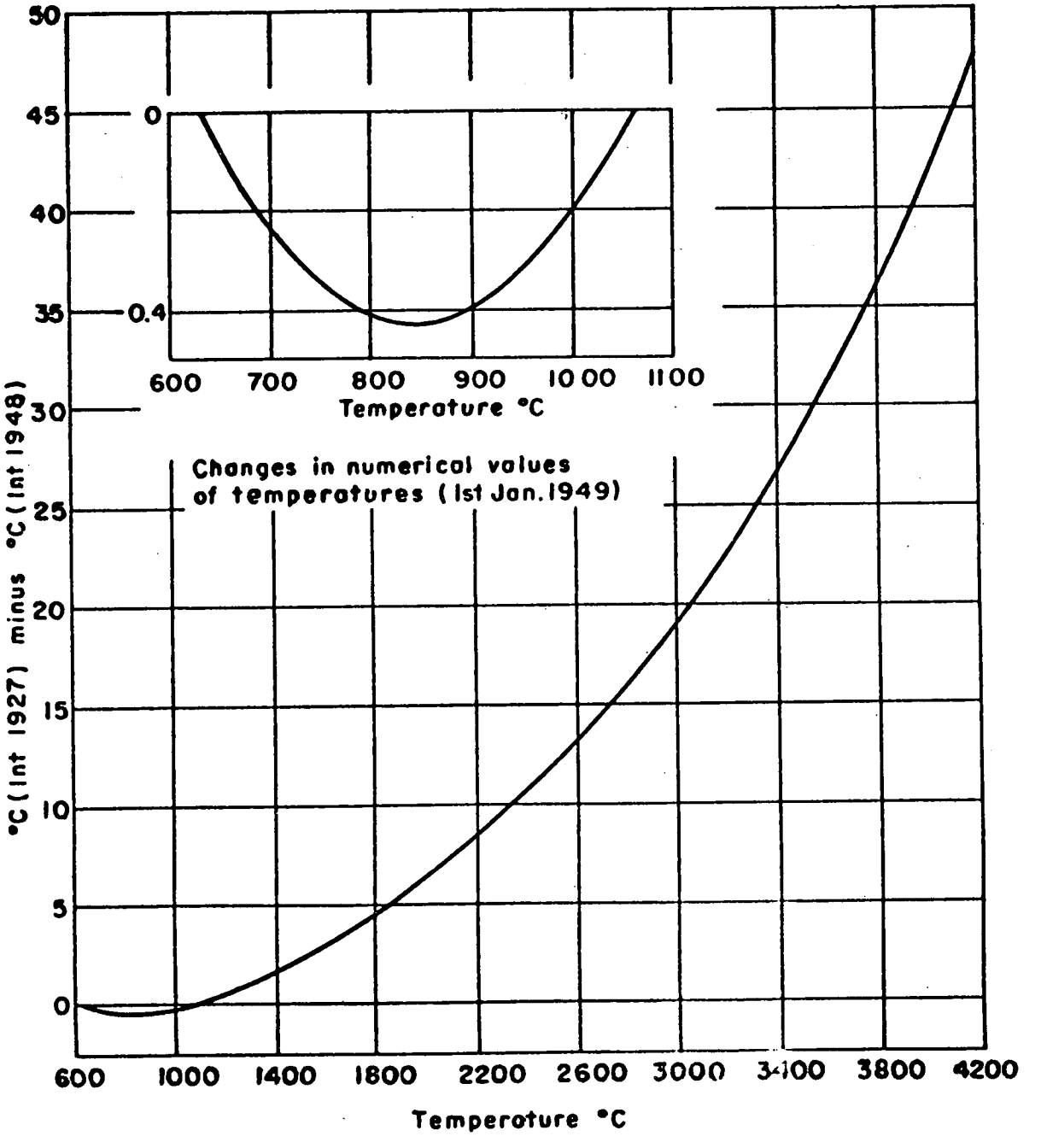

Fig. 1. Differences between the International Temperature Scales of of 1927 and 1948.

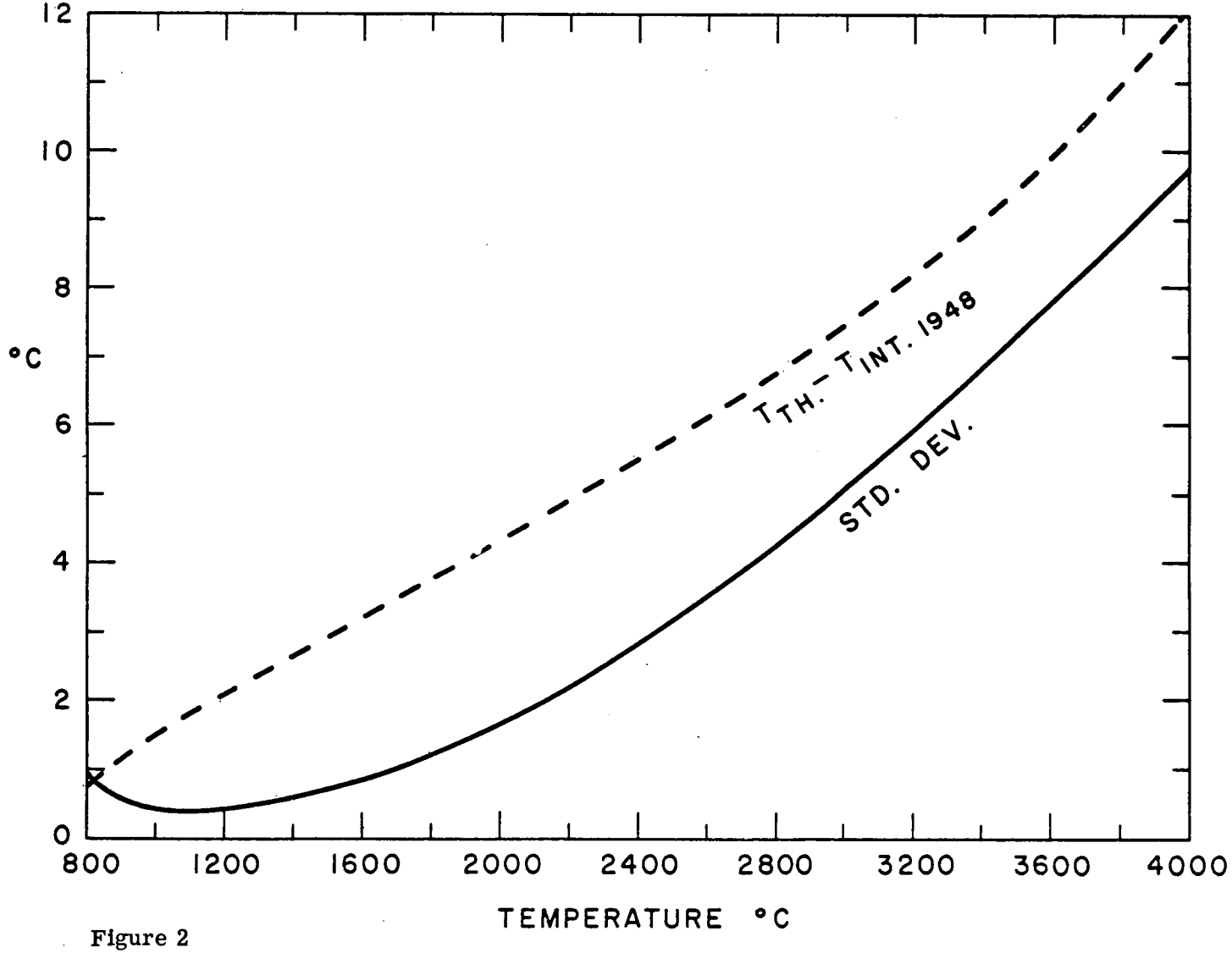
12
10
8
6
4
2
0
°C
800
1200
1600
2000
2400
2800
3200
3600
4000
TEMPERATURE °C
$T_{TH.} - T_{INT.\ 1948}$
STD. DEV.

Figure 2

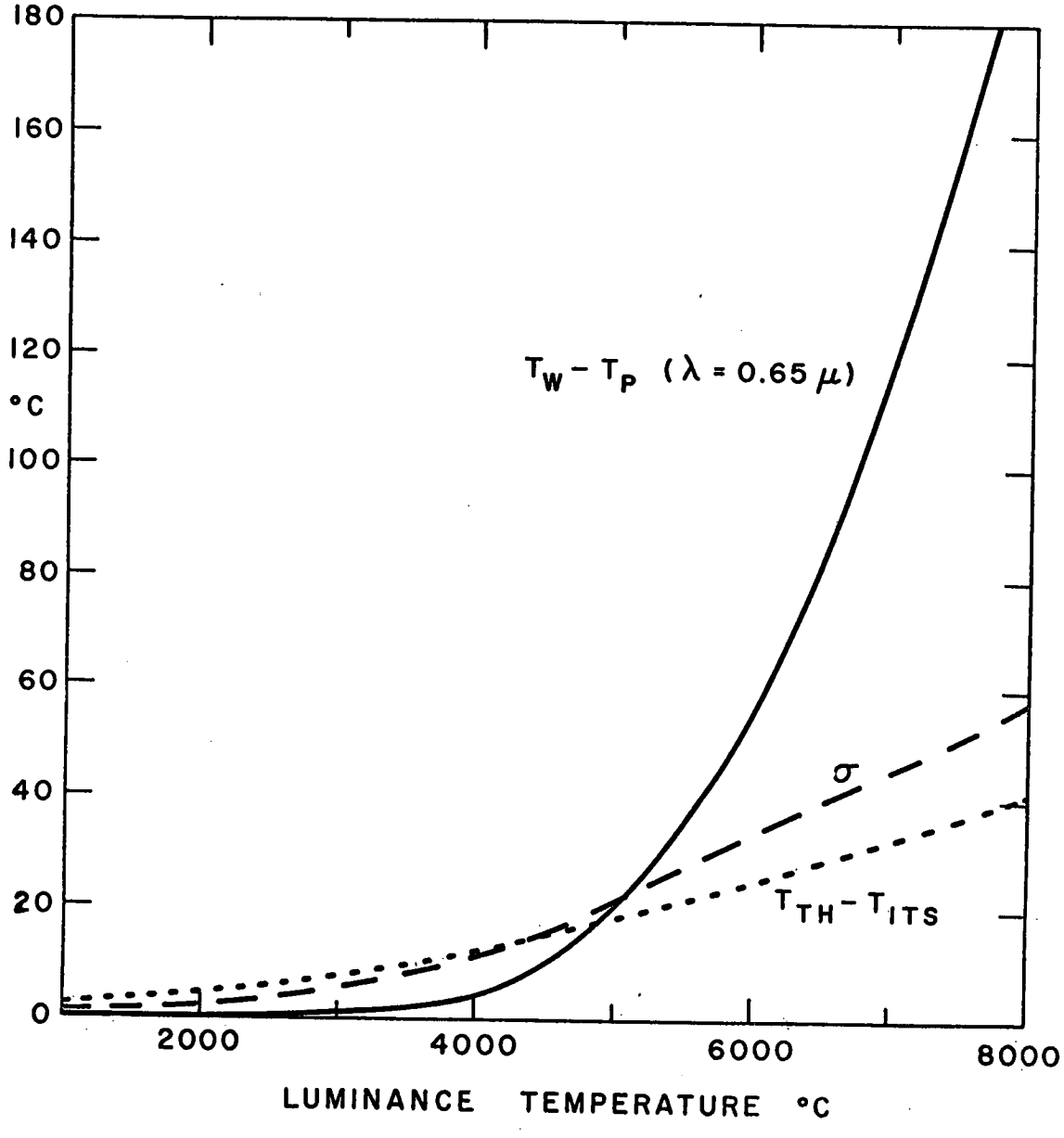
180
160
140
120
°C
100
80
60
40
20
0
2000
4000
6000
8000
LUMINANCE TEMPERATURE °C
$T_W - T_P$ ($\lambda = 0.65\,\mu$)
σ
$T_{TH} - T_{ITS}$

Figure 3.

LES PROPRIETES THERMODYNAMIQUES D'EXCES DES MELANGES BINAIRES DES SELS FONDUS.

I. G. Murgulescu et S. Sternberg

Les propriétés thermodynamiques d'excès des mélanges des sels fondus ont été déterminées surtout par des mesures de f.e.m. pour des systhèmes qui peuvent constituer des piles réversibles de formation. Dans le présent travail on a étandu l'étude des propriétés thermodynamiques d'excès à quelques mélanges des sels fondus pour lesquels les détermination potentiométriques sont difficiles à effectuer.

Dans ce but on a employé la relation connue

$$\ln a = \frac{\Delta H_\theta}{R}\left(\frac{1}{T} - \frac{1}{\theta}\right) + \frac{\Delta C_p}{R}\left(\ln\frac{\theta}{T} - \frac{\theta - T}{T}\right) \qquad (1)$$

qui se trouve à la base des determinations d'activité par la méthode cryoscopique. Pour la mise en valeur de l'expression (1) on a employé les diagrammes de fusion des mélanges. On peut applique la relation (1) dans le cas où par refroidissement cristallise seulement un composant pur. Les grandeurs ΔH et θ représentent la chaleur molaire de fusion, respectivement la température de congélation du composant pur, T la température de congélation du même composant du mélange donné pendant que ΔC_p donne la différence, supposée constante, des capacit és calorifiques molaires du composant pur à l'état solide et liquide. On admet pour l'état standard de chaque composant le sel pur. Dans quelques travaux antérieures (1, 2), nous avons démontré que les activités thermodynamiques calculées à partir des diagrammes de fusion concordent avec celles obtenues à l'aide de la relation Nernst à partir des mesures de la f. e. m. des piles de formation.

Dans les travaux metionnés on a démontré que les termes en ΔC_p peuvent être négligés et que la récalculation des activités obtenue à la température T pour une température de reference T, peut être effectuée à l'aide de la relation

$$RT\ln\gamma_1 = B(1 - N_1)^2 \qquad (2)$$

propre aux solutions "regulaires", dans laquelle B est une constante. Les énergies libres partielles molaires d'excès ont été calculées d'après les relations:

$$\bar{F}_1^E = RT\ln\gamma_1 \quad \text{et} \quad \bar{F}_1^E = RT\ln\gamma_2 \qquad (3)$$

et l'énergie libre integrale d'excès a l'aide de la relation:

$$F^E = N_2\bar{F}_2^E + N_2\bar{F}_2^E \qquad (4)$$

A l'aide des relations (1), (2), (3) et (4) on a calculé les proprietés thermodynamiques d'excès pour 16 mélanges binaires à simple eutectique: LiCl+KCl(RbCl, CsCl); LiBr+KBr, NaCl+RbCl(CsCl); $LiNO_3$+$NaNO_3$(KNO_3, $RbNO_3$, $CsNO_3$); NaF+NaCl(NaBr, NaI), KE+KCl(KBr+KI).

Pour les 4 premiers mélanges on a employé les diagrammes de fusion determinés dans ce travail, pour les autres mélange on a employé les donnés de la littérature. Le terme ΔC_p a été consideré nul chaque fois qu'on n'a pas pu avoir les capacités calorifiques respectives. A fin d'élaborer une classification des sels fondus, on a calulé au cours de ce travail, les énergies libres integrales d'excès F^E aussi pour 17 nouveaux mélanges de sels fondus. Pour ces dernier mélanges les chaleurs partielles molaires F^E, et F_2^E, ont été déduites anterieurement des données potential metriques par nous mêmes ou par d'autres chercheurs.

Dans le tableau 1 sont reproduit les énergies libres in tégrales d'excès calculées d'après la relation (4) pour presque tous les mélanges binaires des sels fondus étudiés jusqu'à présent. Les resultats obtenus prouvent l'existence d'un parallélisme évident entre les valeurs des énergies libres d'excès et l'allure des diagrammes de fusion du mélanges.

1. Les mélanges qui donnent par congélation des cristaux mixtes et qui possedent des énergies libres d'excès positives.
2. Les plupart des mélanges à eutectique simple ont les énergies d'excès integrales trés petites, preque nulles.
3. Quelques-un des mélanges à eutectique simple présentent des énergies libres d'excès négatives. Dans cette catégorie on trouve les mélanges de sels de quelques cations ayant le rayon ionique petit (Li^+, Ag^+) avec des sels de K, Rb, Cs.
4. Les mélanges qui donnent par congélation des combinatisons chimiques possèdent des grandes énergies intégrales d'excès négatives.

Etant donée que les mélanges de sels fondus à l'exception de ceux qui forment des combinaisons chimiques ont l'entropie d'excès pratiquement nulle, on peut poser $F^E \cong H^E$ où H^E est la chaleur de mélange.

Les énergies libres d'excès negatives des mélanges du quatrième groupe ne sont pas inattendues; elles sont dies à la formation d'ions complexes, procés qui découle avec dégajement d'énergie (8, 9, 10, 11).

Il y a une analogie rémarquable entre les mélanges du premier groupe et les solutions solides ioniques. Les chaleurs de mélange des sels fondus de ce groupe sont de même signe et du même ordre de grandeur (300–600 cal/mol) que celles des solutions solides ioniques. De même l'équation parabolique $H^E = BN_1N_2$ (dans la quelle B est une constante) est valable pour les solutions solide: comme aussi pour les mélanges liquides. Dans une note qui va paratre (12) les auteurs ont calculé la chaleur de mélange H^E pour les sels fondus qui donnent au refroidissement des cristaux mixte: en employant la relation:

$$H^E = \frac{NAe^2}{R_o} N_1N_2 \left(\frac{\Delta R}{R_o}\right)^2 \left[\frac{\delta_1}{8}(1 + \sigma(1 - 4N_2) + \frac{\delta_2}{8}(1 + \sigma(1 - 4N_1) + \frac{1}{2}(1 + \sigma)\right]$$

établie par J. Vasastierna pour les chaleurs de mélange des solutions solides ioniques. Ici δ représente l'apport des forces de répulsion, et dépend des coefficients de comprésibilité. (c) et de dilatation (γ) des sels purs; σ donne le degré d'ordre. On a demontré que pour les distance interioniques dans des sels fondus ainsi que pour c et γ il est necessaire de prendre des valeurs très rapprochées a celle correspondant aux sels purs a l'état solide. On a trouvé une concordance satisfaisante entre les chaleurs de mélange déterminées experimentalement par des determinations de f. e. m. et celles calculées par la relation ci–dessus. En partant de cette analogie de proprieés on a consideré que pour ce type de sel fondus il y a une ordre locale "mixte" tres semblable a la structure des réseaux dans les solutions solides ioniques. Il en découle qu'une position dans l'immédiat voisinage de l'ion commun A dans un mélange fondu AB+AC peut être accupée, par n'importe lequel de ces deux ions B et C avec la même probabilité comme dans les réseaux des cristaux mixtes. Pour réaliser une telle structure ionique mixte on a besoin d'une absorbtion d'énergie ce qui explique les énergies positifs tant pour les solutions solides ioniques que pour les mélanges de liquides ioniques qui provennent de la fusion

de ceux–ci.

En maintenant l'analogie entre l'état liquide et l'état solide on a essayé aussi de donner une explication pour le comportement des mélanges a l'eutectique simple, dont la chaleur de mélange est preque nulle. Pour ces mélanges les paramètres reticulaires ont des sels composants diffèrent beaucoup entre eux, c'est a dire le raport

$\frac{R_1 - R_2}{1/2\ (R_1 + R_2)}$ dépasse sensiblement 15–20 %. C'est a cause de quoi, les sels a l'état solide ne forment pas des cristaux mixte et aussi a l'état liquide la formation d'une ordre locale mixte n'est pas possible. Pour les mélanges de sels fondus à eutectique simple il y a donc une ordre locale particulière "quasieutectique." : autour de l'ion commun. A vont se grouper de préférance les ions de signe contraire d'une seule espèce d'où la prédominance des liaisons de type B–A–B et C–A–C. Par consequant, si on mélange deux sels fondus de ce groupe, les énergies d'interaction des ions vont rester les mêmes que pour les substances purres. D'où il s'ensuit que l'énergie de mélange H^E va être nulle, ce–qui explique le comportement des mélanges du 2 eme groupe.

Les mélangès a eutectique simple qui ont des chaleurs de mélange négatives (groupe 3), constituent une exception. La grandeur du rayon ionque de l'argent dans les bromures et dans les clorures est proche de la grandeur de rayon ionique du lithium, ce qui éxplique le comportement semblable des sels de lithium et d–argent. C'est possible que l'anomalie observée pour ces mélanges soit due à la grande polarisation de l'ion de halogène par l'action des ions à petit rayon ionique Li^+ ou Ag^+.

Bibliographie

1. I. G. Murgulescu et S. Sternberg, Revue de Chimie (acad. R. P. Roumani (II), 2, 251, (1957); III, I, 55 (1958)
2. S. Sternberg, Revue de Chimie (Acad. R. P. Roumania) II, 2, 77, (1958).
3. I. N. Hildebrand, E. Salstrom, J. Am. Chem. Soc. 54, 4257, (1932).
4. S. Sternberg et S. Gheorghiu, Studii si Cercetari de Chemie VI, I, 107, (1959).

5. I. G. Murgulescu et D. Marchidan, Revue de Chimie (Acad. R.P.R.) III, 1, 47, (1958).
6. E. Salstrom, T. Ken, T. Powell, J. Am. Chem. Soc. 58, 1948, (1936).
7. E. Salstrom, J. Am. Chem. Soc. 56, 1272, (1934).
8. B. F. Markov, J. K. Delimarski, et I. D. Pancenko, J. Fiz. him. (URSS) 28, 1987 (1954); 29, 51, (1955).
9. M. F. Lantratov, A. F. Albisev, J. phikl. him. (URSS) 26, 353, 722 (1955).
10. B. F. Markov, Ukrain him. jurn. XXI, 6, 703, (1955).
11. E. R. Van Artsdalen, J. Phys. Chem. 59, 2, 118, (1955).
12. I. G. Murgulescu et S. Sternberg, Revue de Chemie (Acad. R.P.R.) VI, I, (1961).

TABLEAU I

La énergie libre integrale d'excès des mélanges binaires des sels fondus ($N_1 = N_2 = 0.5$). *

Les mélanges qui donnent par congélation des cristaux mixtes (groupe 1) F^E, cal/mol.

AgBr+LiBr	à 600°C	+ 470 (3)(P)
AgBr+NaBr	" 600°C	+ 320 (3)(P)
AgCl+NaCl	" 600°C	+ 283 (4)(P)
AgBr+AgCl	" 500°C	+ 527 (5)(P)
AgCl+LiCl	" 500°C	+ 525 (6)(P)

TABLEAU II

Les mélanges à simple eutectique. (groupe 2) F^E, cal/mol

AgCl+KCl	à 500°C	−411(1)(P)
		−465(1)(C)
AgBr+KBR	" 500°C	−370(3)(P)
LiCl+KCl	" 600°C	−595* (C)
LiCl+RbCl	" 600°C	−544* (C)
LiCl+CsCl	" 600°C	−450* (C)
LiBr+KBr	" 600°C	−739* (C)
$LiNO_3$+KNO_3	" 300°C	−715* (C)
$LiNO_3$+$CsNO_3$	" 300°C	−511* (C)

TABLEAU III

Les mélanges a simple eutectique (groupe 3) F^E, cal/mol

NaCl+RbCl	à 600°C	−25*	(C)
NaCl+CsCl	" 600°C	+ 4*	(C)
$NaNO_3$+$RbNO_3$	" 300°C	+69*	(C)
$LiNO_3$+$NaNO_3$	" 300°C	−47*	(C)
NaF+NaCl	" 800°C	+153*	(C)
NaF+NaBr	" 800°C	+190*	(C)
NaF+NaI	" 800°C	+288*	(C)
KF+KCl	" 800°C	+2,5*	(C)
KF+KBr	" 800°C	−32 *	(C)
KF+KI	" 800°C	+184*	(C)
AgCl+$PbCl_2$	" 500°C	−30 (7)	(P)
		−90 (1)	(C)

TABLEAU IV

Les mélanges qui donnent par congélation des combinaisons chimiques. (Groupe 4) F^E, cal/mol.

$PbCL_2$+KCl	à 600°C	−1200(8)(P)
$PbCl_2$+KCl	" 600°C	−1642(8)(P)
$MgCl_2$ +KCl	" 718°C	−1700(8)(P)
$MgCl_2$+RbCl	" 718°C	−3500(8)(P)
$CdCl_2$+KCl	" 700°C	−2000(9)(P)
$ZnCl_2$+KCl	" 600°C	−3500(9)(P)
$CdCl_2$+NaCl**	à 700°C	−900(9)(P)
$ZnCl_2$+NaCl**	à 600°C	−1500(9)(P)
AgBr+RbBr	à 600°C	−645(3)(P)

* $\overline{F_1^E}$ et $\overline{F_2^E}$ calculées dans ce travail à partir des diagrammes de fusion.

** Des mélanges qui dans l'état liquide forment des combinaisions instables.

(P) – Des résultats obtenus par déterminations de f. e. m.

(C) – Des résultats obtenus par la méthode crioscopique.

CALORIMETRY IN LIQUID THALLIUM NITRATE–ALKALI NITRATE MIXTURES

O. J. Kleppa and L. S. Hersh

In an investigation of the binary systems formed by the liquid alkali nitrates (1) the authors have found that the molar enthalpies of mixing are all negative and may be represented by the following simple, approximate relation:

$$\Delta H^M \cong -X(1-X)\ U'\ \delta^2 \text{ kcal/mole.} \qquad (1)$$

In this expression U' is 140 (kcal), i.e., of order of magnitude of the lattice energy of the salts, $\delta = (d_1 - d_2) / (d_1 + d_2)$ where d_1 and d_2 are the sums of the ionic radii characteristic of the two pure components, while X and $(1 - X)$ are the mole fractions of the two components. Although this expression was derived for the alkali nitrates, it is believed that similar expressions are likely to apply also for other essentially ionic mixtures when the two fused salts have the same charge structure and contain a common anion.

More recently, in a study of the binary liquid mixtures of silver nitrate with various alkali nitrates, the authors have demonstrated that in these systems the molar enthalpy of mixing may be represented by a related approximate expression (2).

$$\Delta H^M \cong -X(1-X)\left[(U'\delta^2 - U''\delta)\right] \text{ kcal/mole} \qquad (2)$$

The first term inside the square bracket is identical with the corresponding expression for the alkali nitrates. The second term takes into account the non-ionicity of the silver nitrate. The constant U'' is about 24 kcal, i.e. it is of magnitude comparable to the non-ionic contribution to the lattice energy of this salt. (3) (In ref. 2 the part of equation (2) which is linear in δ contains a small correction term. This may be omitted by adopting an ionic radius for silver of 1.20 A rather than 1.26 A.)

In the present investigation we consider the thallium nitrate–alkali nitrate systems. From data quoted in the recent work of Ladd and Lee (3) we have estimated the non-ionic contribution to the lattice energy of thallium nitrate to be about 15 kcal/mole[3]. In analogy with equation (2) we accordingly write the following tentative, approximate expression for the heats of mixing in the thallium nitrate – alkali nitrate systems:

$$\Delta^{M} = -X(1 - X)\ (140\ \delta^2 - 15\delta)\ \text{kcal/mole} \qquad (3)$$

where

$$\delta = (d_{TlNO_3} - d_{MeNO_3})/(d_{TlNO_3} + d_{MeNO_3})$$

If we base our evaluation of d_{TlNO_3} and δ on Pauling's value for the radius of the thallous ion (1.44 A), equation (3) fails by a wide margin to reproduce the experimental results. However, if we adopt the ionic radius recommended by Brewer et al (4) (1.59 A), the agreement between the experimental values of ΔH^{M} and the calculated values is remarkably good. This is illustrated in the table, where we compare the experimental and calculated values for the equimolar mixtures.

System	$\Delta H^{M}_{0.5}$, exp.	$\Delta H^{M}_{0.5}$, calc., eq. (3)
$(Tl–Li)NO_3$	−220 cal/mole	−230 cal/mole
$(Tl–Na)NO_3$	+64 "	+47 "
$(Tl–K)NO_3$	+110 "	+89 "
$(Tl–Rb)NO_3$	+58 "	+48 "

This agreement lends significant support to the use of semi–empirical relations such as equations (1), (2), and (3) in order to predict heats of mixing in previously unexplored fused salt mixtures. Alternatively, it suggests a possible method for determination of the effective ionic radius in fused salt solutions, and for estimation of the non–ionic contribution to the lattice energy of salts.

References

1. O.J. Kleppa and L.S. Hersh, J. Chem. Phys. (February 1961, in press).

2. O.J. Kleppa, R.B. Clarke and L.S. Hersh, J. Chem. Phys. (1961, in press).

3. M.F.C. Ladd and W.H. Lee, J. Inorg. Nucl. Chem. 13, 218 (1960)

4. L. Brewer, L.A. Bromley, P.W. Gilles and N.L. Lofgren, "The Chemistry and Metallurgy of Miscellaneous Materials," L.L. Quill, editor, pp. 76 – 192 (McGraw–Hill Book Co., Inc., New York, 1950).

IMMISCIBILITY OF SODIUM BORATE AND SODIUM HALIDE IN THE MOLTEN STATE

Boleslaw Ludwik Dunicz and Ronald C. Scheidt

The literature records one limited study of phase diagrams of the molten three-component systems: boron oxide–alkali metal oxide–alkali metal halide. Stålhane (1) used mixtures of sodium chloride at 850° and sodium bromide at 830°C, respectively, with sodium borates of varied basicity. The salts were fused in open platinum crucibles, and the phases were isolated when the melt was poured down a gently slanting cast iron trough. Exposure to air during equilibration caused continuous displacement of halide by oxygen and this reaction was enhanced by the presence of boron oxide. In agreement with Stålhane, the process can be represented by the reaction:

$$4NaX + O_2 + 2B_2O_3 = 2X_2(g) + 4NaBO_2.$$

A reaction suggested by Stålhane as accounting also for the loss of halogen,

$$3NaX + 2B_2O_3 = BX_3(g) + 3NaBO_2,$$

is not possible on the basis of chemical thermodynamical calculations. Also, the preliminary experiments of the present investigators have shown that platinum, as well as gold, crucibles are not suitable for fusions of the kind under consideration, as they undergo gradual corrosion by the melts.

The shortcomings of Stålhane's method and the growing interest in utilizing two-phase molten salts for extraction of some inorganic solutes, prompted an extended and more exact study of the properties of the salts under consideration, with an improved experimental technique. Instead of platinum, a graphite crucible, enclosed in a quartz capsule under vacuum was used. The crucible was tightly closed with a graphite cover, and the salt melt in it could be vigorously agitated without being spilled. The equilibrated melt was solidified in the crucible allowing convenient separation of the original two liquid phases.

This communication will present the results of the study of phase equilibria, at 800° and 980°C, of sodium chloride, bromide and iodide, respectively, with sodium borates of varied basicity. The graphs will becompared with those of Stålhane and discussed.

Reference

1.) B. Stålhane, Z. Elektrochem. 35 : 486 (1929).

DEPOLYMERIZATION OF POLYANIONS BY REACTION OF MOLTEN SALTS WITH THE ATMOSPHERE

C. F. Callis, J. R. Van Wazer, and J. S. Metcalf

Results and Conclusions: A quantitative study has been made on the equilibrium between water vapor and gaseous hydrogen chloride over melts containing sodium, chloride, and polyphosphate ions. The equilibrium results because of a reaction which can be written in ionic form, as follows:

$$H_2O + 2\,Cl^- + (P_nO_{3n+1})^{(n+2)-} = 2\,HCL + (P_{n-x}O_{3n-3x+1})^{[(n-x)+2]-} + (P_xO_{3x+1})^{(x+2)-} \qquad (1)$$

where $\infty > n >$ ca. 3, $n > x$, and n and x are integers.

It can be seen from this equation that the reaction consists of donating an oxygen atom to a polyphosphate chain so as to cause scission of this chain. In other words, the reaction can also be written in the following ionic form:

$$H_2O + 2\,Cl^- + \text{—P(O)(O}^-\text{)—O—P(O)(O}^-\text{)—} = 2\,\text{—P(O)(O)O}^{=} + 2\,HCl \qquad (2)$$

(segment in a polyphosphate chain) (end of a polyphosphate chain)

According to equation 2, two middle groups in a polyphosphate chain are converted to two end groups by the reaction in which one mole of water combines with two equivalents of chloride ion to give two moles of hydrogen chloride.

Since hydrogen chloride and water are very insoluble in molten salts, the equilibrium of equation 1 is readily measured by obtaining the partial pressures of HCl and H_2O over the melt. Attempts to set up an equilibrium constant based on equation 2 and having the following formula

$$K = \frac{P^2_{HCl}/P_{H_2O}\ [a_{ends}]^2}{[a_{Cl^-}]^2\ [a_{middles}]^2} \qquad (3)$$

led to extreme variability in the constant. This is probably attributable to the fact that all P O P segments in a polyphosphate chain are not equally reactive and that, perhaps, P O P segments towards the end of a chain exhibit different equilibrium constants than those in the middle of a long chain. However, partial equilibrium constants of the following form

$$K_{partial} = \frac{p^2_{HCl}/p_{H_2O}}{[a_{Cl}]^2} \qquad (4)$$

were found to be reasonably constant for various fixed ratios of Na_2O/P_2O_5 in the polyphosphate. (This is equivalent to saying that the ratio of $[a_{ends}]^2\ [a_{middles}]^2$ is constant.)

A typical plot of p^2_{HCl}/p_{H_2O} versus [mole fraction chloride]^2 is given in Figure 1, where it can be seen that at high chloride concentrations, there is a deviation from the straight-line function. The activity coefficient of the chloride ion was calculated from this deviation. Typical data are shown in Table I.

Rate studies indicate that equilibrium is obtained very rapidly and that the rate-determining step under most conceivable experimental arrangements is determined by the physical processes of diffusion in the melt and/or sorbing and desorbing the gases.

Experimental Approach: In a series of preliminary experiments, a platinum test tube about 3 ft. long and 1 in. in diameter was sparged with gases containing various fixed ratios of HCl/H_2O, and, in some

cases, helium. The runs were made with different melt compositions and with various melt heights, and it was found that equilibration occurred about as rapidly in a shallow layer of melt as it did when the platinum tube was completely filled. Therefore, another series of studies was carried out in a platinum dish. The approach to equilibrium in this series of studies is shown in Figure 2.

TABLE I

PARTIAL EQUILIBRIUM CONSTANTS AT 800°C. AND FOR VARIOUS SODIUM PHOSPHATES OVER THE RANGE IN Na_2O/P_2O_5 of 1.1 to 1.7

$$K_{partial} = \frac{P^2_{HCl}/P_{H_2O}}{(\text{mole fraction Cl} \times \gamma Cl)_2}$$

Na_2O/P_2O_5 in Phosphate	K partial	Approx. Conc. NaCl (wt.%) Above which γCl Deviates from One
1.098	830	1.5
1.20	350	2.6
1.30	140	2.7
1.40	53.3	2.0
1.50	15.0	4.0
1.60	3.60	4.6
1.67	1.38	3.7

Finally, a new piece of apparatus was developed in which small platinum pans containing thin layers of melt having various compositions were exposed to the gas. In order to freeze the equilibrium corresponding to the temperature under study, the apparatus was contained in a specially built radiant-tube furnace which could be cooled down to room temperature in a matter of seconds. The usual methods of analysis for chloride and for the polyphosphates were employed.

Other Studies: In a paper to be published shortly in J. Am. Chem. Soc., Maier, Mills, Alden, and Owens measured phase diagrams between alkali metal metaphosphates and alkali metal sulfates. In this work, they found considerable depolymerization of the sodium metaphosphate. Indeed, the number-average chain length of the polyphosphate chain which equaled 110 in their original melt was sometimes reduced as low as two (pyrophosphate) in those composition regions consisting of more than 80% Na_2SO_4.

This behavior is attributed to a reaction of the type shown in equation 1, with H_2SO_4 being the off-gas instead of HCl.

Likewise, a series of experiments [R. K. Iler and J. Tauch, Trans. Am. Inst. Engrs., 34, 853 (1941)] on the reaction of silica sand, sodium chloride, and steam has shown that a similar reaction occurs with the condensed silicates. The patent literature also contains empirical descriptions of the reaction studied by us [F. P. Kerschbaum, U. S. Pats. 2,142,943 and 2,142,944 (1939); and C. R. McCullough, U. S. Pat. 2,266,328 (1941)].

From the available information, it appears that there is a general class of reactions of the type reported here. In such reactions, an equilibrium between water vapor and the vapor of a volatile acid is set up over a melt in which the equilibrium reaction involves the polymerization–depolymerization of the inorganic polyanion. Such equilibria are probably most readily observed in the temperature range of 500–1500°C. It seems certain that many investigators in the fields of molten salt mixtures, glasses, etc. have experienced such reactions without being aware of the event. These reactions lead to small but significant changes in properties of the melts and glasses or crystalline mixtures obtained from them.

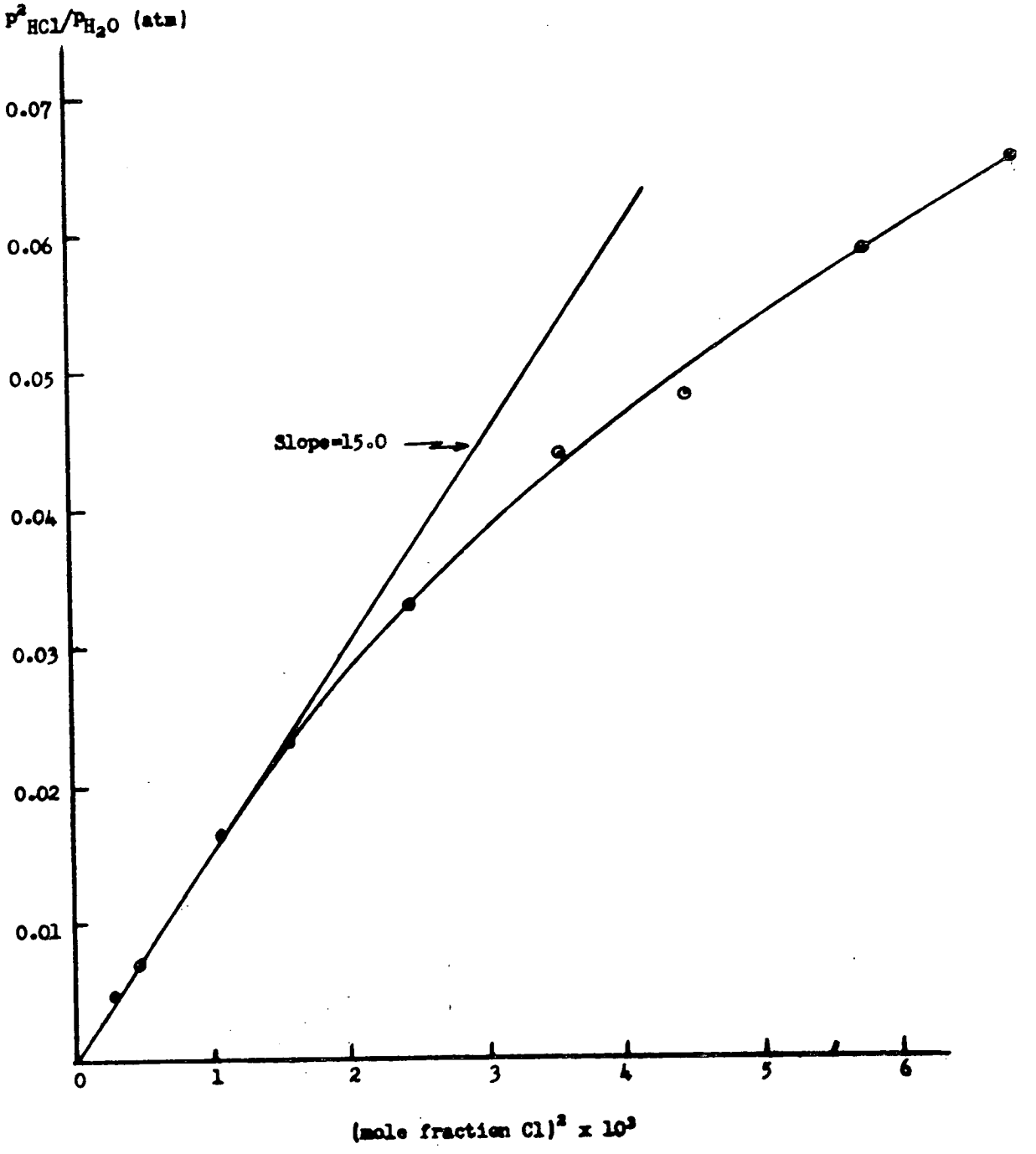

Figure 1 P^2_{HCl}/P_{H_2O} *versus* (mole fraction Cl)^2 for ca. 800°C. and an Na_2O/P_2O_5 mole ratio in phosphate of 1.50.

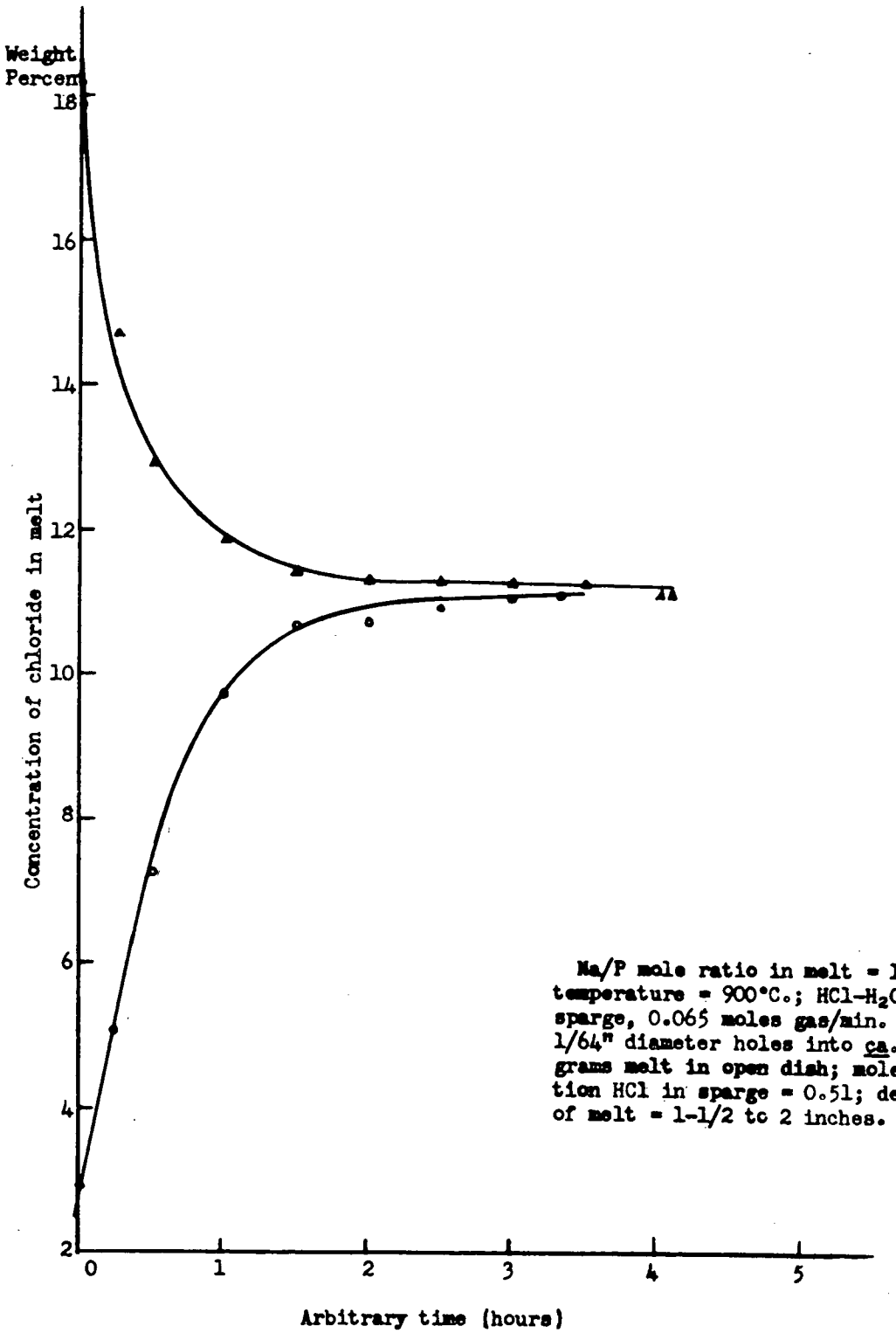

Figure 2 Variation in the concentration of chloride ion in Na_2O-P_2O_5-NaCl melt as a function of the time of sparging with gaseous HCl-H_2O mixture.

SOLUBILITY OF METAL OXIDES IN MOLTEN SODIUM CHLORIDE. THE FIRST TRANSITION SERIES

K. H. Stern

The solubility of metal oxides in molten salts is of some interest in connection with the general problem of metal oxidation is these media. If the initial step in the oxidation is the formation of the metal oxide from metal and O_2 the rate of this reaction will be affected by the solubility and rate of solution of the oxide in the salt. If the oxide is insoluble and forms an adherent coating of the metal, metal oxidation may be quite slow if the oxide does not dissolve in the salt.

In the present work we report a simple chemical study of oxide solubility in fused NaCl at 900° for metals of the first transition series from Ti to Cu.

Experimental Part: Reagent grade materials, well dried, were used. Solubilities were measured by equilibrating the oxide with NaCl in vycor test tubes at 900°. Melts were sampled by dipping cold procelain rods into them.

Results: Titanium. NBS standard sample TiO_2 was used. This oxide is stable at 900°. When heated it turns pale yellow but returns to white on cooling. The melt was equilibrated for five days. No qualitative difference between oxygen and argon atmospheres was noted. Spectroscopic analysis of the melt gives an upper limit of 10^{-5} mole fraction for the solubility.

Vanadium. V_2O_5 is a stable liquid (m.p. 660) at 900°. This was verified by X-ray diffraction of a melted sample. However, the addition of NaCl results in a violent reaction which liberates Cl_2. X-ray diffraction of the product does not correspond to any known pattern, but the compounds V_2O_3, VCl_3, and VO_2 are definitely not formed. The product is undoubtedly a lower-valent oxide or oxychloride.

Chromium. Cr_2O_3 is a stable solid at 900°. However, heating it in the presence of air with NaCl resulted in the rapid formation of a yellow color in the liquid due to $CrO_4^=$ ion. The reaction $Cr_2O_3 + O_2 \rightarrow 2CrO_4$ evidently proceeds in the presence of NaCl only, with the product dissolved in the melt.

In the absence of oxygen the oxide remains green and melts are water white. Spectroscopic analysis shows that the solubility is 10^{-5} mole fraction.

Manganese. The stable oxide at 900° is Mn_3O_4, although small quantities of Mn_2O_3 may be present. Melt compositions varied considerably with the method of preparation of the starting material and atmosphere, but the metal solubility was always 0.1 – 1.0 mole % with the $Mn/O^=$ mole ratio varying from 2.2 to 4.7.

Iron. Fe_2O_3 is the stable oxide. Both in air and argon atmosphere its solubility is low. NaCl melts remain nearly white with perhaps a tinge of faint brown. The solubility is 5×10^{-5} mole fraction Fe.

Cobalt. Co_3O_4, the oxide used in this work is unstable at 900° where it decomposes to CoO. Solutions of the oxide are intense blue, typical of the color of anhydrous Co^{++}. The solubility (argon atmosphere) is 6.6×10^{-3}. The $O^=$ concentration found is much lower, 8×10^{-4}.

Nickel. The solubility of NiO varies somewhat with the source of the starting material (black or green). Solubility of NBS standard NiO is 6×10^{-5}. The $Ni^{++}/O^=$ ratio is quite erratic, perhaps because of the uncertainties involved in the analysis of very low concentrations, but is 1 for nearly all samples (0.04 – 0.85) and tends to decrease with time.

Copper. At 900° both Cu_2O and CuO are equally stable and the equilibrium mixture contains 50% of each oxide. However, only Cu (l) is found in NaCl melts. X-ray diffraction patterns of the quenched melt shows the presence of Cu_2Cl_2. The solubility is >5%.

Discussion: The above results are summarized in Table I.

In spite of the considerable scatter of these data some regularities are apparent:

1. Only oxides of metals having odd atomic number, i.e., an odd number of 3d electrons, show any appreciable interaction with NaCl, i.e., either reaction or solubility. Of the remainder Cr_2O_3 is an exception only in the presence of oxygen.

2. With the exception of V_2O_5 which oxidizes Cl^-, soluble oxides have possibly more than one oxide stable at 900°; all the insoluble oxides (NiO and Fe_2O_3 are included since their solubility is very low) have only one stable oxide.

3. The metal/oxide ion ratio found in the melts for the soluble oxides is much greater than can be accounted for on the basis of a simple solubility, (i.e., $M_n^{+n}O_n \quad mM^{+n} + nO^{=}$); also, since the ratio is >1 the stoichiometry does not correspond to any known oxide stable as a solid.

4. In spite of the considerable scatter of solubilities all the soluble oxides with exception of copper dissolve to the extent 0.001–0.01 mole fraction metal in the melt.

Table I

Solubility of Metal Oxide in NaCl at 900°(a)

Metal	Oxide	Solubility Metal	Solubility $O^{=}$	$M/O^{=}$
Ti	TiO_2	$< 10^{-5}$	not determined	
V	V_2O_5	Reacts to form Cl_2		
Cr	Cr_2O_3(b)	$< 10^{-5}$	not determined	
Mn	$Mn_3O_4(Mn_2O_2)$(c)	1×10^{-2}	1×10^{-3}	10
	$Mn_2O_3(Mn_3O_4?)$	$.8 \times 10^{-3}$	$.4 \times 10^{3}$	2 (air)
	$Mn_2O_3(Mn_3O_4)$	1.6×10^{-3}	8×10^{-4}	4 (argon)
Fe	Fe_2O_3	$\sim 5 \times 10^{-5}$		
Co	$Co_3O_4(CoO)$	6.6×10^{-3}	8×10^{-4}	8 (argon)
Ni	NiO (NBS std.)	6×10^{-5}	$(1\text{–}50) \times 10^{-3}$	.04– .8
Cu	$Cu_2O(CuO)$	$>5 \times 10^{-2}$	$.4 \times 10^{-3}$	>10

(a) Solubilities in mole fraction units.
(b) In air $Cr_2O_3 + O_2 \rightarrow (2CrO_4^{=})_{NaCl}$
(3) Oxide outside parentheses is starting material, oxide in parentheses may also be involved.

ELEKTROCHEMISCHE UNTERSUCHUNG GESCHMOLZENER BORATE UND PHOSPHATE

Ju. K. Delimarski, W.N. Andreewa, K.M. Bojko, G.D. Nasarenko, and T.N. Kapzowa

Es sind die Lösungen von Metalloxyden in geschmolzenem Borax oder Natrium–Meta–phosphat untersucht worden. Die untersuchung umfasste:

a) die chemischen galvanischen Ketten;
b) die Konzentrations–Ketten;
c) die Polarographie;

Es wurden die thermodynamischen Zusatzfunktionen für die in geschmolzenem Borax und Natrium–Meta–Phosphat gelösten Oxyde berechnet. Diese erlauben, die Energie der chemischen Wechselwirkungen bei der Auflosung des Oxyds in der Salzschmelze abzuschützen. Es ist die Bildung von Polyboraten und Polyphosphaten in den Schmelzen festgestellt worden.

Bei der Elektrolyse dieser Systeme wurde das Vorhandensein einer chemischen Polarisation festgestellt, die jedoch die Proportionalität zwischen dem Grenzstrom und der Konzentration nich stört.

THERMODYNAMIC STUDIES ON THE Tl–Bi LIQUID ALLOYS

K. Niwa, M. Shimoji, and O. Mikuni

Introduction: Although thermodynamic values of the Ti–Bi solid alloys were determined by Ölander (1) there have been no reliable electromotive force values of the Tl–Bi liquid alloys, except for the limited data of activities obtained by Wagner and Engelhardt (2) and by Vierk (3): Wagner and Engelhardt measured the electromotive forces of the cell $Tl/Tl^{+}/Tl–Bi$ at 480° and 270°C. Vierk also measured those values on the similar cell only at 459°C. According to Kubaschewski and Catterall's calculation (4), the agreement on the enthalpy of mixing calculated by using the above data is unsatisfactory with each other. This may be due to the small number of experimental runs. The purpose of the present paper is to measure the e.m.f. as detailed functions of temperatures and to obtain the knowledge on activities, entropies, and enthalpies of this system.

Experimental and Results: Electrode concentration cells of the following type were operated:

Tl(liquid)/TlCl in KCl–LiCl/Tl–Bi(liquid).

The details of experimental methods are the same as those described elswhere (5). Measurements were performed over the temperature range of 370~480°C.

The results of this experiment are summarized in Table I. Fig. 1 shows the activities of Tl and Bi along with corresponding data both of Wagner and Engelhardt (751°K) and of Vierk (732°K). It will be noted that there is a reasonable agreement between the present results and the earlier ones. The activity curves show profoundly negative deviations from Raoult's Law. In Table 2 the excess enthalpies and entropies of the Tl–Bi liquid alloys calculated from the present data are given. The enthalpies of mixing based upon the present e.m.f. values come very near by Wittig and Müller's data (6) (measured directly by the calorimetric method) in comparison with earlier e.m.f. values.

It is interesting to compare the present result with the theoretical equations for the energies of alloys. The atomic radii of Goldshmidt is 1.71A for Tl and 1.82A for Bi, but the metallic radii are respectively 1.71A and 1.70A. (7) In the liquid state the cohesion of bismuth atoms may be nearer to the metallic bonding than to the covalent one. Consequently the spheres of both metals may be regarded as having the same radii in the liquid alloys. Then the size effect may be negligible in the Tl–Bi liquid solution. The most prominent contribution to the excess enthalpy is due to the difference of electronegativities of the two metals (Tl:1.5, Bi:1.8) or an electron transfer.

The asymetric behavior of the excess heats can be explained in terms of the electron transfer theory (8,9), if the number of valence electrons is $Z_{Tl} = 3$ for Tl and $Z_{Bi} = 5$ for Bi in accordance with the positions in the periodic table. When the size effect can be neglected, the electron transfer theory of metallic solutions gives

$$\left(\frac{d_{Bi}}{d_{Tl}}\right) \sim \left(\frac{Z_{Tl}}{Z_{Bi}}\right)^{1/3}.$$

Here, d_{Bi} and d_{Tl} are

$$\lim_{X_{Tl} \to 0} H^{e}_{m}/X_{Tl} = d_{Bi}$$

and

$$\lim_{X_{Bi} \to 0} H^{e}_{m}/X_{Bi} = d_{Tl} \text{ (in Tl side)}$$

The predicted relation becomes then

$$\left(\frac{d_{Bi}}{d_{Tl}}\right)_{\text{Theor.}} \approx \left(\frac{3}{5}\right)^{1/3} = 0.84$$

The observed ratio is

$$\left(\frac{d_{Bi}}{d_{Tl}}\right)_{\text{obs.}} \approx 0.6$$

Hence, the form of energetic asymmetry may qualitatively be explained by the electron transfer theory.

Finally, it is interesting to note that the excess entropy has a slightly negative value in the liquid alloys in spite of its positive values in the solid alloys. Probably this may be due to the reason that the covalent bonding of Bi atoms in solid state disappears in liquid state.

Tables 1 and 2 appear on the following page.

TABLE I

E. m. f. and its temperature coefficient in Tl–Bi liquid alloys at 700°K

X_{Tl} (atomic fraction)	E (mV)	$(dE/dT) \times 10^6$ (V/deg)	a_{Tl} (activity)
0.103	273.0	195.0	0.011
0.189	204.0	140.0	0.021
0.255	191.5	117.0	0.042
0.263	184.0	118.0	0.047
0.403	149.0	73.0	0.085
0.432	118.3	64.0	0.141
0.526	91.3	52.0	0.220
0.645	65.8	40.0	0.336
0.741	41.9	28.0	0.499
0.805	24.8	15.5	0.663

TABLE 2

Thermodynamic Values of Tl–Bi liquid alloys

X_{Tl} (atomic fraction)	ΔS_m (cal/deg)	$-S^e_m$ (cal/deg. g atom)	$-\Delta H_m$ (cal / g atom)	$-\Delta H_m$ (Wittig & Müller) (cal/g atom)
0.1	0.59	0.15	354	267
0.2	0.84	0.15	656	494
0.3	1.07	0.13	885	703
0.4	1.22	0.12	1050	888
0.5	1.27	0.11	1136	1026
0.6	1.25	0.09	1146	1083
0.7	1.12	0.08	1068	1025
0.8	0.93	0.06	872	827
0.9	0.59	0.05	555	480

References

1) A. Olander, Z. phys. Chem. (A) 169 (1934) 260.

2) C. Wagner and G. Engelhardt, Z. phys. Chem. (A) 159 (1932) 241.

3) A. L. Vierk, Z. Elektrochem., 547 (1950) 436.

4) O. Kubaschewski & J. A. Catterall, Thermochemical Data of Alloys,

Pergamon Press Ltd. (1956).

5) K. Niwa, M. Shimoji, and O. Mikuni, J. Japan Inst. Metals, 24 (1960) 668.

6) F.E. Wittig and E. Müller, Z. phys. Chem. 21 (1959) 47.

7) L. Pauling, J. Amer. Chem. Soc. 69 (1947) 542.

8) J.H.O. Varley, Phil. Mag. 45 (1954) 887.

9) M. Shimoji, J. Phys. Soc. Japan 14 (1959) 1525.

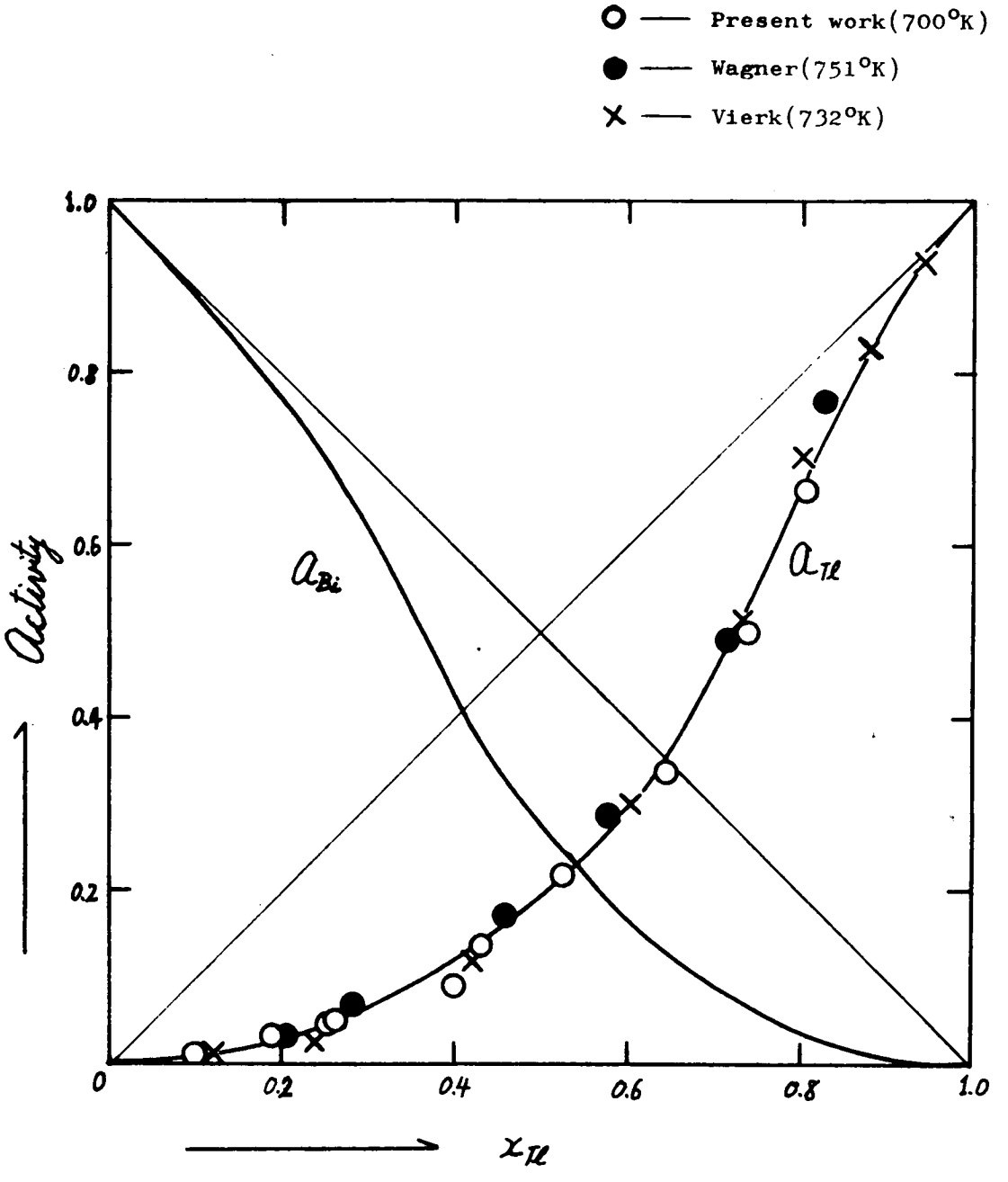

Fig. 1 Activity curves in Tl-Bi solution

ACTIVITY COEFFICIENTS AND ASSOCIATION IN MOLTEN SALT SOLUTIONS: A CRITICAL EVALUATION OF ASSOCIATION CONSTANTS IN RECIPROCAL SALT SYSTEMS

J. Braunstein, M. Blander, R.M. Lindgren, and Alba R.A. Funes

Introduction: Reliable values of association constants are necessary for a comparison with theoretical predictions. In this paper a new method of calculation of association constants is presented. The evaluation of thermodynamic equilibrium constants for the formation of associated species in solutions requires reliable data at low concentrations and a precise thermodynamic analysis of the data. Discrepancies among reported association constants of cadmium ions and halide ions in molten alkali nitrates, for example, probably are the result of the lack of data at sufficiently low concentrations to permit reliable evaluation of thermodynamic association constants, (1, 2, 3). The major advantages of this method over the methods (4, 5, 6) of Leden, Fronaeus, and Bjerrum is that, since the association constants are determined from the dependence of the activity coefficients on the stoichiometric concentrations of the solute components rather than on the concentrations of unassociated species, the calculations are more direct and often simpler. The method is applied to the evaluation of the thermodynamic association constants of silver ions with chloride and bromide ions in molten potassium nitrate.

Experimental: The determination of the activity coefficients of silver nitrate in dilute solutions of silver nitrate and potassium chloride in molten potassium nitrate from the e.m.f. of concentration cells has been described previously (7, 8) Additional data obtained by the same method were used with the earlier data in the evaluation of the association constants. Data were also obtained in the system $AgNO_3$–KBr– KNO_3 at five temperatures ranging from 402 – 500°.

The "Chemical" Interpretation of Activity Coefficients: Deviations from Henry's Law in solutions, if attributed to the presence of associated species, may be treated quantitatively in terms of equilibrium quotients for the associated species, The equilibrium quotients α are defined below for the association of Ag^+ and Cl^- in molten KNO_3, which will be treated specifically.

$$\alpha_1 = \frac{R_{AgCl}}{R_{Ag^+} R_{Cl^-}}$$

$$\alpha_2 = \frac{R_{AgCl_2^-}}{R_{Ag^+} R^2_{Cl^-}} \qquad (1)$$

$$\alpha_{1\,2} = \frac{R_{Ag_2Cl^+}}{R^2_{Ag^+} R_{Cl^-}}$$

etc.

The Ri are the mole ratios, n_i/n_{KNO_3}, of the species which may be present in the solutions. R_{Ag^+} and R_{Cl^-} are the concentrations of "free" Ag^+ and Cl^- ions respectively. The stoichiometric mole ratios of silver nitrate and of potassium chloride may be written as the sums:

$$R_{AgNO_3} = R_{Ag^+} + \alpha_1 R_{Ag^+} R_{Cl^-} + \alpha_2 R_{Ag^+} R^2_{Cl^-} + 2\alpha_{1\,2} R^2_{Ag^+} R_{Cl^-} + \ldots$$

$$R_{KCl} = R_{Cl^-} + \alpha_1 R_{Ag^+} R_{Cl^-} + \alpha_{1\,2} R^2_{Ag^+} R_{Cl^-} + 2\alpha_2 R_{Ag^+} R^2_{Cl^-} + \ldots (2)$$

Equating the activity coefficients of the solute components, $AgNO_3$ and KCl, to the fractions of unassociated Ag^+ and Cl^- ions, $\gamma_{AgNO_3} = R_{Ag^+} \gamma R_{AgNO_3}$ and $\gamma_{KCl} = R_{Cl^-} \gamma R_{KCl}$, and combining the definitions with (2) leads to the relation:

$$\frac{1}{\gamma_{AgNO_3}} = 1 + \alpha_1 R_{KCl} + \alpha_2 R^2_{KCl} + + (2\alpha_{1\,2} - \alpha_1^2) R_{AgNO_3} R_{KCl} + \ldots (4)$$

or

$$\ln \frac{1}{\gamma_{AgNO_3}} = \alpha_1 R_{KCl} + (\alpha_2 - {}^1/_2\, \alpha_1^2) R^2_{KCl} + (2\alpha_{1\,2} - \alpha_1^2) R_{AgNO_3} R_{KCl} + \ldots (4).$$

(3) and (4) are the Maclaurin expansions of $\frac{1}{\gamma_{AgNO_3}}$ and in $\frac{1}{\gamma_{AgNO_3}}$ in the range of concentrations where the species in (1) follow Henry's Law. The association constants can be obtained by extrapolation of the successive derivatives to infinite dilution of the solute components.

$$\lim_{\substack{R_{AgNO_3}\to 0 \\ R_{KCl}\to 0}} \left(\frac{\partial \ln \gamma_{AgNO_3}}{\partial R_{KCl}}\right)_{R_{AgNO_3}} = -\alpha_1$$

$$\lim_{\substack{R_{AgNO_3}\to 0 \\ R_{KCl}\to 0}} \left(\frac{\partial^2 \ln \gamma_{AgNO_3}}{\partial R^2_{KCl}}\right)_{R_{AgNO_3}} = (2\alpha_2 - \alpha_1^2)$$

$$\lim_{\substack{R_{AgNO_3}\to 0 \\ R_{KCl}\to 0}} \left(\frac{\partial^2 \ln \gamma_{AgNO_3}}{\partial R_{KCl}\partial R_{AgNO_3}}\right) = (2\alpha_{1\,2} - \alpha_1^2) \qquad (5)$$

etc.

These extrapolated limits are unique and lead to thermodynamic association constants.

Evaluation of the Association Constants: The association constants of Ag^+ and Cl^- in molten KNO_3 were evaluated from the activity coefficients of $AgNO_3$ in the presence of KCl in molten KNO_3. Large scale plots were made of log γ_{AgNO_3} as functions of the mole ratio of KCl at fixed mole ratios of $AgNO_3$ (7, 8). The slopes of these graphs at zero concentration of $AgNO_3$ were evaluated graphically, plotted as a function of the mole ratio of $AgNO_3$ and extrapolated to $R_{AgNO_3} = 0$.

The concentration of solutes varied between 3×10^{-4} and 3×10^{-3} mole ratio. The graphical extrapolation of the slopes obtained at 385° led to the values $\alpha_1 = 456 \pm 10$ and $(\alpha_{1\,2} / \alpha_1) = 70 \pm 15$ which were obtained from the intercept and the limiting slope of this graph. The value $(\alpha_2 / \alpha_1) = 169 \pm 20$ was obtained by first fitting the experimental activity coefficients of $AgNO_3$ at fixed mole ratios of $AgNO_3$ to the equation $\log \gamma_{AgNO_3} = A R_{KCl} + B R_{KCl}^2$ by the method of least squares; the coefficient B then was extrapolated to zero concentration of $AgNO_3$.

In a similar manner values of α_1 and $(\alpha_{1\,2} / \alpha_1)$ were evaluated for the associations of Ag^+ and Br^- ions in KNO_3 and are listed in Table 1.

Table I

Association Constants for Ag+ and Br^- in KNO_3

T(°K)	α_1 (moles / mole KNO_3)$^{-1}$	$(\alpha_{1\,2} / \alpha_1)$(moles/mole KNO_3)$^{/1}$
675	925	289
711	772	210
725	737	208
747	598	174
773	540	145

The estimated error in α_1 is about 3% except at 402° (675°K) where it is about 5%. The estimated error in $(\alpha_{1\,2} / \alpha_1)$ is about 8%. The values of α_1 and $(\alpha_{1\,2} / \alpha_1)$ and their variations with temperature may be compared with theoretical predictions.

References

1. E.R. VanArtsdalen, J. Phys. Chem. 60 172 (1956).
2. F.R. Duke and M.L. Iverson, J. Phys. Chem. 62 417 (1958).
3. J.H. Christie and R.A. Osteryoung, J. Am. Chem. Soc. 82 1841 (1960).
4. I. Leden, Z. Physik. Chem. A188, 160 (1941).
5. S. Fronaeus, Acta Chem. Scand. 4 72 (1950).
6. J. Bjerrum, "Metal Ammine Formation in Aqueous Solution", P. Haase and Son, Copenhagen, 1941.
7. J. Braunstein and M. Blander, J. Phys. Chem. 64 1038 (1960).
8. M. Blander, F.F. Blankenship, and R.F. Newton, J. Phys. Chem. 63 1259 (1959).

THE THERMODYNAMIC EVALUATION OF ACTIVITIES IN MOLTEN MIXTURES OF RECIPROCAL SALT SYSTEMS.

E. Grjotheim, C. Krohn, and J.M. Toguri

Molten salt mixtures, containing two or more of both cations and anions, can be treated as reciprocal salt systems. On a classical thermodynamic basis it is possible to evaluate formulae for the activities of the single salt components in these systems.

Consider the simplest system, a molten mixture of the ions (Na^+ K^+, Cl^-, and Br^-), as a representative example of these systems. This system has only three independent constituents because of the electroneutrality restriction. To describe the composition of the system, the ionic fractions are chosen as the independent variables:

$$N_{Na^+} = \frac{m_{Na^+}}{m_{Na^+} + m_{K^+}} \quad \text{and} \quad N_{Cl^-} = \frac{m_{Cl^-}}{m_{Cl^-} + m_{Br^-}}$$

where the N's are the ionic fractions and the m's the molar amounts of the respective ions in the mixture.

Four independent thermodynamic equations are imperative to calculate the four unknown activity coefficients, γ_{NaCl}, γ_{KCl}, γ_{NaBr} and γ_{KBr}, in this system.

Primarily, there is the reciprocal salt pair reaction

$$\text{I} \quad NaCl(l) + KBr(l) = NaBr(l) + KCl(l)$$

From tabulated data the standard (Gibbs') free energy, ΔG°_{ex}, can be obtained. If the activity terms in the thermodynamic equilibrium constant of reaction I are replaced by the Temkin terms (1), like

$$a_{NaCl} = N_{Na^+} \cdot N_{Cl^-} \cdot \gamma_{NaCl},$$

the first equation relating the four unknown activity coefficients with a known term results.

$$-\ln\gamma_{NaCl} + \ln\gamma_{NaBr} + \ln\gamma_{KCl} - \ln\gamma_{KBr} = -\frac{\Delta G^\circ_{ex}}{RT} \qquad (1)$$

Next, the anion exchange reaction is considered. This can be written, according to the classical method, as

$$\text{II} \quad N_{Na^+}NaCl(l) + N_{K^+}KCl(l) + {}^1/_2\,Br_2(g)$$

$$= N_{Na^+}NaBr(l) + N_{K^+}KBr(l) + {}^1/_2Cl_2(g)$$

The thermodynamic equilibrium constant for this reaction, in terms of Temkin's activity expressions, will be:

$$K^\circ_{mix} = \underbrace{\left[\frac{N_{Br^-}}{N_{Cl^-}}\left(\frac{P_{Cl_2}}{P_{Br_2}}\right)^{1/2}\right]}_{K^{an}_{mix}} \left(\frac{\gamma_{NaBr}}{\gamma_{NaCl}}\right)^{N_{Na^+}} \left(\frac{\gamma_{KBr}}{\gamma_{KCl}}\right)^{N_{K^+}} \qquad (2)$$

K^{an}_{mix} is the denotation of the "ideal equilibrium constant". Here it is convenient to introduce the change in standard Gibbs' free energy for the same anion exchange in pure sodium–ΔG°_{Na}, respectively pure potassium– ΔG°_K, milieu. Equation 2) then will possess the following form:

$$\ln K^{an}_{mix} = -\frac{1}{RT}\left(N_{Na^+}\Delta G^\circ_{Na} + N_{K^+}\Delta G^\circ_K\right) - N_{Na^+}\ln\left(\frac{\gamma_{NaBr}}{\gamma_{NaCl}}\right)$$

$$-N_{K^+}\ln\left(\frac{\gamma_{KBr}}{\gamma_{KCl}}\right) \qquad (3)$$

The simplified form without the activity coefficient terms of equation 3) has been derived by Flood and Muan (2) by another method, and the general equation

$$RT\ln K^{an}_{mix} = \sum_i N_i\Delta G^\circ_i$$

is known as "Flood's Equation" for exchange equilibria in molten salts.

Equation 3) gives the second connection between the four activity coefficients and the experimentally determinable terms. (K^{an}_{mix} contains concentration terms which are obtainable from equilibrium measurements.) A third relationship is obtained by considering the total exchange of cations in this system. This may be associated with the following reaction:

$$\text{III} \quad N_{Cl^-}\,NaCl(l) + N_{Br^-}\,NaBr(l) + K(g) = Na(g) + N_{Cl^-}\,KCl(l) + N_{Br^-}\,KBr(l)$$

This reaction is analogous to the anion–exchange reaction II. In a corresponding way, a combination of the expression for the equilibrium constant for this reaction with the standard Gibbs' free energy for the same cation exchange in pure chloride and bromide respectively, gives,

$$-N_{Cl^-}\ln\gamma_{NaCl} - N_{Br^-}\ln\gamma_{NaBr} + N_{Cl^-}\ln\gamma_{KCl} + N_{Br^-}\ln\gamma_{KBr} =$$

$$-\frac{1}{RT}(N_{Cl^-}\Delta G^{\circ}_{Cl} + N_{Br^-}\Delta G^{\circ}_{Br}) - \ln K^{cat}_{mix} \qquad (5)$$

where the "ideal equilibrium constant" K^{cat}_{mix} denotes

$$\left[\frac{N_{K^+}}{N_{Na^+}} \cdot \frac{P_{Na}}{P_K}\right].$$

The fourth and last equation between the activity coefficients is obtained from the Gibbs–Duhem, which for this system with ionic fractions may be used in the following form (3)

$$(N_{Na^+} - N_{Br^-})d\ln\gamma_{NaCl} + N_{Br^-}\,d\ln\gamma_{NaBr} + N_{K^+}d\ln\gamma_{KBr} = 0 \qquad (6)$$

An elimination of the three unknown activity coefficients is now possible, and the following expression for $\ln\gamma_{NaCl}$ results,

$$\ln\gamma_{NaCl} = \int_{1}^{N_{Na^+}} \int_{1}^{N_{Cl^-}} \left[(1 - N_{Na^+}) d\ln\left[\frac{N_{K^+}}{N_{Na^+}} \cdot \frac{P_{Na}}{P_K} \right] + (1 - N_{Cl^-}) d\ln\left[\frac{N_{Br^-}}{N_{Cl^-}} \cdot \left(\frac{P_{Cl_2}}{P_{Br_2}} \right)^{1/2} \right] \right] \quad (7)$$

In principle it is possible to determine the ratio of P_{Na}/P_K in the gas phase in equilibrium with the molten ionic mixture (Na^+, K^+, Cl^-, Br^-) for any concentration except at $N_{Na^+} = 0$ or 1. Therefore K^{cat}_{mix} is a single–valued, continuous function of the two variables N_{Na^+} and N_{Cl^-}. By an extrapolation of the experimental values, it is also possible to obtain the values of this function at (O, N_{Cl^-}) and (1, N_{Cl^-}).

Corresponding arguments can be given for the expression K^{an}_{mix}, which also appears to be a single–valued, continuous function of the same two variables. The values of the function at (N_{Na^+}, O) and (N_{Na^+}, 1) must be determined by extrapolation.

The information which exist for $\ln\gamma_{NaCl}$ are:

a) it is a single–valued, continuous function of the two variables N_{Na^+} and N_{Cl^-} existing in the intervals

$$O \leqq N_{Na^+} \leqq 1 \quad \text{and} \quad O \leqq N_{Cl^-} \leqq 1$$

b) for $N_{Na^+} = 1$, the γ_{NaCl} equals the activity coefficient in the binary system NaCl–NaBr, and for $N_{Cl} = 1$ the γ_{NaCl} equals the activity coefficient in the binary system NaCl–KCl.

c) For pure sodium chloride, $N_{Na^+} = 1$ and $N_{Cl^-} = 1$, thus by definition $\gamma_{NaCl} = 1$.

As $\ln\gamma_{NaCl}$ within the discussed concentration range satisfies the conditions for being a total differential, the equation 7) for $\ln\gamma_{NaCl}$ is an exact integral whose value is independent of the path of integration. Hence the integration path selected should be the most convenient one from an experimental point of view. To obtain γ_{NaCl} for an arbitrary concentration ($N^*_{Na^+}$, $N^*_{Cl^-}$) at constant temperature and pressure, the simplest integral results if the integration path is chosen, as follows: $N_{Cl^-} = 1$ from (1, 1) to (N_{Cl}, 1), and $N_{Na^+} = N^*_{Na^+}$ from ($N^*_{Na^+}$, 1) to ($N^*_{N^+}$, $N^*_{Cl^-}$).

A partial integration of equation 6) then gives

$$\ln\gamma_{NaCl} = \left[(1 - N^*_{Na^+}) K^{cat*}_{Cl} - \int_{N^*_{Na^+}}^{1} K^{cat}_{Cl} \, dN_{Na^+} \right.$$

$$\left. + (1 - N^*_{Cl^-}) K^{an*}_{mix} - \int_{N^*_{Cl^-}}^{1} K^{an}_{mix} \, dN_{Cl^-} \right] \qquad (7)$$

K^{cat}_{Cl} is the "ideal equilibrium constant" for the cation exchange in the pure chloride system. Corresponding expressions may be derived in a similar way for the three other activity coefficients in this system.

It is thus possible to calculate the activity coefficient for each salt at any concentration in the mixture when the anion exchange equilibria are known over the whole concentration range for the ternary system, and the corresponding cation exchanges for the two binary systems. From the experimental data analytical functions for the integrand may be found, or the integral may be obtained by other graphical or numerical methods.

It should be stressed that the selection of the integration path will depend upon which experimental data are the most easily determinable.

This method should prove useful for many systems where the entropy of mixing fit Temkin's model. That is in ionic systems where the cations do not differ too much with respect to size and charge. At present, however, complete experimental data which might assess the equations are not available.

References

1) H. Temkin: Acta Physicochim. URSS 20, 411 (1945)

2) H. Flood and A. Muan: Acta Chem. Scand. 4, 364 (1950).

3) H. Flood, T. Forland, and K. Grjotheim: Z. anorg. Chem. 276, 289 (1954).

ACTIVITY COEFFICIENTS IN FUSED SALTS

D.G. Hill, E.S. Woolner, and Alva R. Alvarez

Concentration cells have been studied of the type developed by Blander and others in which silver salt is dissolved in a solvent in which it is stable, in a two compartment cell. Additions of a reactant are made to one compartment, and the change in potential measured as a function of the concentration of added reagent and of original silver salt. We report here the addition of chromate to a solution of silver nitrate in potassium–nitrate and the addition of chloride to a solution of silver sulfate in potassium–lithium sulfate eutectic. Both are stable and reproducible, and permit calculation of activity coefficients which may be compared with those found in other systems and by other experimental means.

Equations for the activity coefficient of a solute in this type of system have been proposed by Flood and Blander. In the limit for small additions of reactant the equations approximate each other:

$$\log \gamma_{AD} = \bar{N}_B \bar{N}_C \frac{\Delta\Sigma}{RT} Z \quad \text{(Flood)}$$

$$\log \gamma_{AD} = \bar{N}_B \bar{N}_C \left(\exp \frac{\Delta\Sigma}{RT} - 1\right) Z \quad \text{(Blander)}$$

where $\Delta\Sigma$ is the excess interaction energy for the formation of an A–C coordination, and Z is the coordination number in the melt. The reactions given here are cases where ionic size and charge differ considerably, so that it is significant that the data approach a linear dependance in dilute solution as both theories demand.

In more concentrated solution Blander's complete equation demands a change in slope depending on the silver ion concentration, A in the symbols above. This was found to be the case in the study in fused sulfate while no dependance was found in the nitrate melt for chromate addition.

The interaction energy as calculated empirically from the two equations is given in Table I as well as two other values from the literature determined in the same manner.

Table I

Solute	Reactant	Solvent	Interaction Energy— (kcal) Flood	Blander
$AgNO_3$	K_2CrO_4	KNO_3	4.5	2.0
Ag_2SO_4	KCl	K_2SO_4 Li_2SO_4	13.5	4.0
$AgNO_3$	K_2SO_4	KNO_3	2.9	1.6
$AgNO_3$	NaCl	$NaNO_3$	43.0	4.6

All the measurements are averages for a number of temperatures, (only in the Ag_2SO_4 case over a range as small as 100°) and are quite constant over this range with the single exception of that calculated from the Flood equation in $NaNO_3$. The interaction energy may also be approximately calculated, as Flood has shown, from the heats of formation of the components of the reciprocal reaction. All the small values are in reasonable accord with this calculation. This would seem to show that the Flood equation is incorrect in two of the cases quoted, but applicable to the other two.

The basic difference in assumptions in the two theories lies in the consideration of the entropy of the solution. Flood considers that the anion reactants are distributed at random on the anion lattice which is believed to represent the arrangement in the melt. The entropy is then given solely by the ion fraction(or equivalent fraction) as Temkin defined it. Blander, on the other hand, assumes that the interaction energy favors a non-random distribution, with the added anions preferentially taking positions around the silver ion. This is treated statistically and results in an entropy expression dependent on the interaction energy, ultimately pracing it as an exponential parameter in the activity coefficient.

It would be expected that higher temperature would favor a random distribution, which is shown by closer agreement in fused sulfates than in fused nitrates, both for chloride additions. The successful applications made by Flood in slags also fall into line. It appears on the basis of the data presently available that the temperature and interaction energy are the important factors. Great differences in size and shape of the ions have less effect than might have been expected.

SELF-DIFFUSION IN MOLTEN SALT SYSTEMS

R. B. Escue and G. Perkins, Jr.

Self-diffusion coefficients, D, for Pb and Cl have been determined for several mixtures of $PbCl_2$ with KCl from 450–575°C and NaCl from 430–595°C by the capillary method. Compositions were chosen to provide data near the congruently melting $2PbCl_2$, KCl and the eutectic of the $PbCl_2$– NaCl system. Carrier-free samples of Pb-210 and Cl-36 were used to activate a portion of the diffusion melt so as to insure the same composition both within and outside of the capillary. Double labeling allowed an evaluation of both diffusion coefficients under identical conditions. After the diffusion period of 48 hours, the residual activities were separated by precipitating the chloride as AgCl prior to the counting.

The temperature range employed was from 10°C above the melting point of the mixture to the maximum permitted by the glassware. Over this range, the diffusion coefficients fitted the relationship $D = A \exp(-\Delta H^*/RT)$. Values for the least-squares straight lines are given for each composition in the following table.

Mole % Salt in $PbCl_2$	D_{Pb} (cm^2/sec)	D_{Cl} (cm^2/sec)
0.0	$7.73 \times 10^{-4} \exp(-6777 \pm 643/RT)$	$8.95 \times 10^{-4} \exp(-6099 \pm 483/RT)$
25.2KCl	$5.03 \times 10^{-3} \exp(-9864 \pm 242/RT)$	$2.34 \times 10^{-3} \exp(-7403 \pm 541/RT)$
33.3KCl	$2.92 \times 10^{-2} \exp(-12796 \pm 995/RT)$	$1.44 \times 10^{-3} \exp(-6608 \pm 573/RT)$
37.0KCl	$1.96 \times 10^{-3} \exp(-8405 \pm 566/RT)$	$1.31 \times 10^{-3} \exp(-6433 \pm 417/RT)$
17.9NaCl	$9.15 \times 10^{-4} \exp(-6705 \pm 671/RT)$	$13.4 \times 10^{-4} \exp(-6545 \pm 644/RT)$
27.0NaCl	$13.9 \times 10^{-4} \exp(-7338 \pm 304/RT)$	$16.8 \times 10^{-4} \exp(-6844 \pm 281/RT)$
34.9NaCl	$12.9 \times 10^{-4} \exp(-7054 \pm 866/RT)$	$13.1 \times 10^{-4} \exp(-6308 \pm 601/RT)$
47.5NaCl	$17.0 \times 10^{-4} \exp(-7325 \pm 999/RT)$	$23.8 \times 10^{-4} \exp(-7236 \pm 1505/RT)$

Overlapping values are observed for the ΔH^* values of chloride at all compositions (ca. 6.5 Kcal) and of lead (ca. 7.0 Kcal) in pure $PbCl_2$ and the mixtures containing NaCl. In the $PbCl_2$ – KCl mixtures, the ΔH^* for Pb shows a maximal value for the composition $*PbCl_2 \cdot KCl$.

Isotherm values of D_{Pb} show a minimum at this same composition for temperatures near the melting point (440°C) which disappears at higher temperatures (550°C).

No satisfactory agreement between experimental conductance values and those predicted by the Nernst–Einstein equation was obtained for either system. If the diffusing species are taken to be $PbCl^+$ and Cl^-, the D_{Cl} should be corrected for that chlorine transported as $PbCl^+$. Application of the Stokes–Einstein relationship to this data for pure $PbCl_2$ and $PbCl_2$–NaCl mixtures predict radii for the diffusing species which are in fair agreement with crystal structure values. A more involved degree of complex ion formation may be responsible for the failure of this equation in the $PbCl_2$ – KCl systems.

THE MECHANISM OF SOLUTION OF ALUMINA IN THE ALUMINUM ELECTROLYTE.

P.A. Foster, W.B. Frank, and L.M. Foster

Recent investigations have established the mechanism and extent of dissociation of molten cryolite. Cryolite, on fusion, ionizes completely as

$$Na_3AlF_6 = 3Na^+ + AlF_6^{3-}$$

with the anion undergoing partial dissociation according to the reaction

$$AlF_6^{3-} \rightleftharpoons AlF_4^- + 2F^-$$

The magnitude of this dissociation has been effectively related to temperature thus permitting more realistic evaluation of certain thermodynamic properties. The use of this knowledge in a structural evaluation of cryolite–alumina melts suggested that aluminum oxide dissolves according to the reaction mechanism

$$3F^- + Al_2O_3 = 3/2AlO_2^- + 1/2AlF_6^{3-}$$

It has never been possible, even in quenched cryolite–alumina fusions, to detect either microscopically or by x–ray the presence of aluminate. This is attributed to the instability as a solid of the $NaAlF_4$ from the cryolite dissociation. The species present in the molten state revert to cryolite and a meta–stable alumina on quenching, and to cryolite and starting α–alumina on slow cooling. However, quenched mixtures of alumina and fused sodium fluoride revealed sodium aluminate and cryolite. It is shown that sodium fluoride on fusion reacts quantitatively with alumina according to the reaction

$$6NaF + 2Al_2O_3 = 3NaAlO_2 + Na_3AlF_6$$

It is also demonstrated that the aluminate formed is insoluble in sodium fluoride, that the observed limited freezing point depression can be attributed to the product cryolite, and that the cryolite formed is responsible for the limited alumina solubility. The relation of alumina solubility to AlF_6^{3-} activity can be used to account for the observed maximum in solubility of alumina in basic (NaF rich) melts and the observed decrease in solubility of alumina in acid (AlF_3 rich) melts.

THE OSCILLOGRAPHIC INVESTIGATION OF THE ELECTROCHEMICAL KINETICS IN FUSED SALTS.

A. V. Gorodisky

A method of rapid electrochemical investigation of fused salts by means of a cathode–ray oscillograph is proposed. The device enables one to obtain the following dependences:

$$i, E;\ \frac{di}{dE}, E;\ \frac{di}{dE}, i;\ \frac{dE}{di}, E;\ \frac{dE}{di}, i;\ i, t;\ E, t;\ \frac{di}{dt}, t;\ \frac{dE}{dt}, t;$$

where i is the current, E the electrode potential, and t is the time. The electrolytic cell is polarized with saw–tooth, square or sinusoidal currents. The investigation is conducted with stationary electrodes. The choice of the correct time of polarization and the automatic electrochemical depolarization guarantee the complete reproducibility of the results obtained.

The data obtained allow one to determine the "superfluous" interelectrode capacity, to calculate ionic diffusion coefficients, and to investigate the electrode polarization in melts. A simple equation for the calculation of the charge curve, (E, t), is proposed.

These measurements, conducted at solid and at liquid electrodes, provide evidence on which to draw conclusions concerning the mechanism of certain electrode processes in fused salts.

ABSTRACTS

of

PAPERS

presented at the

CONDENSED STATE SESSIONS

PREPARATION, STRUCTURE, AND ELECTRICAL PROPERTIES OF THE AB_2 – TYPE SINGLE CRYSTALLINE SELENIDES AND TELLURIDES OF NIOBIUM, TANTALUM, MOLYBDENUM, AND TUNGSTEN

Lothar H. Brixner

The recent resurgence of interest in the phenomenon of thermoelectricity has initiated a rather detailed study of practically all metal tellurides and selenides from lithium to uranium. It appeared that the group V and VIa compounds, particularly those of Nb, Ta, Mo, and W, had, however, been somewhat neglected during these investigations; and the reason for this may be the fact that the selenides and tellurides of these metals thermally dissociate rather than melt and therefore pose a problem with regard to the preparation of single crystalline material. In the literature only the structures of WTe_2 (1), WSe_2 (2) and $TaTe_2$ (3) have been reported. They were obtained on the basis of a powder pattern in the case of WSe_2 and with the help of fine single crystals found in otherwise polycrystalline material for WTe_2 and $TaTe_2$. $MoSe_2$ was described by E. Wendehorst (4), $MoTe_2$ by Morette (5), and in 1907 Bolton (6) stated that Nb does react with selenium to form a compound without giving its composition or structure. No literature reference could be found as to $NbTe_2$ and $TaSe_2$. Also in no case were the electrical properties described. Our investigations were concerned mainly with the preparation of single crystalline material and the determination of the electrical properties of these compounds. As to the first objective we found that a transport reaction in a sealed quartz ampoule is a good general means to prepare single crystals of the discussed selenides and tellurides. Specifically, about 10–20 g. of the previously prepared polycrystalline selenide or telluride are charged into a quartz tube, which is sealed under 10^{-5} mm Hg pressure after about 1 – 3 mg of iodine or bromine have been added. The tube is put into a furnace with a temperature gradient of about 200°C. ($T_1 = 900°C$, $T_2 = 700°C$.) and is surrounded by an inert atmosphere to avoid any possible oxygen diffusion during the transport reaction, which for $NbTe_2$ is proposed to run according to the following mechanism:

$$NbTe_2 + {}^5/_2\, I_2 \rightarrow NbI_5 + 2Te$$

$$NbI_5 \rightarrow Nb + {}^5/_2\, I_2$$

$$Nb + 2\,Te \rightarrow NbTe_2$$

After 10 – 20 hours practically all of the polycrystalline material has deposited at the cooler end of the tube in form of well-defined single crystalline hexagonal platelets, with edges sometimes as long as 5 mm. In the case of $MoTe_2$ a rather perfect example of a screw dislocation growth could be observed. (These and other crystals will be shown on slides.) With this particular compound iodine also completely failed to give any transport and bromine had to be used for the formation of a decomposable bromide as transport medium.

The compositional identity of the originally charged and the transported species was established by comparison of X-ray powder patterns and also by chemical analysis. Some typical analyses for a selenide and a telluride are:

Found: Te 74.02%, Nb 25.56%; calcd. for $NbTe_2$; Te 73.31%, Nb 26.69%

Found: Se 63.24%, Mo 37.28%; calcd. for $MoSe_2$: Se 62.21%, Mo 37.79%

Single crystal data were obtained in a precession camera. The parameters and structures obtained are summarized in Table I:

TABLE I

Structures and Parameters for The Investigated AB_2 (A = Nb, Ta, Mo, W; B = Te, Se) Compounds

Compound	a_o in A	b_o in A	c_o in A	Space Group
$NbTe_2$	10.904	—	19.888	$D_{3d}^5 - R\bar{3}m$
$TaTe_2$	10.904	—	20.075	$D_{3d}^5 - R\bar{3}m$
$MoTe_2$	3.517	—	13.949	$D_{6h}^4 - P6_3/mmc$
WTe_2	14.028 *	3.495	6.270	$D_{2h}^{13} - P\ mmn$
$NbSe_2$	3.439	—	25.188	$D_{6h}^4 - P6_3/mmc$
$TaSe_2$	3.431	—	12.737	$D_{6h}^4 - P6_3/mmc$
$MoSe_2$	3.288	—	12.900	$D_{6h}^4 - P6_3/mmc$
WSe_2	3.280*	—	12.950	$D_{6h}^4 - P6_3/mmc$

*These parameters are in good agreement with the previously reported values.

It can be seen that with the exception of WTe_2 all compounds crystallize in hexagonal structures and all selenides are isostructural. $TaSe_2$ was observed to be dimorphic; its second modification crystallizes in the D_{3d}^5 space group, with $a_o = 3.428$ A and $c_o = 19.100$ A.

The electrical measurements were taken on bars, $^1/_4$" x $^1/_4$" x 2" in dimension, which were pressed at about 50 tsi from single crystalline materials. Since, even after sintering, the densities of these bars were around 90% of theoretical, the given data are only characteristic of this condition. Table II summarizes some fo the electrical and thermal data measured.

These properties shall be discussed and most of them will also be reported as a function of temperature.

As an example for the thermal stability the Ta:Te ratios will be reported as a function of temperature.

TABLE II

Electrical and Thermal Properties of The Investigated AB_2 (A = Nb, Ta, Mo, W; B = Se, Te) Compounds

Compound	ρ, Electrical Resistivity at RT in mΩcm	Electrical Resistivity at liquid N_2 T mΩcm	Seebeck Coefficient S, μ V/°C.	K, Thermal Conductivity watts/deg cm	Figure of Merit deg^{-1}
$NbSe_2$	0.351	0.180	+12		
$TaSe_2$	0.402	0.311	+13		
$MoSe_2$	$3.44 \cdot 10^3$	$4.76 \cdot 10^5$	+900		
WSe_2	$5.00 \cdot 10^2$	$1.50 \cdot 10^4$	−990		
$NbTe_2$	0.262	0.768	−15	0.019	$4.4 \cdot 10^{-5}$
$TaTe_2$	0.364	0.120	−14	0.014	$3.8 \cdot 10^{-5}$
$MoTe_2$	$8.05 \cdot 10^3$	$1.34 \cdot 10^6$	+780	0.020	$3.9 \cdot 10^{-6}$
WTe_2	2.87	0.364	+57		

REFERENCES

1. O. Knop and H. Haraldsen, Can. J. Chem. 34, 1142 – 1145 (1956).

2. O. Glemser, H. Sauer and P. Konig, Z. Anorg. Chem. 257, 241 – 246 (1948).

3. Y.M. Ukrainsky, Russ. J. Inorg. Chem. 4, 1305 – 1306 (1959).

4. E. Wendehorst, Z. Anorg. Chem. 173, 268 – 272 (1928).

5. A. Morette, Compt. Rend. 215, 86 – 88 (1942).

6. v. Bolton, Z. Elektrochem. 13, 149 (1907).

CRYSTAL GROWTH OF SYNTHETIC FLUOR-PHLOGOPITE

Tokiti Noda, Shigeharu Naka, Shigeo Tsujimura, and Nobutoshi Daimon

Synthetic fluor-phlogopite crystallizes from a melt of a composition approximately corresponding to that of the mica. The authors previously reported crystal growth of the mica using aluminous clay crucibles or graphite crucibles in a carbon granule resistance furnace. Clear single crystals of fluor-phlogopite measuring about 5 cm by 5 cm were obtained with 30 kg charge experiments by cooling the melt slowly from 1400° to 1300°C. The solidified mass comprised of randomly oriented mica crystals of various sizes and the yield of large crystals was small.

In the author's laboratory, various techniques of crystal growth such as the stationary crucible technique, the moving crucible technique and the Kyropoulos technique were investigated for the crystal growth of the mica. It was found that the thermal history of the melt affected nucleation seriously, when platinum vessels were used with the stationary crucible or the moving crucible technique. A series of experiments on the effect of heat-treatment of the melt on the nucleation of mica crystals were carried out. Finally the successful growth of clear "mica book" was accomplished with the moving crucible technique by using seed crystals of mica.

1. Effect of heat-treatment of the melt on nucleation of mica crystals.

Fluor-phlogopite crystals sealed in a small platinum vessel were heated to a temperature above the melting point of the mica and cooled with a rate of 7.5°C/min. Temperatures of beginning crystallization or temperatures of undercooling were measured from cooling curves. With a constant holding time of 5 minutes the melts heat-treated either at 1390° or 1395°C solidified at 1375°C, i.e. the equilibrium crystallizing temperature, while with the melt heat-treated at 1400°C, undercooling of about 70°C and with that at 1420°C, undercooling of 100°C were observed. Most of melts heat-treated above 1430°C were cooled down only with a slight exothermic effect and did not separate any visible amount of crystals. The degree of undercooling not only changed with the holding temperature, but also with the time of holding and there was always a region in which appreciable crystallization did not occur. Minute crystals of chondrodite were found along with crystals of mica in the crystallized mass which solidified from the melt of fluor-phlogopite at a large undercooling.

Mica crystals of good quality were found in the crystallized mass, only when the melt crystallized without undercooling or with a slight undercooling. The amount of chondrodite varied with the degree of undercooling, and the amount of mica crystals varied inversely with the amount of chondrodite. With heat-treatments which gave the maximum undercooling, almost all parts of the crystallized mass were composed of chondrodite and glass. It was found that chondrodite crystals once deposited reacted with the residual liquid to form fluor-phlogopite crystals, when the specimen was held at temperatures about 100°C lower than the crystallizing temperature of the mica.

2. Experiments on crystal growth of mica without using seed crystals.
a. The stationary crucible technique.

A furnace used for the experiments had three platinum-rhodium ribbon heater, each one being controlled separately. A platinum crucible containing fluor-phlogopite batch mixture was placed in the furnace and heated up to a temperature above its melting point. A temperature gradient in the crucible was then set by controlling temperatures of the top and bottom of the crucible. The temperature gradient ranged from 10° to 80°C/cm. The melt was cooled with a rate between 0.5° and 90°C/hr. Crystals of good quality of the thickness 0.7~0.6 mm grew with the rate of growth less than 1 mm/hr. Mica crystals grew vertically with their basal planes parallel to the temperature gradient, but the basal planes themselves were not parallel to each other.

b. The moving crucible technique.

A furnace used for the experiments was the type of Stockbarger. Fluor-phlogopite batch mixture was contained in a thin-walled platinum crucible whose conically shaped bottom was held on a platinum rod. The crucible and the rod were encased in a schamotte supporter which was connected with a lowering mechanism. The platinum rod served to cool the cone tip selectively, so that nucleation took place only in the tip. After melting, the crucible was lowered with a constant speed of 0.75 mm/hr. By varying the heat-treatment of the melt, it was verified that excessive heat-treatment resulted aggregates of randomly oriented minute crystals and insufficient melting was a cause of large number of seed crystals. Just to melt down to the tip was the optimum condition for the growth of a few crystals from the tip to the top of the charge. This heat-treatment could only be carried out by a very careful control of the tip temperature. The resulted crystals grew vertically with their basal planes parallel to the direction of lowering, but the basal planes

themselves were not parallel to each other.

3. Experiments on crystal growth of mica using seed crystals.

With the Kyropoulos technique, small plate crystals could be withdrawn from the mica melt, but the growth of the crystals could not be continued because of the decomposition of the melt from the surface. An attempt to grow seed crystals in the mica melt enclosed in a vessel was also failed due to technical difficulties. However, the moving crucible technique was proved to be successful. Seed crystals put their basal planes parallel to each other were placed vertically in the bottom part of a thin-walled platinum square tube vessel and raw batch material was placed on the top of the seed crystal layer. The sealed crucible was placed in a tube furnace having such a temperature gradient as to melt the whole raw material and an upper part of the seed crystal layer. The sealed crucible was placed in a tube furnace having such a temperature gradient as to melt the whole raw material and an upper part of the seed crystal layer. After melting, the crucible was lowered with a predetermined speed. The parallel sheets of seed crystals grew vertically into the batch melt to form so-called "mica book". Sheets of clear crystals were obtained with a lowering speed of 0.4 mm/hr. with a 10 mm by 10 mm width vessel, the temperature gradient being 60°C/cm.

EVIDENCE FOR THE EXISTENCE OF Si_2O_3

V. V. Dadape and J. L. Margrave

Silicon monoxide has attracted considerable attention since it was first reported. (1, 2) Although its vapor phase existence has been established unequivocally by spectroscopic investigations, (3–7) its stability as a solid has been in dispute (8–12) and this problem is yet unsolved. High temperature x-ray diffraction studied (13, 14) of the solid sub-oxide and also the x-ray and electron diffraction analysis of the quenched products (15–19) (formed by the interaction of metal with metal oxide or metal oxide with carbon) have suggested the stable nature of crystalline silicon monoxide. However, some of the x-ray evidence (20–21) has been shown to be not sufficiently clear. Thermodynamic (22–24) and thermochemical (25) studies suggest that the nature of SiO (solid) in relation to Si (solid) + SiO_2 (solid is quite uncertain from room temperature to 1400°K or even above this limit.

Solid silicon monoxide is prepared by heating an intimate mixture of finely powdered quartz and silicon metal (or carbon or SiC), at about 1250°C and 10^{-4} mm. og Hg. The gaseous products are quenched rapidly and the solid product is deposited having an appearance varying in color (light brown if condensed at 800°C and black massive is condensed at 400°C). (19)

The work described in this paper is a part of an attempt to obtain crystalline suboxides of silicon, aluminum and boron employing suitable quenching and/or hot pressing techniques. The paper deals with silicon suboxides only.

Experimental: Strong quenching of the products of vaporization from several mixtures (Si + SiO_2, Al + SiO_2, B + SiO_2, Si + Al_2O_3 and Si + B_2O_3) were effected by heating them in a solar furnace. The temperature gradient between the focal spot and its immediate surroundings is quite high. This helps quick condensation of the vapor from the material which is being heated in the focal spot. Contamination from the container material is avoided as the material in the focal spot acts as its own crucible. The quenched products were subjected to the following studies: (1) oxygen absorption and consequent weight gain: (2) x-ray powder diffraction and (3) infrared spectra. The quenched products were also examined after (1) heat treatment and (11) hot pressing at 800° and 70,000 atmospheres. The high temperature and high pressure experiments were carried out in cooperation with Dr. R. H. Wentorf of the General Electric Company.

Pellets of the mixtures Si + SiO_2 (mol. ratio 1:1; 1:2; 4.32.1 and 2.14:1); Si + Al_2O_3 (2:1); Si + B_2O_3 (1:1); Al + SiO_2 (1:1) were heated in the solar furnace at less than 0.5 mm. pressure in a three liter pyrex flask. The vapor was condensed either on the air-cooled walls of the pyrex flask or on the walls of a liquid air condenser. The temperatures could not be determined accurately because of the interference by the vapors emitted and the lack of data for the high temperature emissivities of the materials. Attainable temperatures at the focal spot include the melting point of pure MgO (2800°C) and of ZrO_2 (2600°C).

Oxygen absorption and weight gain in the condensates: The pale brownish yellow condensates from different mixtures of Si + SiO_2 were oxidized at 900°C in a slow current of oxygen. In each case the weight gain was such that the atomic ratio Si:O in the brownish yellow solid was 1:1.5, which corresponds to the formula Si_2O_3. In other mixtures, where more than

one metal is involved, the oxygen absorption experiments were more complicated due to the presence of two elements capable of forming sub-oxides.

X-ray powder studies: The powder pattern from all the condensates showed lines of weak intensities indicating poor crystalline nature. To improve the crystallinity these condensates were pressed at 800°C and 70,000 atmospheres. In the case of the condensates from Si + SiO_2 mixtures the x-ray powder patterns showed lines which gave a cubic fit for the structure. The solid phase with cubic structure has the unit cell dimension a = 5.77 A. The condensates from other mixtures (Al + SiO_2, Si + Al_2O_3 ....) after hot pressing showed in their x-ray powder patterns lines of the above cubic phase together with those of other suboxides. Table I records the x-ray data for the pressed and unpressed cubic phase. The quenched condensates after oxidation at 900°C showed no lines in their powder patterns indicating that the original crystalline material was converted into an oxidized amorphous form.

Infrared spectra: The infrared spectra at room temperature were run for the light brown-yellow cubic phase (Si_2O_3) and the following absorption bands were observed.

wave-length μ	wave no. cm^{-1}	Absorption
6.15	1625	VW
7.3	1370	VW
9.6	1061	VS(broad) 1162 – 1000 cm^{-1}
11.5	872	W

The most intense band at 1061 cm^{-1} which is intermediate between the absorption bands of amorphous SiO (26, 32) at 1000 cm^{-1} and single crystal silicon (27) at 1105 cm^{-1}, the silicon lattice being contaminated with oxygen.

Conclusions: Strong quenching of the vapor from Si + SiO_2 mixture has yielded a suboxide Si_2O_3 having cubic structure. The crystallinity was found to improve after heat treatment (800°C) under extremely high pressures (70,000 atmospheres). This suboxide has been suggested (28) to be the product of heating silicon oxyhydride at 900°C in an oxygen free atmosphere.

It has also been claimed to be one of the products during evaporation studies on amorphous silicon monoxide (29–31) but the product obtained was always in the amorphous state and hence its nature was undecided. The present work justifies its existence through the studies of (a) oxygen absorption; (b) x–ray powder patterns and (c) infrared spectra. Microscopic examination has also shown the isotropic nature of the crystalline Si_2O_3. The density, however, could not be determined due to the very thin platelets being present.

Table I
X–ray Data for the Cubic Phase Si_2O_3

(a) Quenched condensate
(before hot pressing)

d(Å)	Relative Intensities	Length of unit cell "a"
3.30	Ext. W	5.72
3.12	W	5.83
1.91	W	5.73
1.565	W	5.83
1.43	VW	5.73
1.35	VW	5.73
1.24	Ext. W	5.73
	a_{av} =	5.77

(b) Quenched condensate
(after hot pressing – 800°C and 70,000 atms.)

d(Å)	Relative Intensities	hkl	Length of unit cell "a"
3.35	M	111	5.81
3.08	W	200	5.75
2.0	VW	220	5.70
1.92	VW	300;221	5.75
1.67	VW	222	5.78
1.58	VW	321	5.85
1.22	VW	332	5.72
1.15	VW	500;430	5.75
		a_{av} =	5.76

Intensities: W – weak; VW – very weak; M – medium; Ext. W – extremely weak.

References

1. C. Winkler, Ber. deut. chem. Ges. 23, 2642–48 (1890).
2. H.N. Potter, Trans. Am. Electrochem. Soc. 12, 215–22 (1907).
3. A. De Gramont and C. de Watteville, Compt. rend. 147, 239 (1908).
4. W. Jevons, Proc. Roy. Soc. (London) 106, 174 (1932).
5. P.C. Saper, Phys. Rev. 42, 498 (1932).
6. K.F. Bonhoeffer, Z. physik. chem. 131, 363 (1928).
7. D. Sharma, Proc. Nat. Acad. Sci. (India) A14, 37 (1944).
8. C.A. Zapffe, J. Am. Ceram. Soc. 27, 298–98 (1944).
9. C.A. Zapffe and C.E. Sims, Iron Age 149, (4), 29–31 (1942). (5), 34–39 (1942).
10. W. Biltz and P. Ehrlich, Naturwissenschaften 26, 188 (1938).
11. E. Zintl, W. Baruning, H.L. Grube, W. Krings and W. Morawietz, Z. anorg. u. allgem. Chem. 245, 1–7 (1940).
12. H.N. Baumann, Jr., Trans. Am. Electrochem. Soc. 80, 95–98 (1941).
13. M. Hoch and H.L. Johnston, J. Am. Chem. Soc. 75, 5224–5 (1953).
14. M. Hoch and H.L. Johnston, J. Am. Chem. Soc. 76, 2560 (1954).
15. G. Grube and H. Speidel, Z. Elektrochem. 53, 339–41 (1949).
16. H.D. Erasmus and J.A. Persson, J. Electrochem. Soc. 95, 316 (1949).
17. H. Inuzuka, Mazda Kenkyu Ziiho (Japan) 15, pages 161, 237, 305 and 374 (1940).
18. H. Konig, Optik. 3, 419 (1948).
19. G. Hass, J. Am. Ceram. Soc. 33, 353 (1950).
20. S. Geller and C.D. Thurmond, J. Am. Chem. Soc. 77, 5285 (1955).
21. G.W. Brady, J. Phys. Chem. 63, 1119 (1959).
22. L. Brewer and R.K. Edwards, J. Phys. Chem. 58, 351 (1954).
23. H. Von Wartenberg, Z. Elecktrochem. 53, 343 (1949).
24. H. Schick, Chem. Rev. 60, 331–62 (1960).

25. L. Brewer and F. T. Greene, J. Phys. Chem. Solids, 2, 286 (1957).

26. G. Hass and C. D. Salzberg, J. Opt. Soc. Am. 44, 181 (1954).

27. H. J. Hrostowski and R. H. Kaiser, Phys. Rev. 107, 966 (1957).

28. G. H. Wagner and A. N. Pines, Ind. Eng. Chem. 44, 321–26 (1952).

29. B. C. Weber and P. S. Hessinger, J. Am. Ceram. Soc. 37, 267 (1954).

30. Von E. Cremer, Th. Kraus and E. Ritter, Z. Elektrochem. 62, 939 (1958).

31. E. Cremer, A. Faessler and H. Kramer, Naturwissenschaften 46, 377 (1959).

32. L. E. Howarth and W. G. Spitzer, J. Am. Ceram. Soc. 44, 26–28 (1961).

EFFECTS OF VARIOUS ADDITIONS ON THE SYNTHESIS OF SILICON NITRIDE AND ITS POLYMORPHISM

Hiroshige Suzuki and Toshiyoshi Yamauchi

As for the reaction of pure silicon with nitrogen, a few studies have been reported, and the reaction is known to proceed at a fairly slow rate at such low temperatures as 1200 – 1400°C. Preliminary experiments of the writers have confirmed similary, that when a compact of silicon was nitrided at about 1300°C, a thin layer of white nitride, containing fine whiskers, was produced at the surface, but at the under surface almost all the silicon remained still unreacted. For the production of silicon nitride commerically, iron or alkalline earth fluorides are said to be valuable catalysts in promoting the silicon–nitrogen reaction. No fundamental work is known to the writers, however, on such a nitridation of silicon containing a bit of additions in it. The object of this work was to investigate what would be the effective additions (catalysts), and efforts were made to make clear the nitridation behaviour of such a silicon.

The experiment proceeded in the following manner; Purified silicon powder with a mean diameter of 22.6μ was first taken. Sixteen sorts of metal fluorides were separately added to them, at the ratio of 2 and 4% each. Nitridized for 3 hours at 1385°C (of some of them, experiments were tried at 1265 – 1405°C also). Using 4 N–NaOH and some

mineral acids, the unreacted parts of silicon and additions were dissolved and removed. By measuring the amount of silicon nitride thus produced, the effects of fluorides on the reaction were examined. As the result, the effects of BaF_2, CaF_2 and of some other kind of fluorides could not be observed, while the effects of a group of fluorides – MnF_2, CuF_2, NiF_2, etc. – were ascertained to promote the nitriding reaction remarkably. Besides, it was certain that each fluoride addition affects not only the nitriding rate but polymorphic composition of the nitride produced there; CuF_2, MnF_2, PbF_2 etc. produced a large amount of α –Si_3N_4, and only AlF_3 had an inclination of producing β –Si_3N_4 preeminently. What interested the writers still more was that LiF, NaF, CaF_2 etc. had no effects of promotion on the reaction rate (the volatilization of nitrides was observed to some extent), but they were apt to produce a considerable amount of new crystalline phase which showed the another X–ray diffraction pattern, not belonging to α –Si_3N_4 nor to β –Si_3N_4. It could not yet be confirmed whether this new substance was Si_3N_4 or something which had some other molecular formula. But it is surely a kind of nitride, and the writers tentatively decided to call it "silicon nitride of γ –type".

The results thus acquired in the experiment were examined and compared with m.p., b.p. etc. of the metal fluorides used as additions. No clear relations were found between them. And then the effects of oxides, chlorides, carbonates, sulphates, phosphates, sulphides of the more metals and of isolated metal powders were examined experimentally. In those experiments each addition was measured and used to be 2% of silicon when they would convert to their oxides. After having been pressed into a small disk with 320 kg/cm^2 pressure, silicon powders mixed with additions were heated for 5 hours at 1400°C in the current of nitrogen. The rates of growth of silicon nitrides were examined.

The effects of additions were compares respectively. As a result, $CuCl_2$, CuO, Cu, $CoCl_2$, CrO_3, $MnCO_3$, $FeSO_4$, Al and Cu_2O, Co_2O_3, NiO, Cr_2O_3, Fe_2O_3 etc. showed remarkable rates. The effects of the latter five were especially conspicuous. Six sorts of additions, including the above–mentioned five additions and $MnCO_3$, were further examined with respect to their rates of nitriding reactions, changing their ratio of additions to be 0.5, 1, 2, and 4%, at 3 kinds of temperatures – 1300, 1370 and 1400°C respectively.

An empirical equation for the rate of nitridation of the silicon compacts was as follows:

$$\log x = C + G \log t$$

where x is the rate of reaction, t the duration of reaction, C a constant and G also a constant.

Under the conditions of this experiment, C shows an increase in proportion to the rate of addition and temperature, and G is not much affected by the rate of addition, but by the temperature. When the temperature is as high as 1400°C, C indicates a tendency to be saturated by the rate of addition above 2%. On the other hand, G tends to decline again when the temperature exceeds about 1370°C.

After examining the results fully and making additional experiments, each addition was found to be affected by metallic elements in the addition, whether it may be an oxide or a salt. Such metals as belong to the first group of transition elements were found to be the most effective for the reaction. Consequently, each compound added must be reduced to metal by silicon at or below the nitriding temperature and the metal should be transformed into an intermetallic compound having a low melting point or solid solution with silicon.

It is reasonable to conclude that each metal atom of the compounds may be incorporated into the lattice of Si_3N_4 in the nitridation process, thus contributing to the production of lattice defects. These defects will increase the rate of material transport, and may also be responsible for the development of Si_3N_4 into needle–like crystals; the minute cracks produced by this crystallization will facilitate nitrogen permeation in reaction layer.

Finally, the writers were able to synthesize Si_3N_4 containing above 95% α – phase after nitridation at 1400°C by adding 2% NaF and 1% Co_2O_3, and Si_3N_4 containing almost β –phase after nitriding at 1420° to 1430°C with the addition of 3% AlF_3. Many data reported to date have been confirmed, corrected and supplemented by measuring face spacing, X-ray density, thermal expansion, thermal conductivity and oxidation of these two nitrides.

The writers failed to synthesize pure γ –type silicon nitride, but some properties of it were measured in as wide a range as possible.

THE SYNTHESIS OF CALCIUM TITANATE SINGLE CRYSTALS BY THE FLAME FUSION TECHNIQUE

L. Merker

This investigation was undertaken in order to obtain large single crystals of calcium titanate of high purity in order to determine the physical properties of the material. Calcium titanate occurs in nature as the mineral perovskite, and while transparent crystals of yellow color are occasionally found they are invariably very strongly twinned and chemically not very pure. Previous attempts to synthesize calcium titanate single crystal from fluxed melts have either failed or produced only crystals of very small size (1–2 mm.). Even these small crystals were invariably strongly twinned, to such a degree that it was extremely difficult, if not impossible, to carry out accurate structure determinations. The flame fusion technique was selected for the synthesis of large single crystals of calcium titanate because of its high melting point of 1960 to 2000°C., and also because the flame fusion technique greatly reduces impurity pickup during growth. However, if the growth of calcium titanate crystals is carried out under standard flame fusion conditions, only fractured crystals are obtained which are as badly twinned as the crystals found in nature.

In order to obtain unfractured crystals of up to one inch length and $^1/_2$ inch diameter which are free of strain and twinning, a novel–type boule furnace was devised which permits supplementary heating of the boule during and after growth and eliminates the severe heat shock to which the crystal is subjected when the boule burner is shut off. The supplementary heating serves to reduce the temperature gradient inside the furnace during the growth of the crystal, and allows annealing of the boule "in situ" at temperatures of up to 1500°C. After completed annealing inside the furnace, the boule is allowed to cool slowly at rates from 5 to 30°C. per hour. This growth technique results in a considerable reduction of strain in the crystal and produces unfractured boules which exhibit very little twinning. Twinning is completely eliminated by subjecting the boule to additional annealing at 1700°C., which is carried out in a gas fired furnace. When boules grown by the standard flame fusion technique, i.e., without supplemental heating during growth, are subjected to annealing at 1700°C., no complete elimination of twinning is achieved. Boules which are free of twinning can be sawed, ground and polished without fracturing, and are eminently suitable for the determination of the physical properties of calcium titanate.

These measurements were made with untwinned crystals of 8 x 10 mm. size, and extended to determinations of refractive index, dispersion, specific gravity, hardness, optical transmission range, dielectric constand and loss angle.

The feed material from which the crystals were grown was of very high chemical purity, and was prepared by precipitation of calcium titanyl oxalate ($CaTiO(C_2O_4)_2$) which on calcination at 1000°C. is transformed into calcium titanate of stoichiometric composition and very fine particle size. The calcium titanyl oxalate is obtained by adding a concentrated solution of ammonium oxalate to the combined solutions of calcium chloride and titanium tetrachloride, under carefully controlled conditions of temperature, agitation and dilution. If these conditions are not carefully controlled, the final product will either be off composition or so floury that it cannot be used for growing boules.

The paper discusses briefly the basic principles of growing large single crystals of high melting compounds by the flame fusion technique, with particular emphasis on the growth of calcium titanate crystals. It furthermore describes the design and construction of a novel boule furnace equipped with supplemental heating, and how it can be applied to the growth of large true (i.e., untwinned) single crystals of calcium titanate which prior to this work have not been available from either natural or other sources. The gradual elimination of twinning domains is illustrated by a series of photo-micrographs. The technique for the preparation of a suitable high purity boule feed material is described and is illustrated by spectrographic analysis data as well as electron micrographs. The paper concludes with a tabulation and discussion of some of the more important physical properties of calcium titanate which are the results of measurements made with large untwinned single crystals prepared by the technique described above.

THE PHYSICO-CHEMICAL APPLICATIONS OF ELECTROMAGNETIC LEVITATION.

A. E. Jenkins

Introduction: Although the levitation coil offers many advantages in the control of masses of liquid metals for general physico-chemical purposes, the measurement and control of the temperature of the specimens is made more than usually difficult by the inaccessibility of the liquid mass and the existence of non-black body conditions within the coil. In this connection, the recent investigations by Fogel (1) in Leningrad (1959) illustrate rather clearly the general position in that whilst the melting and casting of 100 grams of titanium and zirconium has been achieved by improvements in general coil design, only approximate temperature measurements could be achieved with the aid of an optical pyrometer and no actual control of the temperature was attempted. Similarly, research into the fuming of iron by the British Iron and Steel Research Association (2) using the levitation method, has been halted after some promising results had been achieved, due to the difficulty of controlling and measuring the temperature of liquid iron spheres. With an acceptable solution to the temperature measurement and control problem, the controlled levitation of a sphere of liquid metal weighing approximately 3 – 5 grams, offers the prospect of a fundamentally new experimental technique for the study of gas liquid metal systems at temperatures where the more usual techniques cannot be used. In addition, however, it should also be possible to examine certain kinetic phenomena, such as are encountered in the vacuum or reactive gas refining of metals since the temperature of the metal surface, the area and degree of surface turbulence, would then be under direct control.

Experimental: A suitable technique has been developed for the levitation of liquid 3 – 5 gram masses of copper, iron and titanium, utilising a levitation assembly described in a previous paper (3). However, the reaction volume is now constructed from a simple pyrex glass tube which is blown to fully occupy the internal volume of the levitation coil. The coil is thus placed wholly outside the gas metal system and liquid metal samples can now be held for an indefinite period within a gas stream passing through the reaction tube. Although the total reaction volume is only approximately 10 cc. the stability of the melt is sufficient to prevent contact with the container walls. Experiments on liquid copper have established that the high frequency generator power input controls are insufficient to maintain the temperature of the specimen constant

once it is completely liquid; any attempt to reduce power under these conditions results in a reduction of levitation force and the specimen falls from the coil. However, using an argon–helium system of gas temperature control, a 3 gram specimen of copper may now be melted and the temperature held constant to within ± 3°C. in the range 1200 – 1550°C. Both flow rate and helium to argon ratio affects the equilibrium temperature of the liquid specimen and this control may be supplemented if required by an adjustable positioning of the reversed upper turns of the levitation coil assembly. It has proved possible to melt and re–solidify specimens whilst levitated, this being an important advantage in certain gas liquid metal studies.

Due to the configuration of the levitation coil specimen assembly, the measurement of the temperature of liquid spheres of metal in the range 1200 – 2000°C, for example, provides a most difficult problem. With the technique as operated at present, there can be no enclosure at the temperature of the sample to provide black body conditions and the range of interest is one for which there is very little reliable infor–mation covering the emissivity of liquid metals. After considering a number of possibilities, the calibration of a reliable optical pyrometer against a micro–probe Pt–PtRh thermocouple was considered to be the most reliable method for measuring the temperature of non–reactive metals such as copper and iron. The final technique used for the copper calibration involved the support of a 1 cm. diameter ball of liquid copper on a vertical carbon tipped refractory pylon, through the centre of which passed a refractory covered microprobe thermocouple. This couple was linked externally to a cathometer which allowed the couple junction to be accurately placed within the coil. Simultaneously, optical pyrometer readings were taken on the curved upper surface of the liquid. Results from these and other similar experiments on liquid copper confirmed the constancy of the Wien relationship in the temperature range 1100 – 1500°C. with an average calculated emissivity of 0.144. Because of the chemical reactivity of liquid titanium a similar technique could not be used for temperature calibration and therefore the Wien relationship was assumed to hold from the melting point to 2000°C. A value of 0.351 for the emissivity of liquid titanium at the melting point (1668°C.) was obtained by observing simultaneously the optical temperature of both solid and liquid metal immediately adjacent to a stable liquid solid interface produced by an induction heated rod of titanium at the tip of which a large molten ball of metal was stabilised by carefully positioning within the levitation coil.

With the attainment of stable levitation conditions within a small reaction volume and satisfactory temperature measurement and control techniques, a series of experiments have now been commenced with the aim of studying the reliability of the new technique for high temperature physico–chemical investigations. A suitable gas train and auxiliary equipment has been constructed to study the copper–oxygen equilibrium using carbon monoxide carbon dioxide gas mixtures carried by an argon helium stream. The possible influence of thermal diffusion within the gas phase on the final result is being examined, and should gross errors be involved, the effect of pre–heating the gas stream will be analysed. A further extension of the investigations into kinetic studies on gas liquid metal and slag liquid metal systems is currently being considered.

References.

1. "Melting of Laboratory Specimens of Metals in Vacuum or an Inert Gas by Levitation Technique". A.A. Fogel. Akad. Nauk. SSSR. 1959, No. 2, pp. 24 – 34. (H. Brutcher Trans. No. 4702).

2. "Summary of Research and Investigation". B.I.S.R.A. (1959).

3. "A Controlled Atmosphere Levitation System". B. Harris, A.E. Jenkins. J. Sci. Inst. 36, 1959, 238 – 40.

PRODUCTION AND MEASUREMENT OF HIGH TEMPERATURES.

John L. Margrave

All of the known refractory materials either sublime, vaporize or melt extensively below 5000°K. and 1 atm. pressure and the dissociation of diatomic molecules (CO, N_2, HF, etc.) limits flame temperatures to about 6000°K. Thus, new approaches and a better understanding of the properties of matter will be required before attaining higher laboratory temperatures than 6000°K. in condensed systems at ordinary pressures, in spite of the fact that one can attain "temperatures" of at least 100,000°K. in electric arcs through partially ionized gases.

Modern research activities include (1) a search for higher melting solids and more stable molecules; (2) the use of oxides and other semiconductors, carbides, borides, silicides, etc. as resistance heaters or susceptors for induction heaters; (3) the use of concentrators to give more uniform induction heating; (4) resolution of container problems by levitation of conducting solids and liquids; (5) the use of high pressures to maintain condensed phases at higher temperatures; (6) the study of fused salts and other high temperature liquids; (7) the study of radiation damage, flash photolysis, flash heating ion sputtering, exploding wires and other techniques for attaining extremely high temperatures for short times in small volumes.

Temperature measurements above 2000°K. are seriously hampered by a lack of (1) reliable experimental data or theoretical predictions for emissivities of solids and liquids; (2) temperature standards; and (3) reliable thermocouples and/or resistance thermometers, especially for high pressure–high temperature studies.

SYMPOSIUM ON CHEMICAL AND THERMODYNAMIC PROPERTIES AT HIGH TEMPERATURES.

Peter E. Glaser and George P. Ploetz

The goal of high temperature research is to obtain a better understanding of the behavior of materials under conditions of extreme temperatures. To permit the experimental investigation of materials, equipment had to be found to generate high temperatures under controlled conditions in the laboratory. Thermal imaging in which an optical system is used to concentrate radiation from a suitable heat source

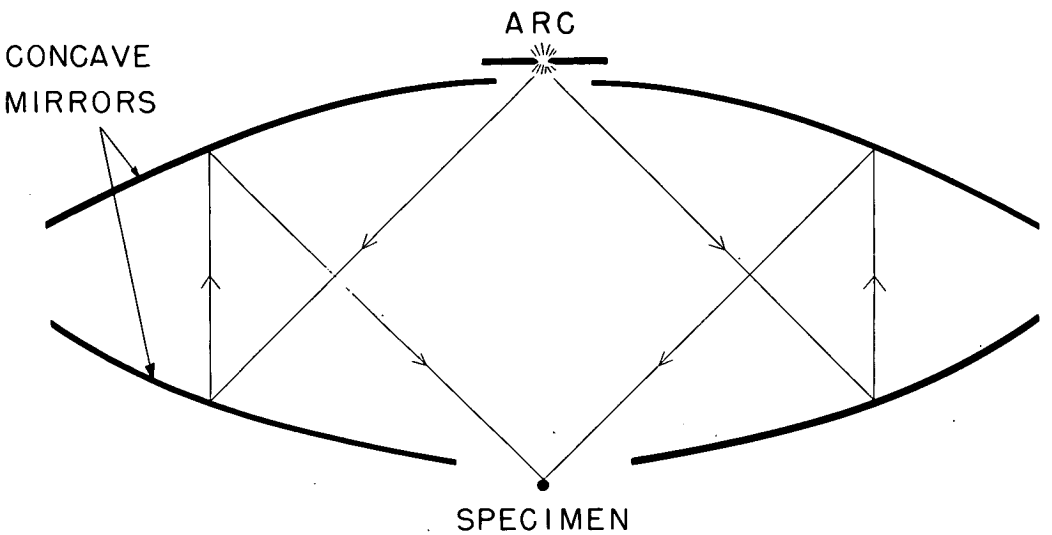

Figure 1

has found its place in studies of high temperature phenomena. Within the past few years as thermal imaging has become an accepted experimental procedure, advances have been made in utilizing these techniques. The recent development of a new optical system suitable for thermal imaging is discussed and its advantages are compared to those of the more conventional optical systems which have been used for imaging purposes. The role of the radiant energy sources, the instrumentation designed to measure the controlling variables, and the imaging techniques which have been developed are discussed. The following topics are treated in greater detail:

Optical System: The new optical system consists of two paraboloids mounted face to face so that the focal point of each falls at the vertex of the other. (See Figure 1.) The effect of the aperture ratio on the radiation entering and leaving the compound reflective optical system is demonstrated. It is shown how holes provided at the vertices of the two paraboloids allow the image to be located completely outside the optical system. Figure 2 shows a thermal imager that uses this optical system. The advantages of this optical system in which both the source and the image are placed outside the system are compared with those of other systems where the source and image are placed within the optical system. Results that are presented give the form of the image obtained in the compound reflective optical system and show the total flux received at the image plane as well as the flux distribution across it. The temperatures which can be achieved with this thermal imager are discussed.

Optical means for enlarging the image and obtaining uniform flux distribution at the image plane are explained and their performance documented.

Radiant Energy Sources: The performance of radiant energy sources presently used for thermal imaging is explained and their drawbacks are mentioned and means of obtaining a source that is stable and uniform across the heated area, and provides a high radiant energy output will be pointed out. In addition to electric arcs, secondary heated surfaces are considered. Such surfaces can be heated by the use of resistance, induction, electron beams, high pressure discharge lamps or radiating plasmas.

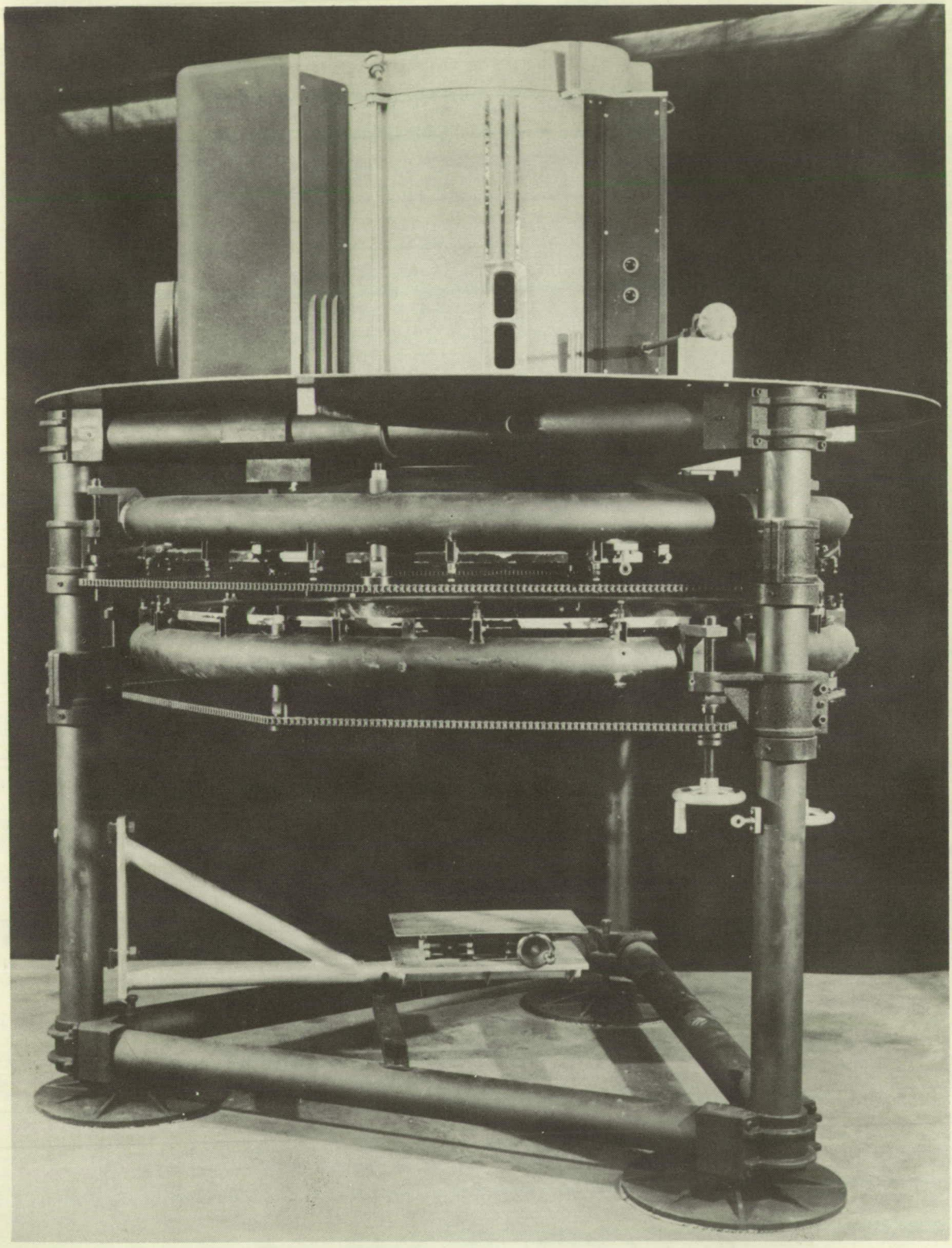

Figure 2

Imaging Techniques: A brief review is given of instruments which have been developed for measuring heat flux and temperatures in thermal imagers. The instruments to be discussed include absolute water cooled calorimeters, radiometers for measuring distribution of radiant energy, and auxiliary copper disc calorimeters.

Attention is given to the measurement of surface temperatures. The role of shutters in the separation of the radiation emitted by the sample from that reflected from the radiant energy sources is discussed. The use of filters to separate the emitted and incident radiant energy is described.

Possible errors which can be caused by temperature measuring instruments operating in conjunction with either shutters of filters are brought out and the potential of new instruments is assessed.

The design of imaging chambers for exposing materials either in a vacuum or a suitable atmosphere is explained and typical chambers are illustrated. (See Figure 3.) It is shown how such a chamber can be easily adapted for the performance of a number of experimental procedures.

Experimental Procedures: The following examples of experimental procedures which have been performed with thermal imagers will be discussed briefly.

a) A description is given of an apparatus which has been designed for growing single crystals. The apparatus includes a powder supply mechanism, a lowering mechanism that operates inside a vertical support tube, and a novel device for preventing powder from settling on the inside surface of the bell jar and thereby reducing the radiant energy flux reaching the crystal. Examples are shown of crystals grown with this apparatus.

b) A study of the degradation of textile materials under thermal pulses is given including pertinent results. An apparatus designed for the analysis of pyrolysis products and consisting of a glass-fronted cell fitted with a gas inlet and outlet tube is illustrated. In this cell the material is exposed to thermal pulses which can be obtained by controlling the motion of shutters. A copper disc calorimeter is switched in place of the sample at the beginning of a test to establish the magnitude of the heat flux reaching the material.

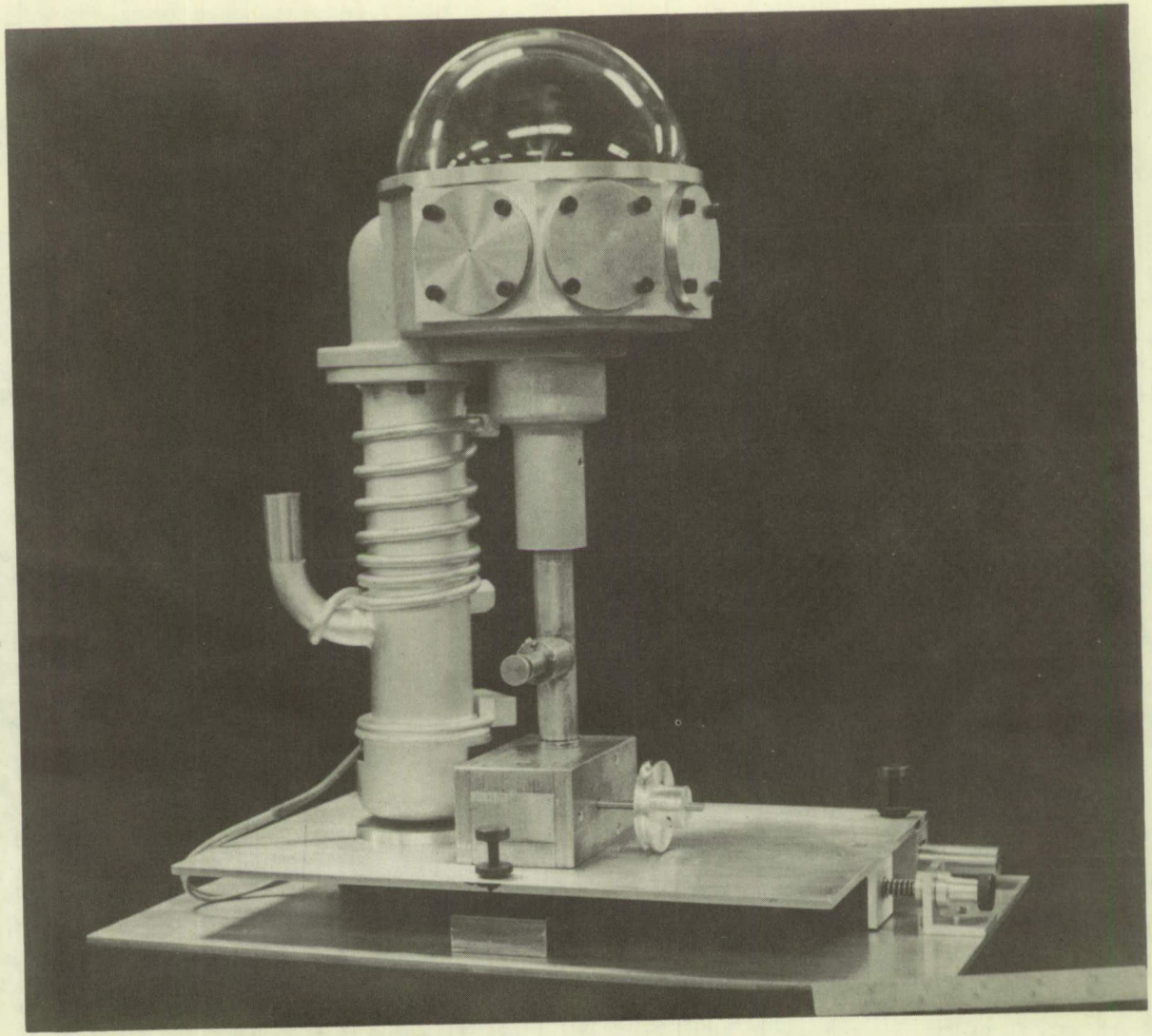

Figure 3.

The products of pyrolysis are then swept into a vapor phase Chromatograph and analyzed.

c) An apparatus for the study of the reaction of heated materials is described. In this apparatus different gases are passed over the material. Methods of examining the product gases as well as establishing the behavior of the material are mentioned.

d) A technique for measuring the thermal conductivity of very small samples of semiconductors is described. The instrumentation developed in conjunction with this apparatus is presented. Results of a few typical measurements are given.

Future Potential: The future possibilities of imaging techniques in the study of chemical and thermodynamic properties is given with special attention to applications of imaging techniques to high temperature mass spectrometry and to the combination of imaging techniques with x-ray studies of the heated material.. The development of improved thermal imagers is projected.

Acknowledgements: Portions of the work reported herein have been carried out under contracts for Air Force Cambridge Research Labs., Bedford, Massachusetts; Office of Naval Research, Washington, D. C.; and Wright Air Development Division, Wright-Patterson Air Force Base, Ohio.

MEASUREMENT AND APPLICATION OF HIGH HEAT FLUXES IN A SOLAR FURNACE.

T. S. Laszlo

Introduction: The advantages of solar furnaces in the measurement of Chemical Thermodynamic Properties have been pointed out before (1). During the present work it has been shown that solar furnaces are also suitable for the generation of high heat fluxes of known, stable intensity and consequently, for the production of high, easily variable, stable temperatures.

Flux Measurements with a Calorimeter: Water cooled absorbing cavities can be used for the absolute measurement of radiant energy. Previous investigations (2) found that the sphere is the most suitable shape for such a cavity.

During the present investigation a new shape was conceived, consisting of a truncated right cone with the smaller end as the orifice. The bottom of the cavity is a right circular cone. With this cavity design only a very small fraction of the surface "sees" the orifice perpendicularly and accordingly reradiation losses are very low. Gouffé's method of blackbody evaluation was applied to this new shape and the results, together with those of Gouffé are presented in Table 1. L is the length of the blackbody, R the radius, s the area of the orifice and S the total surface. Experimental investigations have proven that this shape cavity traps a larger fraction of the incident energy than the sphere.

Table 1
Comparison of Proposed Blackbody Shapes

$\frac{L}{R}$	$\frac{s}{S}$				$\frac{s}{S} - \frac{s}{S_0}$ #		
	Sphere*	Cylinder*	Cone*	Double Cone**	Cylinder*	Cone*	Double Cone*
1	0.500	0.250	0.415	0.175	−0.250	−0.085	−0.325
2	0.200	0.167	0.309	0.094	−0.033	+0.109	−0.106
3	0.100	0.125	0.241	0.059	+0.025	+0.141	−0.041
4	0.059	0.100	0.195	0.041	+0.041	+0.136	−0.018
5	0.039	0.083	0.164	0.030	+0.044	+0.125	−0.009
8	0.016	0.056	0.111	0.015	+0.040	+0.095	−0.001

* Shapes considered by Gouffé

** Shape proposed by present investigation

Comparison of shapes with sphere (s/S_0)

Flux measurements have been performed with this calorimeter in the focal area of a 60-inch diameter solar furnace. During the measurements the normal incidence solar radiation was recorded. Calculated flux values were normalized for 1 Ly/min normal solar incidence and plotted against the position of a flux attenuator as indicated on a linear scale (figure 1).

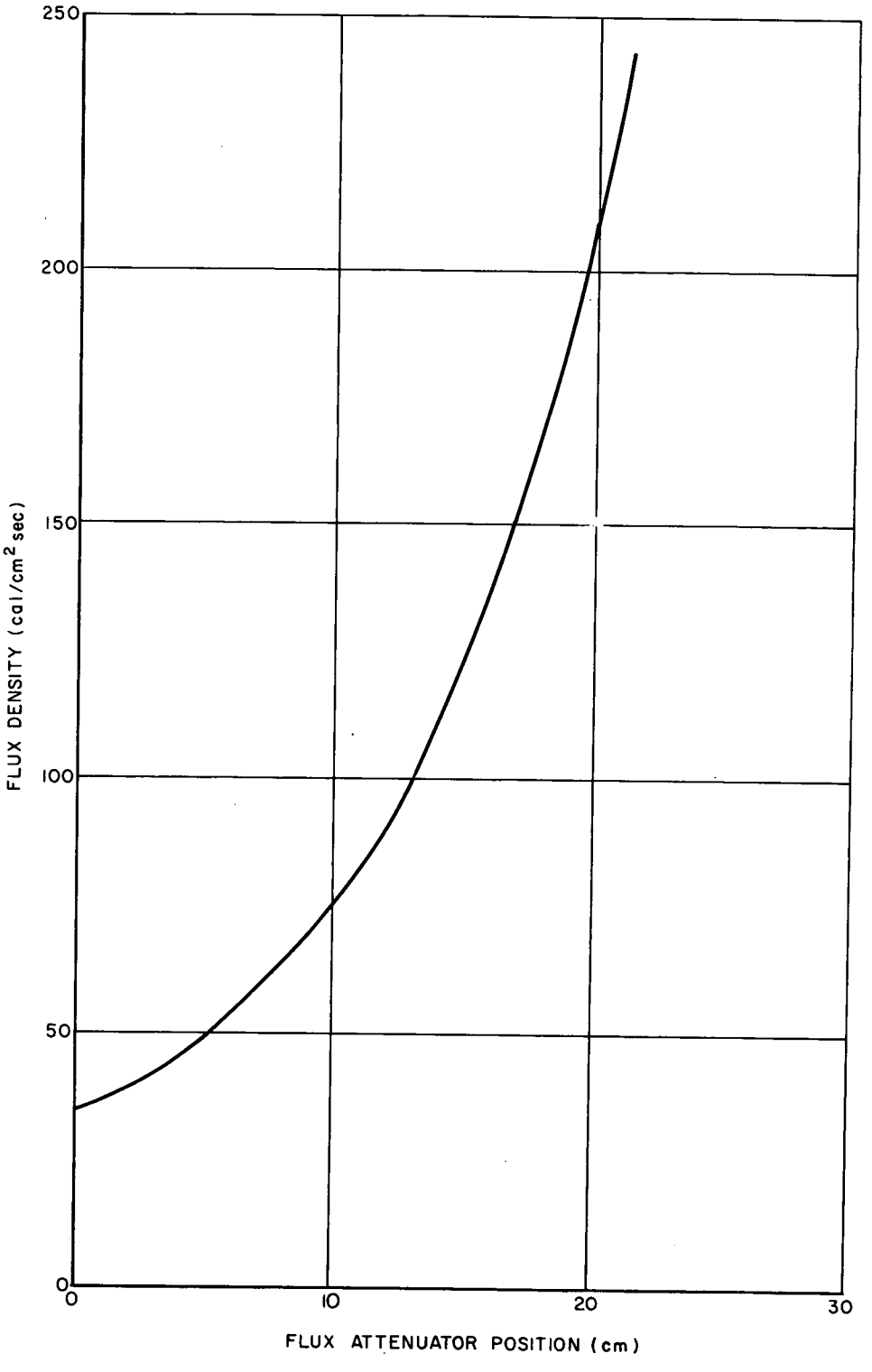

Figure 1 FLUX VERSUS ATTENUATOR POSITION IN THE SOLAR FURNACE
61-5017

The several hundred flux measurements on which this curve is based, prove that the correlation between normal incidence solar radiation and the flux at the focal zone depends only on the position of the flux attenuator. Therefore, the flux at the focal area can be calculated if the normal incidence solar radiation is known from measurements with a commercially available calibrated pyheliometer. This is a very important characteristic of the solar furnace. When a specimen is heated in an image furnace, the flux cannot be directly measured at the same time. It is important however to know the flux impinging on the specimen. In a solar furnace it is possible to calculate this flux at any time during an experiment from the monitored value of the normal incidence solar radiation.

Thus the flux impinging on the specimen is known and the flux emitted by it easily measured with radiometers. Provided no significant heat traffic is caused by conduction and convection, the emissivity of the sample at it s temperature can be calculated from the ratio of the received and emitted flux.

Because of the well-defined correlation between normal incidence solar radiation and flux at the focal area, the solar furnace can also be used as a high intensity radiation standard. The highest intensity standard presently available, the tungsten filament bulb can be used only up to 25 cal/cm^2 sec range are available and can be controlled to a precision of $\pm$ 3%.

Flux Measurement with Radiometers: Calorimetric measurements cannot follow rapid changes in flux and do not give a fine resolution of flux variation across the image area. A modified Gardon radiometer (3) can be used up to the maximum fluxes obtainable in a solar furnace. It has a fast response and very fine resolution. It was found, however, that the camphor soot coating recommended by the manufacturer has two major deficiencies: its emissivity is not constant above 270°C and it tends to burn off in the presence of oxygen when exposed to high heat fluxes.

It is proposed that MgO is a satisfactory coating material for this radiometer. First, because it is stable at elevated temperatures in oxidizing atmosphere and second, it has near linear spectral reflectivity in the visible and near-infrared region. Further, an old contaminated coating can be easily removed with water and a new coating quickly applied. Its slightly hygroscopic nature does not cause difficulties.

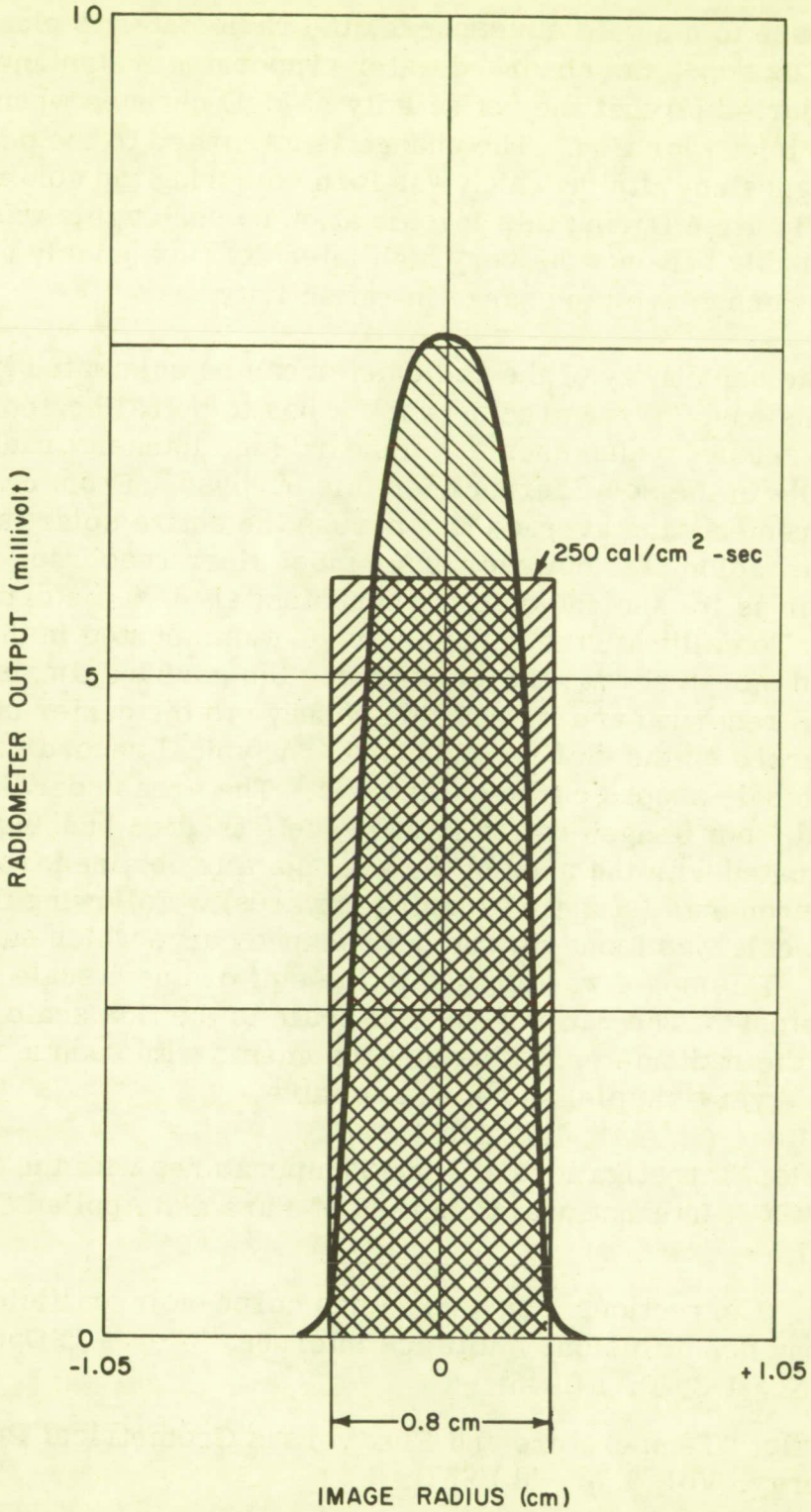

Figure 2 Calibration of Radiometer

If, after exposure to a humid atmosphere, the radiometer is placed in the high heat flux zone, the absorbed water evaporates instantaneously. It has been reported (4) that the reflectivity of MgO changes when exposed to ultraviolet radiation. The change is attributed to the decomposition of magnesium nitride which was formed during the combustion of magnesium in air. During this investigation no such aging was observed, probably because the very high intensity flux quickly completes the reactions which cause the change in reflectivity.

Although the sensitivity of the radiometer can be calculated from its physical dimensions, (5) for precise work it has to be calibrated. A method was developed which uses the standard high intensity radiant energy available in the solar furnace for this purpose. From calorimetric measurements the average flux across the entire solar image is known. The radiometer however has a much finer resolution than the calorimeter as its sensing disc is approximately 1/10 the diameter of the image. To calibrate the radiometer, it was mounted in the focal plane and moved across the image along the horizontal axis. Its emf output was recorded and its position relative to the center of the image was marked on the emf record chart. A typical record thus obtained is the bell-shaped curve on figure 2. The area under the curve was integrated from image edge to image edge (striation running downwards) and equated with the area of the average flux obtained from calorimetric measurements (striation running upwards). Following this an ordinate flux scale was found for the bell-shaped curve which satisfies this equation. This scale was applied to the emf ordinate scale of the radiometer output . The ratio of the emf scale to the flux scale is the sensitivity of the radiometer. Flux measurements with such a calibrated radiometer are very simple, quick and reliable.

REFERENCES

1. T. S. Laszlo: "Investigations at High Temperatures with the Solar Furnace," XVI International Congress of Pure and Applied Chemistry, Paris 1957.

2. A. Gouffé: "Corrections d'ouverture des corps-noir artificiels compte tenu des diffusions multiples internes," Revue D'Optique, Vol. 24, No. 1-3, P. 1 (1945).

3. T. S. Laszlo: "Temperature and Flux versus Geometrical Perfection," Solar Energy, Vol. 1, p. 78)1957).

4. W. E. Knowles Middleton and C. L. Sanders: "The Absolute Spectral Diffuse Reflectance of Magnesium Oxide," J. Opt. Soc. Am. Vol. 41, No. 6, p. 419 (1951).

5. R. Gardon: "An Instrument for the Direct Measurement of Intense Thermal Radiation," Rev. Sci. Inst., Vol. 24, p. 266 (1953).

MESURE DES TEMPERATURES ET ANALYSE THERMIQUE DES SUBSTANCES TRAITEES AVEC LES FOURS SOLAIRES.

M. Foex

Les mesures des températures des substances traitées au moyen des fours solaires sont souvent perturbées par les réflexions parasites du rayonnement utilisé et il est par ailleurs souvent difficile de constituer un corps noir convenable.

La plupart des essais dont il va être question ont été effectués avec un four solaire d'une puissance de 2 KW, comportant un miroir parabolique fixe de 2 mètres de diamètre et de 85 cms de distance focale, placé a l'intérieur d'un laboratoire et éclairé par un héliostat. Il est possible de fermer le laboratoire par des vitrages ou des filtres laissant passer la plus grande partie du rayonnement incident.

On va examiner successivement un certain nombre de procédés utilisés au laboratoire de l'Energie Solaire de MontLouis. Ces procédés sont essentiellement de deux types: ceux comportant l'emploi de filters et ceux utilisant une occultation du rayonnement incident au moment des mesures. La plupart de ces techniques s'appliquent aussi bien aux fours à images qu'aux fours solaires.

Procédés comportant l'utilisation de filtres: On interpose un filtre entre la source à haute température (soleil ou arc électrique) et la zone de traitement de la substance. Ce filtre présente une bande d'absorption bien définie pour certaines longueurs d'onde. On procède aux mesures de températures de la substance traitée au moyen d'un pyromètre optique muni lui-même d'une autre filtre opaque pour le rayonnement du soleil ou de l'arc, à l'exception toutefois d'une bande de transmission correspondant à la bande d'absorption du premier filtre.

Dans une de ces techniques, le rayonnement solaire réfléchi par les miroirs plans orienteurs est filtré par des plaques de plexiglas fermant le laboratoire. Une plaque de 15 mm d'épaisseur absorbe pratiquement la totalité du rayonnement de longueur d'onde voisine de 1, 7 micron et laisse passer environ les 3/4 du rayonnement solaire, sa transparence dans le visible et le très proche infra-rouge étant très grande. Le pyromètre a cellule photoélectrique ou thermopile

utilisé est lui-même muni d'un filtre interférentiel laissant passer uniquement les radiations proches de 1,7 micron. Dans ces conditions il est possible de proceder aux mesures de températures sans être géné par le rayonnement incident.

Une autre méthode, appliquable uniquement dans le cas des fours solaires, consiste à utiliser les bandes d'absorption de l'atmosphère (H_2O, CO_2, O_3). Il est en particulier commode de se servir des bandes d'absorption de la vapeur d'eau dans l'infra-rouge (1,87 et 2,7 microns). L'intensité de ces bandes étant naturellement variables avec la hauteur du soleil, le temps et l'altitude, il conviendra, avant chaque série de mesures de température, de déterminer pour la longuer d'onde considérée, l'intensité résiduelle du rayonnement solaire.

Les méthodes précédentes nécessitent l'emploi de pyromètres à cellules photoélectriques ou à thermopiles, sensibles au rayonnement infra-rouge.

Procédés avec occultation du rayonnement incident: Un procédé très simple consiste, au moment des mesures de température a occulter le rayonnement du soleil ou de l'arc au moyen d'un écran.

On fait passer très rapidement (1/100 ou 1/10 de seconde) devant la substance examinée, au écran obturant le rayonnement incident et on procède pendant ce temps tres court aux mesures de température au moyen d'un pyromètre optique à cellule photo-électrique. Des thermo-piles à réponse rapides sont aussi parfois utilisables. Au cours du passage de l'écran, le produit porté à haute température n'a pas le temps de refroidir.

Notons aussi qu'au lieu d'écrans ou de filtres on peut moduler le rayonnement incident et le distinguer ainsi du rayonnement émis par la substance.

Consitution de corps noirs ou corrections de facteur d'émission: Dans les différents cas précédents il convient naturellement soit de viser les cavités formant corps noir, soit de connaitre le facteur d'émission des substances triatées.

On pourra, par exemple constituer un corps noir en pratiquant dans la substance examinée une cavité relativement peu profonde, mais de faible diamètre.

Pour la mesure de la température d'une substance soumise à l'action du rayonnement solaire il est possible d'utiliser un écran défilant rapidement au voisinage de la surface de la substance traitée. Cet écran qui obture le rayonnement incident présente une face concave métallique polie dirigée vers la surface portée à haute température et réfléchit la plus grande partie du rayonnement émis par cette dernière. On reconstitue ainsi par un jeu de réflexions successives, des conditions analogues a celles du corps noir. La mesure des températures est faite, au moyen d'un pyromètre à résponse rapide, par visée à travers un orifice pratiqué dans l'écran réflecteur, pendant le temps, très court, où cet orifice passe entre la surface portée à haute température et le pyromètre. La substance n'a pas le temps de refroidir sensiblement au cours de ce passage rapide, cependant que l'écran s'échauffe lui'même relativement peu.

Une technique très commode, a été établie pour la mesure des points de solidification des oxydes réfractaires. On réalise un corps noir en centrifugeant la matière fondue de manière à obtenir une cavité dont les parois fondues sont entourées de produit solide en poudre jouant le rôle de calorifuge. Des variations de vitesse de rotation permettent de brasser la matière fondue et d'obtenir une cavité sensiblement isotherme. En combinant cette méthode avec un écran à défilement rapide et un pyromètre à cellules photoélectriques (cesium ou sulfure de plomb) on a pu établir le point de fusion de différents oxydes réfractaires.

On a par ailleurs, au cours de ce travail, mesuré le facteur de réflexion de divers oxydes réfractaires fondus, pour certaines longeurs d'onde. Lorsque l'épaisseur de produit fondu est suffisante tout le rayonnement non réfléchi par la surface de l'oxyde est pratiquement absorbé, le facteur d'émission de ces produits est alors aisément calculable.

Analyse thermique: Efin des essais effectués avec des pyromètres optiques à cellules photoélectriques et des enregistreurs à réponse rapide ont permis de déceler certains phénomènes (transformations allotropiques en particulier) susceptibles de se produire au cours du refroidissement des substances traitées. Ainsi les courbes températures–temps présentent des anomalies dans le cas de la zircone (vers 2360° C) et dans celui de certains sesquioxydes des terres rares Y_2O_3 (vers 2280° C) et La_2O_3 (vers 2100° C).

OXIDE RESISTANCE FURNACE FOR LINEAR THERMAL EXPANSION MEASUREMENTS TO 1900°C.

J. F. Bacon, R. D. Veltri, and J. Y. Whittier

An oxide resistance furnace of a modified Geller (1) design was built to measure the coefficient of linear thermal expansion of those materials which require heating in air to prevent composition change. A quarter–section schematic drawing of this device is shown in Fig. 1. As may be seen in this figure, the furnace has three independent heating stages. The heating elements are eight inner 95% thoria–5% yttria (by weight) rods, an intermediate stage of four Super–Kanthal* U–shape (hairpin) rods, and an outer stage of nichrome V wire wound on an alundum core. The outer nichrome winding serves as a guard ring heater at low temperatures, the Super–Kanthal elements act as a high temperature guard ring and also pre–heat the third stage thoria–yttria elements to the temperature of 1200°C where they become conducting.

The 95% thoria–5% yttria elements used at present are $^{3}/_{8}$ in. in dia and 4 $^{5}/_{8}$ in. long rods. Contact is made to these rods by 85% zirconia, 15% yttria (by weight) blocks $^{3}/_{4}$ in. in dia carrying a 120° conical opening to match the 120° conical end of the heater rod. In turn, external contact is made to each zirconia–yttria block by cementing in a $^{3}/_{16}$ in. dia ball of platinum – 40% rhodium and lead wire. Each thoria–yttria heating element assembly has a resistance of approximately 800 ohms at 1250°C and 75 ohms at 1450°C. However, the individual elements vary sufficiently that separate control circuits are required. Because these elements are not made from the purest grade yttria, they cannot be used above a temperature of 1850°C due to excessive warpage. The four Super–Kanthal elements are supplied by a 5.0 kilowatt transformer whose input voltage is 220 volts and output voltage 32 volts and at their maximum operating temperature of 1700°C actually use 7.1 volts and 140 amperes. The nichrome winding is controlled by a 3.1 kilowatt variable transformer and at 1050°C operates at 220 volts and 5 amperes.

As is shown in Fig. 1, a nested refractory cylinder construction is used with each refractory selected from considerations of thermal shock, chemical compatibility with its nearest neighbors and the temperature which it must stand. The innermost cylinder, together with its top and bottom plates, is made of beryllia because it remains an electrical insulator at high temperatures. The surrounding cylinder and plates are zirconia followed by 3000°F silica brick, then the alundum core for

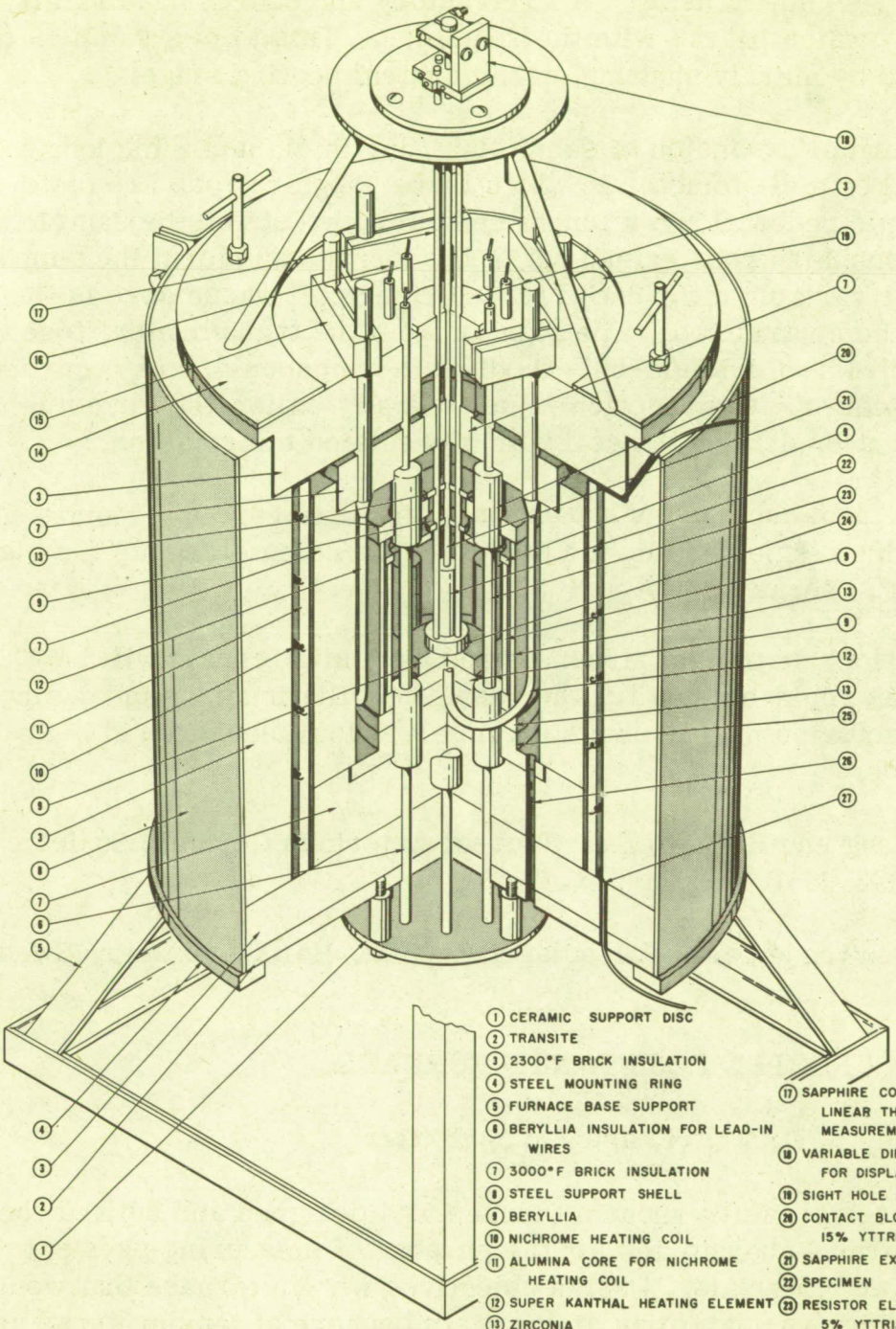

1. CERAMIC SUPPORT DISC
2. TRANSITE
3. 2300°F BRICK INSULATION
4. STEEL MOUNTING RING
5. FURNACE BASE SUPPORT
6. BERYLLIA INSULATION FOR LEAD-IN WIRES
7. 3000°F BRICK INSULATION
8. STEEL SUPPORT SHELL
9. BERYLLIA
10. NICHROME HEATING COIL
11. ALUMINA CORE FOR NICHROME HEATING COIL
12. SUPER KANTHAL HEATING ELEMENT
13. ZIRCONIA
14. TOP SUPPORT RING FOR DISMANTLING
15. ELECTRICAL CONTACT CLAMPS FOR SUPER KANTHAL
16. PLATINUM-RHODIUM LEAD WIRE
17. SAPPHIRE COMPENSATION RODS FOR LINEAR THERMAL EXPANSION MEASUREMENTS
18. VARIABLE DIFFERENTIAL TRANSFORMER FOR DISPLACEMENT MEASUREMENTS
19. SIGHT HOLE FOR OPTICAL PYROMETER
20. CONTACT BLOCKS. (85% ZIRCONIA 15% YTTRIA)
21. SAPPHIRE EXPANSION INDICATOR ROD
22. SPECIMEN
23. RESISTOR ELEMENTS. (95% THORIA 5% YTTRIA)
24. CORUNDUM DISC
25. ALUMINA
26. THERMOCOUPLE WELL
27. ELECTRICAL CONNECTION FOR NICHROME

FIG. 1

HIGH TEMPERATURE OXIDIZING ATMOSPHERE RESISTOR FURNACE

the nichrome winding, an outer refractory shell of 2300°F silica brick and a stainless steel casing. All refractory enclosures have small center caps which lift out with the specimen. This allows samples to be replaced by merely shutting off the central heating stage.

The thermal expansion of samples $^{5}/_{8}$ in. in dia and 2 in. long is determined by a dilatometer in which three sapphire rods are fastened to the sample pedestal and a fourth central rod rests on the sample. The fixed sapphire rods extend out of the furnace and form the support for a linear variable differential transformer coil whose core is then driven by the central rod. The signals from the transformer, together with those from an iridium–60% rhodium thermocouple, are recorded on an x–y plotter. Core motion is periodically calibrated for actual displacement by driving the coil with a precision micrometer.

Future plans include evaluation of $^{1}/_{2}$ in. diameter 95% thoria, 5% yttria heating elements, and the use of thoria–ceria elements for higher temperature operation.

In addition, strontium zirconate and barium zirconate will be evaluated as replacements for the costly beryllia inner cylinder since these refractories may likewise retain electrical insulation at high temperature.

(1) S. M. Lang and R. F. Geller: Journal American Ceramic Society, 34, p. 193 (1951)

* Registered trademark Aktiebolaget Kanthal, Hallstahammar, Sweden

A 2700°C TUNGSTEN RESISTANCE FURNACE.

J. F. Bacon, R. D. Veltri, and J. Y. Whittier

A high temperature vacuum furnace was designed and built at the UAC Research Laboratories for the purpose of measuring physical properties of materials. Design objectives were a furnace that would operate in high vacuum or in an inert atmosphere at temperatures up to 2500°C, utilize readily fabricated heating elements, provide easy access to the specimen chamber, and allow for insertion of instrumentation. Although numerous tungsten resistance furnaces are described in the literature (Refs. 1–5), none fully met these requirements.

The furnace has proven capable of operation at temperatures above 2700°C, and attains a vacuum of 1×10^{-7} mm Hg when the furnace is cold and a vacuum of 3×10^{-5} mm Hg at maximum operating temperature. This design allows complete change of sample with full restoration of vacuum in one hour and utilizes only readily available sheet material for heating elements.

The furnace heating elements, as shown in Fig. 1, are four sheets of either 5 mil tungsten or 7 mil tantalum, 10 in. long and $3\ ^1/_2$ in. wide and arranged to form a rectangular box 9 in. high. Massive water-cooled copper electrodes form the top and bottom of the box. These water-cooled electrodes contain grooves into which the heating elements extend and are clamped by two set screws. On the lower and upper edges of the sheet elements reinforcing strips of 30 mil thick tantalum, 2 in. high and $3^1/_2$ in. wide are fastened on each side. The added thickness forms a temperature transition zone between the full heat of the furnace and the water-cooled electrodes. Because the resistance elements are constrained at each end, they normally tend to buckle on heating due to thermal expansion, but by fastening each heating element to its neighbor by a loop of wire through the mid-point of the element edge, buckling takes place in the form of an English bow and does not interfere with furnace operation. As may be seen in Fig. 1, each electrode is supported by two copper posts which pass through electrically insulated vacuum seals in the bottom plate of the furnace and which supply both water cooling and electrical power to the electrodes.

To prevent excessive heat loss, radiation shielding is used. The main radiation shield is hung from the top electrode and consists of eight tantalum sheets ranging in thickness from 30 mils next to the heating element to 10 mils nearest the cold shell. These shields are arranged in two sets (to eliminate electrical coupling) each covering one-half of the elements. The top and bottom of the heating element box is enclosed with circular tantalum radiation shields. The outer stainless steel vacuum shell is water-cooled by square copper tubing and mirror-finish removable stainless steel insert is placed between the outer shell and the tantalum radiation shields.

The furnace is connected to a standard vacuum system incorporating a 6 in. diffusion pump, 6 in valve with water baffle and liquid nitrogen cold trap. Electrical power for the furnace is supplied by a water-cooled 75 KVA transformer and saturable core reactor having a 440 volt, single phase input and an output voltage continuously adjustable from

1 to 27 volts. Typical power usage at 2700°C is 13 volts and 4600 amperes. The top flange of the furnace (Fig. 1) can be removed and auxiliary equipment such as the thermocouple tower shown in Fig. 2 mounted in its place. By means of a rotating teflon vacuum seal, two tungsten–rhenium thermocouples stored in the tower can be raised and lowered in the heating chamber. It was originally planned to use these thermocouples to explore the uniformity of temperature in the furnace. However, the tungsten member of these thermocouples becomes very brittle after heating so that the thermocouples had to be reinforced with an insulated ceramic sleeve down almost to the thermocouple bead. Since both the beryllia and zirconia sleeves tested become conductive, actual thermocouple usage was restricted to temperatures lower than 2100°C. In place of the thermocouples, temperatures are read by a Pyro* micro–optical pyrometer through the quartz sight–glass and prism shown in Fig. 1. A shutter mechanism is provided to prevent deposits from building up on the sight glass.

In using high temperature furnaces, verification of temperature observations presents difficulties. When the nature of the work permits it, temperatures are determined by using a black body cavity with a ratio of depth to radius of 11.4 to 1. For other work, however, temperatures are read by directly sighting on the edge of the tungsten crucible. Corrections are made for lack of black body conditions by use of a temperature curve obtained by observing the mean melting point of a group of spectroscopic metals including platinum, zirconium, rhodium, hafnium, columbium, iridium, and molybdenum. The micro–optical pyrometer is also regularly calibrated against a tungsten ribbon filament lamp certified by the National Bureau of Standards.

The furnace has now been in operation for a period of eight months. A number of runs have been made at temperatures of 2700°C or greater, and in general, no operational problems have been encountered.

1. E. Anderson and W. Hume–Rothery, J. Less Common Metals, 2 19 (1960).
2. J.M. Dickinson, Fifth National Symposium on Vacuum Technology Transactions (Pergamon Press, New York, 1959), p. 192.
3. J.H. Randall, J. Scientific Instruments, 29, 248 (1952).
4. J. Cohen and W. Eaton, Rev. Sci. Instruments, 31 p. 522 (1960).
5. G.B. Eyerly and W.A. Lambertson, High Temp. Technology (John Wiley and Sons, Inc., New York, 1956), Chap. 13, p. 259.

* Registered trademark The Pyrometer Instrument Co., Inc. Bergenfield, N.J.

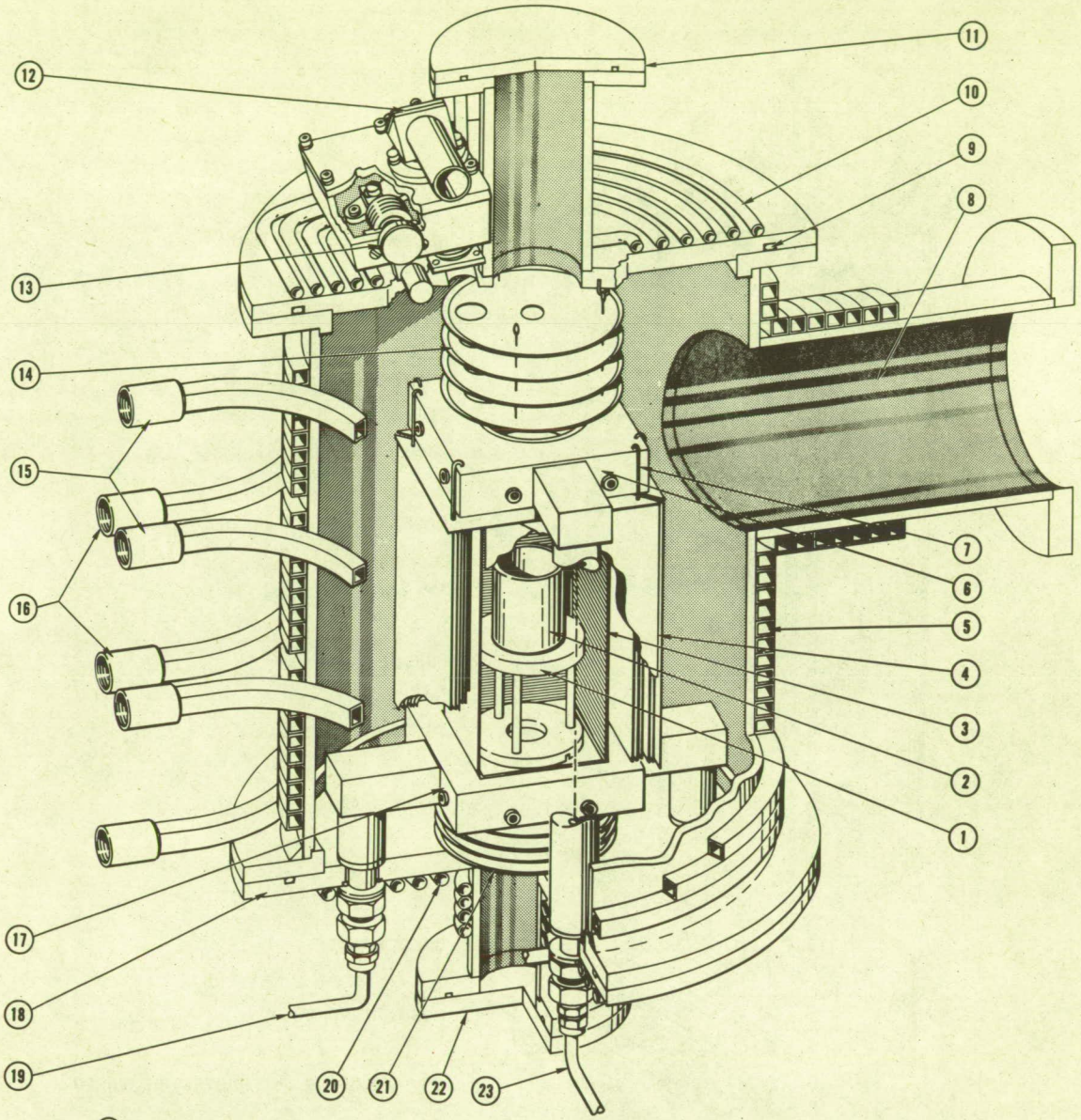

(1) TUNGSTEN PEDESTAL FOR CRUCIBLE
(2) TUNGSTEN CRUCIBLE
(3) FLAT TUNGSTEN HEATING ELEMENT (4)
(4) TANTALUM RADIATION SHIELDS
(5) SIDE COPPER COOLING COILS
(6) TOP WATER COOLED ELECTRODE SUPPORT CONDUCTOR
(7) SUPPORT PIN FOR TANTALUM SHIELDS
(8) TO VACUUM SYSTEM
(9) "O" RING GASKET SEALS
(10) TOP COPPER COOLING COILS
(11) TOP INTERCHANGABLE COVER FOR MEASURING APPARATUS
(12) SIGHT GLASS
(13) PROTECTOR MECHANISM FOR SIGHT GLASS
(14) TOP TANTALUM RADIATION SHIELDS
(15) COOLING WATER IN
(16) COOLING WATER OUT
(17) BOTTOM WATER COOLED ELECTRODE SUPPORT CONDUCTOR
(18) BOTTOM PLATE FOR MOUNTING
(19) WATER IN BOTTOM ELECTRODE
(20) BOTTOM COPPER COOLING COILS
(21) BOTTOM TANTALUM RADIATION SHIELDS
(22) BOTTOM INTERCHANGABLE COVER FOR MEASURING APPARATUS
(23) WATER IN TOP ELECTRODE

FIG. 1 **HIGH TEMPERATURE TUNGSTEN RESISTANCE FURNACE**

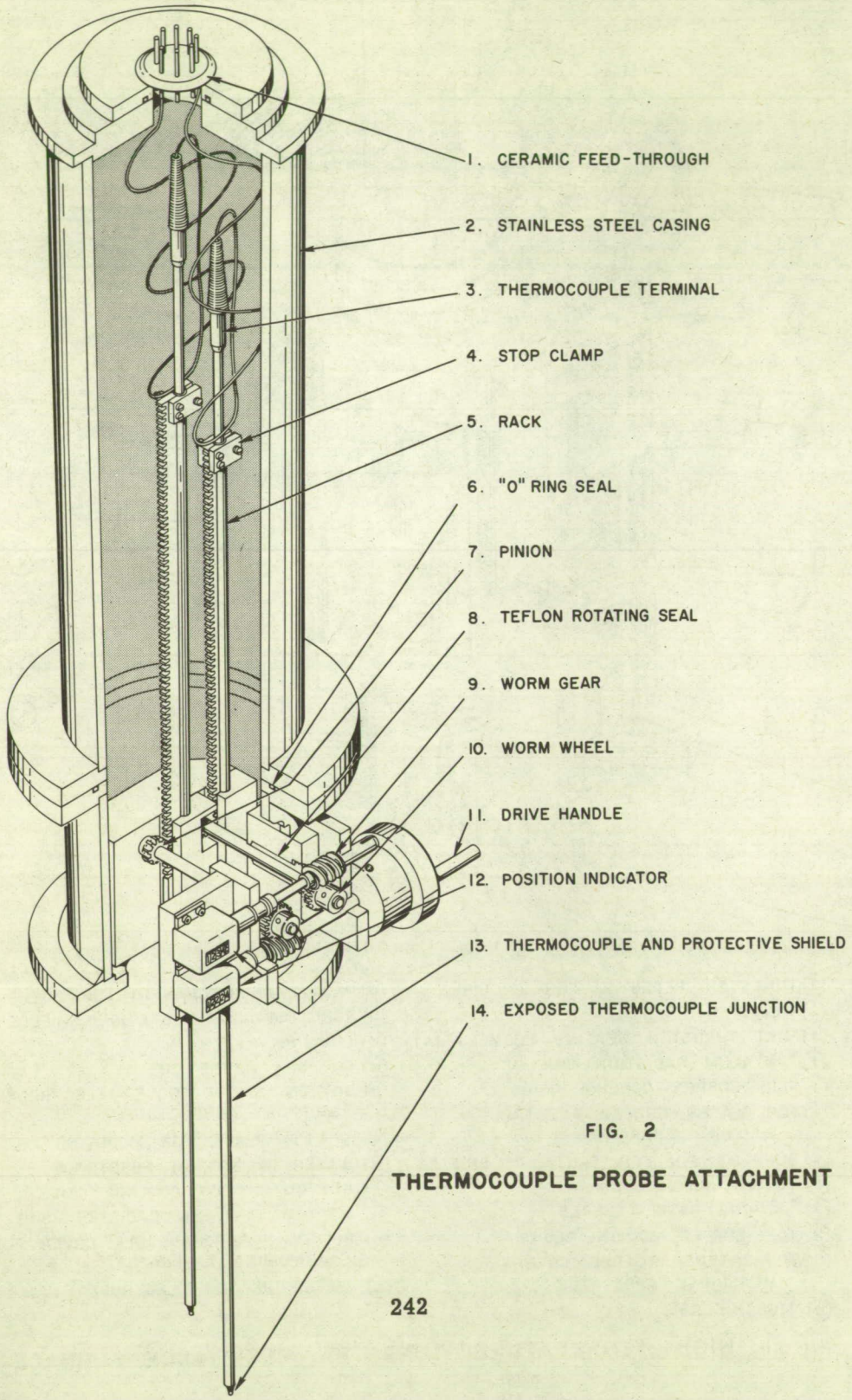

FIG. 2

THERMOCOUPLE PROBE ATTACHMENT

THERMOCOUPLES FOR MEASURING URANIUM DIOXIDE FUEL TEMPERATURES IN-PILE.

A. Harvey

The calibration of high temperature thermocouples was undertaken at Chalk River to meet the need for knowledge of the centre temperature of uranium dioxide fuel elements under reactor operating conditions. From a knowledge of this temperature, the thermal conductivity of uranium dioxide under irradiation can be deduced. If long term measure- could be made, changes in reactor flux could also be followed. A thermo- couple was chosen as the measuring device because of its simplicity, small size, and relative immunity to radiation effects. Since the melting point of UO_2 is around 2800°C, the thermocouples must work up to this temperature.

Two furnaces are being used to provide the high temperatures required for calibration of the thermocouples prior to their in-pile use. The first is a graphite resistance furnace with argon at one atmosphere pressure as the cover gas; the second, a tungsten tube resistance furnace operating in vacuum. The graphite furnace consists of two concentric pieces of graphite pipe surrounded by carbon black as the insulation. The inner tube, which is the heater tube, is 3" OD by $^3/_8$" wall. Its useful length is about 6". The tube is connected by water- cooled brass heads to copper terminal blocks, to which power is supplied from a low voltage transformer having a short circuit capability of 3600 amps and an open circuit voltage of 8.5 volts. The primary of this transformer is supplied from a 30 kva variac, which permits manual control of the furnace power. The argon supply to the furnace tube is introduced at the top and directed to keep the quartz viewing window clear of dirt and condensing vapours. A separate argon supply feeds the annulus outside the heater tube and the carbon black insulation.

The tungsten tube vacuum furnace has as its heater element a tube formed from 0.005" thick tungsten sheet, $^3/_8$" diameter by 6" long. This heater tube is held between two water-cooled heads through which pass holes for sighting the optical pyrometer and bringing out the thermocouple leads. The heater tube is surrounded by radiation shields of tantalum and molybdenum sheet. The current supply to the heater tube is from a manually controlled variac through a low voltage trans- former.

The temperature standard used in all the tests was a Leeds and Northrup optical pyrometer, catalogue No. 8622–C. This pyrometer was calibrated by the National Research Council in Ottawa. Unfortunately, since both furnaces were vertical, the pyrometer had to be sighted through a mirror. While the absorption of this mirror was found by calibration, it introduced an uncertainty of ± 35°C in the temperature readings at 2000°C. Emf readings were made using a Leeds and Northrup type K2 potentiometer with the same standard cell for all the tests. The thermocouple junction was located within a drilled enclosure in a sample block to give black body conditions. For the tungsten/rhenium thermocouple calibrations this block had a length to diameter ratio of 6:1, while for the tungsten/tungsten–26% rhenium thermocouple calibrations this was increased to 10;1. The error in the calibrations due to the optical pyrometer, the sighting mirror, the viewing window and the potentiometer is estimated to be ± 37°C at 2000°C. Other possible sources of error which are not included in this estimate are: (1) drift in temperature between reading of emf and pyrometer; (2) possible absorption by gas or vapour in the furnace tube at high temperatures; (3) departure of the thermocouple wire used from a unique thermocouple emf.

The calibration results obtained are as follows:

Temp. °C (ref. O°C)	W/Re		W/W–26% Re	
	mV	μV/°C	mV	μV/°C
1000	15.85	17.4		
1250	20.01	16.2	20.96	22.2
1500	23.80	13.5	26.12	19.5
1750	26.58	8.8	30.96	19.0
2000	28.38	6.2	35.37	15.7
2250	29.68	3.2	38.85	13.4

Since beryllia has the highest published electrical resistivity values, it was selected as the insulator for these high temperature thermocouples. Pure re–crystallized beryllia insulators were used for the furnace tests, and a simple ohmmeter test gave resistivity values close to the lower values quoted by Campbell. Since, however, BeO and UO_2 form a comparatively low melting eutectic, the insulator has to be protected by a sheath for use in a fuel element.

This decreases the effective resistance between the thermocouple wires by a factor of 2 and means that beryllia becomes useless as an insulator above 2100 – 2200°C.

Checking the compatibility of possible sheath materials with UO_2 was done at the University of Toronto; tantalum and molybdenum appear to be suitable to 2600°C and 2400°C, respectively.

It is proposed to use a tantalum sheathed, beryllia insulated, tungsten/rhenium thermocouple for the measurement of temperatures up to 2200°C in UO_2. These thermocouples are readily available as commercial items in diameters of $^1/_{16}$" and 0.040". Our calibration of this thermocouple pair agrees with those published previously.

While the tungsten/tungsten–26% rhenium thermocouple shows a useful emf output for higher temperatures, the calibration we have obtained differs from that previously published. Another insulator, or a configuration different from that normally adopted, will also be required to make reliable thermocouple measurements at higher temperatures.

THE NATURE OF MICROPHASES IN $CeCd_{\sim 4.5}$ SOLID SOLUTION.

Joe Fred Lemons and Guy R. B. Elliott

Introduction: In order to understand factors which influence the mutual solubility of metals, particularly in narrow phase regions, it is essential to have a method which can detect changes in activity with a high degree of precision. We have reported previously on an isopiestic apparatus which is most effective on selected systems, namely those consisting of a relatively volatile constituent in solution with relatively non-volatile constituents.

Apparatus: The apparatus makes use of the fact that two solutions in contact with the gaseous phase of one of their constituents will tend to adjust in composition with respect to that constituent in such a way as to equalize its vapor pressure in the two solutions. The cerium–cadmium system was chosen as a suitable one for study. The cerium–cadmium alloy is placed in a tantalum cup in one leg of an inverted quartz U tube and is maintained at the temperature selected for study of the system. The other leg of the tube is maintained at a lower temperature so that pure cadmium condensed in this leg has an activity corresponding to the cadmium activity in the particular alloy phase being studied. The intervening section of tube is maintained at an elevated temperature to prevent condensation. This U tube is freely suspended near its mid-point and one end is supported by the arm of an analytical balance. The balance detects with precision the amount of cadmium which has shifted between the two arms of the vessel.

The $CeCd_{\sim 6}$ System: The first system studied using this technique was the cerium–cadmium system in the region near $CeCd_6$. Observations at 857°K and 912°K showed a continuous and pronounced change in activity, even beyond the equilibrium limits of the $CeCd_{\sim 6}$ phase. At 912° the activity coefficient varied from about 1.06 at the phase boundary which appeared at composition $CeCd_{6.118}$ to about 0.810 for the boundary at $CeCd_{5.791}$. Apparently the phase limits are characteristic of no unique bonding effect but result solely from competition for cadmium by the adjacent phases. The slight nonlinearity of the activity–mole fraction relationship has been treated in terms of a model elsewhere (1).

The $CeCd_{\sim 4.5}$ System: A study of a second system, i.e. the cerium cadmium system in the region of the phase usually designated Ce_2Cd_9, resulted, as was expected, in an activity versus mole fraction

relationship similar to that outlined above. The postulated detailed model necessary to correlate the data is somewhat different from that referred to previously and probably involves a simpler system, e.g. the solubility of cadmium in a parent $CeCd_4$ lattice. However, again in this case a characteristic, essentially-linear, large increase in activity coefficient (35%) for a small change of cadmium mole fraction (approximately 0.5%) was observed. The upper curve of Fig. I shows this single phase relationship which exists throughout the composition region $CeCd_{4.5}$ to $CeCd_{4.6}$.

During a period of about two weeks the system remained in this single phase region after which it departed from this meta-stable phase to form several alternating single and two phase regions as seen in Fig. I. It can be seen that several families seem to exist among these phases based on characteristic activity coefficients, i.e. slopes of the curves. These slopes, each of which measures the tolerance for non stoichiometry of a given microphase, vary over a twenty fold range. The intervening two phase regions are in some places extremely narrow, as small as 2.4×10^{-5} change in mole fraction between single phases. These very narrow two phase regions appear in families of phases having both large and small solubility ranges. The data in Fig. I were taken on two different samples over a period of 126 days at temperature. The data for the two samples were normalized to bring the random solution curves into coincidence.

Data for the random solution curve were obtained at various times throughout the investigation. The system showed complete reversibility while this phase was present but the microphases showed much narrower ranges of reversibility. When $CeCd_{\sim 4.5}$ was produced from $CeCd_{\sim 6}$ the random solution always occurred, but the microphases were a matter of accident, and although several families and many individual phases within a family were rediscovered during the investigation it was not possible to return at will to any of them.

The vertical family of curves shown in the lower right hand corner of Fig. I, and enlarged in the insert, is discussed in detail elsewhere (2). This family appears to follow a cyclic relationship showing a proportionate difference cycle 11, 7, 7, 7, 10, 8, 7, 8. The minimum composition change required to form a new phase corresponds to 125 cadmium atoms per million total atoms in the $CeCd_{\sim 4.5}$ alloy, of composition near $CeCd_{4.36}$. It is interesting to find a comparable small change in composition between phases in other regions of the system, notably, the

lower set of curves in the upper left hand region of the diagram where the experimental points are not recorded. This repetition of certain slopes and approximate spacings between single phases throughout the diagram suggests that the same few types of long range effects may be involved in the ordering of various familiies throughout the diagram.

Microphases in terms of ordered dislocations: It is suggested that the existence of phases corresponding to the vertical family of curves can be explained qualitatively be the effect of lattice distortions on the periodicity of conduction electron waves. In a system containing more than one component, composition ranges exist which will introduce defects in the simple parent lattice. Single defects can propogate large lattice distortions in the direction of nearest neighbors. Random defects constitute scattering centers while ordered defects yield reflecting surfaces for some components of the electron waves and a new periodic medium for others. Since the permissible lattice wave form is a property of the parent lattice, the defects might be expected to order in such a way as to permit the electron wave energy to minimize the free energy. This minimization of free energy for a given composition might be accomplished by a specific ordering of defects to produce a single phase or by a mixture of two types of ordering to produce two phases. The result would be that certain defect compositions could not be achieved in a single phase. In other words, certain single phase compositions would be forbidden; we have chosen to think of this as quantization of composition.

For those families exhibiting a high tolerance for nonstoichiometry, it is postulated that a similar effect occurs, except that in this case planes of defect atoms exist which can accomodate a highly variable number of defect atoms without altering the number or basic nature of the electron wave reflecting surfaces.

References

(1) G. R. B. Elliott and J. F. Lemons, J. Phys. Chem. 64, 137 (1960).

(2) G. R. B. Elliott and J. F. Lemons, Phys. Rev. Letters, Submitted for publication.

CADMIUM ACTIVITY (RELATIVE TO PURE LIQUID CADMIUM AT 639 °C)
0.75
0.65
0.55
0.45
0.35
0.25
0.15
0.822
0.820
0.818
0.816
0.814
CADMIUM FORMAL MOLE FRACTION
CeCd4.5
0.28
0.26
0.24
0.22
0.20
0.18
0.16
0.8159
0.8157
0.8155
0.8153

STUDIES ON SOME INTERSTITIAL PHASES OF OXYGEN OR NITROGEN AND TITANIUM, ZIRCONIUM, HAFNIUM OR VANADIUM.

Sven Westman, Bo Holmberg, Claes Nordmark, Tore Dagerhamn and Arne Magneli

The hexagonal close-packed α-modifications of titanium, zirconium and hafnium are all characterized by a remarkable ability to dissolve small non-metal atoms to a large extent. This is especially so with oxygen, which can enter into solid solutions in titanium up to the composition $TiO_{0.50}$, in zirconium up to $ZrO_{0.40}$ and in hafnium up to $HfO_{0.26}$. The solubility limits are independent of the temperature. The solubility mechanism has been thought to imply that the oxygen atoms occupy the major interstices of the metal structures, i.e. the octahedral holes, in a perfectly random way.

The solid solutions exhibit considerable expansions of the c axes with increasing contents of oxygen, and also of a axes up to moderate oxygen concentrations (including the solubility limit in the hafnium system). At the compositions $TiO_{0.33}$ and $ZrO_{0.25}$, however, the lengths of the a axes reach maximum values followed by decreasing values at still higher oxygen contents. An abrupt increase in the rate of expansion of the c axes is observed at the compositions mentioned.

The present investigation, which has been carried out by powder and single-crystal x-ray methods, has revealed that several preparations in the titanium-oxygen and zirconium-oxygen systems give extra x-ray reflections which are not compatible with the idea of random solutions of oxygen in the metals. Thus three different phases have been found to occur in the former system symbolized by TiO_{0+x}, Ti_2O_{1-y} and $Ti_2O_{1-1/3}$ and two phases in the latter system, viz: ZrO_{0+x} and Zr_3O_{1+y}. The hafnium-oxygen solid solution is only represented by HfO_{0+x}.

The phases MO_{0+x} represent random interstitial solutions of oxygen in the α metal structures.

At the composition Ti_2O the phase Ti_2O_{1-y} is of the anti - $Cd(OH)_2$ type. The metal atom positions are slightly removed from those in the hcp structure, viz., parallel to the c axis, away from the oxygen

atom layers. At lower oxygen contents Ti_2O_{1-y} shows randomly distributed oxygen vacancies in the Ti_2O structure. The region of formation of Ti_2O_{1-y} shows a lower oxygen limit of $TiO_{\sim 0.33}$ at about 400°C, the oxygen content necessary for formation of this phase increasing with increasing temperature of annealing.

The phase $Ti_2O_{1-1/3}$ (Ti_3O) represents a superstructure of Ti_2O with one third of the oxygens missing in an ordered arrangement. This phase forms within a very narrow range of composition at temperatures below 400°C.

At the composition Zr_3O the Zr_3O_{1+y} phase is of the Ni_3N type. This ordering of the interstitial atoms has been found to be independent of the heat-treatment of the specimens. At higher oxygen contents the additional non-metal atoms occupy interstitial sites of the Zr_3O structure in random distribution.

The titanium-nitrogen and zirconium-nitrogen systems show solubilities in the hcp region up to the approximate limit $MN_{0.25}$. No indications of ordering have been observed. These phases should thus be symbolized by MN_{0+x}. A phase of a composition around Ti_2N appears to have a metal atom arrangement somewhat distorted from that of the hcp structure.

Samples of the ternary system titanium-zirconium-oxygen, upon quenching from the melting temperature, have been found to contain a phase of ω-type over extensive regions of composition. Thus, at the 1:1 ratio of the metal atom species, single-phase preparations of ω-phase have been obtained within the approximate limits $Ti_{0.5}Zr_{0.5}O_{0.25}$-$Ti_{0.5}Zr_{0.5}O_{0.50}$.

In the vanadium-oxygen system, a phase of analyzed composition $VO_{0.53}$, provisionally called V_2O, has been identified. The crystal structure is so far unknown. The strongest powder diffraction lines may be indexed, however, assuming an orthorhombic unit cell intimately related to the unit cells of "V_4O" and "VO" (high temperature form), representing a distorted arrangement of metal atoms in the transition from the body-centered cubic structure of vanadium metal to the cubic closest packing in the "VO" phase.

The cubic "VO" phase (NaCl-type structure), containing disordered atomic vacancies, is homogeneous between the limits $VO_{0.89}$ and $VO_{1.20}$. The upper composition limit, $VO_{1.20}$, represents an almost completely occupied oxygen lattice (96%), whereas no similar relation defines the lower phase boundary. Using the approximate dimensions of the V_2O cell, however, density data indicate that the vanadium lattice of this phase is completely occupied. It is noteworthy that the boundaries of the high temperature "TiO" phase with the same type of structure ($TiO_{0.64} - TiO_{1.26}$) are defined by 96% and 98% occupancy of the Ti and O lattices respectively.

A further remarkable feature is the difference in the behavior of the lattice parameters of the "TiO" and "VO" phases. The cell edge of VO increases and the TiO cell edge decreases with increasing oxygen content.

Upon annealing, at 800°C, of titanium–oxygen and vanadium–oxygen specimens in the monoxide regions, new phases appear at the compositions $TiO_{1.00}$ and $VO_{1.27}$.

The TiO powder pattern can be indexed assuming a monoclinic unit cell. It may be profitable, however, to think of the structure in terms of a pseudo-cubic cell, all three axes of the NaCl-type subcell being tripled.

Single crystal data seem to justify this view, but the structure has not been solved. However, the superstructure most probably arises from the ordering of the atomic vacancies present already in the disordered, high-temperature form.

For the ordering of metal atom vacancies in $VO_{1.27}$, two homometric models have been worked out. The structures are pseudocubic, the dimensions of the NaCl-type subcell being quadrupled. Actually, the cell is very slightly tetragonally distorted. The ordering process seems to imply clustering of the vacancies. In the model considered the most probable one, hexagonal "discs" of nearest-neighbor vacancies are formed. The mechanism may possibly be regarded as a tendency to layer structure formation. A probably similarly ordered phase, $Ti_{\sim 0.1}\ V_{\sim 0.9})\ O_{\sim 1.2}$, possessing a small field of homogeneity has been prepared. The x-ray powder pattern indicates a strong relationship to the TiO and $VO_{1.27}$ structures. It has not yet been indexed, however.

Acknowledgment: Work, sponsored by the Office, Chief of Research and Development, U. S. Department of Army through its European Research Office, by the Swedish National Science Research Council and by the AB Atomenergi.

DIAGRAMMES DE PHASES FORMES PAR LE SULFURE D'YTTRIUM AVEC LES SULFURES MS DES ELEMENTS BIVALENTS.

J. Flahaut, L. Domange et Mme. M. Patrie

Les sulfures des terres rares Ln_2S_3 forment avec les sulfures MS des métaux bivalents diverses combinaisons, dont certaines possèdent les types structuraux des sulfures inférieurs des terres rares. L'étude comparative de ces combinaisons permet de définir les conditions de formations de ces divers types, dont l'évolution est par ailleurs remarquable à l'intérieur de la série des terres rares.

Nous présentons ici les premiers résultats obtenus avec le sulfure d'yttrium. Pour chacun des 7 systèmes Y_2S_3–MS étudies, le diagramme de phases a été établi entre les températures de 800°C et 1350°C. La courbe de fusion a été déterminée dans quelques cas.

Les phases caractérisées sont schématisees dans le tableau suivant dans l'ordre de la teneur décroissante en yttrium.

système Y_2S_3 –	2 Y_2S_3 –MS	Y_2S_3 –MS	solution solide
MgS	.....	type A	type NaCl
CaS	solution solide γ	type Yb_3S_4	type NaCl
SrS	.....	type B	type NaCl
BaS	.....	type B	.....
CdS	type Y_5S_7	type C	.....
Cr S	type Y_5S_7	type A	.....
MnS	type Y_5S_7	type A	type NaCl
FeS	type Y_5S_7	type A	.....

La dernière colonne de ce tableau concerne des solutions cubiques du type NaCl, formées à partir des sulfures MS purs par addition de Y_2S_3. Ces solutions solides ont une étendue vaziable pour le système

CaS–Y_2S_3 elle atteind la composition 0,22 Y_2S_3–CaS à partir de 1220°C. Pour les systèmes MgS–Y_2S_3 et MnS–Y_2S_3 la composition limite est légèrement supérieure et les paramètres varient beaucoup. Pour le système SrS–Y_2S_3 la solution solide a une importance très restreinte.

Le type A désigne une structure othorhombique assez proche de Yb_3S_4; on l'observe pour la composition MY_2S_4 avec le magnésium, le chrome, le manganèse et le fer. Les rayons ioniques expliquent cette similitude de structure. Dans le cas du magnésium, par exemple, les paramètres sont a = 12,64 kX b = 3,77kX c = 12,69 kX.

Le sulfure CaY_2S_4 existe sous deux variétés cristallines. L'une, α, stable a basse température et jusqu'à 1110°C, est orthorhombique du même type que Yb_3S_4 (1). Elle a pour paramètres: a = 12, 91 kX b = 13,05 kX c = 3,85 kX.

La forme de haute température de CaY_2S_4, désignée par β, présente de grandes analogies avec les types précédents.

Le type B désigne une phase de structure inconnue rencontrée avec les sulfures de métaux de grands rayons ioniques: SrS et BaS.

Le type C de CdY_2S_4 est également inconnu.

La phase γ ne s'observe qu'avec le sulfure de calcium, et présente un domaine d'homogénéité de part et d'autre de la composition 2 Y_2S_3. CaS. Elle est cubique, du type Th_3P_4, structure caractéristique des sulfures des terres cériques de Ln_2S_3 a Ln_3S_4 (2). A 1220°C elle s'étend entre 0,25 CaS. Y_2S_3 et 0,61 CaS. Y_2S_3. Elle n'est stable qu'à haute température et possède un point eutectoide à t = 980°C pour la composition 0,47 Cas. T_2S_3.

Quatre sulfures de formule générale MY_4S_7 possèdent la structure de Y_5S_7 (que l'on retrouve avec Dy_5S_7 et Er_5S_7) (3). Celle-ci est monoclinique. On a, par exemple, avec CrY_4S_7: a = 12,59 b = 3,79 c = 11,39 kX. Le sin β calculé est 0,961. Les rayons ioniques des métaux cadmium, chrome, manganèse et fer sont tres voisins de la valeur moyenne 0,90 kX qui caractérise le rayon yttrium calculé pour le sulfure YS. L'analogie structurale doit être liée à cette propriété.

bibliographie.

(1) J. Flahaut, L. Domange, Mme. M. Patrie et Melle M. Guittard Comptes Rendus 1960 251 p. 1517.

(2) J. Flahaut, M. Picon, L. Domange, Mme. M. Patrie et Melle M. Guittard, Bull. Soc. Chim. 1960 p. 221.

(3) J. Flahaut, Melle M. Guittard, J. Loriers et Mme. M. Patrie. 2e Collogue national sur la chimie des hautes températures. Paris Novembre 1957 Edit. CNRS Paris 1959 p. 51.

SOLID AND GAS-PHASE REACTIONS IN A TANTALUM CARBIDE INCANDESCENT LIGHT SOURCE.

Dexter P. Cooper, Jr., George R. Bird, and Leo Brewer

The unique high melting point of TaC has long suggested its use as an incandescent light source. Patents on TaC lamp filaments appeared as early as 1902 (1) and on a lamp atmosphere in 1937 (2). The principal difficulty encountered in these early investigations involved rapid decomposition of the filament.

The principal species given off from a hot TaC surface are Ta, C_1, C_2, and C_3. There is no evidence of the existence of a gaseous TaC molecule. TaC exists as a single phase f.c.c. system from roughly stoichiometric down to $Ta_1C_{0.8}$ or lower (3, 4), with relative abundances of the evaporating species dependent on the solid composition. For example, at 3100°K the pressure of tantalum over TaC is estimated to vary from 10^{-8} atm. for carbon-saturated TaC to 10^{-7} atm. for $Ta_1C_{0.80}$.

Our work has been directed toward developing a TaC incandescent source possessing high brightness, efficiency, and long life. One objective has been to maintain a partial pressure of hydrocarbons near a hot filament, and so stabilize solid TaC about a fixed carbon composition of high melting point. The first successful method of stabilizing TaC with a carbon atmosphere was based on the use of hydrocarbons and hydrogen[5]. These hydrocarbons equilibrate with the carbon in a hot TaC filament. (The rate of equilibration is inferred from the rapid carburization of metallic Ta filaments in just such an atmosphere). As violent convection currents sweep the hot atmosphere from the

filament toward the glass wall, reactions between carbon from the filament and hydrogen give first CH_4 and C_2H_2, and finally all of the C_1, C_2 hydrocarbons. This cooled gas is then swept back toward the filament. Lamps containing such atmospheres have been operated for more than 50 hours at 3500°K color temperature.

In the absence of free hydrogen, hydrocarbon atmospheres deposit soot on lamp envelopes even at low filament temperatures. By adding hydrogen, it is possible to avoid this soot deposition at filament temperatures up to about 3600°K; however, the presence of appreciable amounts of atomic hydrogen results in large power losses due to dissociation and recombination. At still higher filament temperatures, soot deposition occurs even from these hydrocarbon–hydrogen atmospheres and thus decreases the available carbon, leading to decarburization and failure of the filament. We have eliminated soot formation at high temperatures by adding either bromine or chlorine to hydrogen–hydrocarbon atmospheres. Another important advantage is realized through halogenation of these atmospheres. By adding chlorine, for example, the amount of H_2 required to avoid sooting is reduced from 200 mm. Hg. to 50 mm. or less with a corresponding decrease in power loss.

We have developed a set of microanalyses which may be applied to an operating lamp without gross depletion of the atmosphere. Gas chromatography and mass spectrometry have been accomplished with small sampling manifolds. We have developed a new type of infrared gas microcell for analyses on 1 cm^3 volumes of gas (6). The ratios of C_2H_4/C_2H_2 and C_2H_6/C_2H_2 obtained from typical TaC filament lamps are given in Table I. In this specific example, gas compositions refer to 1 atm. of cold gas; all filaments were operated at 3400–3500°K integrated color temperature and samples were withdrawn from the cold zone.

Table I

Hydrocarbon Ratios from Operating Lamps

Initial Gas Composition 1 ATM Total	$\frac{C_2H_4}{C_2H_2}$ Ratio	$\frac{C_2H_6}{C_2H_2}$ Ratio
0.4% C_2H_4, 30%H_2, 69.6% A	1.2	–
0.4% CCl_4, 6%H_2, 93.6% A	0.58	0.17
0.4% CCl_3 Br, 6% H_2, 93.6% A	0.20	.04

These gas phase reactions are observed to occur with extreme rapidity. Initial species either disappear or drop to steady–state concentration within one minute. Carbon–halogen compounds have not been detected in these atmospheres. Chlorine is present as HCl and bromine is presumed to occur as HBr. Consideration of the observed steady–state hydrocarbon compositions now permits a simple interpretation of the reactions involved. C_2H_2 and CH_4, the only hydrocarbons stable in the 2000 – 3500°K range, are presumably formed from C_1 and C_2 through CH°, C_2H°, and other radicals. As the hot gas convects away from the filament, it is assumed that the extent of reaction to C_2H_4 and C_2H_6 is determined by the persistence of atomic hydrogen. Moreover, halogen acids which accelerate H° recombination would decrease the production of saturated hydrocarbons. Therefore, the drastic shift in C_2 ratios observed on the addition of small amounts of Br clearly indicates the catalytic function of halogens in the intermediate temperature zone.

Monitoring C_2H_2 throughout the life of a halogen–containing lamp shows that degradation of the atmosphere precedes filament failure. Acetylene concentration drops rapidly at first, and then more slowly. As this occurs, the filament holds its physical dimensions, but the electrical resistance rises. This increase in resistance is associated with decarburization and the approach of failure (7). A quantitative account of atmospheric hydrocarbon loss is obtained by weighing the deposits of graphite which form near the ends of the filament at temperatures below 2700°K. The temperature limit for this reaction identifies it as thermal cracking of C_2H_2 to graphite. This reaction may be retarded by geometrical means or by adjustment of atmospheric composition. The addition of Br to a $CCl_4 + H_2$ atmosphere retards the deposition, and this is attributed to production of atomic hydrogen from HBr in the cooler gases sweeping upward toward the filament.

HCN has also been successfully employed to maintain a carbon activity adequate to support TaC filaments. As in the case of hydrocarbon atmospheres, the addition of free hydrogen is required to avoid sooting. Clearly, when HCN is so employed in an operating lamp, acetylene is formed in equilibrium with HCn and nitrogen. Thus the performance of HCN–hydrogen atmospheres can be interpreted in terms of the performance of a hydrocarbon–hydrogen atmosphere which has available an additional reservoir of carbon as HCN in equilibrium with acetylene.

Methods of x-ray crystallography have been employed to establish completeness of initial filament carburization and to verify that only the cubic TaC phase exists throughout the useful life of an operating filament. The Ta_2C hexagonal phase is observed only following the failure and arcing of an operating filament, or when a filament is intentionally operated at low temperature.

As a result of this work, we can report the routine operation of TaC lamps at 3500–3700°K color temperature. These lamps possess useful lives and operate at considerably higher intrinsic brightness than does tungsten. Furthermore, with these atmospheres, we have achieved satisfactory efficiencies. The high intrinsic brightness of TaC suggests such as spectroscopy and pyrometry.

References

1. German Patent DRP 153, 352 (1902) to Siemens and Halski.
2. M.R. Andrews, U.S. Patent, 2,072,788 (1937).
3. F.H. Ellinger, Trans. Am. Soc. Metals 31, 89 (1943).
4. The system Nb–C is very similar in qualitative behavior; see E.K. Storms and N.H. Krikorian, J. Phys. Chem. 64, 1471 (1960).
5. D.P. Cooper, Jr., U.S. Patent 2,596,469 (1952).
6. G.R. Bird, J. Op. Soc. Am., scheduled for April 1961 publication.
7. M.R. Andrews, J. Am. Chem. Soc. 54, 1845 (1932).

OXIDATION KINETICS IN THE MOLYBDENUM–SILICON SYSTEM IN THE 1000° – 2000°C TEMPERATURE RANGE.

J. B. Berkowitz–Mattuck

In order to study solid–gas interactions in the 1000° – 3000°C temperature range, it is necessary to find (a) a suitable container material, in which the reaction under study, and only that reaction, occurs; (b) a means for maintaining and measuring the temperature; and (c) one or more techniques for following the reaction of interest in the vapor, the solid phase, and at the solid–gas interface. Solutions to these problems that have proved satisfactory for studies of the kinetics of reaction of molybdenum and molybdenum silicides with oxygen and oxygen – water vapor mixtures will be described.

A diagram of the apparatus developed for the oxidation studies in this laboratory is shown in the figure. Sample pellets, 0.818 cm in diameter and 0.321 cm in height, are supported by point contact with three alumina or thoria rods at L. The pellets are completely enclosed in a constant–pressure flow system, and have been heated by

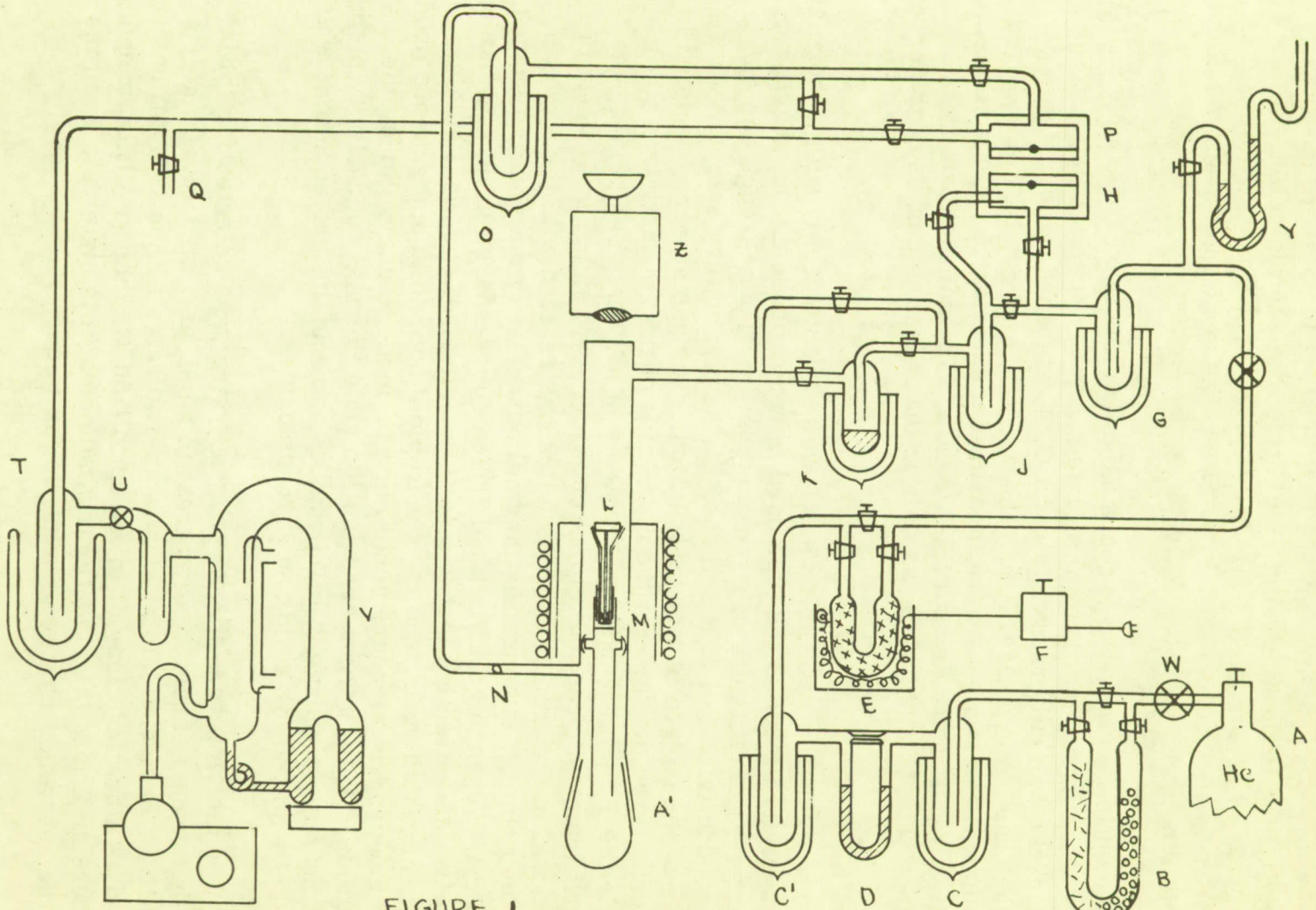

FIGURE 1
DIAGRAM OF APPARATUS

induction to temperatures of 2500°C. Except for a short length of quartz tubing in the immediate vicinity of the sample pellet, the apparatus is constructed entirely of pyrex. The concentrator and radio-frequency coils of a 5 k.w. Sylvania induction unit surround the quartz tube at L.

An optical pyrometer is focussed on an image of the sample pellet in a plane mirror (not shown) situated above the optical flat R. The pyrometer was calibrated against a G.E. standard lamp and viewed through the same optical flat. The spectral emissivities of oxidized and unoxidized samples were measured and emissivity corrections were applied to all of the raw pyrometer data. The non-uniformity in surface temperature of the sample in the induction unit is of the order of $\pm$ 5°C.

The oxidation reactions were followed continuously with a thermal conductivity bridge of the type used in vapor phase chromatography. A helium-oxygen mixture of fixed composition flows through one side of the conductivity cell at H and over the hot refractory sample, where some of the oxygen is lost by reaction. The gas stream, depleted in oxygen, flows out through the other side of the conductivity cell at P. The cells P and H constitute two arms of a Wheatstone bridge, the output from which is fed into a recorder. The signal is directly proportional to the amount of oxygen that has reacted with the sample per unit time. Although the thermal conductivity method was suggested by E.R. Weaver of the National Bureau of Standards in 1951, it has not received the attention that it merits for physical chemical studies. For systems which react with oxygen to yield both solid and gaseous products, two independent measurements must be made to characterize the reaction. Total oxygen consumption via a thermal conductivity method, and net weight change would provide the requisite two equations which could be solved for solid and gaseous oxides.

The molybdenum-silicon-oxygen system was selected for initial study because of the great interest in $MoSi_2$ as a structural material in oxidative environments at high temperatures. Although $MoSi_2$ has been used as a heating element in air up to 1700°C, there is little fundamental understanding of the oxidation resistance of this material. Even the sign of the net weight change on oxidation is in question.

Pure Mo metal was studied first. Previous work had shown that in air, at temperatures between 795° and 900°C, the reaction follows a linear rate law, due to sublimation of $(MoO_3)_x(g)$ and continuous exposure to fresh metal surface to atmospheric attack. In the present research, the oxidation was studied at temperatures above 900°C, and at low oxygen partial pressures, where data was lacking. At partial pressure of oxygen of 3×10^{-3} atm, and temperatures between 1000° and 1700°C, the rate of oxygen pick-up as measured by the thermal conductivity bridge was constant with time at a given temperature and increased with increasing temperature as expected. At a higher oxygen partial pressure, 2×10^{-2} atm, and a temperature of 1226°C, however, the rate of oxygen consumption was found to be high for the first fifteen minutes of the run, and to diminish over the next seven minutes; the high rate then returned for a time, and finally diminished once again. After the run, the pellet was covered with a blue-black layer of $MoO_2(s)$. It is possible that vaporization of $MoO_3(g)$ predominates in regions of rapid linear oxidation, and that $MoO_2(s)$ is providing limited protection in the regions of slow oxidation.

As a first approximation, the oxidation of $MoSi_2(s)$ is expected to yield $MoO_3(g)$ and glassy $SiO_2(s)$. At 1660°C, and an oxygen partial pressure of 2×10^{-2} atm, the thermal conductivity curves showed a high initial rate of oxidation, which began to drop after 6 to 12 minutes. The rate of oxygen uptake continued to fall, and finally approached a value of $4.2 \pm 0.5 \times 10^{-7}$ g^2 cm^{-4} per min^{-1} for all samples. The initial rates of oxidation, however, showed pronounced irreproducibility. Furthermore, net weight gains were observed in some exposures, net weight losses in others. After oxidation, the samples were coated with a dark, shining, glassy surface layer, which recrystallized to β-cristobalite at 1100°C, and the cool walls of the reaction chamber were covered with MoO_3 (s).

At 1660°C, and an oxygen partial pressure of 3×10^{-3} atm, the amound of oxygen picked up by the sample proved to be constant with time, and a protective glass failed to form. When the oxygen partial pressure was raised to 2×10^{-2} atm, the rate of oxygen consumption fell rapidly and approximated a parabolic curve, as above.

The data on $MoSi_2(s)$ are consistent with the formation of $MoO_3(g)$, $SiO_2(s)$, and $Mo_5Si_3(s)$ as oxidation products. The observed initial variations in oxidation rate may be ascribed to porosity and sample composition.

In addition, metallographic evidence for voids in the oxide film suggests an inherently nonreproducible system. Once a protective layer of silica, or ternary oxide has formed, oxidation can proceed only by diffusion of oxygen inward of diffusion of Si outward through the SiO_2(s) layer, or both. The thermal conductivity curves of oxygen pick–up vs time in this region of diffusion–controlled oxidation show occasional blips. These are probably due to bursts of MoO_3(g) which rupture the protective glass momentarily. This type of mechanism, where periodic changes occur in oxidation rate due to changes in the activity of a component at the alloy–oxide interface, was suggested as possible by Webb, Norton and Wagner, but previously had not been experimentally observed.

It is a pleasure to acknowledge the assistance of John Mellor and John T. Larson with the experimental measurements.

LEGIERUNGEN DES PLATINS MIT UNEDLEN METALLEN: EINE NEUE METHODE ZU IHRER DARSTELLUNG.

W. Klemm

Die Verbindungen der Platinmetalle mit unedlen Metallen sind bisher nur wenig untersucht. Das ist bedauerlich, da sich hier eine grosse Anzahl von intermetallischen Verbindungen bildet, die sowohl in ihrem strukturellen Aufbau als auch in ihren physikalischen Eigen – schaften interessante Probleme bieten.

Als ein Beispiel dieser Art wurde in unserem Laboratorium von R. Huch das System Platin–Aluminium durch thermische Analyse untersucht. Dabei zeigte sich, dass die Bearbeitung eines solchen Systems experimentell sehr grosse Schwierigkeiten mit sich bringt, Einmal sind die Schmelzpunkte und die Dichten der Partner sehr verschieden. Von Bedeutung ist ferner, dass das Atomgewicht des Al so klein ist; infolgedessen sind schon kleine, nahezu unvermeidbare Angriffe auf das Aluminium durch den Sauerstoffgehalt des Schutzgases bzw. durch das Gefässmaterial von entscheidender Bedeutung für das atomare Verhältnis. Was in der Literatur über das System Al/Pt aus der thermischen Analyse bekannt war, ist ganz unvollständig und zudem im wesentlichen falsch. Das Zustandsdiagramm zeigt Abb. 1. Es existieren folgende Verbindungen: $PtAl_4$, $PtAl_3$, $PtAl_2$, Pt_2Al_3, PtAl, Pt_3Al_2, Pt_5Al_3, Pt_3Al und eine platinreiche Überstrukturphase dieses Typs mit leichter tetragonaler Verzerrung.

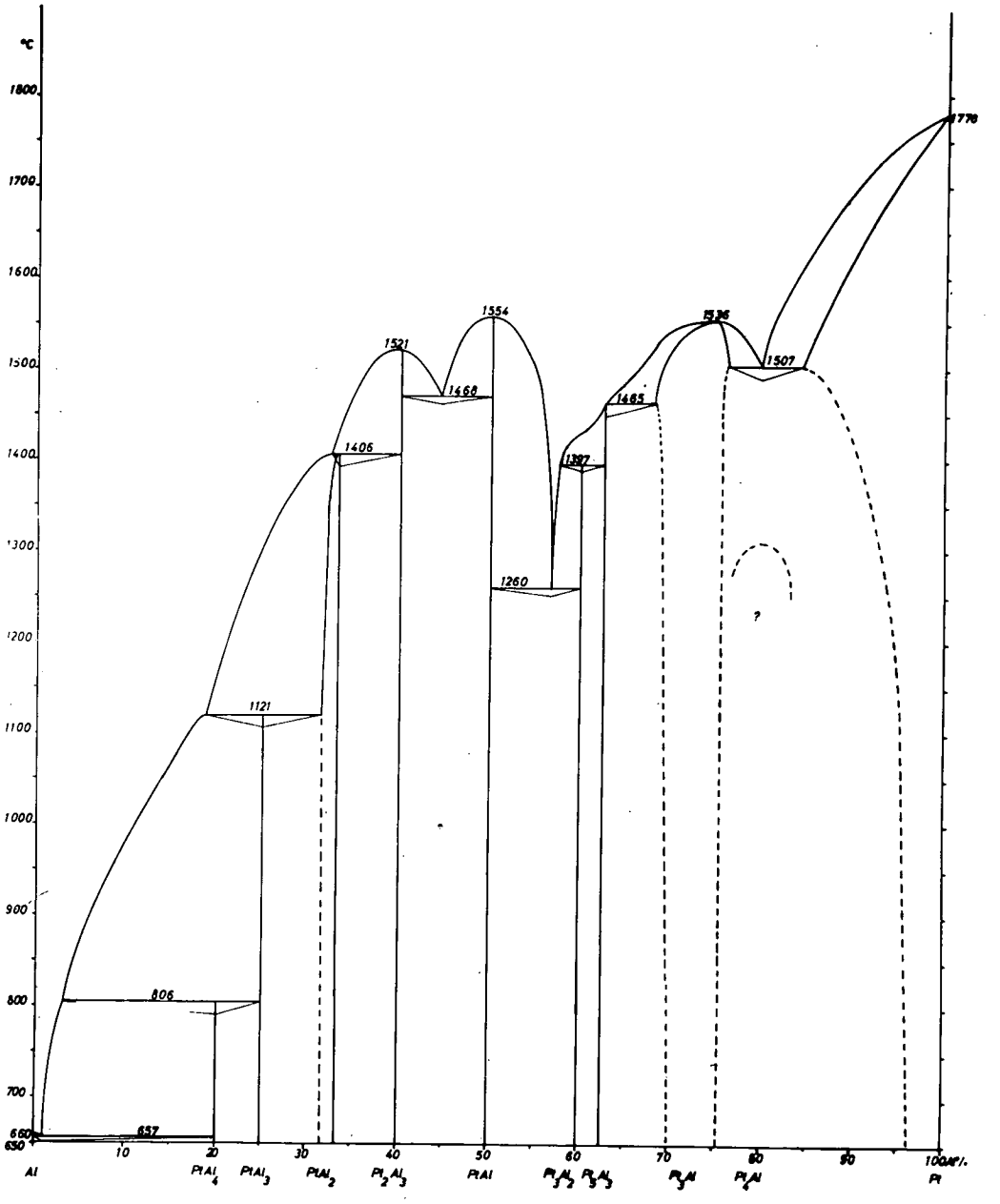

Abb. 1 Das System Platin–Aluminium

Bei diesen Phasen waren die Strukturen von $PtAl_2$ (CaF_2–Typ) und PtAl (FeSi–Typ) schon bekannt. Von den bisher unbekannten Verbindungen konnten die Strukturen von Pt_2Al_3 (Überstruktur des Ni_2Al_3–Typs), Pt_5Al_3 (Rh_5Ge_3–Typ) und Pt_3Al (Cu_3Au–Typ) aufgeklärt werden. Der Aufbau der übrigen Verbindungen konnte noch nicht ermittelt werden; es liegen hier komplizierte Strukturen mit sehr grossen Elementarzellen oder niedriger Symmetrie vor.

Die Schwierigkeiten bei der Untersuchung dieses Systems führten zu dem Wunsch, eine einfachere Methode zur Herstellung von Verbindungen des Platins mit unedlen Metallen zu finden. Dies geschah auf Grund folgender Uberlegung: Wie die Erfahrungen bei der Synthese derartiger Verbindungen zeigten, sind die Bildungswärmen sehr gross. Es bestand daher die Möglichkeit, dass man Legierungen unedler Metalle mit Platin durch Erhitzen von Gemischen der Oxide mit Platin im Wasserstoffstrom herstellen konnte. Diese Versuche wurden von W. Bronger begonnen am System Aluminiumoxid Platin. Es zeigte sich, dass die Komponenten im Wasserstoffstrom schon bei 900°C unter Bildung von Platin–Aluminiumlegierungen reagierten. Wie thermodynamisch zu erwarten ist, ist der Trocknungsgrad des Wasserstoffs von grossem Einfluss. Z. B. kann man bei 1100°C mit Wasserstoff, der über konz. Schwefelsäure getrocknet wurde, nur Pt–Al–Legierungen bis zur Zusammensetzung ~ Pt_4Al erhalten. Verwendet man dagegen scharf getrockneten Wasserstoff (hergestellt entweder mittels Diffusion des Gases durch erhitztes Nickelblech oder durch thermische Zersetzung von Ammoniak, das vorher mit Natrium getrocknet war), so kommt man bis zu der Zusammensetzung Pt_3Al.

Aus diesen Versuchen, insbesondere aus der Abhängigkeit vom Wasserdampfpartialdruck, konnte man thermodynamisch die Bildungswärme der Pt_3Al–Phase abschätzen; es ergab sich pro Formeleinheit eine Bildungs wärme von etwa 23 kcal.

Als besonders angenehm stellte sich bei dieser Methode heraux, dass man Überstrukturphasen, deren Bildung bei der thermischen Analyse vielfach sehr schwer zu erfassen ist, hier besonders leicht herstellen und charakterisieren konnte. So, wurde eine interessante Überstruktur gefunden, bei der die kubische Zelle, die man beim Pt_3Al findet, ganz schwach tetragonal verzerrt wird. Die Röntgeninterferenzen des Pt_3Al–Diagramms spalten teilveise auf und es treten neue schwache Überstrukturreflexe auf, die man allerdings eindeutig nur mit Guinier–Aufnahmen erkennen und vermessen kann. Die Idealzusammensetzung dieser Überstruktur–Phase liegt etwa bei

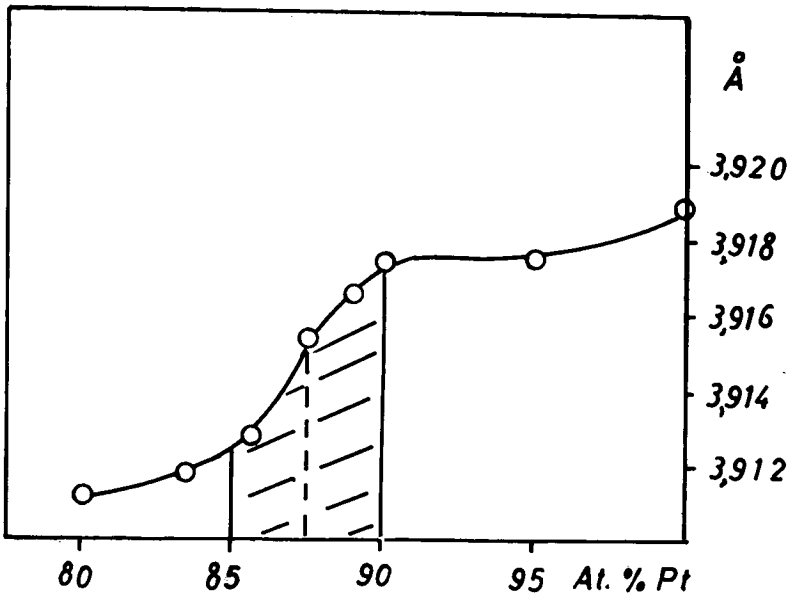

Abb. 2 Feste Lösungen von Mg ind Pt (schraffiert: Gebiet der geordneten Phase Pt_7Mg)

$Pt_{18}Al_3$; die Art der Überstruktur konnte in grossen Zügen aufgeklärt werden, mit den Feinheiten sind wir noch beschäftigt.

Diese Ergebnisse beim System Pt/Al ermutigten uns, auch andere Legierungssysteme zu untersuchen. Es zeigte sich, dass die beschriebene Methode ganz allgemein anwendbar ist, um platinreiche Legierungen mit unedlen Metallen auf bequeme Art herzustellen. Untersucht wurden sehr zahlreiche Platin-haltige Systeme, eingehender die Systeme mit Li, Be, Mg, Ca, Sr, Sc, Y, La und Cr. Bei dem letztgenannten System stellte sich heraus, dass man die bei tiefen Temperaturen gebildete Phase Pt_3Cr, die bisher bei der thermischen Analyse nicht fassbar war, in einfacher Weise herstellen konnte. Bei den Elementen der ersten bis dritten Gruppe wurden folgende Verbindungen hergestellt und zum grössten Teil strukturell aufgeklärt: Pt_7Li, Pt_7Mg, Pt_3Mg, Pt_2Ca, Pt_5Ca, Pt_3Sc, Pt_5La. Als typisch traten dabei auf: die Cu_5Ca-Struktur, die Cu_2Mg-Struktur und die Cu_3Au-Struktur. Charakteristisch ist ferner, dass in den platinreichen Gebieten geordnet Phasen auftreten, die mit der kubisch dichten bzw. hexagonal dichten Kugelpackung Verwandtschaft zeigen. Solche Strukturen sind Pt_7Li, Pt_7Mg und eine Überstrukturphase der ungefähren Zusammensetzung $Pt_{15}Be$. Im Bereich des Homogenitätsgebietes derartiger Überstrukturphasen finden sich charakteristische Änderungen der Gitterkonstanten (vgl. z. B. Abb. 2). Ausserdem wurde festgestellt, dass zwischen dem Cu_5Ca-Struktur-Typ und dem Cu_2Mg-Typ Übergänge auftreten, mit deren Aufklärung wir noch beschäftigt sind.

Diese Ergebnisse haben eine gewisse Bedeutung für das Arbeiten mit Platingeräten. Liegt eine stark reduzierende Atmosphäre vor, so besteht bei Anwesenheit von Oxiden unedler Metalle bei Glühtemperaturen von 1000°, evtl. sogar schon früher, die Gefahr, dass sich Legierungen des Platins mit diesen Metallen bilden.

CRYSTAL STRUCTURE AND STABILITY OF REFRACTORY PHASES.

H. Nowotny

Although combinations having the highest melting point like HfC, TaC or HfC-TaC are known for 30 years, little progress has been made in finding more stable systems. However, many new refractory phases in binary or multicomponent systems suitable for different purposes have been detected. A rather wide variety of refractory phases as far as crystal structure and properties are concerned makes one believe that regularities may be applied, only limited.

In respect to the key of the problem, the bonding in refractory phases, several modern concepts will be reviewed. The paper deals with some new investigations on borides, carbides, nitrides, aluminides, silicides and germanides of transition metals as well as with combinations of these, with special reference to hafnium–systems. The results are to be discussed within the general field of refractories excluding the class of typical oxides.

More intense study revealed the systematic influence of metalloid impurities C, N, O on high melting borides and silicides or N, O on carbides respectively. Very often such small metalloids brought in by preparation technique, like hot–pressing, sintering and powder reaction–method, arc–melting, surface deposition, may change the constitution of the systems.

The most important group of so called monocarbides, mononitrides and others having the simple sodiumchloride structure includes still new problems. Earlier experimental work and theoretical considerations lead to the conclusion that no cubic ScC exists. However carburation of a very pure Sc_2O_3 gives full evidence of a "ScC" or Sc(C, O) having sodium–chloride structure. The lattice parameter (4,50 – 4,48kX. U.) is well above those for ScN and TiC. The melting point of this carbide (carboxide) seems to be placed above 2500°C. The question of the existence of scandium–monocarbide is of special interest in respect to the competition between formation of dicarbides, such as LaC_2 and the very stable monocarbides: Ti (Zr, Mf, V, Mb, Ta)C, governed by the ratio r_x/r_{Me}. An early attempt to prepare MoC with sodium–chloride–type has been promising, but this phase could not be obtained in a pure state; however, Rudy and Benesovsky recently prepared pure MoC having B 1 structure during an investigation of the ternary system: Mo–B–C. Here again the carbon defect seems to play an essential role, known in all monocarbide–phases. There are some hints, that in the monocarbide–group also metal defect in the lattice may appear, with which fact we are familiar in monoxides of transition metals.

Emphasis has been given to the elucidation of Zr and Hf–monoborides, which are closer to the critical Hagg ratio 0,59. Firstly it was found that the B h–type mentioned in literature leads to volume for "ZrB" and "HfB" respectively surprisingly smaller than for the unambiguous monocarbides. Extended homogenous fields for the B h–phase have been noticed in the systems Zr(Hf)–B–C(N), especially concerning the nitrides, but the origin of this phase comes either from the carbide or the nitride.

The lattice parameters of Zr(N, B) or Hf(N, B) are higher than those of the nitrides, and the highest values agree with the literature data. However one can conclude that there is by no means a complete transition although Hf(N, B) mixed crystal is stable up to B/N ≈ 1. HfB stabilized by a small amount of carbon has been shown to be of the FeB (B 27)–type. This corresponds completely to the behavior of TiB. No ternary compound will be formed in all these systems and in a regular manner the mononitride dissolves always more boron or boride than the carbide.

The strong similarity between carbides and nitrides has been pointed out in the formation of complete series of mixed crystals between: HfC–TiN, –ZrN, –HfN and –Nb(N, O) as well as between: HfN–TiC, –ZrC, –NbC and TaC. Together with earlier results one can suppose that the type of bonding seems to be somewhat similar. Using the electrostatic concept for evaluation of lattice energy Baughan calculated an uniform electron affinity ($N \rightarrow N^{3-}$) for high melting mononitrides. One obtains surprisingly fair values extending this method for monocarbides. also. From this follows E ($C \rightarrow C^{3-}$) = –325,4 kcal.

Pseudoternary equilibria have been investigated with respect to HfC and UC. Inasmuch as the volume condition is observed complete miscibility gap while ZrC and UC are completely miscible, or HfN and UN have a relatively small miscibility gap in spite of the unfavourable size factor. It is a remarkable fact that one failed up to now to get mixed crystals in the system: HfN–NbN. A simple thermodynamic calculation adopting regular solutions leads to a mixing enthalpy of some kcal in carbide systems. This confirms a regularity in such a way that the energy is endothermic for metals of the same group and exothermic for metals of different groups.

It should be mentioned that HfC does obviously not exist in a stoichiometric composition; nevertheless HfC is diamagnetic. It is of some interest to note that (Ti, Ta)C at about 50 Mol% TaC also shows a diamagnetic behaviour like ZrC and HfC although TiC and TaC are paramagnetic.

The very high stability of HfC may be seen from the small expansion coefficient, which has been measured by X–ray–method: α (20 – 960°C) = $5,60.10^{-6}$.

Other carbides like $CrUC_2$ and so on will be discussed.

The structural principle in carbides changes in the case of borides and silicides. A typical case in Ti–Mo–B can be discerned in Ti–Mo–monoborides. All three types of monoborides in which the boron–atoms form chains are realized in such a manner that the distances B–B remain constant while the other axes vary in the opposite sense.

One can assume that the diborides replace the role of monocarbides. In the same sense the bonding is explained in an analogous way inasfar as a trigonal sp^2–hybridisation on the boron–atoms is consistent with a strong polar effect. Boron is placed between interstitial and substitution structural principles as is clearly seen in many ternary systems like Me–B–Si (Me = Zr, V, Nb, Ta, Cr, Mo, W). Boron substitutes Silicon in the high–melting silicides like T 1 (W_5Si_3–type) and T 2 (Cr_5B_3–type), but is built in as an interstitial atom in filled up $D8_8$ – phases ($Mo_5Si_3C_x$–type)

A special discussion will be given on the stabilization problem about the $D8_8$ – phases.

While diborides and disilicides have almost no mutual effect a strong electronic factor intervenes in the case of aluminum, which can be seen from the ternary systems: Me–Al–Si (Me = Ti, Zr, Nb, Ta, Cr, Mo, W). The regular sequences of mixed sheets follow from the common structural principle of disilicides. Lowering the valence electron concentration by mixing: $TiSi_2 + MoSi_2 = (Ti, Mo)Si_2$ leads to the $TaSi_2$–type. Another example is the existence of $Mo(Al, Si)_2$ and $W(Al_{0,7-0,3}$ $Si_{0,3-0,7})_2$, which also crystallize in the $TaSi_2$–type.

The observed regularity is confirmed to a wide extend, as it was found the phase NbAlSi to have a crystal structure isotype to $TiSi_2$.

The substitution of silicon by germanium can be interpreted also as a valence electron lowering effect. One has to accept in this family of compounds a higher electron concentration than 4 for Hf, but a smaller than 6 for chromium. While $ZrSn_2$ crystalizes in the homologous $TiSi_2$ – structure, $HfSn_2$ prefers to be isotype with $TaSi_2$. Furthermore, $HfAl_3$ is forming both structures: $ZrAl_3$– and $TaAl_3$–type. Aluminides of transition metals e.g. Nb, Ta have been found to be potentially useful for high temperature application because of the remarkable high oxidation resistance.

PHASES NON STOECHIOMETRIQUES ET THERMODYNAMIQUE.

M. Laffitte

Dans le cadre de l'étude de l'activité chimique des solides, celles des phases non stoechiometriques joue un rôle primordial.

Les premiérs travaux sur ce sujet ont consisté à définir ces phases non stoechiométriques, grâce a une connaissance parfaite de leur structure. La cristallographie a été dans ce domaine un outil très précieux.

Si cette structure dont permettre un jour de calcules dans tous les cas la stabilité des phases non stoechiométriques, nous n'en sommes pas encore là, malheureusement car cette stabilité nous permettrait de prévoir la réactivité chimique de ces phases.

L'énergie libre dont donc être calculée par d'autres méthodes où la thermodynamique peut rendre de grands services, en s'appuyant sur des méthodes expérimentales convenables. Des résultats ont déjà été obtenus par des méthodes diverses. De nombreuses mesures restent à faire et certaines techniques semblent devoir être très frucheuses.

ROLE OF GASEOUS SPECIES AND DEFECT STRUCTURES IN DETERMINING PHASE EQUILIBRIA.*

R.J. Ackermann, R.J. Thorn, and G.H. Winslow

The thermodynamic equilibria between solid and gaseous phases are determined in part by the stabilities of the gaseous species and in part by the stabilities of the solids including those which have defect structures in the crystalline lattice. Consequently there are, in general, three groups under which pressure – composition diagrams can be discussed:

1) Those of systems in which there are several gaseous species of importance but no significant defect structures.

2) Those of systems in which there is a single gaseous species so that the nature of the diagrams is determined by the stabilities of the lattices and defects.

*Based on work performed under the auspices of the US Atomic E n. Comm.

3) Those of systems in which the behavior is determined by both gaseous species and defect structures.

A typical example in the first group is that displayed by the aluminum–oxygen system. The second type is observed in the iron–oxygen system. There are several examples in the third group which are interesting to discuss because of the complexities which can occur. Among the binary systems in this group are those composed of oxygen and the individual metals titanium, zirconium, vanadium, chromium, molybdenum, tungsten, and uranium. Herein only the zirconium–oxygen system will be analyzed.

In the case of aluminum and aluminum oxide the precise values for the mutual solubilities are unknown but undoubtedly very small. There are several gaseous species which are important, viz. aluminum, oxygen, and gaseous oxides of formulas Al_2O and AlO. The free energies of formation of all of these have been derived from the best available measurements (See R. J. Ackermann and R. J. Thorn, "Vaporization of Oxides" in Progress in Ceramic Science, Vol. I, Editor, J. E. Burke, Pergamon Press Inc., New York, to appear). From these data one can construct the phase diagram.

One is particularly encouraged to attempt a quantitative evaluation of the pressure – composition diagram for at least part of the iron–oxygen system because the published measurements (L. S. Darken and R. W. Gurry, J. Am. Chem. Soc., 67, 1398 (1945); Ariya, Morozova, and Shneider, J. Gen. Chem. U. S. S. R. 24, 37 (1954)) are sufficiently accurate that one can examine quantitatively the thermodynamic analysis of the theory of non-stoichiometric compounds as formulated by Schottky and Wagner (W. Shottky and C. Wagner, Z. Phys. Chem. B 11, 163 (1930)), and developed by Lachler (J. R. Lachler, Proc. Roy. Soc. A 161, 525 (1937)) and Fowler (R. H. Fowler and E. A. Guggenheim, Statistical Thermodynamics, Cambridge University Press, Cambridge, 1939; and J. S. Anderson, Proc. Roy. Soc. A185, 69 (1946)). Apparently there have been no attempts to examine quantitatively the data for the wustite phase with the objective of deriving the parameters associated with the defects. Such is attempted herein by use of the equations as summarized by Anderson. These are obtained by assuming that the "energy of interaction between defects can be represented as the sum of the contributions of those pairs of defects that occur as nearest neighbours in a completely random distribution" and that "the vibrational partition function of an interstitial... atom, and of the atoms adjacent

to a vacant lattice site or to an interstitial atom, is taken to be identical with those of atoms in a perfectly ordered lattice." The resulting, pertinent equations are as follows:

1. For small deviations from stoichiometry in FeO_n

$$\frac{\lambda_o(n)}{\bar{\lambda}_o} = \frac{n}{2\delta} + \left[\left(\frac{n}{2\delta}\right)^2 + 1\right]^{1/2} \qquad (1)$$

in which λ_o is the absolute activity of atomic oxygen in FeO_n, $\bar{\lambda}_o$ refers to the hypothetical ideal compound FeO, and δ is the intrinsic disorder or ratio of vacancies-to-sites in the stoichiometric compound.

2. For large deviations from stoichiometry and equilibrium between two solid phases such as magnetite and wustite with cation vacancies in the wustite,

$$\frac{\lambda_o(\theta^h)}{\lambda_o(1/2)} = \frac{\theta^h}{1-\theta^h} \; e^{-(1-2\theta^h)\frac{E_{hh}}{kT}} \qquad (2)$$

in which $\lambda(1/2)_H$ is the absolute activity of atomic oxygen in the two phase region, θ is the fractional cation sites vacant, and E_{hh} is the interaction energy between vacant sites. (3) For large deviations from stoichiometry in a single phase region

$$\frac{\lambda_o(\theta^h)}{\bar{\lambda}_o} = \frac{\theta^h}{1-\theta^h} \; \frac{1-\delta}{\delta} \; e^{-(2\delta-2\theta^h)\frac{E_{hh}}{kT}} \qquad (3)$$

and or

$$\frac{\bar{\lambda}_o}{\lambda_o(\theta^i)} = \frac{\theta^i}{1-\theta^i} \; \frac{1-\theta}{\delta} \; e^{-(2\delta-2\theta^i)\frac{E_{ii}}{kT}} \qquad (4)$$

in which θ^i is the ratio of interstitials to lattice sites.

4. For both vacancies and interstitials in FeO_{1+x}

$$\theta^h - \theta^i = \frac{x}{1+x} \quad . \qquad (5)$$

Although the data reported by Darken and Gurry indicate that stoichiometric FeO does not exist at temperatures near 1000°K, the more precise data by Ariya, Morozova, and Shneider indicate that the slope of the oxygen pressure vs composition approaches zero asymptotically near the stoichiometric compound. Consequently upon initiating an examination of wustite by use of the equations given above one must recognize that stoichiometric FeO may exist. Using the data given by Ariya, Morozova, and Shneider in equation (1) one obtains values of δ ranging from 0.024 to 0.26. Hence, as one might suspect because of the rather large deviations from stoichiometry, equation (1) is not applicable. If one assumes that only cation vacancies are present, then one should be able to describe the behavior of FeO_{1+x} by means of equations (2) and (3). At the two phase boundary between wustite and magnetite Ariya, Morozova, and Shneider found an oxygen to iron ratio of 1.0975 in the wustite phase at 1104°K. Using this information in equation (2) one obtains a value of −6211 cal/mole for E_{hh}. When this value is employed in equation (3), however, one does not obtain a constant value of δ for varying θ^h. Therefore equations (2) and (3) do not describe the behavior of the wustite phase. It is necessary consequently to investigate both vacancies and interstitials.

The absolute rate of effusion of vapor subliming from solid zirconium dioxide contained in a tungsten cell has been measured as a function of temperature and composition (R.J. Ackermann and R.J. Thorn, manuscript to be published). It has been found that at constant temperature near 2400°C the rate of effusion decreases with decreasing ratio of oxygen – to – zirconium in the solid phase between values of 2.00 and 1.96. The rate increases between ratios of 1.96 to about 1.90 and at a ratio of 1.96 the solid sublimes congruently. From measurements of the effusion rate as a function of temperature for both the stoichiometric dioxide and the oxide exhibiting minimum volatility it is possible to derive certain thermodynamic properties. The free energy of formation of the gaseous dioxide has been found to be given by the equation

$$\Delta F_f^\circ (ZrO_2 g) = -94,000 + 5.1T. \qquad (6)$$

The decrease in volatility in the region between an oxygen – to – zirconium ratio of 2.00 and one of 1.96 can be explained by assuming

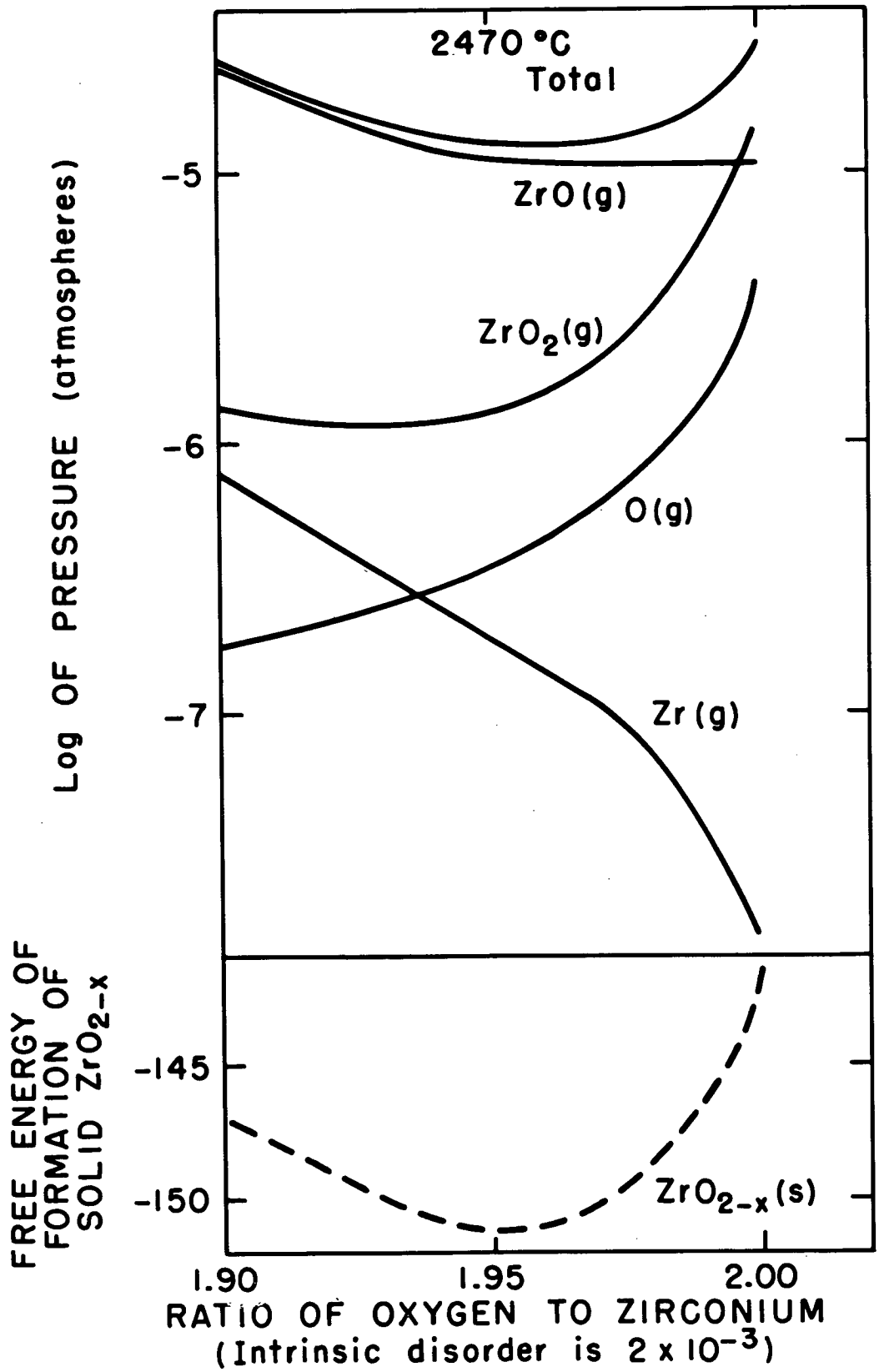
2470 °C
Total
ZrO(g)
ZrO_2(g)
O(g)
Zr(g)
-5
-6
-7
Log OF PRESSURE (atmospheres)
-145
-150
ZrO_{2-x}(s)
FREE ENERGY OF FORMATION OF SOLID ZrO_{2-x}
1.90
1.95
2.00
RATIO OF OXYGEN TO ZIRCONIUM
(Intrinsic disorder is 2×10^{-3})

that oxygen ion vacancies are created in the zirconium dioxide lattice. Employing the measured thermodynamic properties of gaseous dioxide and monoxide and the measured volatility at $ZrO_{1.96}$ in equation (1), one finds that the intrinsic disorder in the stoichiometric dioxide at about 2470° is 2×10^{-3}. These data permit the calculations of the theoretically expected partial pressures of the various gases in equilibrium with the dioxide phase of varying composition as shown in Figure I. The variation of the free energy of formation of the condensed phase, ZrO_{2-x}, with composition is shown by the dashed line in the bottom of the figure. The properties of the monoxide gas is the most important of those of the gases in determining the volatility behavior. There is a significant change in the free energy of formation over the composition range studied. This change together with the properties of the gaseous monoxide are the principal factors which determine the total pressure.

SUR LA FORMATION DE DIFFERENTS ETATS ORDONNES DANS LES PHASES NON STOECHIOMETRIQUES REFRACTAIRES.

R. Collongues, J. Lefevre, M. Perez Y Jorba, et F. Queyroux

L'intervention des phénomènes de non stoechiométrie en chimie minérale est reconnue depuis fort longtemps. Cependant dans les domaines où prédomine nettement le caractère ionique des liaisons, par exemple dans la chimie des oxydes, les probabilités de formation de phases non stoechiométriques étendues sont assez réduites à température moyenne. A haute température, au contraire, l'accroissement de l'agitation thermique entraîne la possibilité d'existence de phases présentant de nombreux défauts ponctuels: substitutions ou lacunes. Par exemple la phase spinelle $MgAl_2O_4$ qui est sensiblement stoechiométrique jusqu'à 1200°C possède au voisinage de la température de fusion (2000°C environ) un domaine d'homogénéité s'étendant de $MgAl_2O_4$ (50 % mol Al_2O_3) à $Mg_{0,1}Al_{2,6}O_4$ (93 % mol Al_2O_3).

Les études de chimie minérale à haute température permettent donc la préparation de phases présentant des écarts importants à la stoechiométrie. Au cours de traitements thermiques convenables, l'arrangement des défauts ponctuels peut être modifié et de nombreuses structures nouvelles peuvent apparaître. Nous nous sommes proposés l'étude de la structure et des transformations de ces phases non stoechiométriques a l'aide de quelques exemples choisis dans la chimie des super-réfractaires à base de zircone. Dans ces phases les défauts

ponctuels peuvent être constitués soit uniquement par des substitutions: ce sera le cas des systèmes $ZrO_2 - MO_2$; soit par des substitutions et des lacunes: ce sera le cas des systèmes $ZrO_2 = M_2O_3$.

Phases presentant des ecarts a la stoechiometrie par substitution: Des exemples de telles phases se rencontrent dans les systèmes formés par la zircone avec les oxydes de métaux tétravalents. Nous avons étudie plus spécialement le système $ZrO_2 - GeO_2$ dans un domaine de composition compris entre la zircone pure et le composé $ZrGeO_4$ (50 % GeO_2) (1, 2, 3, 4) Trois phases de structures voisines apparaissent dans ce système:

1. La solution solide primaire de l'oxyde de germanium dans la zircone quadratique dont le domaine d'homogénéité s'étend de ZrO_2 à $Zr_{0,9}Ge_{0,1}O_2$ La structure est de type fluorine déformé;

2. la phase non stoechiométrique dérivant du composé Zr_3GeO_8 dont le domaine d'homogénéité s'étend de $Zr_{3,2}Ge_{0,8}O_8$ à $Zr_{2,8}Ge_{1,2}O_8$. Sa structure a été déterminée par l'étude du composé correspondant Hf_3GeO_8 formé par les oxydes d'hafnium et de germanium;

3. la phase non stoechiométrique dérivant du composé $ZrGeO_4$ dont le domaine d'homogénéité s'etend de $Zr_{1,2}Ge_{0,8}O_4$ à $ZrGeO_4$. Sa structure est de type scheelite.

Il convient de remarquer que les structures de ces trois phases dérivent simplement de la structure de la zircone quadratique. Les positions des cations sont les memes dans les différentes mailles. Le réseau des anions subit une légère distorsion afin d'assurer la configuration tétraèdrique autour des ions Ge^{4+}. On passe successivement du motif Zr_4O_8 au motif Zr_3GeO_8 par substitution ordonnée d'un ion Zr^{4+} par union Ge^{4+} puis de Zr_3GeO_8 à $ZrGeO_4$ par le même processus.

Il semble donc que les phases Zr_3GeO_8 et $ZrGeO_4$ puissent être considérées comme les surstructures de type A_3B et A B d'une même solution solide s'étendant de la zircone quadratique au composé de type scheelite $ZrGeO_4$ A l'intérieur de chacun des trois domaines monophasés du diagramme d'equilibre les paramètres a et c de la maille quadratique varient régulièrement et le rapport c/a augmente quand la teneur en oxyde de germanium augmente.

Phases non stoechiometriques lacunaires: On recontre de remarquables

exemples de ces phases dans l'étude des systèmes zircone – oxydes de terres rares (5, 6, 7, 8).

La solubilité des oxydes de terres rares (autres que l'oxyde de lanthane) dans la zircone quadratique est très élevée. Il se forme une solution solide lacunaire de formule $Zr^{4+}_{1-x}\ M^{3+}_{x}\ O^{2-}_{2-x}\ \square_{\frac{x}{2}}$ s'étendant aux environs de 2000°C de 0 à plus de 50 % mol. M_2O_3 ($O < x < 0,7$).

Pour une composition voisine de $2ZrO_2 - M_2O_3$ ($x = 0,5$) un ordre peut s'établir dans la réparitition des cations et des lacunes de la structure de cette solution solide. Une nouvelle structure apparait alors: elle est de type pyrochlore. Cette phase ordonnée est d'autant plus stable que le rayon ionique de l'element des terres rares est plus élevé: dans les systèmes $ZrO_2 - La_2O_3$ et $ZrO_2 - Nd_2O_3$ elle est stable jusqu'à la température de fusion; dans les systèmes $ZrO_2 - Sm_2O_3$ et $ZrO_2 - Gd_2O_3$ son domaine de stabilité cesse respectivement à 1900°C et 1550°C. Ces températures sont des températures de transition ordre – désordre au-dessus desquelles la phase ordonnée pyrochlore donne naissance à la solution solide désordonnéede type fluorine. A mesure que l'on s'éloigne de la composition stoechiométrique, la température de transition ordre–désordre diminue. Enfin, dans les systèmes $ZrO_2 - Dy_2O_3$ et $ZrO_2 - Yb_2O_3$, la structure ordonnée n'apparait pas.

Il est intéressant de noter que de simples considérations géométriques permettent d'interpréter d'une manière satisfaisante l'étendue des domaines d'homogénéité des phases ordonnées dans les différents systèmes étudiés.

Pour des teneurs supérierues en oxydes de terres rares d'autres structures ordonnées ont été mises en évidence dans les systèmes ZrO_2–Dy_2O_3, ZrO_2–Yb_2O_3, ZrO_2–Sc_2O_3.

Il apparait ainsi, dans ces systèmes, diverses possibilités de formation de structures nouvelles correspondant à des états d'ordre différents d'une même phase non stoechiométrique. La formation de ces surstructures se traduit vraisemblablement par des modifications sensibles des propriétés de la phase suivant les traitements thermiques subis.

BIBLIOGRAPHIE

1. J. Stöcker, M. Moser et R. Collongues, Collogue Nal sur la Chimie des Hautes Températures, Paris (1957); p. 39.

2. J. Lefevre et R. Collongues, Bull. Soc. Chim. Fr. 1966 (1959).

3. J. Lefevre et R. Collongues, C.R. 251 – 1016 – 1960.

4. R. Collongues, J. Lefevre, H. Mondange et M. Perez y Jorba Journées d'Etudes sur la Silice – Bruxelles (Septembre 1960).

5. M. Perez Y Jorba, R. Collongues et J. Lefevre – C.R. 249 – 1237 – 1959.

6. J. Lefevre, R. Collongues et M. Perez Y Jorba – C.R. 249 – 2329 – 1959.

7. M. Perez Y Jorba et R. Collongues – Bull. Soc. Chim. Fr. 1967 – 1959.

8. J. Lefevre, M. Perez Y Jorba et R. Collongues – Soc. Chim. Fr. 1969 – 1959.

REACTIONS BETWEEN BETA–SPODUMENE AND SUBSTANCES ISO–STRUCTURAL WITH SILICA: I, PHASE EQUILIBRIA IN THE SYSTEM BETA–SPODUMENE– $AlPO_4$.

M. K. Murthy

Beta–spodumene ($Li_{20}.Al_2O_3.4SiO_2$) and its solid solutions with silica have very low thermal expansion properties and therefore have found many commercial applications. Also, there are a number of phosphates, $AlPO_4$, PBO_4, $MnPO_4$, $FePO_4$, and $GaPO_4$ which are iso–structural with silica. $AlPO_4$ exists in all the three crystalline modifications that are exhibited by silic quartz, tridymite and cristo–balite. The system beta–spodumene–$AlPO_4$ has been studied by solid state reaction and by the conventional quench techniques. Phase equili–brium data are presented.

REACTIONS IN THE SYSTEM Si–B–O.

H. F. Rizzo, M. P. Davis, W. R. Foster

The compatibility joins for the system Si–B–O have been established at temperatures of 1000°C and 1100°C. A study of reactions in the binary systems B–O, B–B_2O_3, Si–O, Si–B_2O_3, and Si–B revealed the formation of several compounds, SiB_4, SiB_6, B_7O, and α – rhombohedral B. At 1000°C compatibility joins exist between SiO_2 and SiB_4, SiB_6, –B, and B_2O_3. At 1100°C, joins were found between SiO_2 and SiB_4, SiB_6, B_7O, and B_2O_3. The synthesis of all the above mentioned compounds can be accomplished by reacting Si and B_2O_3 in varying proportions, as governed by the compatibility joins.

HETEROGENEOUS REACTIONS INVOLVING OXIDATION AND REDUCTION AT HIGH TEMPERATURES AND PRESSURES.

H. P. Eugster, D. R. Wones, and A. C. Turnock

Oxidation and reduction reactions can be controlled by hydrogen diffusion through the wall of the charge container in a hydrothermal experiment. Externally heated stellite vessels are used. The temperature range is 200 to 900°C. Fluid or gas pressure up to 5000 bars is applied and measured through a pressure lead.

The charge container is a tube of platinum, silver, or palladium, sealed by welding the ends. It maintains the bulk composition of the charge except for hydrogen. The oxygen content of the charge may be adjusted by the amound of water added to the solids.

The hydrogen fugacity is buffered by a water–plus–solids redox system, which surrounds the inner tube and is again enclosed by a thick, malleable, outer container. The outer container, made of gold, is less permeable to hydrogen and therefore allows the buffer to come to equilibrium values of the partial pressures of hydrogen, oxygen, and water, with the solids at the specified conditions of temperature and total pressure. The following redox pairs have been used: (1) $Cu_2O + Cu$, (2) $Fe_2O_3 + Fe_3O_4$, (3) $NiO + Ni$, (4) $Fe_3O_4 + SiO_2 + Fe_2SiO_4$, (5) $Fe_3O_4 + Fe_{1-x}O$, (6) $Fe_{1-x}O + Fe$, (7) $Fe_3O_4 + Fe$, and (8) $Fe_2SiO_4 + SiO_2 + Fe$.

The diffusion of hydrogen through the walls of the inner container is fast enough at temperatures above about 400°C to maintain equal pressures, with some exceptions. The partial pressures of hydrogen of buffers (1) and (2) above are very low, of the order 10^{-2} (1) and $10^{-1.5}$ atm. (2) and are not effective at temperatures of less than about 450°. Also, the rate of diffusion through silver is less than the rate through platinum, and equilibrium is not found below 500°.

Within the charge container, the gas phase will consist of water, hydrogen, and oxygen, and the partial pressures of these three are related by the dissociation constant of water. When the partial pressure of hydrogen comes to equilibrium at the same values, providing that the dissociation constant is the same for both the buffer and the charge vapor phases. This will be correct if there is negligible solubility of the solids in the vapor. We have worked with solids of Na, K, Fe, Mg, Al, and Si, and our experience is that the effect of their solubility in the vapor, changing the partial pressure of oxygen from that of the buffer, cannot be observed.

For the buffers listed above, data on the fugacity of oxygen has been compiled and extrapolated down to 400°, and the fugacity of hydrogen in a coexisting aqueous phase has been calculated. There are many other reactions that might be used as buffers.

The effect of total pressure on the values of the partial fugacities of hydrogen and oxygen of the buffers has been calculated and shown to be very small.

The compounds studied by this method were complex silicates of iron. When platinum is used as the inner charge container, there is a problem of loss of iron into the platinum by alloying. This was avoided by either wrapping an inner portion of the charge in an unsealed wrapping of silver foil, or by substituting a silver container for the platinum one. Platinum is most permeable to hydrogen, and it can be used with buffers (1), (2), and (3) above, where the oxygen pressure is high enough to prevent alloying. Silver tubes are now used with buffers (4) to (8).

This buffer arrangement has been applied to phase–equilibria studies of some rock–forming silicates of iron. Stoichiometric synthesis of the following minerals has been achieved:

Annite	$KFe^{+2}_3AlSi_3O_{10}(OH)_2$
Biotite series	$K(Fe^{+2}, Mg)_3AlSi_3O_{10}(OH)_2$
Oxybiotites	$K(Fe^{+2}, Fe^{+3})_3AlSi_3O_{10}(OH)_2$
Septechlorites	$(Fe^{+2}, Al)_6(Si, Al)_4O_{10}(OH)_8$
Spinel series	$FeO(Fe, Al)_2O_3$
Amphiboles (W. G. Ernst)	$Na_2(Fe^{+2}, Mg)_3(Fe^{+3}, Al)_2Si_8O_{22}(OH)_2$

The phase equilibria of these minerals has been determined as a function of temperature, partial fugacity of oxygen, and the total pressure. The importance of controlling the oxygen pressure in regard to stoichiometric synthesis is emphasized by the correlation of change of composition of the above minerals, by oxidation of the ferrous iron, with increasing oxygen pressure.

For the reaction annite = kalsilite + leucite + fayalite + water

$$KFe^{+2}_3AlSi_3O_{10}(OH)_2 = KAlSiO_4 + KAlSi_2O_6 + Fe^{+2}_2SiO_4 + H_2O$$

the value of water fugacity is $\log_{10} f_{H_2O} = -\frac{11200}{T} + 13.35.$

For the reation annite = sanidine + magnetite + hydrogen

$$KFe^{+2}_3AlSi_3O_{10}(OH)_2 = KAlSi_3O_8 + Fe^{+2}Fe^{+3}_2O_4 + H_2$$

$$\log_{10} f_{H_2} = -\frac{9215}{T} + 10.99.$$

Using published values for the heats of formation of sanidine, leucite, magnetite, fayalite, and water, the following heats of formation from the elements have been derived:

Annite	−1235 kcal/mol
Arthorhombic kalsilite ($KAlSiO_4$)	−408 "

The solvus in the spinel series, which opens out in the temperature range 500 to 900°C, controls the locations of the tie–lines in the system Fe–Al–O. These tie–lines are also contour lines for oxygen pressure. Information on these tie–lines, and the entropy of mixing of the spinels, was obtained by these buffered hydrothermal experiments.

RECHERCHES SUR LE SYSTEME CaO–MgO–WUSTITE.

Vittorio Cirilli, Aurelio Burdese

En poursuivant des recherches précedentes qui avaient permis d'établie la possibilité de coexistence à l'état solide de chaux et de wustite à température élevée et en presence de liquide, les études ont été étendues au système ternaire CaO–MgO–wustite.

Les essais expérimentales ont été conduits en déterminant les équilibres de réduction des différents solides jusqu'à leur température de fusion.

Dans le champ du système CaO– "FeO" on a confirmé la possibilité de formation d'un eutectique (1120°C) entre solutions solides de wustite en chaux ("FeO" = 9,5 % mol.) et de chaux en wustite (CaO = 9,0 % mol.)

En utilisant des atmosphères controllées pour maintenir les échantillon à la limite inférieur d'oxydation il n'a pas été possible d'obtenir des solutions solides (Fe, Ca)O, contenant jusqu'à 33 % mol. de chaux dont l'éxistence a étée recemment admise.

L'eutectique CaO– "FeO" correspond au minimum de la température de fusion même dans le système ternaire CaO–MgO– "FeO". Le diagramme d'état est caractérisé par deux champs de cristallisation primaire, divisés par una ligne qui joint l'eutectique CaO–MgO avec l'eutecti que CaO– "FeO". Sur cette ligne on trouve en condition d'équilibre des solution solides (Mg, Fe)O, contenant de petites quantités de chaux, avec des solutions solides saturées de wustite en chaux.

THE SYSTEM IRON OXIDE–MANGANESE OXIDE IN AIR.

Arnulf Muan and Shigeyuki Somiya

Phase relations in the system iron oxide–manganese oxide in air have been determined in the temperature interval from 800 to 1585°C.

The quenching method was used in this study. Oxide samples made up from pure chemicals were heated in air until equilibrium was established among condensed phases and gas. The samples were then quenched

rapidly to room temperature and the phases present determined by X-ray and occasionally by microscopic examination. The equilibration runs were made in a conventional vertical tube quench furnace with resistance winding of an 80% platinum 20% rhodium alloy. Accurate d-spacing measurements for quantitative determination of compositions of solid solution crystals were carried out on a GE-XRD-3 spectrometer unit, using NaCl as internal standard in all samples. Boundary curves in the liquidus temperature region were determined by reflected light examination of polished samples under an ore microscope. Although the very fluid liquids occurring in this system gave rise to extensive formation of dendritic quench crystals even upon most rapid quenching, these crystals could be distinguished by shape and size from those grown under equilibrium conditions in contact with liquids at the high temperatures of the quench runs.

Phase relations in the system iron oxide–manganese oxide in air, based on data obtained in the present investigation, are shown in Fig. 1. The system is not binary because both iron and manganese are present in varying degrees of oxidation. The two components Fe_2O_3 and Mn_2O_3 have been chosen for purpose of easy illustration of the phase relations. Designations used in labeling crystalline phases in the diagram are : Hematite (Fe_2O_3 with some Mn_2O_3 in solid solution), spinel (a solid solution between magnetite (Fe_3O_4) and high hausmannite (Mn_3O_4)), Mn_2O_3 (containing some Fe_2O_3 in solid solution).

The most prominent features of the diagram are as follows: The decomposition of hematite to magnetite, which in air takes place at 1390°C in the pure iron oxide system, decreases to a minimum of 997°C as manganese oxide is added. Decomposition of Mn_2O_3 to tetragonal Mn_3O_4, which takes place at 877°C in pure manganese oxide in air, increases to a maximum of 932°C as iron oxide is added. Inversion from the tetragonal to the cubic form of Mn_3O_4, which takes place at approximately 1160°C in the system Mn–O, decreases to a minimum of 932°C upon iron oxide addition. Phase assemblages and temperatures of two isobaric binary invariant situations in the system are as follows: At 997°C hematite with ~13 wt. % Mn_2O_3 in solid solution, Mn_2O_3 with ~ 64 wt. % Fe_2O_3 in solid solution, spinel (~ 60 wt. % Fe_3O_4, 40 wt. % Mn_3O_4) and gas ($pO_2 = 0.21$ atm.) coexist in equilibrium. At 932°C spinel (~ 30 wt. % Fe_3O_4 70 wt. % Mn_3O_4), Mn_2O_3 with ~42 wt. % Fe_2O_3 in solid solution and tetragonal Mn_3O_4 with ~2 wt. % Fe_3O_4 in solid solution are present together with gas ($pO_2 = 0.21$ atm.) in stable equilibrium. Liquidus temperatures decrease very slightly from either

end of the system, with solidus as well as liquidus curves having a minimum of approximately 1565°C.

A plot of d-spacing for (440) reflections of the spinel phase versus composition shows a distinct change in the slope of the curve at approximately 32 wt. % Mn_3O_4, as illustrated in Fig. 2. In this graph are plotted data obtained in the present investigation as well as those obtained by previous investigators. (1–5) Although the d-spacing values determined in the present study are slightly higher than those of Montoro, (2) the slopes of the curves are very similar, and the same characteristic break in slope is seen to be present in both curves.

Only very small changes in d-spacings with compositions of the hematite and Mn_2O_3 phases were observed, in agreement with the findings of Montoro. (2) X-ray methods were therefore not suitable for determining compositions, and hence boundary curves, where the solid solution crystals above were involved.

REFERENCES

1. E.J.W. Verwey and M.G. Von Bruggen, "Structures of Solid Solutions of Fe_2O_3 in Mn_3O_4," Z. Krist., 92, 136–138 (1935).

2. V. Montoro, "Miscibilita frai Sesquiossi di Ferro e di Manganese," Gasz. Chim. Ital., 68, 728–33 (1938).

3. H.J. Van Hook and M. L. Keith, "The System Fe_3O_4–Mn_3O_4," Am. Miner., 43, 69–83 (1958).

4. Brian Mason, "Mineralogical Aspects of the System FeO–Fe_2O_3–MnO–Mn_2O_3, "Geol. Foren. Forhandl., 65, 95–180 (1943).

5. Sidney Roy Butler, "A Study of the Variations in the Valence and Distribution of Iron and Manganese and their Effect on the Magnetization and Crystal Structure of Manganese Ferrite," Ph.D. Dissertation, The Pennsylvania State University, January 1960.

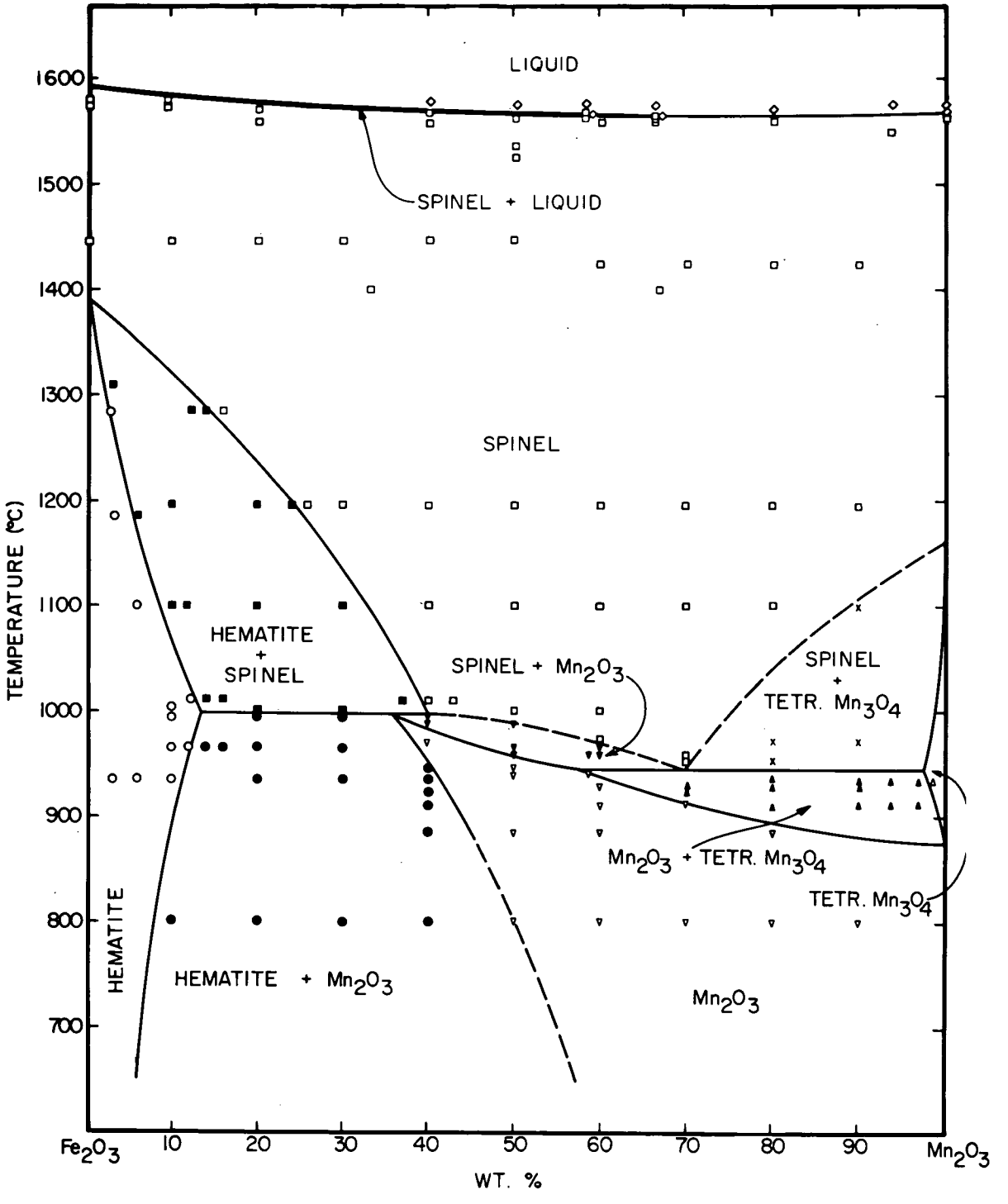

Fig. 1 Diagram showing phase relations in the system iron oxide-manganese oxide in air, as determined in the present investigation. A different symbol is used to designate each phase assemblage, as seen from the diagram.

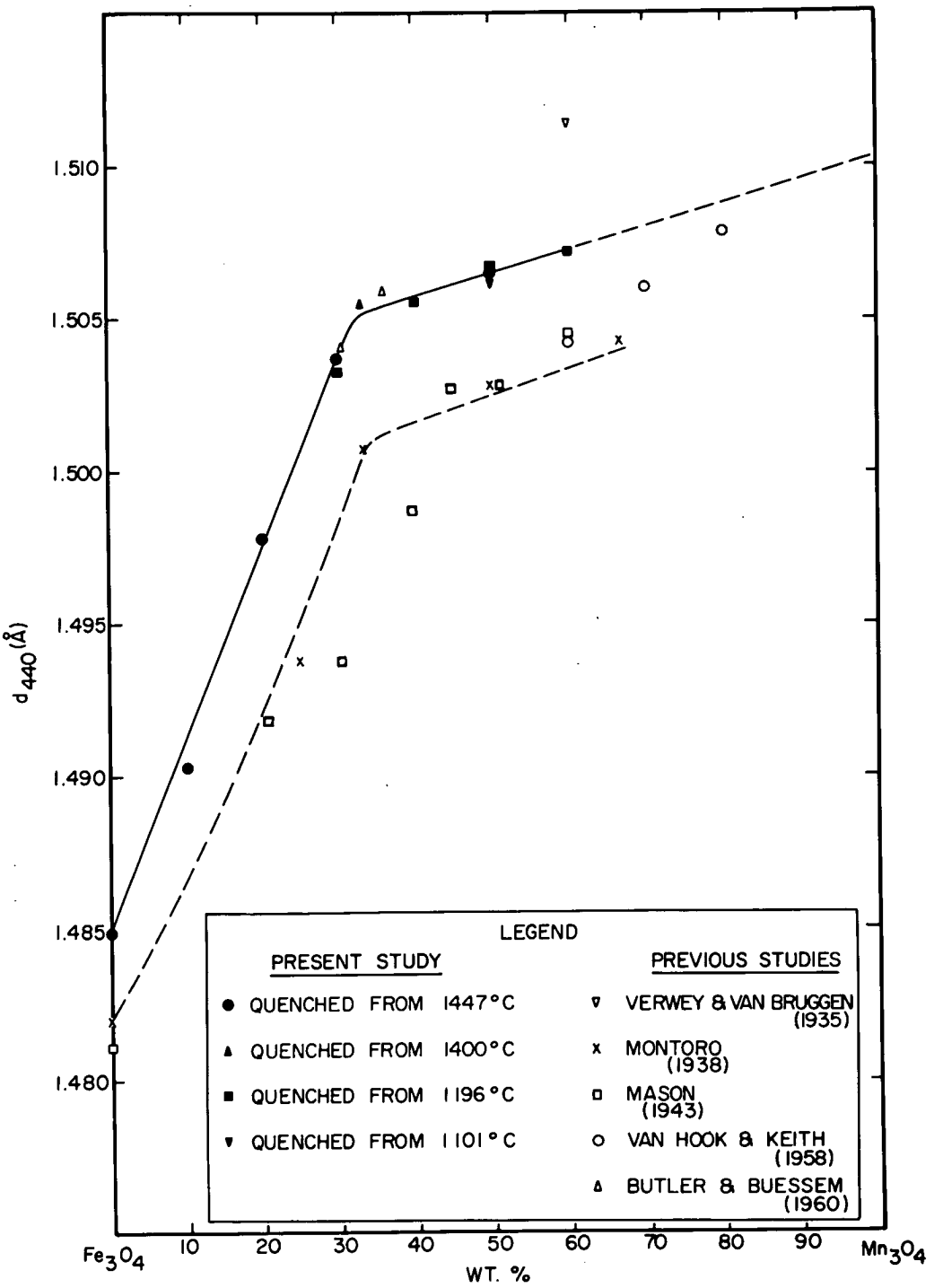

Fig. 2 Diagram showing variation in d-spacing with composition for (440)-reflection in spinel solid solutions, as determined in the present investigation and as reported in previous literature.[1-5]

UBER DAS VERHALTEN VON EISENOXYDEN BEI HOHEREN TEMPERATUREN.

Hans von Wartenberg, Horst Heinrich Weizenkorn u. Oskar Glemser

Das zur Verwendung kommende Eisenoxyd wird durch Oxydation von Eisendraht mit CO_2 bei 1160°C hergestellt.

Eine Iridiumbirne wird mit Hilfe eines Tammann–Ofens mit Iridiumrohr als Heizkörper auf 1800 – 2200°C (Grenze der Beanspruchbarkeit für Iridium) erhitzt. Die Temperaturmessung geschieht mit einem optischen Pyrometer. Nach Errichen der jeweiligen Versuchstemperatur wird ein Eisenoxydstäbchen bekannten Gewichts in die Birne eingeworfen, wonach bei Normaldruck nur an der oberen Grenze des Temperaturintervalls, bei vermindertem Druck jedoch auch im unteren Teil des Gebiets, Verdampfung einsetzt. Der Volumenzuwachs, der durch die Verschiebung einer Quecksilberkugel in einer Kapilare gemessen wird, gestattet Rückschlüsse auf die Molmasse.

PHASE EQUILIBRIUM AND CRYSTAL CHEMICAL RELATIONSHIPS IN RARE EARTH SYSTEMS

I. Warshaw and Rustum Roy

The phase equilibrium and crystal chemistry in rare earth oxide, aluminate and silicate systems were investigated in an effort to obtain further information on the effect of slight changes in ionic radius on compound formation and liquid immiscibility, on the possible sub–groups of the lanthanon elements, and on the problems which will be encountered when the rare earth oxides react with alumina or silica, two of the most widely used oxides in high–temperature technology.

The phase equilibrium and crystal chemical relationships involved in simple rare earth sesquioxide systems and binary systems containing these oxides and alumina or silica were determined by a number of high–temperature techniques. In the solution of the problems encountered, hydrothermal techniques and an iridium "strip–furnace" were used extensively. The use of hydrothermal techniques to aid diffusion in the solid state made it possible to attain equilibrium at lower temperatures; the strip–furnace made it possible to observe reactions which took place up to 2400°C. Not only were the phase equilibrium relationships in these systems defined but a clearer understanding was obtained of the extent of the liquid mixcibility gap which one might expect in all binary silicate systems as well as in rare earth silicate systems.

Contrary to what has been published previously, the polymorphic transformations of all the rare earth oxides are reversible under equilibrium conditions. Furthermore, the transformation temperatures of nearly all the polymorphs are considerably lower than reported previously. Finally, none of the rare earth sesquioxides exists in more than two polymorphic forms. Only A–type oxides of lanthanum and praseodymium were obtained, while the C–type oxide of neodymium was observed as well. Both B and C polyporphs, high– and low– temperature forms respectively, were found for the rare earths samarium through dysprosium, whereas C–type is the only form of sesquioxide with the smaller rare earths.

A new rare earth aluminate compound, $2Ln_2O_3 \cdot Al_2O_3$, forms with many of the smaller rare earth ions. The identification of this compound along with recognition of the fact that the metastable 1:1 compound, the distorted perovskite–type, tends to form readily in the systems containing the small rare earths dysprosium through erbium and yttrium has made it possible to clarify many conflicting results reported previously. The metastable compound forms from the liquid state or by the reaction of oxides. It is now clear that, while the 1:1 compound is metastable when containing rare earths smaller than terbium, the garnet–type 3:5 compound formed with terbium and all the smaller rare earths is stable and melts congruently without undergoing any inversion. The rare earth aluminate systems containing elements larger than europium are simpler than the rest since they contain only one compound, perovskite–type 1:1, which melts congruently.

Compounds form at only two compositions, $Ln_2O_3 \cdot SiO_2$ and $Ln_2O_3 \cdot 2SiO_2$, in all the rare earth silicate systems. Although there are

only two possible compositions, there is a large number of compounds because there are as many as five different structures for only one of these compositions. Except for lanthanum orthosilicate, which is unique, the 1:1 silicates fall into two groups depending on the size of the rare earth ion. One consists of the orthosilicates of praseodymium through terbium, the other of those of all the smaller rare earths. The rare earth pyrosilicates fall into three groups: pyrosilicates of the large ions, lanthanum through europium, those of the intermediate rare earths, gadolinium through holmium, and the 1:2 silicates of the small rare earths. Moreover, the first two groups each have low- and high-temperature polymorphs. Yttrium pyrosilicate occupies an intermediate position between the latter two groups. It exhibits polymorphism, but the low-temperature form is like that of the intermediate group while the high-temperature polymorph is similar to the only form of the small rare earth pyrosilicates.

The changes in the extent of the liquid miscibility gap in the rare earth oxide–silica systems are quite striking. While the extent of this gap increases, as one might expect, with decreasing radius of the modifier cation, the liquidus temperature of the two-liquid region rises sharply in those systems involving the last three oxides, and the primary phase below the two-liquid dome is no longer cristobalite but a rare earth silicate. While this change of the primary phase which can exist in equilibrium with the two liquids was recognized previously, it was not believed to be common. This study has shown not only that such occurrences are more common in silicate systems than previously anticipated but also that the extent of the liquid miscibility gap can be clearly related, at least empirically, to the ionic radius of the modifier cation.

The results of this investigation indicate that the rare earths should be divided into three, rather than two, separate groups, comprising the large, intermediate and small rare earths. This is clearest in the case of the sesquioxides, where the groups consist of lanthanum to neodymium, samarium to dysprosium, and holmium to lutetium.

From the silicate studies the elements most probably would be grouped as lanthanum to eruopium, gadolinium to holmium, and erbium to lutetium. The latter elements, erbium to lutetium, and certainly thulium to lutetium, definitely comprise a third group of the rare earths. This statement is based especially on the fact that thulium, yttrium and lutetium behave so differently from all the other rare earths in the formation of immiscible silicate liquids.

TUNGSTEN–YTTRIUM OXIDES.

Hans J. Borchardt

Five new phases have been found to result from reaction of WO_3 with Y_2O_3 in air which can be described by the formula $WO_3 \cdot X(YO_{1.5})$ where X has the values 2/3, 2, 15/4, 9/2 and 6. These are shown in the pseudobinary phase diagram of the system WO_3–Y_2O_3, Fig. 1.

Phase I has been formed by heating a pressed pellet of the mixed oxide powders in a platinum vessel at temperatures as low as 750°. No evidence was found for the formation of phase II below 1000°C nor for the formation of phases III, IV and V below 1100°C when heating the corresponding oxide mixtures for one week. At temperatures between 750°C and 1000°C, Y_2O_3 rich compositions react to form a sixth new phase which has a composition, approximately 75% $YO_{1.5}$. This phase appears to persist indefinitely at temperatures below 1000°C. It disappears on heating at 1100°C. It does not reappear when any of the higher temperature phases are annealed at 1000°C. This evidence, together with the fact that it has resisted efforts to form it free of any other phases, suggests that it is a metastable phase. The X–ray powder diffraction patterns of phases I and II have not been indexed because of their complexity. Phase III can be indexed on the basis of a hexagonal elementary cell having $a = 2 \times 3.688$A and $c = 9.39$A. The strong reflections of phase IV can be indexed on the basis of a monoclinic elementary cell with $a = 3.688$A, $b = 6.445$A, $c = 9.390$A and $\beta = 90°$. The prominent lines of phase V can be described with a hexagonal elementary cell with $a = 3.688$A and $c = 9.32$A. These three phases may be different distortions of a fluorite type structure.

No evidence for homogeneity ranges about the cited composition could be obtained by X–ray powder diffraction methods.

Phase I melts congruently at 1495 ± 5°C. It forms a eutectic with WO_3 at a composition, approximately 30 mole % $YO_{1.5}$ and a temperature of 1155 ± 5°C. Phase II melts incongruently at 1700 ± 20°C. Phases I and II form a eutectic at approximately 47 mole % $YO_{1.5}$ which melts at 1455 ± 10°C. Phases III, IV and V all melt above 2200°C. X–ray diffraction of the quenched melts suggests that phases III and IV melt congruently. The X–ray pattern of phase V quenched from the melt can be indexed on the basis of a face–centered cubic unit cell with a lattice parameter of 5.276A. This indicated that phase V undergoes a phase

FIG. 1

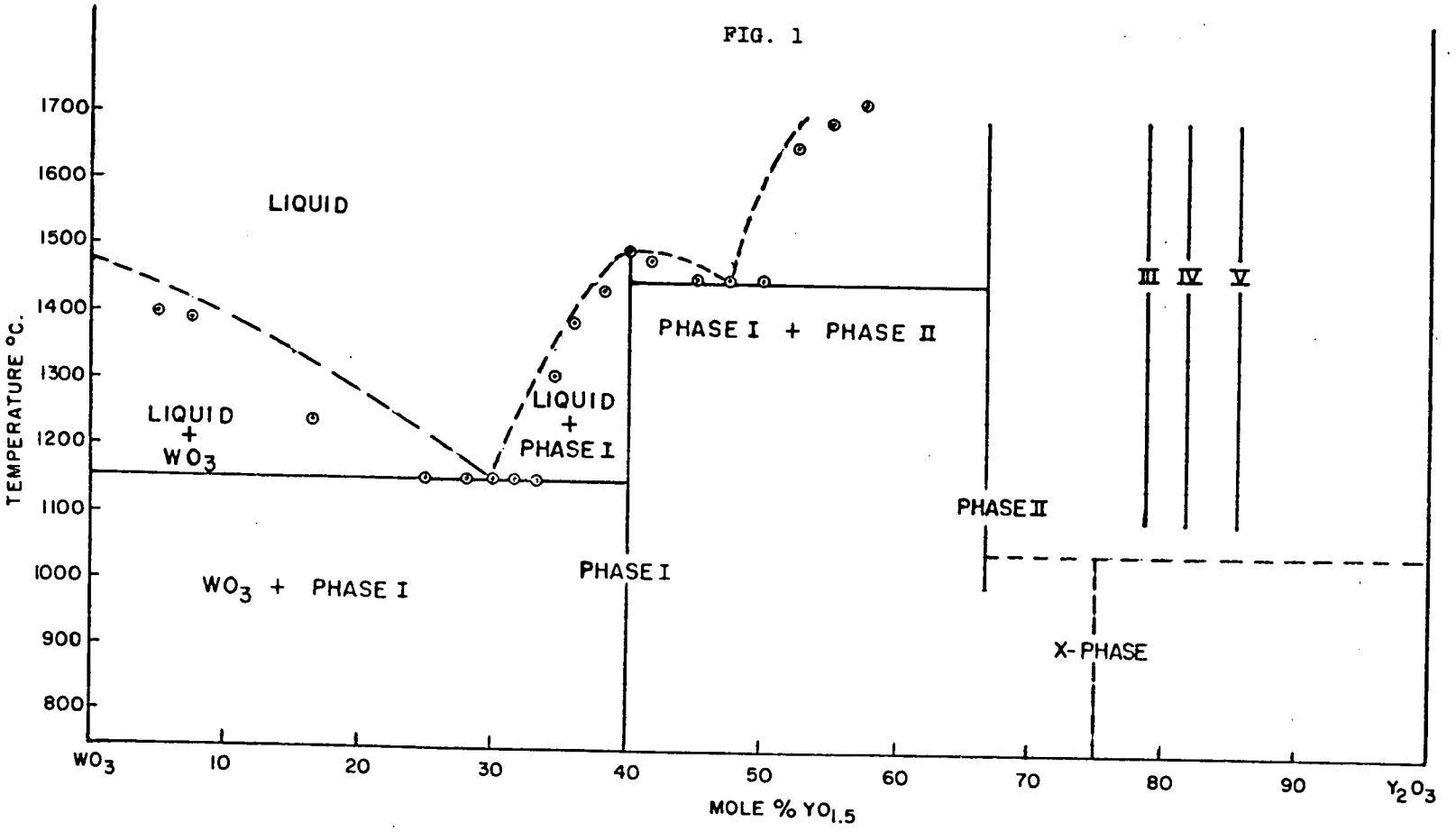
LIQUID
LIQUID + WO3
LIQUID + PHASE I
PHASE I + PHASE II
WO3 + PHASE I
PHASE I
PHASE II
X-PHASE
III
IV
V
TEMPERATURE °C.
1700
1600
1500
1400
1300
1200
1100
1000
900
800
WO3
10
20
30
40
50
60
70
80
90
Y2O3
MOLE % YO1.5

transformation at some temperature between 1700°C and its melting point.

Various compositions of WO_2–Y_2O_3 were reacted in argon at 1400°C. The reaction products were elemental tungsten and the same phases as are observed when WO_3 –Y_2O_3 are reacted in air. The overall stoichiometry corresponds to the disproportionation of WO_2 to WO_3 and W, the former reacting with Y_2O_3 to yield the several new phases.

Yttrium metal reacts with the several new phases to form elemental tungsten and Y_2O_3. No evidence could be obtained for alloy formation or other interaction between the metals yttrium and tungsten.

The above observations are summarized in the form of a ternary composition diagram of the system W–Y–O. From this diagram it is concluded that no phases, other than those discussed above, form from the elements W, Y, O at one atmosphere total pressure in the temperature range 1100–1400°C. Excluded from this conclusion are compositions in the range WO_3–WO_2–Phase I, which were not investigated.

Six independent methods were employed to determine the oxygen content of the several cited phases. No major deviation from stoichiometry were detected. With the stoichiometric formula as $WO_Z \cdot X(YO_{1.5})$, Z cannot be less than 2.95 and a more reasonable lower limit is 2.99.

A small variability in oxygen content was detected through resistivity measurements in various partial pressures of oxygen at elevated temperatures . With phase II at 1000°C, the resistivity increases as the partial pressure of oxygen is lowered from one atmosphere. It goes through approximately a ten-fold increase and then returns to near its original value in pure argon. As the resistivity passes through a maximum, the sign of the Seebeck coefficient changes indicating that donor levels are present in one case and acceptor levels in the others. A quantitative interpretation of these results will be presented.

OXIDATION CHARACTERISTICS TO 2600 F OF SEVERAL MATERIALS EVALUATED FOR LEADING EDGES OF HYPERSONIC AIRCRAFT.

John M. Novak

Oxidation tests in flowing air were conducted on a number of materials evaluated for use as leading edges of hypersonic aircraft.

The paper describes the results obtained on cylindrical specimens 1" x 3/8" diameter of the following materials: unalloyed molybdenum, molybdenum (1/2 Ti) alloy, diffusion coated molybdenum disilicide, material systems, dense silicon carbide, siliconized graphite, molybdenum disilicide, and a cermet with a nominal composition of 60% tungsten, 25% chromium and 15% alumina. Test temperatures were 1700, 2000, 2300 and 2600 F. All the specimens were exposed to air flow rates of 1500 lb/ft^2. hour and a Reynolds number of 3.5×10^4 to 3.5×10^5. In addition specimens of unalloyed molybdenum and the 1/2 Ti molybdenum alloy were exposed to mass air flow rates of 500 lb/ft^2. hour and 4000 lb/ft^2. hour. The test conditions approximated flight mass velocities, free stream V, and Reynolds number parameters nominally associated with the leading edges of hypersonic flight vehicles. The oxidation data for the bare metals appears to fit the Arrhenius rate equation

$k = Ae^{-\frac{Q}{RT}}$. The Q value was obtained by fitting the best straight line to a plot of log k vs 1/T.

Oxidation tests were also conducted on molybdenum (1/2 Ti) alloy, on coated molybdenum (1/2 Ti) alloy, and on siliconized graphite using specimens simulating leading edge shapes. The specimens were wedges nominally 2-1/2" in length, by 1" in height with a 1/2" base. The wedge samples were tested at 2000 F, at 2450 F, at air mass flow rates of 500, 1500 and 5000 lb/ft^2. hour. The data for the bare molybdenum alloy was plotted and fits the Arrhenius equation based on a limited number of samples. Data obtained on the wedges is compared to the data obtained on the cylindrical specimens.

NASA - Langley Field, Va.